



**AALBORG
UNIVERSITY**

Aalborg Universitet

A novel method for solving problems in linear dynamics using bi-orthogonality relations

Ledet, Lasse Søgaard

Publication date:
2019

Document Version
Publisher's PDF, also known as Version of record

[Link to publication from Aalborg University](#)

Citation for published version (APA):

Ledet, L. S. (2019). *A novel method for solving problems in linear dynamics using bi-orthogonality relations*. Aalborg Universitetsforlag.

General rights

Copyright and moral rights for the publications made accessible in the public portal are retained by the authors and/or other copyright owners and it is a condition of accessing publications that users recognise and abide by the legal requirements associated with these rights.

- Users may download and print one copy of any publication from the public portal for the purpose of private study or research.
- You may not further distribute the material or use it for any profit-making activity or commercial gain
- You may freely distribute the URL identifying the publication in the public portal -

Take down policy

If you believe that this document breaches copyright please contact us at vbn@aub.aau.dk providing details, and we will remove access to the work immediately and investigate your claim.

**A NOVEL METHOD FOR SOLVING
PROBLEMS IN LINEAR DYNAMICS
USING BI-ORTHOGONALITY RELATIONS**

**BY
LASSE SØGAARD LEDET**

DISSERTATION SUBMITTED 2019



AALBORG UNIVERSITY
DENMARK

A novel method for solving problems in linear dynamics using bi-orthogonality relations



AALBORG UNIVERSITY
DENMARK

By
Lasse Søgaaard Ledet

Department of Materials and Production
Solid and Computational Mechanics Research Group
Aalborg University, Denmark

PhD Thesis
2019

Dissertation submitted: June, 2019

PhD supervisor: Sergey V. Sorokin, Prof., DSc, PhD, MSc
Department of Materials and Production,
Aalborg University, Denmark

PhD committee: Associate Prof. Thomas Møller Søndergaard (chair.)
Aalborg University
Professor Lars Vabbersgaard Andersen
Aarhus University
Professor Goran Pavic
National Institut of Science (INSA)

PhD Series: Faculty of Engineering and Science, Aalborg University

Department: Department of Materials and Production

ISSN (online): 2446-1636
ISBN (online): 978-87-7210-453-9

Published by:
Aalborg University Press
Langagervej 2
DK – 9220 Aalborg Ø
Phone: +45 99407140
aauf@forlag.aau.dk
forlag.aau.dk

© Copyright: Lasse Søgaard Ledet

Typeset in L^AT_EX and printed in Denmark by Rosendahls, 2019

Preface

This thesis has been submitted to the Faculty of Engineering and Science at Aalborg University in partial fulfilment of the degree of Doctor of Philosophy in Mechanical Engineering. The work has been carried out at the Department of Materials and Production at Aalborg University and at the Department of Mechanics and Materials at Grundfos Holding A/S in the period from June 2016 to June 2019 including a three-month research stay at the Mechanical Engineering Department at University of Auckland, New Zealand from February to May 2018. The work has been carried out as an Industrial Research Project entitled “*Vibro-acoustics of centrifugal pumps*” funded partly by Grundfos Holding A/S and partly by the Innovation Fund Denmark under the grant number 5189-00011B. The support is gratefully acknowledged.

The thesis is prepared as a collection of papers introduced by an extended summary and with an associated online Annex. The Annex can be accessed using either the QR-code below (smartphone) or through the link provided in the caption. The full link can be found in [1].



Online Annex, [1]: forms.gle/Acx78Y5CN897XjVXA

In the Annex the reader will find most of the figures embedded in the extended summary in full size. Further, as the thesis is conducted under the Danish Research Program “*Erhvervsforsker*” (Industrial PhD) part of the extended summary will focus on industrial impact of the research conducted. To accommodate the industrial needs ‘Plug-N-Play’ Matlab tools have been developed. The tools are elaborated in Chap. 2, while examples of various analysis and functionalities provided by the tools can be found in the Annex. The industrial partner, Grundfos, is a Danish pump manufacturer and therefore discussions and emphasis in the extended summary may, at times, be directed towards centrifugal pumps. The technical terminologies and basic knowledge required is, however, limited to a minimum, but should the reader find the need for a quick brush-up on centrifugal pumps, a short introductory video with the basic concepts, terminology and working principle of the centrifugal pump can be found in the Annex as well.

Acknowledgements

I would like to take this opportunity to express my sincerest gratitude to my brilliant supervisor; Prof. Sergey V. Sorokin for always being available and patient and for his encouraging spirit, his enthusiasm and his many suggestions and ideas. Thanks for the countless number of interesting discussions and the extreme effort put into reviewing and editing manuscripts. The support has been beyond compare. Also, a special thanks to my colleagues at Aalborg University for the always joyful DCAMM trips and to my office mate Christian Krogh for our daily discussions. Further, a special thanks also to Prof. Brian Richard Mace and Dr. Michael Joseph Kingan, whom I visited during my stay in Auckland. I am most grateful for the valuable knowledge with which you contributed and for the interesting discussions and most competent supervision. Also, a special thanks to Prof. John Chapman for his comments to manuscripts and for the always encouraging discussions and suggestions during his visits in Aalborg.

My sincerest gratitude also goes to my industrial supervisors: Brian Lundsted Poulsen (Mechanics specialist), Jan Balle Larsen (Sound & Vibration specialist) and Nicholas Engen Pedersen (Fluid mechanics specialist) for the many good discussions, support and the valuable knowledge with which you contributed and for always prioritising your time to assist whenever needed. Also, thanks to the rest of the Mechanics & Materials department at Grundfos for keeping a fun work environment and, of course, for the enjoyable department trips; Thanks to the Sound and Vibration Laboratory for their continuous support, help whenever needed and, not least, their sweets; And thanks to the Hydraulics department for providing the needed CFD data.

Finally, a very special thanks to those who deserve it most: My family and friends, for constantly reminding me about other important things in life and for their worthy attempt in trying to understand my work (*“Something with water in pipes”*). Lastly, I owe my sincerest gratitude to my Significant Other; Esin Severinova, for her everlasting love and support.

Aalborg, 2019

Lasse Sjøgaard Ledet

Abstract

This thesis is concerned with a novel approach to analyse dynamic systems. Dynamic systems appear everywhere in nature and may be everything from chaotic to almost static (quasi-static) in behaviour. They appear in almost all areas of science ranging from physics and engineering science to sociology and psychology. More specifically, this thesis is concerned with time-invariant linear dynamic systems, which is likely the most considered type of dynamic systems in science; Yet the thesis primarily addresses examples from the field of vibro-acoustics (fluid-structure interaction) as this have particular interest for the industrial partner; Grundfos Holding A/S.

A novel approach for analysing the behaviour of linear dynamic systems has been developed. The method is based on specially derived bi-orthogonality relations which have origin in the classical reciprocity relation (or theorem). Application of the bi-orthogonality relation provides, for a broad class of problems in e.g. waveguide theory, convenient analytical closed-form solutions. These explicit solutions offer full transparency when analysing e.g. the energy conveying properties and thus permit an increased insight into the physical phenomena occurring in waveguides. Likewise, the method offers insight into the formation of standing waves when extended to what is called 'finite' waveguides, that is, waveguides subjected to boundary conditions. The novel approach of bi-orthogonality developed here is found to be an efficient tool for solving a wide range of problems in physics such as, for example, in mechanics, acoustics, electromagnetics, seismics, optics and even quantum mechanics as well as any coupled problem of the latter. From an industrial viewpoint the study and enhanced physical understanding of performance of vibro-acoustic waveguides related to pipe systems are of particular interest for Grundfos. Therefore, the main focus and examples presented through the thesis are related to an elastic fluid-filled cylindrical shell even though the methods have been shown to apply much beyond vibro-acoustic waveguides. As receiving pipe systems may be vastly different it is the aim to study these properties in a generic way such as to identify critical excitations, in terms of frequencies, modes and transmission paths, that will be critical for all systems, no matter their size and shape. This is accomplished by the advantages and transparency offered by the solution through bi-orthogonality and has led to the development of two Matlab Tools: Tool 1 to enhance the understanding of wave propagation and energy transmission phenomena of the receiving pipe system and Tool 2 to characterise, based on CFD data (Computational Fluid Dynamics), the acoustic sources generated and emitted by centrifugal pumps.

Resumé

Denne afhandling omhandler en ny metode til analyse af dynamiske systemer. Dynamiske systemer forekommer overalt og kan være alt fra kaotiske til næsten statiske (kvasi-statiske) af natur. De forekommer i næsten alle felter af videnskab, lige fra fysik og ingeniørvidenskab til sociologi og psykologi. Mere præcist omhandler denne afhandling tids-invariante lineære dynamiske systemer, som med al sandsynlighed er blandt de mest betragtede typer af dynamiske systemer i videnskaben. Dog fokuserer afhandlingen primært på eksempler fra feltet; vibro-akustik (fluid-struktur interaktion), da dette er særligt interessant for den industrielle partner; Grundfos Holding A/S.

En ny metode til analyse af lineær dynamiske systemer er udviklet. Metoden er baseret på specielt udledte bi-ortogonalitets relationer, der har sin oprindelse fra den klassiske reciprocitets relation. Brugen af bi-ortogonalitets relationer giver, for en bred vifte af problemer i f.eks. bølgelederteori, eksplicitte analytiske udtryk, som tillader fuld transparens i analyse af f.eks. energi transmissionsegenskaberne for en bølgeleder, og dermed tillader en øget indsigt i de fysiske fænomener, der forekommer i bølgeledere. Ligeledes er metoden videreudviklet til bølgeledere med en endelige længde, det vil sige, bølgeledere der er pålagt et sæt af randbetingelser, og metoden bidrager derved også med indsigt i formationen af stående bølger. Den nye metode baseret på bi-ortogonalitets princippet har vist sig at være et effektivt redskab til at løse en lang række problemer i fysikken f.eks. i mekanik, akustik, elektromagnetisme, seismologi, optik og endda kvantemekanik, såvel som koblede problemer af disse. Fra et industrielt perspektiv er det interessant for Grundfos at udforske og øge den fysiske forståelse for performance af, specielt, vibro-akustiske bølgeledere relateret til rørsystemer. Fokusområdet samt eksemplerne præsenteret gennem denne afhandlingen er derfor primært baseret på en elastisk væskefyldt cylindrisk skal, selvom metoden har vist sig anvendelig for meget mere end blot vibro-akustiske bølgeledere. Da rørsystemerne kan være meget forskellige, er formålet at undersøge disse egenskaber på generisk vis, således kritiske excitationer, i form af frekvenser, modes og transmissionsveje, der er kritiske for alle systemer uanset deres facon, kan identificeres. Dette kan netop imødekommes ved brug af bi-ortogonalitets metoden, som derved har ført til udviklingen af to industrielle Matlab Tools: Tool 1 til at øge forståelsen for bølgeudbredelse og energi-transmissions-fænomener i rørsystemer og Tool 2 til at karakterisere, baseret på CFD data (Computational Fluid Dynamics), akustiske kilder genereret og udsendt fra centrifugal pumper.

Dissemination

The present thesis is submitted as a collection of scientific papers with an introductory extended summary. The following contains a brief description of the main dissemination carried out during the PhD study.

Peer-reviewed publications included in the Thesis

- A) L. S. Ledet & S. V. Sorokin, Bi-orthogonality relations for fluid-filled elastic cylindrical shells: Theory, generalisations and application to construct tailored Green's matrices, *Journal of Sound and Vibration*, 417 (2018), 315–340, doi:10.1016/j.jsv.2017.12.010
- B) L. S. Ledet & S. V. Sorokin, On the application of the bi-orthogonality relations for analysis of linear dynamical systems, *Journal of Sound and Vibration* (under review)
- C) L. S. Ledet & S. V. Sorokin, (Bi)-orthogonality relation for eigenfunctions of self-adjoint operators, *Philosophical Transactions of the Royal Society A*, doi:10.1098/rsta.2019.0112
- D) L. S. Ledet & S. V. Sorokin, Using the Finite Product Method for solving eigenvalue problems formulated in cylindrical coordinates, To be published in: *Journal of Physics: Conference Series*, 13th Intl. Conf. on Recent Advances in Structural Dynamics (RASD), Lyon, 2019
- E) S. V. Sorokin, E. Manconi, L. S. Ledet & R. Garziera, Wave propagation in helically orthotropic elastic cylindrical shells and lattices, *International Journal of Solids and Structures*, 170 (2019), 11–21, doi:10.1016/j.ijsolstr.2019.04.031
- F) L. S. Ledet, S. V. Sorokin & J. B. Larsen, Experimental analysis, simulation and decomposition of vibrations in not perfectly axi-symmetric pipes, In proceedings: *NAFEMS World Congress (NWC17)*, Stockholm, 2017. Available: https://www.nafems.org/publications/resource_center/nwc17_481/. [Accessed 08 May 2019]

Other relevant peer-reviewed publications

- G) L. S. Ledet & S. V. Sorokin, A novel approach to solve eigenvalue and forced response problems in waveguide theory by means of bi-orthogonality relations, To be published in: *Journal of Physics: Conference Series*, 13th Intl. Conf. on Recent Advances in Structural Dynamics (RASD), Lyon, 2019

- H) L. S. Ledet & S. V. Sorokin, Vibro-acoustics of infinite and finite elastic fluid-filled cylindrical shells, *Procedia Engineering*, 199 (2017), 1362–1367, *10th Intl. Conf. on Structural Dynamics (EuroDyn)*, Rome, 2017, doi:10.1016/j.proeng.2017.09.356
- I) L. S. Ledet, S. V. Sorokin, J. B. Larsen & M. M. Lauridsen, Bi-orthogonality conditions for power flow analysis in fluid-loaded elastic cylindrical shells: Theory and applications, In proceedings: *5th Noise and Vibration – Emerging Methods (NOVEM)*, Dubrovnik, 2015, <https://vbn.aau.dk/en/publications/bi-orthogonality-conditions-for-power-flow-analysis-in-fluid-load> [Accessed 30 May 2019]

Dissemination through talks

- 5 Conference talks: Paper D and F-I
- 2 Symposium talks: 2017 DCAMM Symposium (Danish Center for Applied Mathematics and Mechanics), 2019 DCAMM Symposium
- >3 Miscellaneous technical talks: Aalborg University (several occasions), Grundfos Holding A/S (several occasions) and University of Auckland
- >3 Non-technical talks: Dissemination to PhD students from other academic fields (several occasions); Dissemination of science to kids and young adults: 2 talks at “Science festival – Science on Visit” (DK: “Naturvidenskabsfestival – Videnskaben på Besøg”) at Hals and Terndrup school (main school, 14–16 years)

This thesis has been submitted for assessment in partial fulfilment of the PhD degree. The thesis is based on some of the submitted/published scientific papers and conducted dissemination listed above. Parts of the papers are used directly or indirectly in the extended summary of the thesis. Each scientific paper appended as part of the collection of papers is associated with a co-author statement which is made available to the assessment committee and are otherwise available at the Faculty.

Contents

Preface	iii
Abstract	v
Resumé	vii
Dissemination	ix
1 Getting Acquainted	1
1.1 Dynamic systems	1
1.2 Academic scope	6
1.3 Key concepts and theoretical background	8
2 Industrial Impact	19
2.1 Industrial scope	19
2.2 Tool 1: Wave propagation in pipe systems	23
2.3 Tool 2: Source characterisation from CFD simulations	27
2.4 Concluding remarks	34
2.5 Future work	34
3 Summary & Conclusions of the Papers	37
3.1 Description of papers	37
3.2 Future work	47
References	49
A Bi-orthogonality relations for fluid-filled elastic cylindrical shells: Theory, generalisations and application to construct tailored Green’s matrices	51
B On the application of the bi-orthogonality relations for analysis of linear dynamical systems	97
C (Bi)-orthogonality relation for eigenfunctions of self-adjoint operators	131
D Using the Finite Product Method for solving eigenvalue prob- lems formulated in cylindrical coordinates	149

E	Wave propagation in helically orthotropic elastic cylindrical shells and lattices	163
F	Experimental analysis, simulation and decomposition of vibrations in not perfectly axi-symmetric pipes	185

Getting Acquainted

“ Science means constantly walking a tightrope between blind faith and curiosity; between expertise and creativity; between bias and openness; between experience and epiphany; between ambition and passion; and between arrogance and conviction – in short, between an old today and a new tomorrow. ”

– Heinrich Rohrer

1.1 Dynamic systems

A dynamic system can indeed be many things! But common for all of them is that we may understand them as systems that varies in time. It is therefore not difficult to imagine that this covers a whole lot of areas, not just in science and mathematics, but also in e.g. economics, sociology, psychology, anthropology etc. A dynamic system can have everything from, mildly speaking, a very rich behaviour to a more subtle, yes even steady, behaviour. The most violent behaviours of dynamic systems are highly non-linear in nature and are known as chaotic systems – studied in the field of Chaos theory. In general, a chaotic system is a system with a vigorous transient behaviour characterised by being highly sensitive to what is known as initial conditions. Thus, the slightest change in initial conditions could, potentially, cause a dramatic change in the response of the system, if not immediately then as time passes. Imagine, for instance, a chaotic universe where slight changes in initial conditions during the big bang would change completely the world as we know it. To this day it is still uncertain why matter exceeds anti-matter – Could this be the remains of a chaotic beginning of our universe?

Moving on from this rather philosophical example to more tangible ones, we in fact see chaotic systems everywhere in nature today, ranging from engineering science to climate and even to road traffic. Probably the first modern encounter of such violently (or chaotically) behaved systems was made by the famous Mathematician and Meteorologist Edward Norton Lorenz, who by pure serendipity noticed that a very small round-off error in his initial conditions of a weather simulation completely changed the weather forecast over as little as a few months. This led Lorenz to present his peculiar findings at the 139th meeting of the American Association for the Advancement of Science and in his quest for a proper title he came up with: “Predictability: Does the flap of a butterfly’s wings in Brazil set off a tornado in Texas”, [2]. Today this is known as the “Butterfly effect” and has led to the famous saying: “A butterfly flapping its wings in Brazil can create a hurricane in Texas“ – just one of many formulations. The chaotic behaviour observed by Lorenz is now known as a Lorenz system. What exactly has been the inspiration for the butterflies is unsaid but it may have had something to do with the solution to the system, seen in Fig. 1.1, which is known as the Lorenz attractor.

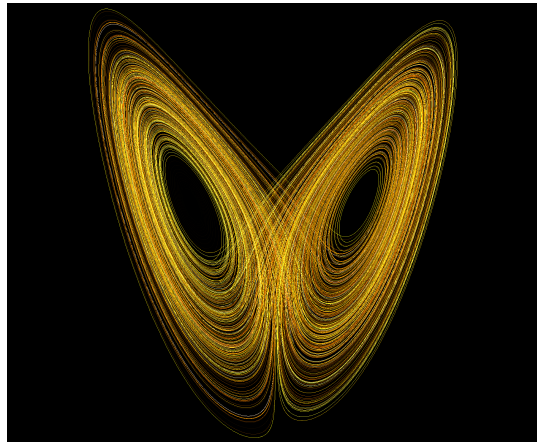


Fig. 1.1: The chaotic Lorenz attractor. As time passes the solution sporadically orbits the two equilibrium states of the problem. The way in which the solution orbits the equilibrium change radically depending on the initial conditions. Source: https://pt.wikipedia.org/wiki/Ficheiro:Lorenz_system_r28_s10_b2-6666.png [Accessed 14-05-2019].

On the opposite extreme a dynamic system may behave so smooth and nicely that they are almost static and may in this case, by a reasonable assumption, be treated as a static system. Such systems are known as quasi-static systems. Quasi-static systems are likely more apparent in our daily lives and therefore of great importance in engineering science. In many of the products and structures we engage with in our daily lives the static performance often governs the design and construction thereof. Within mechanics, quasi-static systems are, for instance, useful for assessing the stress/strain (load/deformation) state and even fatigue life of a product/structure. For example, determining how much (quasi) static load a structure can carry before collapsing.

Somewhere in-between these two extremes lie the dynamic systems relevant for this thesis, namely genuine dynamic systems obeying linearity. In general, linear dynamic systems reveal themselves everywhere in nature and science and are, as the quasi-static ones, very important for the architecture of our daily encounters. Limited to physics, much of what we use, see, hear and feel may be sufficiently represented by a linear dynamic system such as, for instance, vibrations through a structure, traffic noise, the signal on a cell phone, internet, the light and colours we see etc. And maybe even more intriguing, yet not likely a daily encounter, is the peculiar field of quantum mechanics, which may also be represented as a linear dynamic system through the Schrödinger equation.

An important part of linear dynamic systems is the field of stationary (or steady state) dynamics. This is referred to as time-harmonic (or time-invariant) systems, in which we assume a simple harmonic (or periodic) behaviour of the system i.e. $\exp(-i\omega t)$. Thus, we say that we have transformed (or decomposed) the problem into the frequency (or Fourier) domain. This simplification is indeed useful as differentiation transforms into multiplication. Should we, on the other hand, at a later stage want to assess the transient effects we may recover this by collecting all information from the time-harmonic system. Thus, time-harmonic problems are certainly among the most considered problems in linear dynamics and do also constitute the problems considered in this thesis.

1.1.1 Waves

Common for the linear dynamic systems is that the dynamic behaviour is caused by waves, although they may appear in various forms e.g. as electromagnetic waves, sound waves or mechanical waves. In general, waves may be either dispersive or non-dispersive. Non-dispersive waves have a constant relation between wavenumbers, K (defined as the inverse of the wavelength), and frequency, ω , whereas dispersive waves do not. Waves in unbounded medium (free space) in e.g. acoustics and electromagnetics are non-dispersive whereas waves in semi-bounded medium (guided waves) are generally dispersive.

Application of waves in the field of electromagnetics are vast and occur in everything from tele- and radio communication, to remote controls, to optics, to nuclear energy and in many other places, see for example Fig. 1.2. All the latter cases are examples of electromagnetic waves although quantum physics suggests that light does not always behave as a wave.

Waves also appear in the form of acoustic waves (or sound waves). Obviously, we use this in daily communication with other beings, when listening to music or, on a more unpleasant note, perceive it as noise, in whichever form it may be e.g. a passing car, construction, wind (flow-induced) or even music. In the field of acoustic waves we also find fluid-borne sound/noise. This is commonly used, for example, by fishermen to locate prey by sonars, which are also used to map the landscape of the world and its oceans.

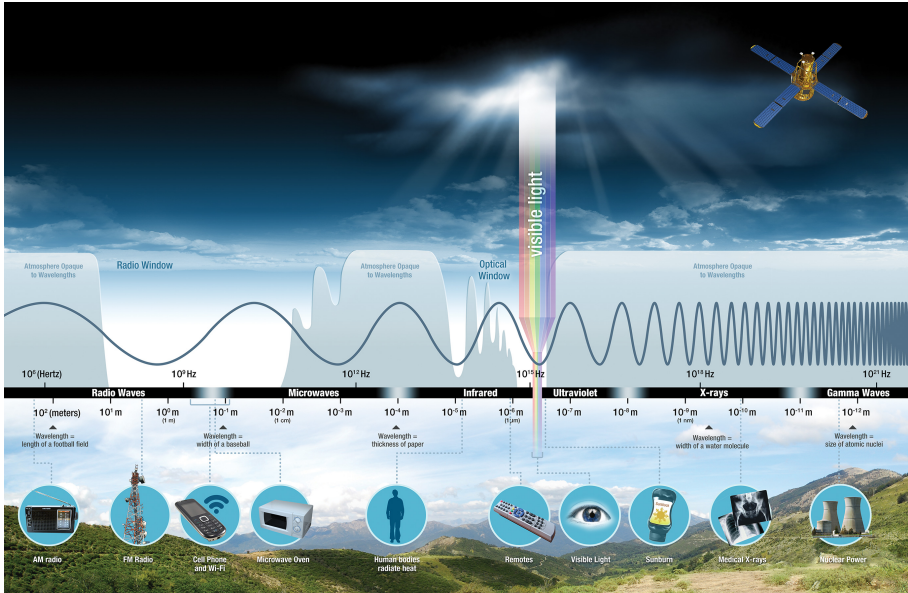


Fig. 1.2: The electromagnetic spectrum and its applications. For enlarged version access: www.nasa.gov/analogs/nsrl/why-space-radiation-matters [Accessed 14-05-2019].

Mechanical waves also appear in many places. They may be thought of as waves propagating through solids, for example, through the ground when a train is passing or under construction when pillars are being slammed into the ground or during an earthquake. As one can imagine from the latter examples, mechanical waves couple with acoustic waves and are in fact responsible for the noise/sound radiated from structures/products. Therefore, some refer to propagation of mechanical waves as structure-borne sound/noise. In the field of continuum mechanics, the course of air-, fluid- and structure-borne sound is a sub-field known as vibro-acoustics (sometimes called structural acoustics or fluid-structure interaction problems). Even though the methods developed in this work are in no way restricted to vibro-acoustics, this sub-field is of prime interest and we shall thus introduce this concept in more detail in Sec. 1.1.3.

1.1.2 Vibrations

In addition to waves and wave propagation we shall in this work also focus on vibrations. To distinguish between the two, we may say that waves are something found only in unbounded (or infinite) structures e.g. those mentioned just above. For purposes elaborated in Sec. 2.1 we have in this thesis a special interest in infinite fluid-filled pipes. Vibrations, on the other hand, is something found in bounded (or finite) structures. In some sense we may therefore say that vibrations are wider explored than waves. Nevertheless, vibrations are indeed composed of the waves present in an unbounded structure, however, as the boundaries confine the waves to remain within the structure they do not

propagate but instead form what is called standing waves. Standing waves can be formed in several ways, the most common of which is known as resonance- or eigenfrequencies. In this sense, the formation of standing waves occurs because the waves are constantly being reflected at the boundaries and so the standing waves are formed by constructive interference (superposition) of the reflected waves. Naturally, this occurs only at specific frequencies, which then compose the spectrum of eigenfrequencies. At other frequencies destructive interference occurs and we have what is known as anti-resonances. Since standing waves, eigenfrequencies and vibrations are all composed of the waves in an unbounded medium/structure the study of waves is of significant interest. The same can be said about waves in other areas of science.

Eigenfrequencies (or resonances) are a virtue of all finite structures and thus a naturally occurring phenomenon. In fact, a finite continuous structure has an infinite number of eigenfrequencies, dispersed vividly throughout the entire spectrum of frequencies. Unfortunately, eigenfrequencies are generally perceived as an undesirable phenomenon, in particular, when excitation frequencies and eigenfrequencies coincide. This often results in a compromise of the structural integrity, leading, usually, to a prompt failure. The most famous example of this is probably the Tacoma bridge. In simple words, we may say that eigenfrequencies are structural weak 'points' (frequencies) where the structure is prone to excitation i.e. only a little effort is required to get a large response. Of course, one can think of places where this is convenient but in general we prefer engineering structures to be somewhat under control. Vibrations in general, on the other hand, find very useful applications, for example, as indicators (a vibrating cell phone) or for music e.g. a vibrating guitar string or loud speaker membrane.

1.1.3 Vibro-acoustics

As already mentioned, vibro-acoustics is a field within continuum mechanics that deals with coupling of a structure and an acoustic medium, e.g. air or water. One of the most tangible and probably best examples (known by most) is the famous cup-phone, see Fig. 1.3. For those unfamiliar, the working principle of the cup-phones relies, as oppose to the newer versions, not on electromagnetic waves but on good old-fashioned vibro-acoustics. Acoustic waves generated by the 'caller' excite the 'phone' (cup) and thus air-borne sound is converted into structure-borne sound (vibrations) that propagates through a pre-tensioned

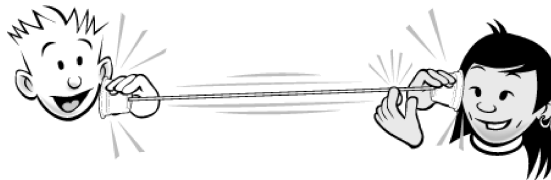


Fig. 1.3: The vibro-acoustic cup-phone. Source: https://www.exploratorium.edu/science-explorer/ear_guitar.html [Accessed 30-05-2019].

string into the receiver cup where it is converted back into air-borne sound heard by the receiver. Although this is an excellent example for illustrating vibro-acoustics, I do, however, believe we should be grateful for the invention of the radio-wave-based phone. It just seems more handy for long distance calls.

In vibro-acoustics we distinguish between what is known as light and heavy fluid loading. In heavy fluid loading the forces exerted by the fluid on the structure is equally important as the structural forces exerted on the fluid. In other words, we have heavy fluid loading when the presence of a fluid changes the characteristics of the waves/vibrations in the structure and vice versa. In such cases it is necessary to treat the problem as a fully (two-way) coupled one. The light fluid loading may be understood as the coupling being so weak that essentially only the structure exerts significant forces on the fluid i.e. a one-way coupling.

Imagine a vibrating structure, say, the string of a guitar. Vibrations of the string causes the air pressure to fluctuate locally around the string and sound is radiated. If the back response of the air is not sufficient to change the vibration characteristics of the string, we have a weak coupling and thus a light fluid loading. In this case we may greatly simplify the analysis of sound radiation to consider the structural surface vibrations as acoustic sources and use well-established methods of acoustics to calculate the radiated sound field at a far distance (far-field). In general, the assumption of weak fluid coupling is valid when the acoustic medium (fluid) is air. However, when the vibrating structure is for instance a loud speaker membrane, it is almost certain that loud speaker and hearing aid manufactures will object to this as being a simple one-way (weak) coupling. Thus, heavy fluid loading may also be a matter of the level of detail required. In Chap. 2 we shall use this approach of one-way coupling when deducing acoustic sources from CFD simulations, however, here with the acoustic sources mapped to the structure and the weak coupling may therefore also apply reversely for some structures. Other examples of exotic coupled (Multiphysics) problems are e.g. thermo-acoustics, Piezoelectrics and all the way to psychoacoustics, bioacoustics and human-structure interaction.

1.2 Academic scope

In the framework of this thesis, in particular, the heavy fluid loading in terms of structures submerged into or conveying water is of interest. Such types of structures are widely exploited in e.g. the oil, gas and pumping industry. Vibro-acoustic problems involving heavy loading have been studied for many years and in recent times using mainly numerical tools and methods. Certainly, numerical tools offer great flexibility to the type of structures that can be assessed, however, numerical solutions unfortunately tend to mask the understanding of the underlying physical mechanisms governing the observed phenomena. Therefore, the academic scope of this thesis is to enhance our understanding of the

wave dispersion and propagation phenomena displayed by such vibro-acoustic waveguides. Further, the transmission of energy through different transmission paths (structure or fluid) and other intriguing occurrences in such waveguides are of interest here, in particular, for pipe and pipe-like structures. Why these structures are of special interest is elaborated in Chap. 2. Likewise, it is of interest to understand in detail how waves form to create standing waves for a given set of boundary conditions. Therefore, the aim is to develop methods and tools for both semi-bounded problems i.e. waveguides, and for fully bounded standing wave (or vibration) problems, sometimes referred to as 'finite' waveguides.

To get full transparency of the phenomena displayed by these waveguides analytical tools are inevitable. Unfortunately, such solutions are not available for the type of (finite/infinite) waveguides of interest here as they are transcendental in nature (has an infinite number of solutions) and further, even retrieving approximate solutions through numerical tools can be challenging for these problems. Nevertheless, to get full transparency, the tools and methods to be developed should preferably be analytic, or at least semi-analytic.

The challenges of solving such vibro-acoustic waveguide problems involving heavy fluid loading typically arise, because the equation system becomes ill-conditioned due to coupling of essentially rigid and compliant constituents and because the problem has an infinite number of solutions as the structure supports an infinite number of waves; Thus, the solution eventually becomes approximate. This complicates greatly the solution process and inflicts issues such as convergence and accuracy of the solution, which are then important to address.

The main methods developed in this work are based on the rather novel concept of bi-orthogonality relations. In brief, bi-orthogonality relations reveal closed-form analytical solutions by simple substitution into the formulas derived in Paper A and C. Then, the challenge of finding solutions to such waveguide problems resolve to just finding the bi-orthogonality relations for the problem at hand. Fortunately, the derivation of bi-orthogonality can be generalised to so-called self-adjoint operators (as shown in Paper C) and thus covers many problems in science. The history and state-of-the-art of bi-orthogonality relations may be found in Paper A–C.

Additionally, the extension from infinite waveguides to finite ones (boundary value problems) is done through the Boundary Integral Equations Methods and as shown in Paper B application of the bi-orthogonality relation also, in this framework, provides great advantages both to accommodate the mathematical challenges but, in particular, to accommodate understanding of how and which waves are engaged in the formation of standing ones. The state-of-the-art related to this can be found also in Paper A through C.

Moreover, as emphasised already throughout the introduction, linear dynamic systems appear on the same form almost everywhere in science and therefore it is natural to also generalised the methods and tools to cover a

much broader range of problems also in other realms of physics, for example, in electromagnetics, optics, quantum mechanics, seismics and beyond.

Finally, review of the state-of-the-art of the current methods and tools applicable for the scope of this thesis is relegated to each paper.

1.3 Key concepts and theoretical background

With the very basics of vibro-acoustics and linear dynamic systems covered this section serves to introduce some key concepts and theoretical background relevant for the present thesis, which will, to the unfamiliar at least, help ease the reading of the appended papers. First, we are, as stated already, confined to linear dynamics. When dealing with vibro-acoustics this means: linear constitutive laws (linear materials/acoustic medium) and small displacements/pressure amplitudes so that the problem may in general be expressed as

$$Lu(X, t) = F(X, t) \quad (1.1)$$

where L is a linear partial differential operator acting on the field $u(X, t)$, $F(X, t)$ is an external (known) forcing and X and t are, respectively, the spatial and temporal coordinates, which, for typical physics problems, are confined by $X \in \mathbb{R}^3$ and $t \in |\mathbb{R}|$. Note that Eq. (1.1) may also be a system of equations i.e. on matrix-vector form. For problems in linear dynamics the superposition principle applies and the solution may be found in the form of an eigenfunction expansion, see Eq. (1.2).

$$u(X, t) = \sum_n^{\infty} A^{(n)} \Psi^{(n)}(X) \Phi^{(n)}(t) \quad (1.2)$$

where $u(X, t)$ solves the partial differential equation (PDE) from Eq. (1.1), $\Psi^{(n)}(X) = \psi_1^{(n)}(x_1)\psi_2^{(n)}(x_2)\psi_3^{(n)}(x_3)$ are the eigenfunctions associated with the spatial coordinates, $\Phi^{(n)}(t)$ the temporal eigenfunctions and $A^{(n)}$ the unknown amplitudes.

As already mentioned we also confine ourselves to time-harmonic systems and therefore take $\Phi^{(n)}(t) = \exp(-i\omega t)$. In the same way we assume also time-harmonic forcing and thus take $F(X, t) = F(X) \exp(-i\omega t)$. Moreover, we consider also the system to be conservative i.e. a system in which no energy escapes, change state or in other ways dissipate. Thus, we say that energy is conserved and so exclude any type of damping.

Finally, the general system presented in Eq. (1.1) may represent both a waveguide and a classical boundary value problem – also referred to as, respectively, a semi- and fully bounded problem. As bi-orthogonality relations are derived for the semi-bounded domains the obvious starting point of this thesis will be the waveguides, which may then later be used to solve the subsequent boundary value problem.

1.3.1 Waveguide theory

From an industrial viewpoint there is a particular interest in studying vibro-acoustic waveguides, as explained in Sec. 2.1. In general, a waveguide, as implied by the name, supports what is called guided waves, that is, structures supporting a (finite or infinite) number of waves which then propagate in a preferred direction. Visually, waveguides may therefore be perceived as a structure that has at least one direction extending to infinity. Mathematically this corresponds to a boundary on which there are no prescribed boundary values. This definition is a rather abstract one and is treated further in Paper C. On the other hand, the fully unbounded (free space) problem is typically not understood to be a waveguide as waves propagate freely in all directions and are thus not guided.

The terminology, waveguides, is broad and extends also to electromagnetic and optical waves etc. Waveguides in vibro-acoustics comes in various forms and shapes e.g. the infinite Bernoulli-Euler beam (purely mechanical), an infinite fluid layer bounded by plates or an infinite fluid-filled cylindrical shell. In a waveguide the waves are usually dispersive as oppose to e.g. free space acoustic waves. Dispersive waves are characterised by their dispersion relation, which is found from the governing equation, Eq. (1.1), by employed the eigenfunctions, Eq. (1.2), and equating to zero the determinant of the system; Hence the characteristic equation defines the waveguide properties. Each solution to this equation corresponds to what is known as a free wave. The dispersion relation may be expressed on the general form

$$f(K, \omega) = 0 \quad (1.3)$$

where K are wavenumbers (possibly $K = [k_{x_1}, k_{x_2}, k_{x_3}]^T$) and ω the angular frequency. For most of the problems considered here the waveguide, and thus dispersion relation, is symmetric and may thus be expressed as

$$f(K^2, \omega^2) = 0 \quad (1.4)$$

which means that the dispersion relation is expressed only in even powers of K and ω . The solutions to the latter equation then reveal the (K, ω) -dispersion diagram shown in Fig. 1.4 for a fluid-filled shell where $K = [k_{x_1}, k_{x_2}]^T = [k, m]^T$. In this case k is a function of m i.e. $k(m)$ where m is an integer due to periodicity of the cylindrical shell. For waveguides with a mathematically continuous cross-section such as the fluid-filled shell (a beam has only a point) there exists an infinite number of solutions to the dispersion relation. These problems are denoted transcendental problems/waveguides and are generally difficult to solve due to the ill-conditioned nature of the dispersion relation. However, the Finite Product Method presented in Paper D indeed proves powerful for approximating and solving such problems.

As seen from the figure, symmetry of the waveguide (and dispersion relation) manifests itself also in the dispersion diagram. I.e. for each $k^{(n)}$ wave

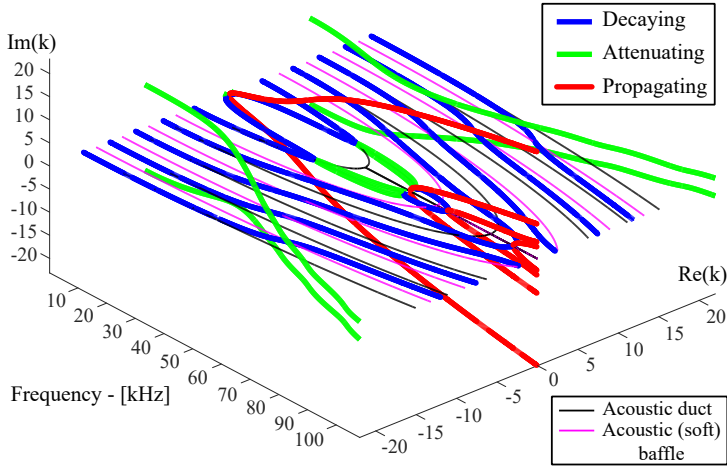


Fig. 1.4: Example of a 3D dispersion diagram for a fluid-filled shell together with the decaying waves from an acoustic duct with rigid and soft walls. Source: Paper A.

there exists an identical opposite going wave, $k^{(-n)} = -k^{(n)}$. We see also that the waves are widely dispersive and in fact some waves more than others (non-dispersive waves appear as straight lines in the dispersion diagram). From the dispersion diagram alone, a lot of valuable information about the waveguide and its properties can be deduced. This is explored in Paper E for an unsymmetric waveguide (orthotropic shell); But, in fact, the dispersion diagram also reveals valuable information about 'finite' waveguides, as shown in Paper B. Moreover, we can deduce information about the energy transferring properties of each wave through their group velocity, c_g , and phase velocity, c_p .

In general, there exist three types of waves (as also indicated in Fig 1.4), namely propagating waves, attenuating waves and decaying waves. The wave types may be defined alone by the domain to which the wavenumbers belong. This is shown in the table in Fig. 1.5 together with the behaviour of the associated eigenfunctions, $\exp(kx)$ (attenuating waves not shown).

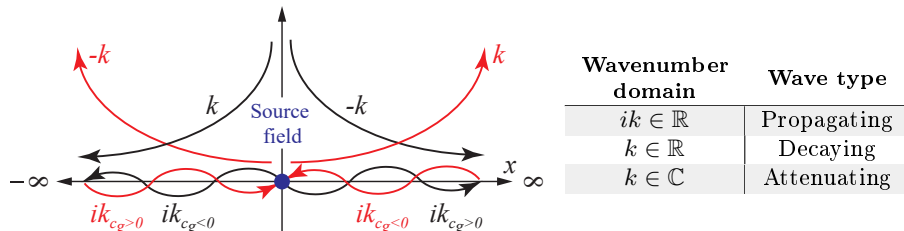


Fig. 1.5: Different wave types and the behaviour of the associated eigenfunctions. Eigenfunctions/waves in black satisfy radiation/decay conditions while waves in red are non-physical. Based on the eigenfunction: $\exp(kx)$. Complex (attenuating) waves are not illustrated.

As illustrated the waves (eigenfunctions), black in Fig. 1.5, satisfy radiation

and decay conditions, which simply says that waves must decay/attenuate away from a source field just as energy must radiate away from the source. The radiation condition (sometimes called Sommerfeld's radiation condition) is ensured by taking, for waves propagating in the positive direction, only waves with a positive group velocity i.e. $c_g = \frac{d\omega}{dk} > 0$, and for waves propagating in the negative direction, only waves with a negative group velocity, see e.g. Paper A or E. Waves not satisfying these conditions are non-physical as waves do not grow unboundedly towards infinity nor does energy spontaneously radiate from infinity towards the source. In particular, waves with positive group velocity and negative phase velocity are an intriguing phenomenon. These are discussed further in Paper E.

Each free wave of a waveguide is also associated with a number of state variables (vectors). The state variables are usually decomposed into forces, Q , and kinematic (displacement) variables, U . For instance, a Bernoulli-Euler beam features shear force and moment as forces and transverse displacement and rotation as kinematic variables. The relation between the force and kinematic state variables are given by the differential operator, \mathcal{L} .

$$Q(X) = \mathcal{L}U(X) \quad (1.5)$$

In general, $U(X) = u(X)$ only when the differential operator, L , from Eq. (1.1) involves harmonic operators, while $U(X)$ contains also derivatives e.g. $\nabla u(X)$ when bi-harmonic operators are present (as in the Bernoulli-Euler beam). For systems of equations the size of the matrix-vector system of Eq. (1.1) and (1.5) may therefore differ, see e.g. Paper A–C. Furthermore, the formulation of state variables i.e. \mathcal{L} , is not unique as they may be derived from different techniques e.g. the variational principle, first principles or the governing PDE. This is elaborated in Paper C. Either way we may write the solution for the state variables in terms of modal coefficients, see Eq. (1.6).

$$\begin{aligned} Q(X) &= \sum_n^{\infty} A^{(n)} \bar{Q}^{(n)}(\tilde{X}) \Psi^{(n)}(X_m) \\ U(X) &= \sum_n^{\infty} A^{(n)} \bar{U}^{(n)}(\tilde{X}) \Psi^{(n)}(X_m) \end{aligned} \quad (1.6)$$

where the inner relation between the entries in the modal coefficient vectors $\bar{Q}^{(n)}(\tilde{X})$ and $\bar{U}^{(n)}(\tilde{X})$ is derived easily from e.g. the governing PDE and the model coefficients will thus depend on coordinates not in the propagation direction, \tilde{X} i.e. X_m is the preferred direction(s) of wave propagation. This is elaborated in Paper A–C. In this framework the unknowns reduce to the modal amplitudes, $A^{(n)}$, while the modal coefficients prove to hold important properties when the waveguide is symmetric according to Eq. (1.4). This is elaborated and utilised in the Paper A–C.

Finally, the time-averaged total energy flow of a free wave (without amplitudes, $A^{(n)}$) is defined from the state variables as in [3] i.e. as the inner product

of forces with the complex conjugated of the velocities (time derivative of kinematic variables), see Eq. (1.7). In case of time-harmonic waveguides this may be reduced to the equation on the bottom.

$$\begin{aligned}
 N^{(n)} &= -\frac{1}{2}\text{Re} \left(\left\langle Q^{(n)}, \dot{U}^{(n)*} \right\rangle_{\partial V} \right) \\
 \Downarrow \\
 N^{(n)} &= \frac{\omega}{2}\text{Im} \left(\left\langle Q^{(n)}, U^{(n)*} \right\rangle_{\partial V} \right)
 \end{aligned} \tag{1.7}$$

where the inner product, $\langle \cdot, \cdot \rangle$, is taken over the a cross-section of the waveguide, indicated by ∂V i.e. over the coordinates, \tilde{X} . Thus, the inner product imply the scalar product between $Q^{(n)}$ and $U^{(n)}$ integrated over ∂V i.e. $\langle \cdot, \cdot \rangle = \int_{\partial V} \cdot \text{nd}\tilde{S}$

1.3.2 Green's function

The method of Green's function is a very well established method that finds applications in almost any field of linear dynamics including those mentioned in Sec. 1.1. It was introduced by the remarkable, mostly, self-taught George Green in his Essay: “*An Essay on the Application of Mathematical Analysis to the Theories of Electricity and Magnetism*” dating back to 1828, [4]. Here he introduced the concept of what is today known as Green's functions, which is the fundamental solution to any system of linear PDE's. In essence, Green's function constitutes the response (or field) to a system driven by a point/impulse function, that is, the delta function. The method of Green's function is useful for both the spatial and temporal domain and is used in many fields of engineering and science. For instance, it is equivalent to, what in structural dynamics, is known as Duhamel's integral, [5], (the response to a temporal impulse), which in the field of control theory typically is known just as the impulse response function, [6] (usually treated in the Laplace-domain). In any case Green's method offers much simplification and flexibility to the problem at hand.

Formally, Green's problem may be perceived as an auxiliary problem useful for solving more general problems. Thus, the general form of Green's method, left in Eq. (1.8), helps to solve the general problem on the right. In this format we have already assumed time-harmonics and thus we shall apply Green's method only in the spatial domain throughout the thesis.

$$LG(X, X_0) = \delta(X - X_0) \qquad Lu(X) = F(X) \tag{1.8}$$

Here $G(X, X_0)$ is the Green's function which depends upon the spatial observation point, X , and excitation point, X_0 . As before, the system may be on matrix-vector form.

A primitive way to illustrate the advantages and auxiliary properties of the Green's function is by multiplying the left of Eq. (1.8) by $F(X_0)$ and taking the inner product over the volume in X_0 i.e. $\langle \cdot, \cdot \rangle_{V_0}$.

$$\langle LG(X, X_0), F(X_0) \rangle_{V_0} = \langle \delta(X - X_0), F(X_0) \rangle_{V_0} = F(X) \tag{1.9}$$

Comparing the right of Eq. (1.8) and Eq. (1.9) we may write

$$\begin{aligned} \langle LG(X, X_0), F(X_0) \rangle_{V_0} &= Lu(X) \\ \Downarrow & \\ L \langle G(X, X_0), F(X_0) \rangle_{V_0} &= Lu(X) \end{aligned} \quad (1.10)$$

and readily conclude that

$$u(X) = \langle G(X, X_0), F(X_0) \rangle_{V_0} \quad (1.11)$$

Thus, the solution to the general problem in Eq. (1.8) is simply found as a convolution of the applied load with Green's function as the kernel. This offers great flexibility for changing driving functions, $F(X)$, and moreover the Green's function is often much easier to obtain than the solution to the actual problem.

When the problem above is a system of equations the Green's function may more appropriately be denoted Green's matrix (or tensor) i.e.

$$G(X, X_0) = \begin{bmatrix} g_1^{01} & g_2^{01} & g_3^{01} \\ g_1^{02} & g_2^{02} & g_3^{02} \\ g_1^{03} & g_2^{03} & g_3^{03} \end{bmatrix} \quad (1.12)$$

where each row is the solution to a given fundamental loading condition i.e. the first row solves the following problem

$$\begin{aligned} LG^{01}(X, X_0) &= \delta^{01}(X - X_0) \\ \Downarrow & \\ \begin{bmatrix} l_{11} & l_{12} & l_{13} \\ l_{21} & l_{22} & l_{23} \\ l_{31} & l_{32} & l_{33} \end{bmatrix} \begin{Bmatrix} g_1^{01} \\ g_2^{01} \\ g_3^{01} \end{Bmatrix} &= \begin{Bmatrix} \delta(X - X_0) \\ 0 \\ 0 \end{Bmatrix} \end{aligned} \quad (1.13)$$

and the second row the problem with $\delta^{02}(X - X_0) = [0, \delta(X - X_0), 0]^T$ etc. As already mentioned in Sec. 1.3, the solution, and thus Green's function, is sought as an expansion on eigenfunctions and may, as for the state variables in Eq. (1.6), be expressed via modal coefficients as

$$G(X, X_0) = \sum_n^{\infty} A^{(n)}(X_0) \bar{G}^{(n)}(\tilde{X}) \Psi^{(n)}(X_m) \quad (1.14)$$

where the amplitudes $A^{(n)}(X_0)$ will depend on the excitation point, X_0 , and $\bar{G}^{(n)}(\tilde{X})$ are the modal coefficients related to Green's function. Again by introducing the modal coefficients, the unknowns of this system of equations have reduced to 'only' the infinite number of amplitudes, $A^{(n)}(X_0)$.

There are several ways of composing the equation system to find, if not exact, then approximate solutions (amplitudes) for such transcendental Green's functions. Most common is likely using the state variables associated with Green's

solution, truncate their expansions and construct, besides the mandatory continuity and load conditions, additional equations based on, for instance, Galerkin orthogonalisation. Either way convergence of the solution becomes a necessary issue to address. However, as we shall see in both Paper A, B and C, this is very conveniently handled when using the method of bi-orthogonality to solve such problems. This method simply allows complete decoupling of the problem and thus analytical closed-form solutions for each of the amplitudes, $A^{(n)}(X_0)$ i.e. no truncations are needed to solve the problem. Moreover, for the Green's function to be of any physical relevance it must satisfy the radiation and decay conditions mentioned in Sec. 1.3.1. This is discussed in detail in Paper A.

With the solution to the forcing problem for any given load already known (by way of Green's method) an energy flow analysis, as presented in Paper A, may readily be conducted. As mentioned in Sec. 1.3.1 this requires the associated state variables. In the framework of Paper A, we refer to these as the Green's matrices where the principal matrix corresponds to the kinematic variables and the second matrix to the forces. The Green's matrices thus refer to the response of all state variables (kinematic and force) to a point source/excitation. As mentioned in Sec. 1.3.1 the size of the state vectors may differ from the size of the governing PDE system when a bi-harmonic operator is present. In particular, this is the case for the Bernoulli-Euler beam, in which the fundamental solution for a moment load corresponds to the solution to the derivative of the delta function i.e. $\frac{\partial \delta(X-X_0)}{\partial X_0}$.

In vibro-acoustics we refer to the state variables (Green's matrices) as forces and displacements, Q and U , (Paper A and B) and as $\mathcal{L}q$ and q in more general terms (Paper C) where \mathcal{L} corresponds to the differential operator from Eq. (1.5). With known Green's matrices the energy flow analysis may be carried out following Eq. (1.7) or [7].

$$\begin{aligned} N\Sigma &= \frac{\omega}{2} \text{Im} (\langle Q, U^* \rangle_{\partial V}) \\ &= \frac{\omega}{2} \sum_n^\infty \sum_j^\infty \text{Im} (\langle Q^{(n)}, U^{(j)*} \rangle_{\partial V}) \end{aligned} \tag{1.15}$$

where each term of the scalar product (contained in the inner product) constitutes the energy flow in a physical transmission path. The energy analysis for the fluid-filled shell at a given frequency is shown in Fig. 1.6. Here we see that even though the fluid-filled shell is loaded by an acoustic source, the energy rapidly escapes to the structure in which it is carried as axial and torsional (membrane) deformation energy to the far-field. Detailed energy analysis of this type indeed provides the necessary understanding of the wave propagation and energy transmission properties sought in this thesis.

Further, as seen from Eq. (1.15) the calculation of energy flow becomes tedious for transcendental problems because each force and displacement constitutes an infinite expansion. As will be seen in Paper A and C this may be

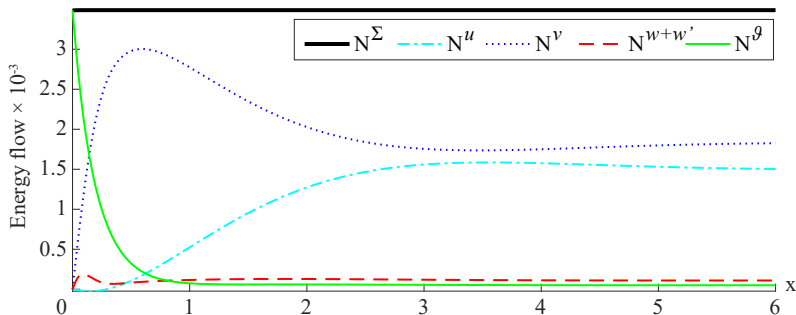


Fig. 1.6: Example of the energy flow in an elastic fluid-filled cylindrical shell. The transmission paths are, respectively: axial, torsional, bending (radial and moment) and fluid. Total energy is conserved. Source: Paper A.

greatly simplified when using the method of bi-orthogonality.

Since the fluid-filled shell is a symmetric waveguide the energy flow is skew-symmetric with respect to the excitation point, $x = 0$. In Paper E a more interesting energy flow analysis is conducted, namely for a conservative helical orthotropic (unsymmetric) waveguide. In the same way as in Fig. 1.6 the energy is conserved, however, when the symmetry is disrupted the energy conveyed to the left and the right is no longer the same. This provides means for tailoring the energy carrying properties of waveguides to e.g. be conveyed only in one direction while being reflected in the other. As an example (from the field of optics) one may think of a pair of sunglasses with a mirror lens; You can look people in the eyes while they are not able to look into yours. This indeed also constitutes a good example of tailoring of spectral properties to certain frequency ranges i.e. while the optical spectrum passes, most of the ultraviolet spectrum is reflected.

1.3.3 Boundary Integral Equations Method

When it is desired to proceed from the infinite waveguide to a 'finite' one it is convenient to apply the Boundary Integral Equations Method (BIEM). This method is widely used in, for example, mechanics, acoustics and civil engineering, see e.g. [8–10], but is also well-known in other areas of physics, for example, as the surface/Green's function integral equations method in Nano-optics, [11] or as the Method of Moments in electromagnetics, [12]. As the practical interest of the present thesis is on vibro-acoustics we shall, however, stick to the BIEM convention. The simple idea of the BIEM is to formulate a set of Boundary Integral Equations (BIE) based on an auxiliary problem (for which the solution is known in advance) and then solve them together with some prescribed boundary conditions. There is no unique choice of an auxiliary problem, however, there are some preferred choices amongst. For now it is convenient to choose the Green's problem for the infinite waveguide already treated in the previous section. Although we are not restricted to Green's problem it is indeed advan-

tageous. In a general format, we have the same problem as that of Eq. (1.8) i.e.

$$LG(X, X_0) = \delta(X - X_0) \quad Lu_{bvp}(X) = F(X) \quad (1.16)$$

where the left equation is the Green's problem from Eq. (1.8) and the right equation the 'finite' waveguide problem, which is similar to the infinite waveguide problem, in that, $u_{bvp}(X)$ is acted on by the same differential operator, L . However, additional requirements apply, and the state variables must therefore satisfy prescribed boundary conditions. The right-hand equation then constitutes a boundary value problem in the classical sense, as implied by the subscript (which we however omit in the following). The additional conditions that must be satisfied at each boundary may be written in the general form as

$$Q(X)|_{\partial V} - \mathbf{Z}(X)U(X)|_{\partial V} = 0 \quad (1.17)$$

where $\mathbf{Z}(X)$ is the prescribed boundary impedance (force-to-displacement ratio) at the boundaries ∂V . For the fluid-filled shell example the boundary conditions are concerned with forces and displacements at each end of the shell i.e. at $x = a$ and $x = b$.

To formulate the BIE's we first formulate what in the field of mechanics is known as Somigliana's identity (equivalent to the Kirchhoff integral known from acoustics). There are many ways to arrive at Somigliana's identity (corresponding to the derivation of state variables). However, for convenience we shall derive it from the governing PDE. Thus, we multiply the right hand equation of Eq. (1.16) with $G(X, X_0)$ and the left hand equation by $u(X)$, take the inner product over the volume, V (in coordinate X), and subtract the right hand equation from the left to arrive at

$$\begin{aligned} \langle \delta(X - X_0), u(X) \rangle_V &= \\ u(X_0) &= \langle LG(X, X_0), u(X) \rangle_V - \langle Lu(X), G(X, X_0) \rangle_V + \langle F(X), G(X, X_0) \rangle_V \end{aligned} \quad (1.18)$$

We see here that the left-hand-side reduce by virtue of the property of the delta function and thus emphasise why Green's problem is a convenient choice of auxiliary problem. Then, by partial integration of the first two terms on the right-hand-side, it is fairly easy to show that these inner products reduce to an integral over the bounding surface, ∂V , and the latter equation reduces to Somigliana's identity in Eq. (1.19). For some problems, e.g. in acoustics, the volume integral of the first two terms vanishes by way of Green's identity, in which case the integral becomes the well-known Kirchhoff integral.

$$\begin{aligned} u(X_0) &= \\ \langle Q_G(X, X_0), U(X) \rangle_{\partial V} &- \langle Q(X), U_G(X, X_0) \rangle_{\partial V} + \langle F(X), G(X, X_0) \rangle_V \end{aligned} \quad (1.19)$$

Here $u(X_0)$ is the solution (transformed into X_0) to the boundary value problem where the first two terms on the right-hand-side constitute the homogeneous

solution and the last the particular solution. $F(X)$ is a known external load, $Q_G(X, X_0)$ and $U_G(X, X_0)$ are the known state variables related to Green's function (and therefore depend on the excitation point, X_0), while $Q(X)$ and $U(X)$ are the yet unknown functions belonging to the boundary value problem and must therefore satisfy Eq. (1.17). As the inner product over the volume of these variables have vanished they need only be determined at the boundaries. This reformulation of the problem by help of an auxiliary problem conveniently reduces the dimensionality from a formulation in the volume to a formulation only on the surface. This is one of the main advantages of the BIEM.

Further, in Paper C it is shown that the reduction to a surface formulation is possible whenever the differential operator L is self-adjoint and so Eq. (1.19) may be thought of as a generalisation of Green's identity. Nevertheless, by help of the bi-orthogonality relation the problem formulation may be reduced even further to an algebraic boundary identity, thus getting rid of all the tedious integrals. This is the essence of Paper B.

To solve the boundary value problem i.e. find the unknowns from Eq. (1.19), we formulate a number of Boundary Integral Equations simply by letting X_0 in Somigliana's identity move towards each boundary separately and from inside the domain. Then, by whichever technique preferred, the BIE's are solved together with the boundary conditions from Eq. (1.17) and the BIEM emerges. For a fluid-filled shell this corresponds to letting X_0 move, first, towards the boundary at $x = a$ and then towards b . This leads to two BIE's for each Somigliana identity and in this case a total of 10 BIE's.

If the BIEM is solved by discretising the boundaries into elements and formulating the BIE's for each element the integrals dissolve to summations and we get what is known as the Boundary Element Method (BEM). This is almost certainly the most popular method for solving the BIE's. Compared with the classical Finite Element approach (defined for a volume) the BEM requires only a boundary mesh and thus much less elements, in particular, when large domains and high frequencies are considered. However, one drawback of the method is that the equation system is fully populated – as oppose to a sparse system in FEA. Other than that, the BIE's acquire singular points/integrals when the excitation and observation point coincide, which is an artefact of Green's function. Then, as always, the choice of strategy becomes a trade-off. In Paper B, however, it is shown how the bi-orthogonality relation can be used, for a rather broad class of problems, to completely resolve the BIE's to algebraic modal boundary identities. This immediately obviates the need for discretisation methods as well as all concerns regarding singularities. Further, for some special sets of boundary conditions the equation system may be factorised completely (becomes diagonal) and closed-form solutions emerge.

Industrial Impact

“ The science of today is the technology of tomorrow ”

– Edward Teller

The present thesis is conducted under the Danish research program “*Erhvervsforsker*” (Industrial PhD) supported partly by the Innovation Fund Denmark and partly by the Danish pump manufacturer, Grundfos Holding A/S. As part of the program the Innovation Fund supports industrial relevant research through researchers employed by companies while being dedicated to a specific academic research project, evaluated under the requirements for obtaining a PhD degree. The purpose of the program is to strengthen Danish companies’ competitiveness and innovation internationally. Therefore, the PhD thesis should, besides being academically novel, contain research with industrial impact for Grundfos.

Throughout this chapter the required preliminary knowledge about centrifugal pumps is limited to a minimum. Should the reader, however, not be entirely familiar with certain terminologies and therefore finds the need for a quick brush-up, a short introductory video can be found in the online *Annex*, [1] (QR code found in Preface). This video covers the basic concepts of centrifugal pumps including working principle and most commonly used terminologies in the pumping industry. Further, details can be found in *The Centrifugal Pump* book by Grundfos, [13].

2.1 Industrial scope

With an annual production of more than 17 million pump units Grundfos is one of the world’s leading pump manufactures. Among others the main products are circulators for heating and air conditioning as well as other centrifugal pumps for industry, water supply, sewage and dosing. Today Grundfos is the

largest manufacturer of circulators in the world, covering approximately 50% of the world's market. Grundfos is represented in more than 55 countries with headquarters in Bjerringbro, Denmark and employs more than 19,000 people worldwide. Grundfos was founded by Poul Due Jensen in 1945 and is a family business, owned entirely by family, employees and the Poul Due Jensen Foundation. As a company Grundfos is known for being a high-end brand, delivering high quality and best-in-class energy efficient solutions to their customers. Grundfos is, and wants to remain, a trendsetter in the market, pushing the limits for what is possible. Moreover, Grundfos is known for taking responsibility in the world when it comes to sustainability, climate change, solutions for water scarcity and pollution etc. and are also known to be a strong supporter of the UN's Sustainable Development Goals 6 (Clean water and sanitation) and 13 (Climate action). For more information about Grundfos visit: Grundfos.com.

2.1.1 Motivation

The main business of Grundfos is moving water, sometimes over short distances with a high pressure, sometimes over long distances with a high flow and sometimes both with a high pressure and flow. The source of water range from fresh water for drinking to water for sanitation or heating/cooling applications, thus spanning temperatures from 0°C to 180°C (-40°C to 240°C for special liquids). In other cases, the pump medium is sewage/waste water where multiphase flow is indeed a frequently occurring phenomenon. For these applications the pumps are usually submerged directly into the waste water and one can imagine that a breakdown in such an environment is, to say the least, a sticky situation.

Indeed the latter cases all fall within the category of heavy fluid loading (as discussed in Sec. 1.1.3) and in all cases vibro-acoustics play a vital role for the performance and durability of the entire pump/supply system. Fig. 2.1 shows a few cases where vibrations in the pipe system has caused (rapid) fatigue as a consequence of formation of standing waves, better known as excitation of eigenfrequencies. Although this figure shows two cases where the pipe system fails just after the pump this is not necessarily always the case. Since waves propagate, reflect, interact and convert throughout the entire pipe system the structural integrity may be compromised anywhere in the pipe system depending, of course, on the level of excitation, on how the standing waves form, how the fluid and structure interacts, how the energy carrying transmission paths interchange along the system etc. Here the latter two depend on how and which of the guided waves that are excited by the given load. This may therefore lead to failures much further down the system and need not necessarily be in the form of leakage but may also appear in the form of noise pollution generated in e.g. the pipes or valves and emitted from (heat) radiators, walls, floors, ceilings etc. An example of this is shown in Fig. 2.2 where a pipe junction downstream from the pump has suffered fatigue damage as a consequence of vibrations and thus required in-situ repair.



Fig. 2.1: Breakdown in a waste water system as a consequence of excessive vibrations. Top: Auto-coupling, on which the pump is mounted, wrecked by fatigue. Bottom: Fatigued welding in flange connection leaking water.

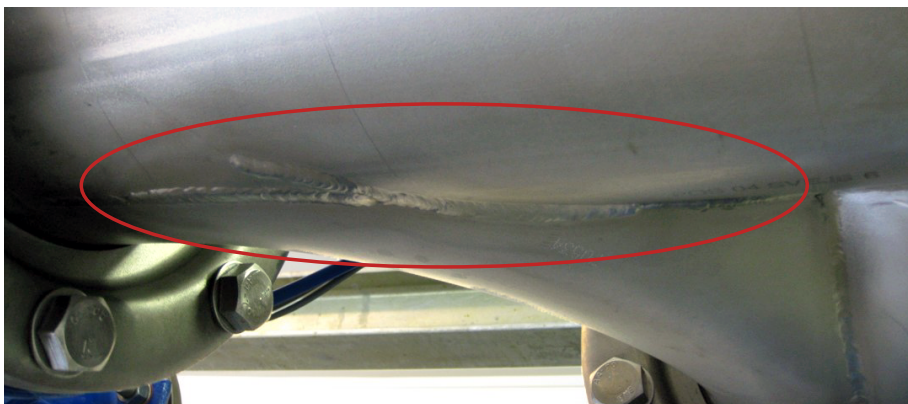


Fig. 2.2: Fatigue failure of a downstream pipe junction caused by vibrations. In-situ repair required.

In addition, Grundfos always strives to optimise the pumps to be more energy efficient and consume less resources (e.g. materials), yet they should remain robust while pushing the structural performance to the limit, making the products, essentially, prone to noise and vibration issues. Unfortunately, with an increase in energy efficiency comes also an increase in the acoustic emission and with an optimised mechanical design comes, in some cases, compliance and in other cases increased rigidity, none of which helps to improve the air-, fluid- or structure-borne sound performance of the pump. Therefore, Grundfos has an increasing focus on improving, alongside with the efficiency and structural performance, also the vibro-acoustic performance of these pumps and this is not an easy task.

Furthermore, to accommodate better energy performance, reducing CO₂ emission and the usage of resources, narrowing product variants is an important step for Grundfos. This means simply extending the application range of some variants to cover the range of others. In pumps this means, for the fixed-speed-pumps, to add frequency converters to allow for variable speed, and, for the already variable-speed-pumps, to extend the range to cover sometimes up to three times the normal rpm range. This has many great advantages for both Grundfos, customers and climate, however, one of the main challenges is that the spectrum of vibro-acoustic excitations/sources generated and radiated by the pump increase accordingly, making it vital that the vibro-acoustic performance of pumps can be assess in advance.

2.1.2 Challenges

As the pump acts as a power supply to the system it is no surprise that the vibrations are inevitably caused by the dynamics introduced by the pump. However, many of the latter discussed failures can easily be prevented by, first of all, following the installation guidelines of the pump manufacturer e.g. on how to properly fixate the pump but maybe more important by ensuring that the pipe system is also properly fixated. But even in these cases problems may arise. Why? In the design of pump systems the dimensioning of the pump is determined alone by the pipe system and supply requirements of the customers i.e. pressure and flow. While this is sufficient criteria in statics it is not so in dynamics, as the pump and pipe system interact through the fluid and thus way beyond just at the interface. Despite this, pipe systems and pumps are only very rarely designed to accommodate one another. Unfortunately, as a pump supplier, Grundfos has only very limited (if any) control over the design of the actual pipe system, which indeed complicates solving these vibration problems from a Grundfos perspective. In other words, while the excitation levels, frequencies, modes etc. are controlled by Grundfos, the formation of standing waves and how easily they may be excited are in some way controlled by the customers and are therefore beyond Grundfos' control.

Moreover, as pipe systems (for the same pump) may behave as everything from an infinite (non-reflective – wave propagation) to a (almost) fully reflective

system, it covers the entire range of impedances from 0 to ∞ . For this reason, even knowing specific impedances of one (or several) customer's system does not help to solve the issues for others. Besides, retrieving such impedances, whether from numerical models or experiments, requires a huge effort and yet it still only represents one system out of many. Thus, from a Grundfos perspective this problem must be treated in the most generic way possible. Inarguably, this leads us back to the study of waves and propagation of waves as well as the acoustic sources/mechanical excitations generated by the pump and transmitted into the received pipe system. Therefore, an increased understanding of these phenomena at an early stage in the design phase constitutes the industrial scope of the present PhD thesis.

To accommodate these challenges two Matlab tools have been developed: Tool 1 to assess, in a generic way, the propagation of waves and energy transmission properties of the receiving pipe system and Tool 2 to deduce acoustic sources from the many CFD simulations (Computational Fluid Dynamics) done in the early stage of a design.

2.2 Tool 1: Wave propagation in pipe systems

This tool is based on the work done in Paper A, B and D, however, with many additional engineering functionalities and post processing features than those presented in the papers. A picture of the main page of the tool is seen in Fig. 2.3. The tool is concerned with various levels of detail, some useful for the design engineer to understand/verify that the excitation characteristics of a specific design (Tool 2) does not coincide with critical frequencies or modes, while other features are useful for detailed studies as those needed for troubleshooting and for intuitively optimising designs.

Depending on the readers experience with wave propagation in cylindrical structures it may be appropriate to continue with Paper A before proceeding here. Paper F also covers some of the very basics of vibration of cylindrical shells (without fluid) and may also help to improve the understanding.

The purpose of this tools is, in a generic way, to be able to predict (or estimate) how prone a pipe system is to various excitations and frequencies. Since the system is, as mentioned, generally unknown (and beyond Grundfos' control) the best and most generic model is based on the infinite fluid-filled shell waveguide addressed in Paper A. This model depends only on the material (fluid/structure) and cross-sectional properties of the waveguide. Both material and cross-sectional properties are determined a priory by the flow and pressure required and by standards. Thus, the outlet dimension of the pump is predetermined and compatible with the standard's requirements. Hence, the parameters do not depend on a specific customer's system and the fluid-filled shell waveguide is therefore the most generic system to study.

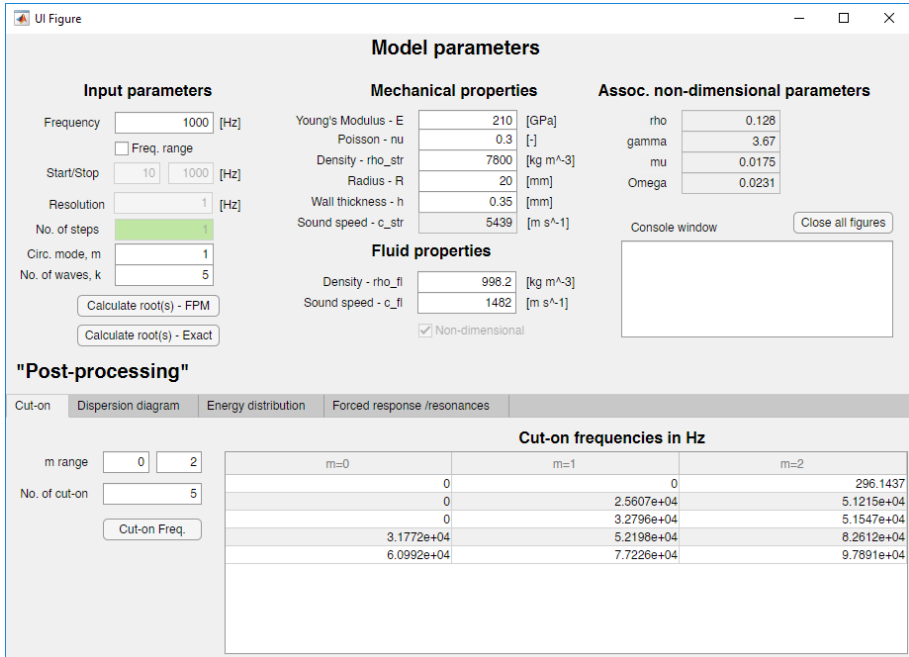


Fig. 2.3: Main page – The tool is initialised when the root (wavenumber) calculation is carried out. After the post processing the tabs below become available. 'Cut-on' tab can be used without initialisation. Full size figures can be found in the online *Annex*, [1].

In general, the vibro-acoustic performance of the pipe system may be assessed based on generic properties of the system, studying for instance the wave propagation properties (wave dispersion) and the fundamental solutions provided by Green's method i.e. the energy propagation/transmission properties of the system. This gives indeed valuable physical insight of the system and its governing vibration phenomena and allows to deduce generic information about, for instance, which frequencies, modes and transmission paths are critical to excite. Common for all pipe systems, no matter their actual formatting i.e. reflective properties (boundary conditions), is that the critical modes, frequencies and transmission paths of the infinite fluid-filled shell are critical for all systems. Further, the tool also provides means for judging whether certain excitations (frequencies, modes and transmission paths) are likely to radiate noise. In summary the features of Tool 1 are:

Main page – Wavenumber calculation, Fig. 2.3: Before the post-processing tabs are available (except the 'Cut-on' tab) the wavenumbers at a specific frequency and in some cases over a range of frequencies are needed. The material and cross-sectional properties of the fluid-filled shell are typed in together with the desired frequency or frequency range (incl. frequency resolution) and the circumferential mode of interest. Then the tool is initialised by calculating the wavenumbers either based on the Finite Product Method alone (Paper D)

or by solving the exact dispersion relation (where the solution from the FPM is used as an initial guess).

Tab 1 – Cut-on frequencies, Fig. 2.3: Presented in table format (and bar plot) the cut-on frequencies are calculated based on the specified number of cut-on frequencies (rows) and number of circumferential modes (columns) desired. The cut-on frequencies are found at $k = 0$ where attenuating/decaying waves transform into propagating ones. Note that this does not account for cut-on frequencies of waves experiencing locking, see Paper E. The response at and in the vicinity of a cut-on frequency is always substantial no matter the system and should thus be avoided whenever possible. The tab may be used without initialisation.

Tab 2 – Dispersion diagram, Fig. 2.4: Plots the dispersion diagram either in the 3D ($f, \text{Re}(k), \text{Im}(k)$)-space (Fig. 1.4) or as two 2D plots, one for the real and one for the imaginary part (imaginary waves are the propagating waves in this framework). The feature requires initialisation with a frequency range specified. To enhance the physical understanding of the wave dispersion and interaction phenomena, the dispersion diagrams for, respectively, an in-vacuo shell, a rigid and soft baffle (cylindrical acoustic duct with rigid or soft walls) may be mapped into the dispersion diagram. The feature is useful for understanding details of the wave and interaction phenomena occurring in fluid-filled pipes.

Fig. 2.4: Plot of dispersion diagram in either 3D or 2D.

In particular, this becomes interesting for compliant pipes such as PVC pipes or rubber hoses (linear approximations only) where the fluid-structure interaction appears much stronger.

Tab 3 – Energy distribution, Fig. 2.5: Allow detailed analysis of how the energy is distributed and carried throughout the waveguide i.e. a transmission path analysis (TPA). This analysis is useful since the energy carrying transmission paths (membrane, torsional, bending and fluid – see Fig. 1.6) tend to persist in the finite systems as this is in general determined more by the waveguide properties and frequency than the boundaries (at least in the relatively low frequency range, which is the main interest in this work). The transmission path analysis is based on the theory in Paper A. The feature handles both frequency range and single frequencies. If a range is specified, frequencies from this set can be selected individually without re-initialising. It holds several practical engineering features divided into, respectively, a load dependent and load independent part. The most essential features are: TPA similar to the

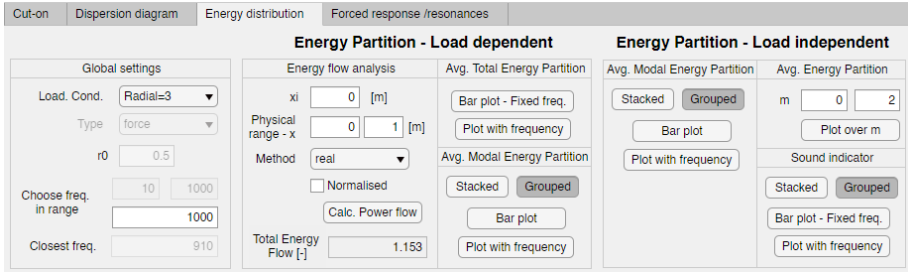


Fig. 2.5: Sound indication, transmission path and energy flow analysis.

energy flow analysis from Fig. 1.6; The partition of modal energy into transmission paths and waves, that is, how much energy (out of the total energy) is carried in each wave and through which transmission paths i.e. governance of waves; TPA comparing different circumferential wavenumbers and finally a sound indicator. The sound indicator utilises the displacements at the surface of the shell to hint towards potential noise pollution; I.e. if, for example, the radial displacement is governing the response, the pipe system is likely to be emit air-borne noise, whereas an axial or fluid governed response is not likely to produce noise.

Tab 4 – Eigenfrequencies (beta-version), Fig. 2.6: Calculates the eigenfrequencies (sweep of determinant over frequency) based on the method presented in Paper B. The length of the pipe is specified together with five impedance conditions at each boundary (force-to-displacement or pressure-to-velocity ratio) – corresponding to the five state variables. The feature is useful

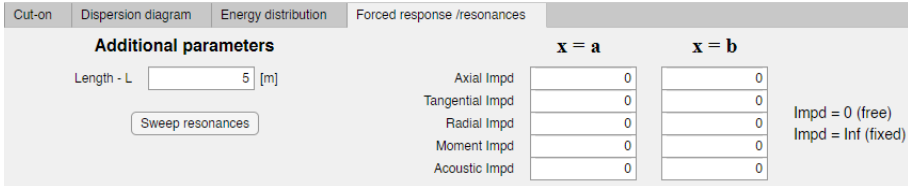


Fig. 2.6: Eigenfrequency analysis

for studying the eigenfrequencies/standing waves in specific pipe systems. However, proper impedances for the different variables for a specific system is rarely known and moreover difficult to retrieve from both models or experiments. The feature may therefore be more useful for sensitivity/limit-case studies e.g. studying the extremes of the eigenfrequency spectrum.

Finally, note that the tool provides fast computations only by virtue of the developments in Paper A (analytical solution using bi-orthogonality) and Paper D (the Finite Product Method). Further, the detailed modal energy transmission analysis is possibly only by way of the proof of linearity of energy shown also in Paper A (and C).

More examples of analyses using Tool 1 can be found in the online *Annex*, [1], or using the QR code found in the Preface.

2.3 Tool 2: Source characterisation from CFD simulations

This tool is based partly on work done in Paper F and during my time at the University of Auckland. The purpose of the tool is to utilise the detailed results obtained from CFD simulations to deduce information about the acoustic sources generated by the pump and emitted through the pipe system. The tool consists of two tabs, see Fig. 2.7. The main tab is intended for hydraulic development engineers to assess and improve the acoustic performance of their designs and the second intended for a more detailed study of the acoustic sources, as that needed for troubleshooting and by the engineers at Grundfos' Sound and Vibration Laboratory. Theoretical details regarding the source characterisation is elaborated in Sec. 2.3.1.

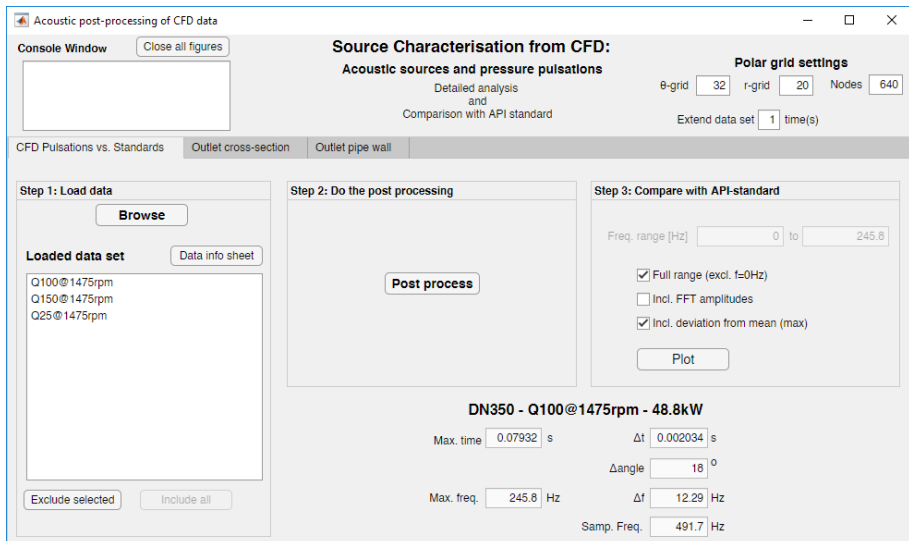


Fig. 2.7: Main page used by hydraulic development engineers to compare pressure pulsations of different designs with recent standards (API). Different designs at different operation points may also be compared individually.

Main page (Tab 1) – Comparison with API-standard, Fig. 2.7: In step 1 a number of pump designs, in terms of CFD data sets, are loaded into the tool. In step 2 the data is processed through a calculation of the peak-2-peak pressure pulsations at different frequencies for all designs loaded into the tool. In step 3 the results are compared to the maximum allowable pulsation levels from recent standards, see Fig. 2.8 (in lack of better standards the API-standard for reciprocating pumps is used, [14]). This allows evaluating different designs or a specific design at various operation/design points (where Q100 is the design point of the pump – corresponding to the best efficiency point) and thus conclude whether a specific design satisfies the API requirements for the

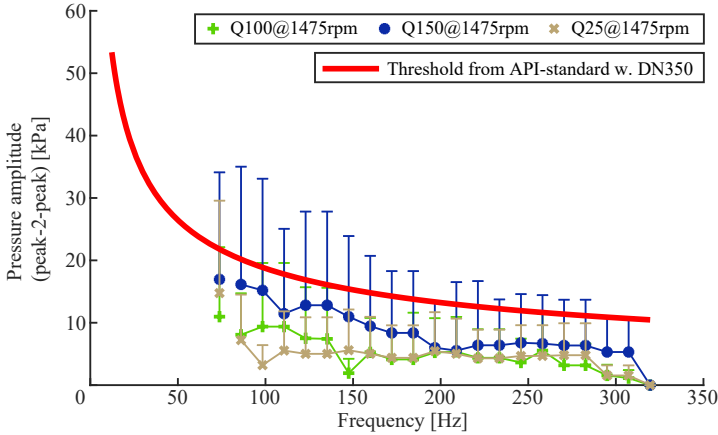


Fig. 2.8: Example of comparison of a specific design at different operation points with the requirements from the API-standard. Q150 means 150% flow compared to the design point (Q100). Performance at other rpm's may also be included. Symbols indicate the mean pulsations over the outlet cross-section and bars the maximum pulsations found in a single CFD-cell.

various operation points. Furthermore, the feature may also be used to compare designs individually.

Tab 2 – Detailed analysis, Fig. 2.9: Each data set from the main tab can be loaded individually into the detailed analysis (or as a separate file if needed) to enhance understanding of which particular frequencies and modes the pump is emitting at a specific operation point. In the detailed analysis, the frequency

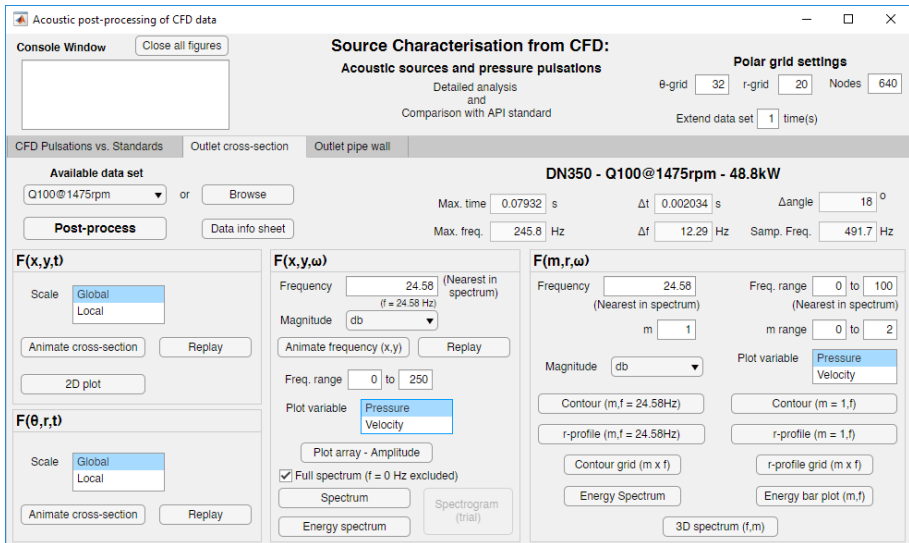


Fig. 2.9: Detailed analysis of each design at a specific operation point. Permits to assess if critical frequencies and/or modes from Tool 1 are excited in this design.

response of the data can be assessed in its original coordinate set i.e. $F(x, y, \omega)$, to assess the frequency content. Further, the response may also be decomposed into its circumferential modes following Paper F i.e. $F(m, r, \omega)$, see Fig. 2.10.

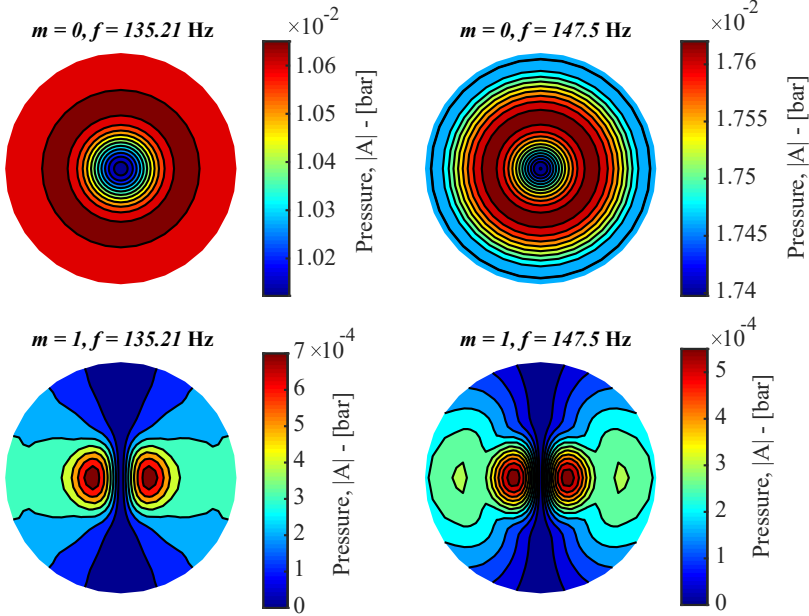


Fig. 2.10: Example of CFD data decomposed into frequency and modal response. Of the frequencies and modes displayed we see that the plane wave ($m = 0$) at $f = 147.5$ Hz is the governing acoustic source.

When this is compared to the information retrieved from Tool 1 it is possible to conclude whether critical circumferential modes are significantly excited at critical frequencies e.g. near cut-on frequencies, and thereby compare different designs in detail. The detailed analysis tab also has several other interesting features such as calculation of the energy content in each circumferential mode at each frequency.

Tab 3 – Mechanical excitations from fluid (alpha-version): The pressure from the surface along the outlet pipe (from CFD simulations) is decomposed into its frequency and modal (circumferential) content to deduce the mechanical excitations generated by the pump at the fluid-structure interface. The excitations may be mapped onto the structure as a radial mechanical excitation of the pipe system i.e. a one-way coupling. This procedure is in an early stage of being tested and implemented and is therefore still an early alpha-version.

As a side note, it is interesting to see that if the response is also decomposed into axial modes (wavenumbers along the pipe, k) a significant amount of acoustic energy propagates with the mean flow. This is caused by vortical structures carried with the flow.

Finally, a rather interesting fact deduced from this tool is that there is a slight rotation in the flow (and pressure) and therefore all the acoustic circumferential modes deduced are in fact spinning helically (discussed in Paper E) as they propagate through the pipe system i.e. they propagate through the system with $\exp(im\theta)$ and not $\cos(m\theta)$ as normally expected. Thus, the receiving pipe system is excited by a rotating force (pressure).

More examples of analyses using Tool 2 can be found in the online *Annex*, [1], or using the QR code found in the Preface.

2.3.1 Theoretical background

At Grundfos CFD simulations have been used for several decades to improve and optimise the hydraulic efficiency of pumps. These CFD simulations are based on hydraulics alone and hence do not account for any acoustics. As the main outcome when designing or improving a pump is a series of CFD simulations at different operation points (and for different designs), it will be beneficial to reuse those to get an insight or indication about the acoustic sources generated by the pump. Thus, to avoid having to build additional (very complicated) aeroacoustic models to get the full acoustic information (sources), it would be highly advantageous to try and extract information about the acoustic sources from the existing CFD data. Although the CFD simulations are generally of very high quality they differ much from the aeroacoustic models, for example, by assuming rigid walls and incompressible fluids. Nevertheless, the deduced sources may still provide reasonable information about which sources are generated and whether they are critical or not according to Tool 1. Besides, proper aeroacoustic models for centrifugal pumps are extremely complicated and time consuming since it requires solving fully compressible Navier-Stokes equations and, in all likelihood, with full account for transient behaviours such as turbulence. Similarly, the model should ideally also feature impedance boundaries (rather than rigid) corresponding to the compliance (and damping) of the structure. In addition to being a very complicated problem by nature, it also requires grid refinements compared to the conventional CFD models in order to capture a reasonable frequency range. Although it seems that the hydraulic CFD simulations are far from the aeroacoustic models there are, however, still hope that they can provide reasonable acoustic sources.

As already mentioned an aeroacoustic model is needed to get full account of the acoustic sources generated by the pump. In this case, where the interest is mostly far-field wave propagation through a pipe system (a linear phenomenon), we would prefer to use these non-linear acoustic sources in a linear acoustic environment. This can be done by using Lighthill's acoustic analogy developed by James Lighthill, [15]. Nowadays there exists indeed many variations of Lighthill's acoustic analogy, some of most famous being: Curle, Ffowcs-Williams Hawkins, Morfey, Lilley, Howe, Goldstein etc. see [16], where the most general (and complicated) is probably the Ffowcs-Williams Hawking (FW-H) shown in Eq. (2.1), formulated for a varying density field, $\rho(X, t)$. De-

tails and technicalities of the model are left out and should be found in [17]. The FW-H analogy is indeed relevant for the centrifugal pump as it accounts also for sound generated by rotating surfaces such as the blades found in a rotating impeller of a centrifugal pump (originally developed to assess the noise pollution from helicopters).

$$\left(\frac{\partial^2}{\partial t^2} - c^2 \nabla^2\right) \rho(X, t) = \frac{\partial^2 T_{ij}}{\partial x_j \partial x_j} - \frac{\partial}{\partial x_i} \left(p_{ij} \delta(f) \frac{\partial f}{\partial x_j} \right) + \frac{\partial}{\partial t} \left(\rho_0 v_i \delta(f) \frac{\partial f}{\partial x_i} \right) \quad (2.1)$$

The simple idea of an acoustic analogy, whichever of the latter is taken, is to combine and manipulate the mass and momentum equations to the above form, in which we recognise the left-hand-side as the (acoustic) wave equation. Note that this equation is in fact exact, nonetheless, very complicated due to its non-linear form. In principle, this complicated equation should be solved on its own, but instead we regard the right-hand-side as known acoustic sources i.e. an external driving function, and the acoustic far-field may then be calculated straightforwardly using linear acoustics. What is left is then to determine the acoustic sources on the right-hand-side which is exactly the scope of Tool 2.

These sources have, in the acoustic terminology, simple interpretations: The first term is known as Lighthill's tensor and describes the noise generated by quadrupoles in the volume, typically, attributed to turbulences. The second term is a dipole source generated by pressure fluctuations at the surfaces (though this is not immediately clear from the equation), known as surface noise, see [18]. The last term constitutes monopole sources generated by volume fluctuations at the surfaces.

Nonetheless, using the full FW-H method for source characterisation of centrifugal pumps is pointless (mainly) for two reasons: 1) From Paper C it is clear that the solution to this problem constitutes a convolution (volume integral) over the entire source region i.e. in this case the entire CFD domain. Deriving and calculating these solutions is therefore a very tedious matter. Further, literature suggests that the quadrupole sources (generated by turbulence) are not sufficiently represented by conventional CFD. However, it is suggested in e.g. [9] that the quadrupole sources can, by reasonable account, be deduced from CFD simulations when Large eddy simulation turbulence models are used. This is rarely used for standard CFD simulations of centrifugal pumps due to low Mach numbers and further, as it rapidly increases the computational costs of the CFD simulations themselves.

2) It is argued in many references, see e.g. [10, 18], that for decreasing Mach numbers the main noise generating mechanism becomes dipole noise. Fortunately, in centrifugal pumps the representative Mach number is indeed low – in the very extreme case no more than ≈ 0.06 . This means that the flow-induced noise is generated almost entirely by pressure fluctuations. Fortunately, this

is well captured by the available CFD simulations and our hope of extracting valuable source information from the CFD simulations thus persist.

Note that in some extreme cases e.g. during cavitation, turbulent noise will affect the noise radiated significantly but as this is never an intended operation regime for a pump it is out of scope of this thesis. Further, the monopole (volume) sources are typically only vaguely present in the flow of centrifugal pumps but does, however, appear occasionally when the internal fluid and structure interacts strongly which, by the rigid wall assumption, is not captured by CFD simulations and is thus also out of scope.

By the latter arguments the acoustic source characterisation may be confined to considering only the dipole (pressure) sources. Further, we need only consider the sources (essentially integrate) over the permeable outlet surface of the pump as the CFD simulations involve the entire domain of the centrifugal pump (including the rigid surfaces) and thus, all surface noise (source information) generated at other internal surfaces is already contained in the information at the permeable surface. Then the far-field wave propagation problem may easily be solved by, essentially, integrating the dipole sources over this surface as suggested by the acoustic analogies. However, as we are interested in understanding the acoustic source generating mechanisms in a centrifugal pump, it is not convenient to just solve the propagation problem but instead, decompose the dipole sources on the permeable surface into its frequency and modal content, and as a consequence avoid integration over the permeable surface.

With this in mind the technique used to deduce the acoustic sources may be based on the same technique used in Paper F to decompose vibration response into circumferential modes. Since the fluid (acoustic) domain and thereby the CFD data is continuous over the cross-section of the outlet of the pump (as oppose to the measurements on the circumference of the pipe in Paper F) the method presented in Paper F need be slightly extended. The output of the CFD simulations used is the pressure profile at the outlet cross-section of the pump as a function of time. The pressure data is known only in discrete points associated with each cell of the CFD grid, see Fig. 2.11(a). To ensure sufficient quality of the data we require data for least one full revolution of the impeller. Preferably, this revolution should be from a steady solution to avoid transient start/stop effects and further, with a mass flow condition at the outlet of the pump as a pressure condition is expected to somewhat disrupt the pressure fluctuations. Likewise, the resolution of the CFD data (time-step) determines the frequency range we can consider and thus, the time-step should be small enough that several harmonics are included (and ideally so that we are free of aliasing issues).

Decomposition (or transformation) of the data from time to frequency domain is straightforward and is done using a Fast Fourier Transformation (FFT) i.e. $\mathcal{F}_t : F(x, y, t) \rightarrow F(x, y, \omega)$. This is done for each cell. The transformation into the spatial domain (circumferential modes) follows directly from Paper F

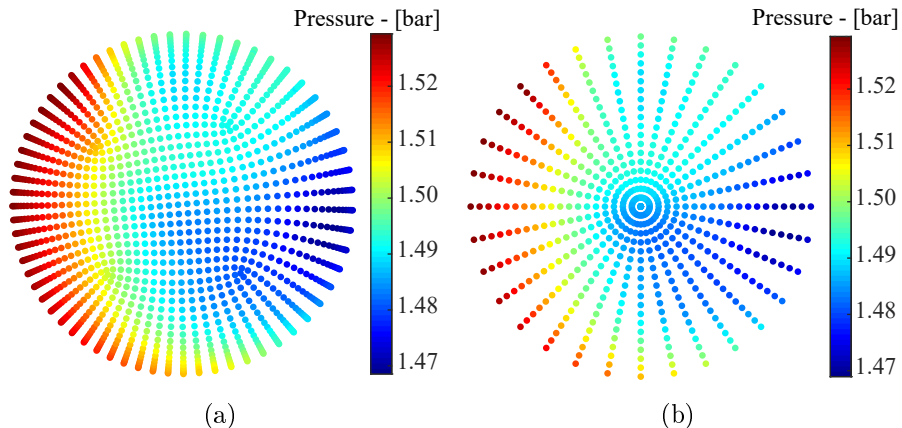


Fig. 2.11: Pressure profile at a given time-step at the outlet cross-section of the pump. (a) original CFD grid and (b) an example of a structured polar grid onto which the data is mapped before spatial decomposition.

i.e. a spatial FFT. However, as the FFT requires equidistant data points this becomes more cumbersome. As discussed in Paper F the FFT is highly sensitive to deviations in equidistant grid points and therefore the CFD grid need be (without exception) fully structured in terms of polar coordinates. As a fully structured polar grid is not plausible for the CFD simulations the data must be mapped from the original grid onto a structured grid before the spatial FFT is performed i.e. $F_{xy} : F(x, y, t/\omega) \rightarrow F(\theta, r, t/\omega)$, see Fig. 2.11(b). This may be done in either the time or frequency domain and will obviously lead to a loss of information if the grid is not chosen sufficiently. Then on the structured grid we perform the spatial FFT, $\mathcal{F}_\theta : F(\theta, r, t/\omega) \rightarrow F(m, r, t/\omega)$. The output of the decomposition of CFD data into acoustic sources is thereby the cross-sectional response at each frequency for each circumferential mode as seen in Fig. 2.10.

Finally, we have so far only considered sources/excitations generated in the fluid by the pump (Tool 2) and how they propagate through the pipe system, of course, accounting for the interaction with the pipe system through the fluid-filled shell model (Tool 1). Similarly, it is of interest to also deduce the mechanical forces exciting the system at the pump/pipe interface. Characterising these mechanical excitations, on the other hand, becomes much more complicated, as it requires accurate calculations of the vibration levels of the entire pump based on the different loads exciting the structure – some of which are not yet quantified. These sources may arise from e.g. the motor (electromagnetic forces), unbalance, hydraulic forces etc. To deduce the excitations at the pump/pipe interface a (very) high fidelity model of the mechanics of the pump is required and further, an investigation and quantification of the governing sources in the pump (besides the hydraulic sources) is necessary. This procedure of predicting the vibration levels (and thus the mechanical excitations of the pipe system) for an operating pump is of high interest and thus constitutes an essential part of the future work.

2.4 Concluding remarks

As mentioned, the industrial scope of this PhD thesis is, in a generic way, to assess the vibro-acoustic sources/excitations generated in a centrifugal pump and how they will propagate into the receiving system. Since Grundfos has no control over the actual supply system, the receiving system studied in the thesis must be chosen as the one of most general character. Therefore, the infinite pipe system is considered (Tool 1) as its properties are characterised only by the pump outlet and the material properties (both standardised). Although only some systems behave infinite it permits generic conclusion for critical excitation of frequencies, modes and transmission paths. The acoustics sources (Tool 2) may, following the acoustic analogies, be deduced from the pressure fluctuations (predicted by CFD simulations) on the permeable outlet surface of the pump. The acoustic sources deduced from several designs and/or operation points may be compared with the requirements from the most recent standards. Further, the acoustic sources may be decomposed into their frequency and modal content, which matches also the output of Tool 1 and thus allow mutual conclusions to be drawn.

Both developed tools have several levels of technical detail, some intended as 'Plug-N-Play' design tools for the hydraulic and mechanical engineers in the early design phase and others intended for specialists for troubleshooting and detailed study of the source generating and propagating mechanisms. Both tools are intended for early use and do thereby not rely on any experimental fitting parameters and therefore neither on any prototypes. Thus, through these tools the vibro-acoustic performance of centrifugal pumps may, in an overall sense, be accounted for already from the initial designs. This is only treated at a much later stage in Grundfos today (after, sometimes, several prototypes). To build these tools the knowledge obtained through the Papers A, B, D, F is crucial, whereas Paper E is interesting from the viewpoint of minimising the energy transmission into the pipe system by tailoring the outlet pipes.

Finally, common for both tools is that we consider the pump as an 'ideal' source not affected by and interacting with the system in which it is operating. This assumption may seem contentious but is nonetheless valid in most cases. On the other hand, accounting for both full fluid-structure interaction internally in the pump and interaction with the entire pipe system becomes extremely complicated and yet it is senseless because two systems are rarely alike.

2.5 Future work

From an industrial viewpoint the most apparent topics of future work are:

- In Tool 1 only the ideal sources related to Green's function are considered. Ideally, actual mechanical and acoustic sources are known e.g. through Tool 2 and therefore the actual energy transmission properties related to

these excitations/sources should be implemented in Tool 1. As shown in Paper A and C this is simply done by a convolution with the Green's function. Nevertheless, at low frequencies the energy carrying properties are determined mainly by the waveguide properties and therefore only sometimes by the excitation type and location (in acoustics).

- As mentioned, impedances for actual systems may vary from everything in-between low to high impedance and, in fact, in the presence of valves and orifices, they may even be complex-valued. As these are basic components in a pipe system, it may be interesting to implement and study the effect of complex-valued impedances in Tool 1. This means that the dispersion diagram need be extended to cover also complex frequencies, which makes this a complicated task.
- When experimental results are available e.g. similar to those in Paper F or as pressure pulsations along or around a pipe, it is always desirable to compare these with the numerical simulation models. For convenience and to ensure a unified framework and terminology, it is desirable to treat the comparison in one tool. Therefore, creating a fourth tab for Tool 2 to process experimental data is desired. Further, this allows to implement the methods developed in Paper F and thereby account for modal leakage in the experimental data such that the comparison between numerical and experimental results becomes transparent to this leakage.
- Source characterisation from both simulation models and experiments is a very complicated matter and, in this thesis, only a naive attempt is done to extract just some valuable information from the existing models regarding the acoustic sources. Though the methodology is based on sound aeroacoustic theory a lot of additional work can be done on this subject to improve even further. This subject is believed to have sufficient depth for a separate PhD study. In such a study a first attempt could be to develop further the method already initiated in tab 3 (Tool 2), but requires, other than that, probably also advanced aeroacoustic modelling and experimental validation, while keeping in mind that the existing CFD models (or at least without a significant increase in computation time) must be at the core of the source characterisation. In addition, deducing mechanical excitations from structural simulations should also be considered in such a study and as already discussed in Sec. 2.3.1 this is indeed a complicated task.
- In Paper E it is illustrated, at particular frequencies at least, that waveguide properties may be tailored to emit energy only in one direction for a given rotating force excitation. 'Fortunately' the centrifugal pump generates rotating forces and thus, it is interesting to study if special pipe sections or pump outlets can be designed such that close-to-zero energy is emitted (through the structure) to the receiving system. And in this regard, how will this affect the performance of the pump itself.

Summary & Conclusions of the Papers

“ To raise new questions, new possibilities, to regard old problems from a new angle, requires creative imagination and marks real advance in science. ”

– Albert Einstein

In the following each paper from the collection of papers included in the thesis is summarised. The summary includes a brief motivation prior to the summary and lastly the main conclusions and scientific contributions are listed for each paper separately. Finally, the extended summary is concluded with a number of selected topics of future work interesting from an academic viewpoint. Some conclusions, scientific contributions or topics of future work may, in view of the extended summary, seem to be rather unsupported and perhaps even appear out-of-the-blue. In this case the full overview and details offered by the paper(s) may be necessary.

3.1 Description of papers

Below, each paper is briefly summarised following the structure: Motivation, summary and main conclusions and scientific contribution.

3.1.1 Paper A

Under the title: *“Bi-orthogonality relations for fluid-filled elastic cylindrical shells: Theory, generalisations and application to construct tailored Green’s matrices”* Paper A deals with the classical vibro-acoustic waveguide problem of

free/forced guided wave propagation in a fluid-filled elastic cylindrical shell formulated in the framework of thin shell theory. In the presence of a compressible (inviscid) fluid this waveguide supports an infinite number of waves. In this paper a novel method based on special bi-orthogonality relations is developed. The method permits deriving analytical closed-form solutions to this otherwise complicated transcendental problem.

First, the free wave problem, in terms of the dispersion relation, is solved. This problem is on its own challenging due to the transcendental and ill-conditioned nature; The former caused by the continuous compressible fluid and the latter by coupling of rigid and compliant constituents. Finding these solutions may however be greatly simplified using the method of Finite Products developed in Paper D. In the formulation of the free wave problem a set of modal coefficients are introduced, defined as coefficients independent of the waveguide direction. These coefficients hold special properties denoted Class properties and are essentially what makes up the powerful bi-orthogonality relation. Second, the bi-orthogonality relation for this particular problem is easily derived directly from the reciprocity relation using only the Class properties of the modal coefficients. Following the same logic, the derivation of bi-orthogonality relations is generalised to cover any waveguide with uniform symmetric properties. This is generalised further in Paper C to cover entire operators obeying self-adjointness. Then, through the formulation of tailored Green's matrices, it is demonstrated how to find the unknown modal amplitudes independent of each other and on algebraic form using just the bi-orthogonality relation. Through conventional techniques this typically proves to be yet another challenge due to the transcendental nature of the problem. This methodology applies to all the fundamental loading cases involved in the formulation of Green's matrix and moreover simple relations between the amplitudes from different loading conditions are also derived.

In order to gain confidence in the method and show its robustness, as that required by engineers, completeness and (uniform) convergence of the solution is proved. In addition, it has been found that unconverged solutions may be easily spotted visually in the energy flow analysis since an unconverged solution disrupts continuity across the excitation point. This leads to the derivation of exact error measures possible because the convergence targets are now well-known. Thus, the method provides an instantaneous measure of convergence for any truncated solution. Finally, it is shown that the total energy flow may be derived from the bi-orthogonality relation. This fact immediately leads to the proof that the total energy flow is a linear quantity because the bi-orthogonal property ensures that all cross-products vanish, leaving only the principal (diagonal) terms. Further, this derivation also shows that only propagating waves contribute to the total energy flow and computation of the energy flow may thus be much simplified.

Main conclusions and scientific contribution

- The derivation of the bi-orthogonality relation is generalised to uniform symmetric waveguides. Its derivation emerges directly from the reciprocity relation using the Class properties of the modal coefficients. The derivation is shown explicitly for the fluid-filled shell.
- Using bi-orthogonality the modal amplitudes of Green's function may be found individually and independent of each other.
- The convergence properties of a solution derived through bi-orthogonality permits instantaneous assessment of convergence through exact error measures and further, from the energy flow analysis unconverted results are readily visible.
- The explicit relation between the total energy flow and bi-orthogonality relation have been shown and have led to the proof that total energy flow obeys linearity. This greatly simplifies calculation of the total energy flow.

3.1.2 Paper B

This paper entitled: “*On the application of the bi-orthogonality relations for analysis of linear dynamical systems*” considers how to apply the bi-orthogonality relation in the framework of the Boundary Integral Equations Method (BIEM) and may thus be seen as an extension of Paper A. In BIEM the solution to the infinite (or unbounded) waveguide problem is exploited to solve the subsequent 'finite' (or fully bounded) waveguide problem and essentially, to explore how propagating waves form into standing waves (eigenfrequencies). As implied by the title the method applies to problems in linear dynamics, confined to uniform symmetric domains e.g. uniform symmetric waveguides with a preferred direction of propagation as considered in Paper A. Thus, the method applies equally well in other realms of physics such as, for instance, electromagnetics, optics, acoustics, seismics and even quantum mechanics. In this paper, however, we consider three examples (of diverse complexity) from mechanics and vibro-acoustics (respectively, a Bernoulli-Euler beam, a fluid-loaded membrane and the fluid-filled shell from Paper A)

First, the concept of modal coefficients, Class properties and derivation of bi-orthogonality from Paper A is briefly summarised. The Boundary Integral Equations (BIE) arise from Somigliana's identity and is therefore our point of departure. Then by relatively simple means Somigliana's identity is reformulated to modal form by expanding each state variable in the identity on its eigenfunctions and take advantage of the bi-orthogonality relation to, eventually, reduce Somigliana's identity to modal form. Then, by formulation of the BIE's from the modal Somigliana's identity it becomes obvious that the integral equations vanish, and the BIE's thus resolve completely to algebraic modal identities which we denote: Modal boundary identities. Technicalities of the procedure are then illustrated for the three examples. When Somigliana's identity involves also forcing terms the identities may still be resolved but are

in this case denoted the inhomogeneous modal boundary identities. With the BIE's fully resolved only the boundary conditions remain and setting up the equation system for an arbitrary set of boundary conditions is therefore done using the boundary identities and a modal projection technique based on the bi-orthogonality relation. For the forcing problem the procedure is the same.

Then for two special sets of boundary conditions (denoted Class consistent boundary conditions) the optimal choice of projection vector is easily identified from the bi-orthogonality relation. For this choice the equation system factorises completely, no matter the complexity of the problem, leading to the fundamental canonical eigenfrequency equations: $\sin(kL) = 0$ and $\cos(kL) = 0$. The eigenfrequencies are then found simply by substituting the solution, k , from the latter canonical eigenfrequency equations into the dispersion relation and use, for instance, the finite product method of Paper D, to find the eigenfrequencies. This allows also identification of eigenfrequencies directly from the dispersion diagram as the intersection of the propagating wave branches with horizontal lines corresponding to the solutions of the canonical eigenfrequency equations. Finally, the modal projection method implies, as in Paper A, that boundary conditions have become convergence targets and thus immediately permits the same error measures introduced in Paper A. In case of an unconverged solution caused by a prematurely truncated solution, the solution will be exact, however, to a set of boundary conditions similar, but not identical, to those prescribed. In the limit, however, the prescribed boundary conditions are of course recovered. Contrary, no such conclusions can be deduced from unconverged solutions in conventional techniques e.g. in the Boundary Element Method. Lastly, perspectives on the possibility to introduce this method into the framework of Wave Finite Element, extension to cover also unsymmetric problems and how convergence may relate to experiments where boundary conditions are rarely ideal, have been discussed.

Main conclusions and scientific contribution

- The Boundary Integral Equations may be fully resolved to simple modal boundary identities between amplitudes at different boundaries. It is done by reducing Somigliana's identity to modal form using decomposition and the bi-orthogonality relation. These identities can be derived both for the homogeneous and inhomogeneous problem.
- With the boundary identities used, the equation system is concerned only with the boundary conditions and does thereby not require any of the technicalities related to BIEM. Further, two special sets of boundary conditions can be identified for which the eigenfrequency spectrum emerges directly from the dispersion relation (or diagram), also for transcendental problems.
- Using the modal projection method, the boundary conditions converge to the prescribed ones in the limit, while unconverged results appear as exact solutions for another, yet similar, set of boundary conditions. As

in Paper A this permit exact error measures and thus an instantaneous measure of convergence for arbitrary truncation orders.

3.1.3 Paper C

With the title: “*(Bi)-orthogonality relation for eigenfunctions of self-adjoint operators*” it should be no surprise that the scope of Paper C is to generalise much further the range of problems for which bi-orthogonality may be used. Thus, Paper C is a generalisation of bi-orthogonality relations beyond the results in Paper A where they were generalised to uniform symmetric waveguides. In this paper we progress to cover entire operators i.e. operators that are self-adjoint and with at least one empty boundary (explained in the paper). Such operators very often constitute the core of problems treated in e.g. applied mathematics, physics or science as a whole and cover, for instance, problems (differential operators) derived from the variational principle. With this generalisation it becomes clear that bi-orthogonality is not confined to any particular realm of physics and further, covers also coupled multiphysics problems thereof. To illustrate the derivations we use a non-trivial example: a fluid-loaded plate with preferred direction of wave propagation in the radial direction i.e. formulated in cylindrical coordinates.

To show that bi-orthogonality exists for general self-adjoint operators we start at the very core of the problem: The governing partial differential equation. From this we may formulate the self-adjoint condition and through partial integration reduce to the reciprocity relation. In this general format deriving bi-orthogonality from reciprocity requires a different approach than that outlined in Paper A. This is essentially done by showing that the bi-orthogonality relation can be obtained as a linear combination of characteristic equations for the eigenfunctions involved. In the framework of the waveguide example this constitutes a linear combination of dispersion relations for the involved waves. Through the non-trivial example, it becomes obvious that in e.g. cylindrical coordinates, the formulation of correct modal coefficients (those ensuring bi-orthogonality and having Class properties according to Paper A) may be deduced only from what is denoted the essential state variables (forces/displacements).

With bi-orthogonality derived it is illustrated how to apply these to solve the subsequent forcing problem. This procedure follows exactly the same steps as for deriving bi-orthogonality and eventually by applying bi-orthogonality, an analytical closed-form solution emerges. When applied to the example we identify the Wronskian and note that the expression for the unknown modal amplitudes reduce to the same simple form derived for the fluid-filled shell in Paper A. Finally, the relation between total energy flow and the bi-orthogonality relation is derived in this general format as it was done for the specific problem in Paper A. This again proves linearity of the total energy flow and further, shows that only the essential state variables contribute to the energy flow. For the fluid-loaded membrane example this implies that the terms associated with

e.g. Poisson's ratio produce no net flow of energy. Lastly, perspectives on how to generalise further to 'finite' waveguides through the Boundary Integral Equations Method (as done in Paper B for a special class of problems) is discussed.

Main conclusions and scientific contribution

- The bi-orthogonality relation is generalised to the eigenfunctions of self-adjoint operators. They are obtained as a linear combination of characteristic equations for the relevant eigenfunctions and are thus invariant to the choice of coordinate system. Further, the bi-orthogonality relation consists only of essential components of the state variables.
- The solution to the inhomogeneous (forcing) problem may be found in closed-form when using the bi-orthogonality relation i.e. the modal amplitudes may be found independently. Further, by the invariance of the bi-orthogonality relation, the solution is on strong form.
- The relation between bi-orthogonality and the total energy flow is derived and linearity of the total energy flow is thus proven in this general format. Thereby it is shown that only the essential components produce a non-zero net flow of energy.

3.1.4 Paper D

As suggested by the title: *“Using the Finite Product Method for solving eigenvalue problems formulated in cylindrical coordinates”* Paper D focuses on extending the Finite Product Method (FPM) to problems formulated in cylindrical coordinates. The purpose of the FPM is to introduce accurate and simple polynomial approximations of transcendental equations similar to those found in Paper A. As mentioned in Sec. 3.1.1 such problems are usually difficult to solve, mainly due to their transcendental and ill-conditioned nature. The FPM has already been developed for the trigonometric functions (sine/cosine), see [19], however, for some problems in cylindrical coordinates the transcendental equation to be solved may rather involve Bessel functions (or a fraction of Bessel functions). Thus, this paper is concerned with extending the FPM to cover also Bessel functions. Although we focus again in this paper on the vibro-acoustic example from Paper A (fluid-filled shell) the FPM is in no way restricted to such waveguide problems and may thus find many convenient applications elsewhere. The FPM for Bessel functions proves particularly strong in the presence of fractions of Bessel functions where properly adjusted approximation orders ensure almost exact cancelling of Runge's phenomenon, thus providing an excellent accuracy of the approximate solution for such problems.

First, the transcendental dispersion equation to be solved is presented. It consists of combinations of polynomials and a fraction of Bessel functions of first kind of integer order m (not restricted to integer orders). Then the transcendental terms (Bessel functions) are replaced by their equivalent infinite product representations, which may be found in literature. In this representation the

zeros of the respective Bessel functions are needed and are also available in literature (or mathematics software). The infinite products are then split into a finite and an infinite product part by N_i , where N_i is denoted the approximation order. The infinite part is neglected and the FPM emerges in a very simple way, reducing the transcendental equation to a polynomial equation. Further, in the presence of fractions the approximation order for each Bessel function, say, (N_1, N_2) , need be chosen properly to ensure cancelling of Runge's phenomenon. The relation between the approximation orders, N_1 and N_2 , were previously found using Stirling's approximation and by ensuring correct limit behaviours. However, it is found that by arranging the zeros used in the infinite products into a sorted set of ascending order we may simply truncate anywhere in the sorted set and by including all zeros up until the truncation we automatically ensure correct limit behaviour and the cancelling of Runge's phenomenon. This holds likewise for multiple fractions of Bessel functions. For the example considered in the paper this corresponds to the two possible approximation orders (N_1, N_1) or $(N_1, N_1 + 1)$, corresponding to a lead of either the denominator or numerator. Finally, accuracy of the solution is studied by comparing with the solution to the actual transcendental equation. From this study conservative, but simple, validity ranges of high accuracy are deduced. Lastly, the reason for the excellent performance of the FPM is discussed. This owes to periodically occurring grid points which are points where the approximate (FPM) dispersion relation is exact. Also, the dispersion diagram is compared to the different 'limit' waveguides i.e. the in-vacuo shell and the cylindrical acoustic duct with both rigid and soft walls.

Main conclusions and scientific contribution

- The FPM is extended to cover also problems formulated in cylindrical coordinates i.e. the FPM is derived for Bessel functions of first kind. Advantages of the FPM is its arbitrarily high accuracy, no spurious roots but most importantly its simplicity.
- The correct approximation orders in the presence of fractions of Bessel functions may be determined directly from a sorted set of the zeros involved in the infinite product representation of the transcendental terms. This immediately ensures correct limit behaviour and the cancelling of Runge's phenomenon without having to formally carry out any of these, sometimes, tedious analyses.
- Simple and conservative measures for the validity range of the FPM are deduced based on the chosen approximation order.

3.1.5 Paper E

With the title: "*Wave propagation in helically orthotropic elastic cylindrical shells and lattices*" the scope is to study the behaviour of a helically orthotropic cylindrical shell in which the orthotropy is defined by an angle and orthotropic

material properties. This may be thought of as for instance a fibre reinforced cylinder. The purpose is to study the wave propagation properties of such a waveguide as well as how the two orthotropy parameters, angle and material, affect the dispersion diagram. The shell is modelled using three different methods: 1) an analytical model based on thin shell theory, 2) the Wave Finite Element Method (WFEM) and 3) a lattice structure consisting of beam elements – also in the framework of WFEM.

First the analytical model is introduced and the dispersion diagrams for several orthotropy parameters are shown. A breaking of symmetry is observed when the orthotropy parameters do not correspond to an isotropic shell. The symmetry breaking manifests itself in the dispersion equation as a polynomial having both even and odd powers of the wavenumbers, nevertheless, with real valued coefficients which ensures that symmetry is always preserved for the decaying and attenuating waves. The symmetry breaking shows interesting behaviours, among others, the existence of waves with a positive phase velocity but a negative group velocity. The symmetry breaking as well as other interesting phenomena e.g. veering and locking of waves are studied in detail for changing angles and material parameters. These phenomena are not observed in the isotropic shell and the orthotropic shell thus permits tailoring to attain special wave propagation properties. Then, the analytical model is compared with the WFEM which uses solid rather than shell elements. Despite the discrepancy the correlation between the models is good. For the simplified lattice structure (consisting of beam elements of various stiffness) the same behaviour and tendencies are observed. Finally, an energy flow analysis for a rotating radial force is conducted in order to study the energy carrying properties of such orthotropic shells. Here it is found that the symmetry breaking leads to an uneven distribution of energy propagation in each direction, which for symmetric waveguides split into equal shares. Thus, it is shown that the orthotropic shell can be tailored to have different energy flow propagating in each direction, and in fact, the waveguide may be tailored to have more or less all energy propagating to the right and only very little energy propagating to the left – at least for some frequencies. Moreover the total energy at a fixed frequency is studied for varying fibre angles and it is found that the total energy may increase drastically for some angles, explained here by cut-on/cut-off of propagating waves which corresponds to a significant change of the waveguide properties.

Main conclusions and scientific contribution

- Breaking of symmetry of the propagating wave branches appears as soon as both the angle and material parameters of orthotropy are chosen different from the isotropic values – explained by even and odd powers of the wavenumber in the dispersion equation. The symmetry is retained for the decaying and attenuating waves, since the dispersion equation has only real valued coefficients. All symmetry is recovered when the angle of orthotropy aligns with the cylindrical coordinates or when the material

parameters are chosen as isotropic.

- For orthotropic parameters the energy flow carried by the waveguide for a rotating applied force is no longer the same to the right and left. Thus, at specific frequencies the orthotropic shell may be tailored to control the energy flow to have, for example, close-to-all energy propagating to, say, the right. Further, the energy carrying properties to the left and right are sensitive to the parameters of orthotropy as they may cause radical changes to the waveguide properties e.g. changing cut-on/cut-off frequencies.

3.1.6 Paper F

Under the title: “*Experimental analysis, simulation and decomposition of vibrations in not perfectly axi-symmetric pipes*” this paper deals with a comparison of experimental and simulation results (model validation) when a significant amount of modal leakage is present (caused by experimental sources of error). In many physics and engineering applications we see axi- and quasi axi-symmetric structures. For such structures the experimentally measured response may be decomposed into to circumferential modes by having accelerometers placed equidistantly around the circumference, allowing for increased physical understanding of the behaviour of the structure and of the response produced by these individual modes. However, this procedure is particularly prone to experimental sources of error and therefore the decomposed spectra usually become inconclusive because the response belonging, essentially, to one mode, leaks into the decomposed spectrum of others. This is called modal, or in a more general sense, spectral leakage. Modal leakage is inevitable and therefore the methods presented in this paper are developed to provide a much clearer interpretation in model validation in the presence of significant leakage as well as a method to distinguish authentic resonances from spurious (leaked) ones both by simple additional post processing of existing experimental data. In particular, this paper deals with mechanical structures (pipes), but the methods developed are equally valid for use in e.g. electromagnetics to decompose the forces in a motor etc.

First, a sensitivity study using a mathematical model (based on thin shell theory) is conducted, testing the effect of various experimental sources of errors on various decomposition techniques. Here it is found that the main error is, by far, caused by misplacement of accelerometers, which are meant to be placed equidistantly around the circumference. In the mathematical model it is shown that even slight (random) perturbation of the equidistant positions with just $\pm 0.1\%$ (corresponding to just $\pm 0.4\text{mm}$ of the circumference of the test pipe) introduce significant leakage into the decomposed results and in fact enough that it becomes incomparable with the initial mathematical model from which it was decomposed. Therefore, no matter how carefully tests are conducted, modal leakage is inevitable. Then, to accommodate model validation we need, instead, to introduce similar leakage into the mathematical model. In the paper

two simple methods for this are presented: one where the mathematical model is simply decomposed with slightly perturbed 'measuring points' (as done in the sensitivity analysis) and one where the decomposed experimental spectrum is used as a scaling in the ideal mathematical model. While the latter method is very simple it provides only visual aids as the relative errors remain unchanged; The former method is much stronger and provides also better relative comparisons. Further, a method for how to distinguish modes of the decomposed spectrum and conclude on whether they are authentic or not is developed. This method is based on additional post processing of the experimental results. The method simply compares two decomposition techniques where one is assuming symmetry. These two methods have different sensitivities to the misplacement and therefore the decomposed response at the resonances are different when the resonance is spurious (i.e. belongs to another mode), while they coincide when the resonance is authentic. Finally, spectral leakage is discussed in terms of aliasing. In the time domain this can be handled by filtering techniques, however, in the spatial domain no such techniques exist. Therefore, the number of equidistant measurements points needed are determined by the last circumferential mode with cut-on frequency in the chosen frequency spectrum. For compliant structures such as PVC pipes, the cut-on frequencies decrease and the number of necessary measurement points around the circumference must be increased if the same frequency range is to be covered. So far, the cut-on frequencies need be determined mathematically.

Main conclusions and scientific contribution

- It is found that the root cause of modal leakage in circumferential decomposition owes to, just slight, misplacement of measurement points, making modal leakage inevitable. The sensitivity to misplacement is extremely high.
- A method for model validation in the presence of significant modal leakage is developed. Leakage is introduced in the mathematical model either using the experimental (decomposed) data as a scaling or by perturbing 'measurement points' in the mathematical model before decomposition.
- A method for distinguishing authentic and spurious resonances in a decomposed spectrum is developed based on additional data processing alone. By comparing two decomposition methods that are based on different assumptions the decomposed results coincide only when the resonances are authentic.

3.2 Future work

Based on this collection of papers a few interesting selected topics of future work are listed below. To comprehend, in full, the perspectives and potentials of the following topics of future work a detailed overview of the papers may be necessary.

- In relation to Paper B the method developed for solving boundary value problems by resolving integral equations into the algebraic modal boundary identities and using the modal projection method is yet confined to problems for uniform symmetric waveguides. In Paper C derivation of bi-orthogonality is, however, generalised to cover self-adjoint operators and therefore extending the methods of Paper B to also cover self-adjoint operators in general is indeed of great interest. Potentially this can reveal closed-form solutions (for Class consistent boundary conditions) for very complicated boundary value problems.
- In relation to Paper C it is interesting whether the bi-orthogonality relations can be extended further to cover also operators that are not self-adjoint (unsymmetric). As the bi-orthogonality relation has proven to be related to the dispersion (characteristic) equation and thus invariant, it is likely that bi-orthogonality relations exist also for unsymmetric operators e.g. for the orthotropic shell treated in Paper E. If such bi-orthogonality relations can be found and generalised it will reveal analytical closed-form solutions for many indeed very complicated semi-bounded problems and therefore have a huge impact in the field of linear dynamic systems and, in particular, in waveguide theory.
- Incorporating the bi-orthogonality relations into a numerical framework such as, for instance, the much used Wave Finite Element Method is indeed an interesting extension of the methods developed in Paper A–C. The standard output of the numerical tools used for assessing waveguide properties provide wavenumbers and related mode shapes. Since the bi-orthogonality relation is composed exactly of these two things, formulating the bi-orthogonality relations in such a framework may be possible. If it is possible the bi-orthogonality relations may be used to straightforwardly solve the subsequent forcing problem using the explicit formula from Paper C which is nothing but the inner product of properly defined state vectors (eigenmodes).
- In addition, the findings of Paper B can potentially be utilised in a numerical framework to obtain the dispersion curves related to the propagating waves. From the solution for Class consistent boundary conditions in Paper B it is known that there is an explicit relation between the spectrum of eigenfrequencies and the wavenumbers of propagating waves and hence the spectrum of eigenfrequencies may be converted into a spectrum of wavenumbers. Then by gradually changing the length of the structure the

dispersion diagram may be obtained. One advantage of this is that there will be no spurious roots.

- Often in experimental vibration analysis the main source of error is related to uncertainties in the actual boundary conditions, yet the sensitivity to these conditions is often very high, affecting, sometimes radically, the spectrum of eigenfrequencies. It is therefore of particular interest to characterise the actual boundary impedances to accommodate model validation. When using the modal project method from Paper B the boundary conditions converge in the limit as all necessary waves are included in the solution and therefore it is interesting to adopt e.g. inverse characterisation techniques, to characterise the boundary conditions. This may also provide insight into which particular waves that are difficult to constrain in practise and thus hint towards less sensitive boundary conditions useful for experiments and perhaps even real-life systems.
- Studying limit cases of the eigenfrequency spectrum for varying boundary impedances is of significant interest for real-life pipe systems to determine and possibly minimise the diversity of the spectrum. Moreover, it may also be interesting to compare the different limit cases with the Class consistent solutions obtained in Paper B, to see whether these solutions, in fact, constitute the limits of the eigenfrequency spectrum. If so, is it then possible to approximate the spectrum for an arbitrary set of boundary conditions based on the Class consistent spectrum alone and thus evade solving the actual system of equations.
- In Paper D the Finite Product Method has shown to be a simple and strong tool for approximating the dispersion relation such that the wavenumbers are easily found. So far, the FPM is developed only for trigonometric functions and through the developments in Paper D, also for Bessel functions of first kind. As it is indeed a strong tool, it is interesting to study in more general terms, to which type of characteristic equations the FPM may be applied i.e. in which realms of physics, for which types of transcendental functions and for which types of fractions of transcendental functions.

Indeed there are many more interesting topics of future work that can be thought of. The topics above are, however, the author's first choice of topics that could potentially have a significant impact on the future of engineering science. This concludes the extended summary, yet the appended collection of scientific papers still remains.

References

- [1] L. S. Ledet, Online Annex – PhD Thesis (2019), Short link: <https://forms.gle/Acx78Y5CN897XjVXA>; Direct link: https://drive.google.com/drive/folders/1c0nlfy-xi0o1HgPJSc-SIDethd8G2_US?usp=sharing.
- [2] E. N. Lorenz, Predictability; Does the Flap of a Butterfly’s wings in Brazil Set Off a Tornado in Texas?, in: 139th Meet. Am. Assoc. Adv. Sci., 1972.
- [3] L. Cremer, M. Heckl, B. A. Petersson, Structure-Borne Sound - Structural Vibrations and Sound Radiation at Audio Frequencies, 3rd Edition, Springer, 2005. doi:10.1007/b137728.
- [4] G. Green, An Essay on the Application of Mathematical Analysis to the Theories of Electricity and Magnetism, Nottingham, England, 1828.
- [5] S. S. Rao, Mechanical Vibrations, 5th Edition, Prentice, 2011.
- [6] C. L. Phillips, J. M. Parr, Feedback Control Systems, 5th Edition, Pearson, 2011.
- [7] G. Pavic, Vibrational energy flow in elastic circular cylindrical shells, J. Sound Vib. 142 (2) (1990) 293–310. doi:10.1016/0022-460X(90)90558-H.
- [8] L. Andersen, S. R. K. Nielsen, Boundary element analysis of the steady-state response of an elastic half-space to a moving force on its surface, Eng. Anal. Bound. Elem. 27 (2003) 23–38. doi:10.1016/S0955-7997(02)00096-6.
- [9] J. Chen, Y. He, L. Gui, C. Wang, L. Chen, Y. Li, Aerodynamic noise prediction of a centrifugal fan considering the volute effect using IBEM, Appl. Acoust. 132 (2018) 182–190. doi:10.1016/j.apacoust.2017.10.015.
- [10] A. Ali, C. Rajakumar, S. M. Yunus, Advances in acoustic eigenvalue analysis using boundary element method, Comput. Struct. 56 (5) (1995) 837–847. doi:10.1016/0045-7949(95)00012-6.
- [11] T. M. Søndergaard, Greens Function Integral Equation Methods in Nano-Optics, 1st Edition, CRC Press, 2018.

- [12] W. C. Gibson, *The Method of Moments in Electromagnetics*, Chapman & Hall/CRC, 2008.
- [13] Grundfos Research and Technology, *The Centrifugal Pump*, Grundfos, 2008, http://www.grundfos.com/content/dam/GlobalSite/Industries&solutions/Industry/pdf/The_Centrifugal_Pump.pdf.
- [14] A. P. Institute, *API standard 674 – Positive Displacement Pumps - Reciprocating*, 3rd Edition, American Petroleum Institute, 2016.
- [15] M. J. Lighthill, On sound generated aerodynamically I. General theory, *Proc. R. Soc. A* 211 (1107) (1951) 564–587. doi:10.1098/rspa.1952.0060.
- [16] C. L. Morfey, M. C. M. Wright, Extensions of Lighthill’s acoustic analogy with application to computational aeroacoustics, *Proc. R. Soc. A* 463 (2085) (2007) 2101–2127. doi:10.1098/rspa.2007.1864.
- [17] J. E. Ffowcs Williams, D. L. Hawkings, Sound Generation by Turbulence and Surfaces in Arbitrary Motion, *Philos. Trans. R. Soc. London. Ser. A, Math. Phys. Sci.* 264 (1151) (1969) 321–342. doi:10.1098/rsta.1969.0031.
- [18] N. Curle, The Influence of Solid Boundaries upon Aerodynamic Sound, *Proc. R. Soc. Lond. A. Math. Phys. Sci.* 231 (1187) (1955) 505–514. doi:10.1098/rspa.1955.0191.
- [19] C. J. Chapman, S. V. Sorokin, The finite-product method in the theory of waves and stability, *Proc. R. Soc. A Math. Phys. Eng. Sci.* 466 (2114) (2010) 471–491. doi:10.1098/rspa.2009.0255.

Paper A

Bi-orthogonality relations for fluid-filled elastic
cylindrical shells: Theory, generalisations and application
to construct tailored Green's matrices

Lasse S. Ledet & Sergey V. Sorokin

*Department of Materials and Production, Aalborg University,
Fibigerstraede 16, 9220 Aalborg East, Denmark*

Published in:

Journal of Sound and Vibration, Vol. 417, pp. 315–340, 2018.

doi:10.1016/j.jsv.2017.12.010

© 2017 Elsevier Ltd. All rights reserved.
The layout has been revised.

Bi-orthogonality relations for fluid-filled elastic cylindrical shells: Theory, generalisations and application to construct tailored Green's matrices

Lasse S. Ledet^a, Sergey V. Sorokin^a

^a*Department of Materials and Production, Aalborg University, Fibigerstraede 16, 9220 Aalborg, Denmark*

Abstract

The paper addresses the classical problem of time-harmonic forced vibrations of a fluid-filled cylindrical shell considered as a multi-modal waveguide carrying infinitely many waves. The forced vibration problem is solved using tailored Green's matrices formulated in terms of eigenfunction expansions. The formulation of Green's matrix is based on special (bi-)orthogonality relations between the eigenfunctions, which are derived here for the fluid-filled shell. Further, the relations are generalised to any multi-modal symmetric waveguide. Using the orthogonality relations, the transcendental equation system is converted into algebraic modal equations that can be solved analytically. Upon formulation of Green's matrices, the solution space is studied in terms of completeness and convergence (uniformity and rate). Special features and findings exposed only through this modal decomposition method are elaborated and the physical interpretation of the bi-orthogonality relation is discussed in relation to the total energy flow which leads to derivation of simplified equations for the energy flow components.

Keywords:

Bi-orthogonality relations, Modal decomposition, Tailored Green's matrices, Symmetric waveguides, Energy flow, Convergence and error calculation

1. Introduction

In this paper we address the classical problem of time-harmonic wave propagation in a thin elastic fluid-filled cylindrical shell loaded by an inviscid compressible fluid without mean flow. This is a subject broadly covered in literature on applied mathematics, see e.g. [1–6]. Among other applications, this formulation is used to address transmission of vibro-acoustic energy which is of primary interest in e.g. the oil and gas industry as well as in larger pumping systems conveying waste water or distributing domestic water to inhabitants. While the analysis of free waves in such a waveguide is a well-established subject, a forced response in various excitation conditions has not yet been fully explored. To cover arbitrarily distributed acoustic and structural sources it is convenient to derive Green's matrices i.e. to study the response to an excitation modelled as delta-functions. In this formulation of the problem it is

Nomenclature

c_{fl}	Fluid sound speed – [m s ⁻¹]	V	Non-dim. circumferential amplitude
c_{str}	Structural sound speed $\equiv \sqrt{\frac{E}{\rho_{str}(1-\nu^2)}} – [m s^{-1}]$	w	Non-dim. radial displacement $\equiv \frac{\tilde{w}}{R}$
E	Young's modulus – [Pa]	W	Non-dim. radial amplitude
h	Shell thickness – [m]	w'	Non-dim. rotation
k	Non-dim. axial wavenumber $\equiv \tilde{k}R$	W'	Non-dim. rotation amplitude
m	Non-dim. circumferential wavenumber	x	Non-dim. axial coordinate $\equiv \frac{\tilde{x}}{R}$
N^u	Non-dim. axial energy flow $\equiv \frac{1-\nu^2}{EhRc_{str}} \tilde{N}^u$	γ	Sound speed ratio $\equiv \frac{c_{str}}{c_{fl}}$
N^v	Non-dim. torsion energy flow $\equiv \frac{1-\nu^2}{EhRc_{str}} \tilde{N}^v$	ϑ	Non-dim. acoustic velocity $\equiv \frac{\tilde{\vartheta}}{c_{fl}}$
N^w	Non-dim. transverse energy flow $\equiv \frac{1-\nu^2}{EhRc_{str}} \tilde{N}^w$	\mathcal{V}	Non-dim. amplitude of acoustic velocity
$N^{w'}$	Non-dim. bending energy flow $\equiv \frac{1-\nu^2}{EhRc_{str}} \tilde{N}^{w'}$	θ	Non-dim. circumferential coordinate
N^θ	Non-dim. acoustic energy flow $\equiv \frac{1-\nu^2}{EhRc_{str}} \tilde{N}^\theta$	κ	Non-dim. radial wavenumber $\equiv \sqrt{k^2 + \gamma^2 \Omega^2}$
N^Σ	Non-dim. total energy flow $\equiv \frac{1-\nu^2}{EhRc_{str}} \tilde{N}^\Sigma$	μ	Thickness-to-radius ratio $\equiv \frac{h}{R}$
p	Non-dim. acoustic pressure $\equiv \frac{1}{c_{fl}^2 \rho_{fl}} \tilde{p}$	ν	Poisson's ratio – [-]
P	Non-dim. amplitude of acoustic pressure	ξ	Excitation point in x
q_l	Non-dim. external structural forces $\equiv \frac{1-\nu^2}{E} \tilde{q}_l, (l = 1, 2, 3)$	ρ_{fl}	Fluid density – [kg m ⁻³]
Q_4	Non-dim. moment $\equiv \frac{1-\nu^2}{Eh^2} \tilde{Q}_4$	ρ_{str}	Structural density – [kg m ⁻³]
Q_l	Non-dim. forces $\equiv \frac{1-\nu^2}{Eh} \tilde{Q}_l, (l = 1, 2, 3)$	ρ	Density ratio $\equiv \frac{\rho_{fl}}{\rho_{str}}$
Q_l	Non-dim. amplitude of structural forces/moment, $(l = 1, \dots, 4)$	ϕ	Non-dim. velocity potential $\equiv \frac{\tilde{\phi}}{c_{fl}R}$
r	Non-dim. radial coordinate $\equiv \frac{\tilde{r}}{R}$	Φ	Non-dim. amplitude of velocity potential
r_0	Excitation point in r	ω	Angular frequency – [rad s ⁻¹]
R	Shell radius – [m]	Ω	Non-dim. frequency $\equiv \frac{\omega R}{c_{str}}$
T	Non-dim. external acoustic source $\equiv \frac{R}{c_{fl}} \tilde{T}$	$J_m(x)$	Bessel-function of first kind of order $m \in \mathbb{Z}$
u	Non-dim. axial displacement $\equiv \frac{\tilde{u}}{R}$	$\delta(x)$	Dirac delta-function
U	Non-dim. axial amplitude	$\text{sgn}(x)$	Signum function
v	Non-dim. circumferential displacement $\equiv \frac{\tilde{v}}{R}$	$ x $	Module of x
		i	Complex operator
		$*$	Complex conjugated
		$'$	Derivative with respect to x
		\mathbf{U}	U as a matrix or vector
		$-$	Indicates modal coefficients
		\sim	Indicates dimensional quantities
		$0f$	Indicates loading condition
		$\binom{n}{m}$	Modal components of circumferential, m , and axial wavenumber, n , e.g. $\{k_m^{(n)} \equiv \mathbb{C} \mid n, m \in \mathbb{Z}, n \neq 0\}$.

expedient, on the one hand, to consider detailed analysis of the energy redistribution and mode conversion in the near-field to gain additional physical insight. On the other hand, the mathematical issues of completeness and convergence need to be addressed.

To understand the energy redistribution and mode conversion in the near-field e.g. from pump to pipe or across flange connections, an accurate coupled vibro-acoustic model of an infinite pipe needs to be formulated. In this paper we adopt the tailored Green's function/matrices as introduced in [5]. These functions deviate from the canonical free-space Green's function of acoustics, in that they satisfy additional boundary conditions – continuity at the fluid-structure interface. Here we consider only the tailored Green's matrices (excitation by ideal sources), while the generation of vibro-acoustic energy internally in a pump is not treated here. Due to the versatility of Green's formulation, see e.g. [7, 8], we can easily generalise to arbitrary sources generated by a pump or to finite and/or compound pipes with arbitrary boundary conditions and/or transition properties using the Boundary Integral Equations Method (BIEM), see e.g. [2–4, 7–14]. However, in the heavy fluid-loading format the problem becomes transcendental and the accuracy of the near-field solution is compromised by the computational efficiency when solved using the conventional weak solution form (integral average). Thus, the purpose of this paper is to improve both accuracy and computational efficiency of the solution by solving the forced vibration problem using modal decomposition (strong form).

The formulation of Green's matrix is based on the eigenfunction expansion method with the eigenvalues derived from the dispersion equation. This method is the most commonly used method in vibro-acoustic problems. In [3, 15–17] authors have employed specially derived orthogonality relations to decompose the governing equations into uncoupled algebraic modal equations which can easily be solved analytically; providing the strong solution form of Green's matrix. The decomposition is analogue to the decomposition of circumferential modes by orthogonality of trigonometric functions, see e.g. [2–4, 13, 14], however, with more advanced orthogonality relations between the involved eigenfunctions. In [3] this modal decomposition method was used for the acoustic duct where the 'more advanced' orthogonality relation reduces to orthogonality of cylindrical functions i.e. Bessel-functions, see relation in e.g. [18–20]. On the other hand, similar relations have been derived in [16, 17, 21–28] for plates, strips, layers, laminates, springs, beams, shells etc. and facilitated in e.g. [15–17] to analytically derive modal amplitudes for a strip, beam, spring and shell.

In this paper, we derive similar orthogonality relations for the elastic fluid-filled cylindrical shell and use these to decompose the transcendental forced vibration problem into algebraic modal equations. More importantly the orthogonality relations are generalised to any symmetric waveguide supporting wave-pairs, that is; waveguides having similar properties in opposite direction (\pm wavenumbers). The generalisation is done utilising Class properties similar to those defined in [29] and has to the best of the authors' knowledge not been done before.

The paper is structured as follows: Section 2 presents the governing equations, dispersion curves, definition of modal coefficients and Class properties. In Section 3 the (bi-)orthogonality relations for the fluid-filled shell as well as for general symmetric waveguides are derived. Section 4 illustrates how the (bi-)orthogonality relations are

used to decompose the equation system and derive modal amplitudes for Green's matrix analytically. With the general solution established using the modal decomposition method completeness and convergence (uniformity and rate) of the solution (Green's matrices) is assessed in Section 5. Finally, Section 6 highlights convenient features obtained using this method and further, derives and discuss the relation between the (bi-)orthogonality relation and the total energy flow. Details regarding the governing equations can be found in Appendix A.

2. Free waves in an elastic fluid-filled cylindrical shell

To assess vibrations in a fluid-filled shell considered as a multi-modal waveguide we employ the standard formulation for the fluid-structure interaction problem of a thin elastic cylindrical shell filled with an inviscid compressible fluid with no mean flow. The model is formulated in the framework of Novozhilov-Gol'denweizer's shell theory and standard linear acoustics and all necessary equations are derived from the action integral assuming time-harmonic vibrations. Details of the derivation of the equations of motion may be found in, for instance, [1, 2, 6].

In the following all equations are converted into non-dimensional form and the time-dependence, $\exp(-i\omega t)$, is omitted. Further, the axi-symmetry of the shell allows the m -spectra to be decoupled (indicated by the subscript, m) and each circumferential wavenumber can therefore be considered separately such that the circumferential-dependence, $\exp(-im\theta)$, may also be omitted. Similarly, the spatial distribution in the axial and radial direction is $\exp(kx)$ and $J_m(\kappa r)$, respectively. For consistency, details regarding the governing equations, conversion into dimensional quantities etc. are given in Appendix A and the definition of non-dimensional parameters in the nomenclature.

The waveguide properties of the fluid-filled shell are found from the dispersion equation deduced from the determinantal equation of Eq. (1).

$$\begin{vmatrix} d_{11} & d_{12} & d_{13} \\ d_{21} & d_{22} & d_{23} \\ d_{31} & d_{32} & d_{33} \end{vmatrix} = 0 \quad (1)$$

where the elements of the linear algebraic equation system are given in Eq. (2).

$$\begin{aligned} d_{11} &= -k^2 + \frac{1-\nu}{2}m^2 - \Omega^2 & d_{12} &= -\frac{1+\nu}{2}km = -d_{21} & d_{13} &= -\nu k = -d_{31} \\ d_{22} &= -\frac{1-\nu}{2}k^2 + m^2 - \Omega^2 + \frac{1}{12}\mu^2 \left[m^2 - 2(1-\nu)k^2 \right] \\ d_{23} &= m + \frac{1}{12}\mu^2 \left[m^3 - (2-\nu)k^2m \right] = d_{32} \\ d_{33} &= 1 + \frac{1}{12}\mu^2 (k^2 - m^2)^2 - \Omega^2 - \frac{\rho}{\mu}\Omega^2 J_m(\kappa) \left[\frac{dJ_m(\kappa r)}{dr} \Big|_{r=1} \right]^{-1} \end{aligned} \quad (2)$$

The dispersion curves for the fluid-filled shell vibrating in (a) bending mode, $m = 1$ and (b) $m = 3$, with the following non-dimensional parameters: $\rho = 0.1282$, $\gamma = 3.7773$ and $\mu = 0.0175$, are shown in Fig. 1 (colours recommended). These parameters are used throughout the paper and are similar to those in [2] against which the model is also validated. The latter non-dimensional parameters correspond to, for instance, a water-filled steel-shell with the properties: $E = 210$ GPa, $\nu = 0.3$, $\rho_{str} = 7800$ kg m⁻³, $R = 20$ mm, $h = 0.35$ mm, $\rho_{fl} = 1000$ kg m⁻³, $c_{fl} = 1440$ m s⁻¹.

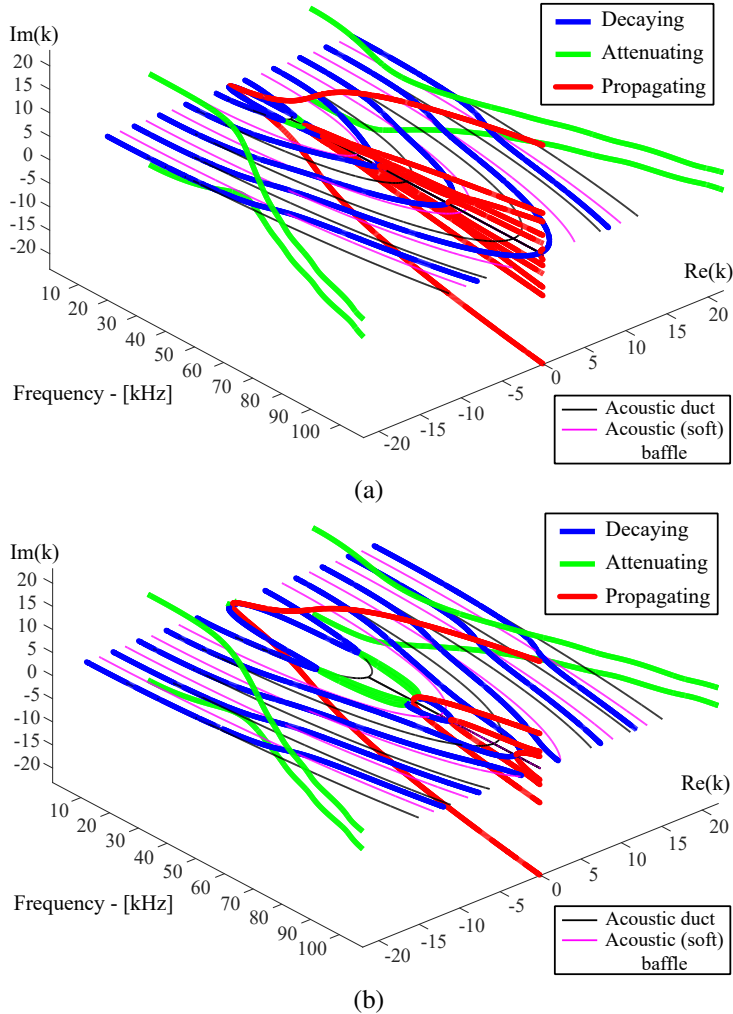


Fig. 1: Dispersion of free waves in a fluid-filled shell with the non-dimensional parameters: $\rho = 0.1282$, $\gamma = 3.7773$ and $\mu = 0.0175$ vibrating in (a) bending mode, $m = 1$ and (b) $m = 3$. Only decaying waves are shown for the acoustic duct and soft baffle. Colours recommended.

In the figures the dispersion curves are confined to displaying only the first 18 waves of the otherwise infinite number of waves carried by this type of waveguide. In the

absence of an acoustic medium ($\rho \rightarrow 0$), however, the dispersion equation reduces to a polynomial of 4th order in k^2 and 3rd order in Ω^2 . At any frequency this empty cylindrical shell supports only four pairs of waves, propagating/decaying in positive/negative direction of the waveguide (axial, x). The analysis of these waves is a standard subject fully covered in literature, see e.g. [30–32]. However, as soon as the interaction of a shell with a compressible fluid is introduced the dispersion equation becomes transcendental. Besides the four pairs of structure-originated waves, it captures infinitely many fluid-originated waves. Identification of these structure- and fluid-originated waves is based on inspection of the modal coefficients introduced in Eq. (3). This is also a subject already widely explored by other authors, mentioned in e.g. [1, 6, 32], and will therefore not be treated further in this paper.

In turn we note that at low frequencies higher order waves (blue) tend towards the waves of the acoustic duct (black) as seen in the figure. This entails that these higher order waves see the shell as rigid (a duct). However, as the frequency increase the fluid-originated (higher order) waves are influenced considerably by the structure such that at a certain frequency each fluid-wave collide with a wave of the acoustic (soft) baffle (magenta). This implies that the particular fluid-wave sees the shell as compliant (pressure release). Finally, by inspection (mapping of the imaginary waves onto the real plane) it can be shown that for increasing frequencies the location of these pressure release (acoustic baffle) points of the higher order fluid-waves tend towards the first structure-originated propagating wave. In particular, these frequencies are interesting for the near-field analysis as we may expect, besides a significant energy content, a substantial fluctuation/exchange of energy in the near-field response.

In terms of the scope of this paper it is, however, more interesting to note that Fig. 1 reveals certain important symmetry characteristics of such waveguides considered here. From the figure it is seen that the waveguide properties are symmetrically dispersed with respect to any of the coordinate planes – even for negative frequencies (not shown). The symmetry of the waveguide properties for negative frequencies is readily explained by the modelling of a time-harmonic conservative system in which energy does not dissipate, while the symmetry of positive/negative going waves are explained by the symmetry of the waveguide itself. The dispersion equation, Eq. (1), is formulated in even powers of the wavenumbers i.e. k^2 . From this it is clear that the waveguide supports wave-pairs of $\pm k$ and this defines its symmetry. Waveguides of such properties are, for instance, the elastic layer, [15, 23], the empty shell, [2], the acoustic duct and the fluid-filled shell without mean flow, [3]. In case of mean flow, the latter waveguides do not retain these symmetry properties i.e. spatial symmetry alone does not define a symmetric waveguide. In the following we will treat only symmetric waveguides as defined here.

2.1. Modal coefficients

Each wavenumber, $k_m^{(n)}$, found from the dispersion equation corresponds to a free wave in the fluid-filled shell i.e. $\{k_m^{(n)} \in \mathbb{C} \mid n, m \in \mathbb{Z}, n \neq 0\}$, which is characterised by its displacements, forces and velocity potential. Here we distinguish between the modal coefficients (indicated by $\bar{\cdot}$) defined as coefficients independent of the waveguide direction and the modal response involving modal coefficients, amplitudes and

the waveguide dependence, see Eq. (3) or Appendix A for further details. For definiteness, in what follows, the modal coefficients are defined by scaling the amplitudes with the amplitude of the lateral component of the displacement vector as seen in Eq. (4). This scaling can, however, be chosen freely.

$$\begin{aligned}
u_m^{(n)}(x) &= U_m^{(n)} \exp(k_m^{(n)} x) = \bar{u}_m^{(n)} W_m^{(n)} \exp(k_m^{(n)} x) \\
v_m^{(n)}(x) &= V_m^{(n)} \exp(k_m^{(n)} x) = \bar{v}_m^{(n)} W_m^{(n)} \exp(k_m^{(n)} x) \\
w_m^{(n)}(x) &= W_m^{(n)} \exp(k_m^{(n)} x) = \bar{w}_m^{(n)} W_m^{(n)} \exp(k_m^{(n)} x) \\
w_m^{\prime(n)}(x) &= W_m^{\prime(n)} \exp(k_m^{(n)} x) = \bar{w}_m^{\prime(n)} W_m^{(n)} \exp(k_m^{(n)} x) \\
\phi_m^{(n)}(x, r) &= \Phi_m^{(n)}(r) \exp(k_m^{(n)} x) = \bar{\phi}_m^{(n)}(r) W_m^{(n)} \exp(k_m^{(n)} x) \\
\vartheta_m^{(n)}(x, r) &= \mathcal{V}_m^{(n)}(r) \exp(k_m^{(n)} x) = \bar{\vartheta}_m^{(n)}(r) W_m^{(n)} \exp(k_m^{(n)} x) \\
p_m^{(n)}(x, r) &= P_m^{(n)}(r) \exp(k_m^{(n)} x) = \bar{p}_m^{(n)}(r) W_m^{(n)} \exp(k_m^{(n)} x) \\
Q_{lm}^{(n)}(x) &= Q_{lm}^{(n)} \exp(k_m^{(n)} x) = \bar{Q}_{lm}^{(n)} W_m^{(n)} \exp(k_m^{(n)} x) \\
&\quad \text{for } l = 1, \dots, 4
\end{aligned} \tag{3}$$

The latter modal coefficients are expressed in Eq. (4)–(6), where the displacement coefficients are derived from the linear equation system in Eq. (1), the force coefficients from the action integral (see Eq. (A.6)) and the velocity potential and acoustic variables from, respectively, the continuity condition in Eq. (A.4) and standard linear acoustics.

$$\begin{aligned}
\bar{u}_m^{(n)} &= \frac{U_m^{(n)}}{W_m^{(n)}} = \frac{d_{12}d_{23} - d_{13}d_{22}}{d_{11}d_{22} - d_{12}d_{21}} = \frac{\mathcal{P}_o(k^3, k^1)}{\mathcal{P}_d(k^4, k^2, k^0)} & \bar{w}_m^{(n)} &= \frac{W_m^{(n)}}{W_m^{(n)}} = 1 \\
\bar{v}_m^{(n)} &= \frac{V_m^{(n)}}{W_m^{(n)}} = -\frac{d_{11}d_{23} - d_{13}d_{21}}{d_{11}d_{22} - d_{12}d_{21}} = \frac{\mathcal{P}_e(k^4, k^2, k^0)}{\mathcal{P}_d(k^4, k^2, k^0)} & \bar{w}_m^{\prime(n)} &= \frac{W_m^{\prime(n)}}{W_m^{(n)}} = k_m^{(n)}
\end{aligned} \tag{4}$$

where $\mathcal{P}_o(k^3, k^1)$ is an odd polynomial in k^3 and k^1 , \mathcal{P}_e is an even polynomial and \mathcal{P}_d an even polynomial in the denominator. The coefficients of each polynomial are defined from the linear equation system in Eq. (1).

$$\begin{aligned}
\bar{Q}_{1m}^{(n)} &= k_m^{(n)} \bar{u}_m^{(n)} + m v \bar{v}_m^{(n)} + v \bar{w}_m^{(n)} \\
\bar{Q}_{2m}^{(n)} &= \frac{1-\nu}{2} \left[k_m^{(n)} \bar{v}_m^{(n)} - m \bar{u}_m^{(n)} \right] + \frac{1}{12} \mu^2 \left[2k_m^{(n)} (1-\nu) \bar{v}_m^{(n)} + 2k_m^{(n)} (1-\nu) m \bar{w}_m^{(n)} \right] \\
\bar{Q}_{3m}^{(n)} &= -\frac{1}{12} \mu^2 \left[k_m^{3(n)} \bar{v}_m^{(n)} - (2-\nu) m^2 k_m^{(n)} \bar{v}_m^{(n)} - (2-\nu) m k_m^{(n)} \bar{v}_m^{(n)} \right] \\
\bar{Q}_{4m}^{(n)} &= \frac{1}{12} \mu \left[k_m^{2(n)} \bar{w}_m^{(n)} - m^2 v \bar{w}_m^{(n)} - m v \bar{v}_m^{(n)} \right]
\end{aligned} \tag{5}$$

$$\bar{\phi}_m^{(n)}(r) = \frac{\Phi_m^{(n)}(r)}{W_m^{(n)}} = -i\Omega\gamma \left[\frac{dJ_m(\kappa_m^{(n)} r)}{dr} \right]_{r=1}^{-1} J_m(\kappa_m^{(n)} r) \tag{6}$$

$$\bar{\vartheta}_m^{(n)}(r) = k_m^{(n)} \bar{\varphi}_m^{(n)}(r) \quad \bar{p}_m^{(n)}(r) = i\Omega\gamma \bar{\phi}_m^{(n)}(r)$$

2.2. Properties of modal coefficients

By virtue of the symmetry of the waveguide (wave-pairs) it is seen that the modal coefficients in Eq. (4)–(6) have certain even/odd properties in k . For instance, $\bar{u}_m^{(n)}$ and $\bar{w}_m^{\prime(n)}$ are seen to be odd functions of k , while $\bar{v}_m^{(n)}$ and $\bar{w}_m^{(n)}$ are seen to be even functions. Likewise, if we consider the remaining modal coefficients in Eq. (5)–(6) we can divided these into classes of similar properties – consistent with the definition by D. J. Mead in [29]. Hence, the modal coefficients can be divided into classes of odd properties in k (Class A) and of even properties in k (Class B), as seen in Eq. (7).

$$\begin{aligned} \text{Class A – odd:} & \quad \left\{ \bar{u}_m^{(n)} \quad \bar{Q}_{2m}^{(n)} \quad \bar{Q}_{3m}^{(n)} \quad \bar{w}_m^{\prime(n)} \quad \bar{\vartheta}_m^{(n)}(r) \right\} \\ & \hspace{15em} (7) \\ \text{Class B – even:} & \quad \left\{ \bar{Q}_{1m}^{(n)} \quad \bar{v}_m^{(n)} \quad \bar{w}_m^{(n)} \quad \bar{Q}_{4m}^{(n)} \quad \bar{p}_m^{(n)}(r) \right\} \end{aligned}$$

From these classes some interesting properties can be observed. First, associated modal force/displacement coefficients are always of opposite Class e.g. $\bar{u}_m^{(n)}$ and $\bar{Q}_{1m}^{(n)}$. This is obvious as their product (and energy flow) must change sign when waves in the opposite direction are considered, see e.g. [11, 17, 29]. Second, if the amplitudes are scaled with $U_m^{(n)}$ rather than $W_m^{(n)}$ the Class A components, as defined here, become Class B components and vice versa. If, on the other hand, they are scaled with $V_m^{(n)}$ the Class definitions remain as defined here. This entails that the Class properties of the components may change (even \Leftrightarrow odd) but always generic for all components in the Class. These Class properties are, fortunately, generic properties of any symmetric waveguide.

3. (Bi-)orthogonality relation

In the previous section it was discussed that a fluid-filled shell with no mean flow constitutes a symmetric waveguide with convenient even/odd properties for its modal coefficients. Application of these properties are, based on e.g. [3, 15, 17, 21], hypothesised to reduce the complexity of the fluid-filled shell problem and permit derivation of essential formulae important to the physical interpretation of symmetric waveguides. Initially, we consider the conventional reciprocity relation in Eq. (B.1), formulated for any two general solutions at any two arbitrary locations; $x = a$ and $x = b$, see e.g. [21]. Derivation of the reciprocity relation for the fluid-filled shell can be found in [2]. The structure of this relation is dictated by the variational principle, which constitutes the correct pairs of generalised forces and displacements necessary to assemble the reciprocity relation. By virtue of 'by parts integration' each pair contains components of each Class (A and B) and the correctness of the formulation of forces/displacements is ensured through the Hamiltonian derivation.

If the reciprocity relation is written for any two free waves it reduces to the conventional orthogonality relation, see e.g. [16, 21–27, 33], which is characterised by wavenumbers $k_m^{(n)}$, $k_m^{(j)}$ and the modal response of Eq. (3). The relation thereby expands to Eq. (8) – shown in non-dimensional form with arbitrary amplitudes $W_m^{(n)}$ and

$W_m^{(j)}$.

$$\begin{aligned} & \left[\bar{Q}_{1m}^{(n)} \bar{u}_m^{(j)} + \bar{Q}_{2m}^{(n)} \bar{v}_m^{(j)} + \bar{Q}_{3m}^{(n)} \bar{w}_m^{(j)} + \mu \bar{Q}_{4m}^{(n)} \bar{w}'_m^{(j)} + i \frac{\rho}{\gamma^3 \mu \Omega} \int_0^1 \bar{p}_m^{(j)}(r) \bar{\vartheta}_m^{(n)}(r) r dr \right. \\ & \left. - \bar{Q}_{1m}^{(j)} \bar{u}_m^{(n)} - \bar{Q}_{2m}^{(j)} \bar{v}_m^{(n)} - \bar{Q}_{3m}^{(j)} \bar{w}_m^{(n)} - \mu \bar{Q}_{4m}^{(j)} \bar{w}'_m^{(n)} - i \frac{\rho}{\gamma^3 \mu \Omega} \int_0^1 \bar{p}_m^{(n)}(r) \bar{\vartheta}_m^{(j)}(r) r dr \right] \quad (8) \\ & \times W_m^{(n)} W_m^{(j)} \left[\exp([k_m^{(n)} + k_m^{(j)}]b) - \exp([k_m^{(n)} + k_m^{(j)}]a) \right] = 0 \end{aligned}$$

where the integral reduces to Lommel's integral which has a convenient analytical solution, see e.g. [18, 20].

Since the amplitudes are arbitrary and $a \neq b$ the relation is satisfied only when either of the expressions in square brackets are satisfied. The latter expression appears from the limits in the reciprocity relation and is satisfied only for opposite going waves of the same properties i.e. $n = -j$ ($\equiv k_m^{(n)} = -k_m^{(j)}$), and is therefore of no further interest. Equating to zero the former expression gives the modal (coefficient) orthogonality relation, which can by the Class properties be shown not to be satisfied for $n = -j$ and to be trivial, nonetheless satisfied, for $n = j$.

The trivial case, $n = j$, is not an authentic relation between waves of the dispersion equation since no degenerate roots exist in undamped conservative waveguides (as considered here). This was studied in [32] where it was shown that dispersion curves (waves) do not intersect but rather veer away or lock into complex (attenuating) waves to be unlocked again at higher frequencies. Nevertheless, intersection occurs (only) in the special case when waves transform from one type to another e.g. at cut-on frequencies ($k = 0$), where, for instance, decaying waves transform to propagating. Hence, the modal orthogonality and thereby the conventional orthogonality relation in Eq. (8) satisfying $n = j$ is not complete in its definition of orthogonality of waves. This entails that the modal orthogonality relation may be generalised further.

3.1. Derivation of the bi-orthogonality relation

Following [28] we consider the modal orthogonality relation for any two distinct wavenumbers, $k_m^{(l)}$ and $k_m^{(j)}$.

$$\begin{aligned} & \left[\bar{Q}_{1m}^{(l)} \bar{u}_m^{(j)} + \bar{Q}_{2m}^{(l)} \bar{v}_m^{(j)} + \bar{Q}_{3m}^{(l)} \bar{w}_m^{(j)} + \mu \bar{Q}_{4m}^{(l)} \bar{w}'_m^{(j)} + i \frac{\rho}{\gamma^3 \mu \Omega} \int_0^1 \bar{p}_m^{(j)}(r) \bar{\vartheta}_m^{(l)}(r) r dr \quad l \neq -j \right. \\ & \left. - \bar{Q}_{1m}^{(j)} \bar{u}_m^{(l)} - \bar{Q}_{2m}^{(j)} \bar{v}_m^{(l)} - \bar{Q}_{3m}^{(j)} \bar{w}_m^{(l)} - \mu \bar{Q}_{4m}^{(j)} \bar{w}'_m^{(l)} - i \frac{\rho}{\gamma^3 \mu \Omega} \int_0^1 \bar{p}_m^{(l)}(r) \bar{\vartheta}_m^{(j)}(r) r dr \right] = 0 \quad (9) \end{aligned}$$

Now, subtract the latter by the modal orthogonality relation from Eq. (8) and let l be the opposite going wave of n such that $k_m^{(l)} = k_m^{(-n)} = -k_m^{(n)}$, then the identities in

Eq. (10) hold by virtue of the Class properties in Eq. (7).

$$\begin{aligned}
\text{Class A: } \quad & \bar{u}_m^{(l)} = -\bar{u}_m^{(n)} & \bar{Q}_{2m}^{(l)} = -\bar{Q}_{2m}^{(n)} & \bar{Q}_{3m}^{(l)} = -\bar{Q}_{3m}^{(n)} \\
& \bar{w}_m^{(l)} = -\bar{w}_m^{(n)} & \bar{\vartheta}_m^{(l)}(r) = -\bar{\vartheta}_m^{(n)}(r) & \\
\text{Class B: } \quad & \bar{Q}_{1m}^{(l)} = \bar{Q}_{1m}^{(n)} & \bar{v}_m^{(l)} = \bar{v}_m^{(n)} & \bar{w}_m^{(l)} = \bar{w}_m^{(n)} \\
& \bar{Q}_{4m}^{(l)} = \bar{Q}_{4m}^{(n)} & \bar{p}_m^{(l)}(r) = \bar{p}_m^{(n)}(r) &
\end{aligned} \tag{10}$$

Employing the latter identities we arrive at the reduced relation in Eq. (11) valid for $n^2 \neq j^2$.

$$\bar{Q}_{1m}^{(j)} \bar{u}_m^{(n)} + \mu \bar{Q}_{4m}^{(j)} \bar{w}_m^{(n)} = i \frac{\rho}{\gamma^3 \mu \Omega} \int_0^1 \bar{p}_m^{(j)}(r) \bar{\vartheta}_m^{(n)}(r) r dr + \bar{Q}_{2m}^{(n)} \bar{v}_m^{(j)} + \bar{Q}_{3m}^{(n)} \bar{w}_m^{(j)} \quad n^2 \neq j^2 \tag{11}$$

This relation comprises two relations as the indices n and j are interchangeable – following directly from the derivation. The relation(s) is denoted “*The bi-orthogonality relation*” which is valid for an elastic fluid-filled cylindrical shell with no mean flow and is, to the best of the authors’ knowledge, derived here for the first time. The bi-orthogonality relation (either one) provides the complete definition of (bi-)orthogonality of waves of different magnitude i.e. orthogonality of wave-pairs, and holds also for the special case of degenerate wave-pairs, $k_m^{(\pm j)} = k_m^{(\pm n)} = 0$, where waves transform e.g. from decaying to propagating waves.

The corresponding orthogonality relation valid for any two waves of the dispersion equation is written as in Eq. (12) in terms of the modal response. Note that the r -dependence of the acoustic variables are omitted hereinafter.

$$\left[\bar{Q}_{1m}^{(j)} u_m^{(n)} + \mu \bar{Q}_{4m}^{(j)} w_m^{(n)} - i \frac{\rho}{\gamma^3 \mu \Omega} \int_0^1 p_m^{(j)} \vartheta_m^{(n)} r dr - \bar{Q}_{2m}^{(n)} v_m^{(j)} - \bar{Q}_{3m}^{(n)} w_m^{(j)} \right]_{x=a}^{x=b} = 0 \quad n \neq j \tag{12}$$

Comparing the conventional orthogonality relation in Eq. (8) with the orthogonality relation in Eq. (12) (and the corresponding one with interchanged indices) it is seen that the conventional orthogonality relation is separated into two relations. As will be discussed in Sec. 6.3 the (bi-)orthogonality relation is a much stronger statement than the conventional orthogonality relation from the viewpoint of physical interpretation and application – especially in forced vibration problems as will be seen in Sec. 4.

Further, it is clear from this derivation, in particular Eq. (10), that given the Class properties it is straightforward to derive the (bi-)orthogonality relation for symmetric waveguides as it follows directly from the Classes i.e. the kinematic variables of Class A gather (with their respective counterparts) on one side of the equality sign and the force variables of Class A (also with their respective counterparts) on the other, see Eq. (11).

Finally, useful limit cases can be retrieved from the bi-orthogonality relation for the

elastic fluid-filled cylindrical shell. For instance, we can retrieve the bi-orthogonality relation for the empty shell by letting ρ go to zero and γ to infinity or for the classical Bernoulli-Euler (BE) beam by assuming an empty shell, vibrating in breathing mode ($m = 0$) with no Poisson coupling ($\nu = 0$) between u and w or for the acoustic duct by letting ρ and γ go to infinity. The corresponding bi-orthogonality relations are shown in Eq. (13). Remark that the bi-orthogonality relation for the acoustic duct reduce to orthogonality of cylindrical functions (Bessel-functions).

$$\begin{aligned}
\bar{Q}_{1m}^{(j)} \bar{u}_m^{(n)} + \mu \bar{Q}_{4m}^{(j)} \bar{w}_m^{\prime(n)} - \bar{Q}_{2m}^{(n)} \bar{v}_m^{(j)} - \bar{Q}_{3m}^{(n)} \bar{w}_m^{(j)} &= 0 && \text{(Empty shell)} \\
\mu \bar{Q}_{4m=0}^{(j)} \bar{w}_0^{\prime(n)} - \bar{Q}_{3m=0}^{(n)} \bar{w}_0^{(j)} &= k^{(j)2} k^{(n)} + k^{(j)3} = 0 && \text{(Bernoulli-Euler beam)} \quad (13) \\
\int_0^1 \bar{p}_m^{(j)} \bar{\vartheta}_m^{(n)} r dr &= \int_0^1 J_m(\kappa_m^{(j)} r) J_m(\kappa_m^{(n)} r) r dr = 0 && \text{(Acoustic duct)} \\
&&& \text{for } n^2 \neq j^2
\end{aligned}$$

Notice here that the relation for the empty shell and BE beam, also derived in [17], constitutes algebraic equations because the shell/beam is a 1D waveguide and supports a finite number of waves – 8 and 4, respectively. The relation for the acoustic duct, used in [3], is, however, formulated on integral form as it is a continuous waveguide in r (2D) and thereby captures infinitely many waves. For the fluid-filled shell the relation is on mixed algebraic-integral form because the waveguide is a composite waveguide comprising both 1- and 2D components. Finally, note that verification of each of these relations can easily be done by substituting any two waves (not opposite going, $\pm k$) of their dispersion equation into the relation.

3.2. Generalisation of the (bi-)orthogonality relation for symmetric waveguides

From Sec. 3.1 it follows that the general reciprocity relation for the fluid-filled shell with no mean flow can be used to formulate the orthogonality relation and further the bi-orthogonality relation for wave-pairs by utilising symmetry of the waveguide (Class properties). This generalisation is therefore valid for eigenfunctions of any symmetric waveguide.

For a waveguide with the aforementioned symmetry properties the generalised forces and displacements can be formulated in terms of modal coefficients with Class properties similar to those defined in Sec. 2.2. For the n^{th} free wave, displacements, $\mathbf{U}^{(n)}(x)$, and forces, $\mathbf{Q}^{(n)}(x)$, may be written as in Eq. (14).

$$\begin{aligned}
\mathbf{U}^{(n)}(x) &= \mathbf{U}^{(n)} f^{(n)}(x) = \begin{pmatrix} \bar{\mathbf{U}}_A^{(n)} \\ \bar{\mathbf{U}}_B^{(n)} \end{pmatrix} U^{(n)} f^{(n)}(x) \\
\mathbf{Q}^{(n)}(x) &= \mathcal{L}_{B/A} \mathbf{U}^{(n)}(x) = \begin{pmatrix} \bar{\mathbf{Q}}_B^{(n)} \\ \bar{\mathbf{Q}}_A^{(n)} \end{pmatrix} U^{(n)} f^{(n)}(x)
\end{aligned} \tag{14}$$

where $\mathbf{U}^{(n)}(x)$ is a function of the coordinate, x , along the waveguides' propagation direction, $\mathbf{U}^{(n)}$ is the amplitude vector, $f^{(n)}(x)$ is a harmonic function, $U^{(n)}$ is the scaling

amplitude and $\bar{\mathbf{U}}_{A/B}^{(n)}$ and $\bar{\mathbf{Q}}_{A/B}^{(n)}$ are the modal coefficients with Class A and B properties. Note that the modal coefficients may be im-/explicit functions of variables not in the propagation direction such as frequency and spatial coordinates. Further, $\mathbf{Q}^{(n)}(x)$ is derived from the generalised displacements through a differential operator of 'Class derivatives', $\mathcal{L}_{B/A}$, meaning that $\bar{\mathbf{U}}_A^{(n)}$ transforms to $\bar{\mathbf{Q}}_B^{(n)}$ and $\bar{\mathbf{U}}_B^{(n)}$ to $\bar{\mathbf{Q}}_A^{(n)}$ when acted on by the differential operator. Hence, the elements of $\mathbf{U}^{(n)}$ corresponds directly to the elements of $\mathbf{Q}^{(n)}$ as discussed in Sec. 2.2 i.e. $\bar{\mathbf{U}}_A^{(n)} \sim \bar{\mathbf{Q}}_B^{(n)}$ and $\bar{\mathbf{U}}_B^{(n)} \sim \bar{\mathbf{Q}}_A^{(n)}$.

From these generalised forces and displacements, the general reciprocity relation is formulated as the inner product, $\langle \cdot, \cdot \rangle$, between force/displacement vectors. The conventional orthogonality relation is then retrieved from the general reciprocity relation by considering any two free waves, n and j , as seen in Eq. (15).

$$\left\langle \left\langle \begin{matrix} \mathbf{U}^{(j)}(x) \\ \mathbf{Q}^{(j)}(x) \end{matrix}, \begin{matrix} \mathbf{Q}^{(n)}(x) \\ -\mathbf{U}^{(n)}(x) \end{matrix} \right\rangle \right\rangle_{x=a}^{x=b} = \left\langle \left\langle \begin{matrix} \mathbf{U}_A^{(j)} \\ \mathbf{U}_B^{(j)} \\ \mathbf{Q}_B^{(j)} \\ \mathbf{Q}_A^{(j)} \end{matrix}, \begin{matrix} \mathbf{Q}_B^{(n)} \\ \mathbf{Q}_A^{(n)} \\ -\mathbf{U}_A^{(n)} \\ -\mathbf{U}_B^{(n)} \end{matrix} \right\rangle \right\rangle U^{(j)} U^{(n)} [f^{(j)}(x)f^{(n)}(x)]_{x=a}^{x=b} = 0 \quad (15)$$

where the sign in front of $\mathbf{U}^{(n)}(x)$ can be placed arbitrarily and $-$ is omitted here and in what follows.

As implied by the inner product, modal coefficients are integrated over explicit variables not in the propagation direction as seen, for instance, for the acoustic part in Eq. (11), the acoustic duct in Eq. (13), the elastic cylinder of general cross-section in [28] or the elastic layer in [15, 16, 23]. Thus, as implied by the inner product, Eq. (15) is valid for any waveguide symmetric in the propagation direction.

As before, since the amplitudes are arbitrary for free-waves and $a \neq b$, only the square brackets are of interest. Again, the harmonic functions ensure that $[f^{(j)}(x)f^{(n)}(x)]_{x=a}^{x=b} = 0$ only for opposite going waves ($k_m^{(j)} = -k_m^{(n)}$), whereas the modal orthogonality relation, Eq. (16), is ensured for all other waves of the dispersion equation. As discussed, there exist no degenerate roots in the dispersion equation of undamped conservative symmetric waveguides, see e.g. [32], and so Eq. (16) does not constitute the complete definition of orthogonality of waves in symmetric waveguides.

$$\left\langle \left\langle \begin{matrix} \mathbf{U}_A^{(j)} \\ \mathbf{U}_B^{(j)} \\ \mathbf{Q}_B^{(j)} \\ \mathbf{Q}_A^{(j)} \end{matrix}, \begin{matrix} \mathbf{Q}_B^{(n)} \\ \mathbf{Q}_A^{(n)} \\ -\mathbf{U}_A^{(n)} \\ -\mathbf{U}_B^{(n)} \end{matrix} \right\rangle \right\rangle = 0 \quad n \neq -j \quad (16)$$

Instead, to arrive at the bi-orthogonality relation, we expand the relation to wave-pairs rather than individual waves and apply linearity of the inner product as seen in

Eq. (17).

$$\begin{aligned}
\left\langle \begin{pmatrix} \mathbf{U}_A^{(j)} \\ \mathbf{U}_B^{(j)} \\ \mathbf{Q}_B^{(j)} \\ \mathbf{Q}_A^{(j)} \end{pmatrix}, \begin{pmatrix} \mathbf{Q}_B^{(n)} \\ \mathbf{Q}_A^{(n)} \\ -\mathbf{U}_A^{(n)} \\ -\mathbf{U}_B^{(n)} \end{pmatrix} \right\rangle &= \left\langle \begin{pmatrix} \mathbf{U}_A^{(j)} \\ \mathbf{U}_B^{(j)} \\ \mathbf{Q}_B^{(j)} \\ \mathbf{Q}_A^{(j)} \end{pmatrix}, \begin{pmatrix} \mathbf{Q}_B^{(-n)} \\ \mathbf{Q}_A^{(-n)} \\ -\mathbf{U}_A^{(-n)} \\ -\mathbf{U}_B^{(-n)} \end{pmatrix} \right\rangle = 0 \\
\Downarrow & \\
\left\langle \begin{pmatrix} \mathbf{U}_A^{(j)} \\ \mathbf{U}_B^{(j)} \\ \mathbf{Q}_B^{(j)} \\ \mathbf{Q}_A^{(j)} \end{pmatrix}, \left[\begin{pmatrix} \mathbf{Q}_B^{(n)} \\ \mathbf{Q}_A^{(n)} \\ -\mathbf{U}_A^{(n)} \\ -\mathbf{U}_B^{(n)} \end{pmatrix} \pm \begin{pmatrix} \mathbf{Q}_B^{(-n)} \\ \mathbf{Q}_A^{(-n)} \\ -\mathbf{U}_A^{(-n)} \\ -\mathbf{U}_B^{(-n)} \end{pmatrix} \right] \right\rangle &= 0
\end{aligned} \tag{17}$$

Again, confer to the Class properties of the modal coefficients the following identities hold:

$$\mathbf{Q}_A^{(-n)} = -\mathbf{Q}_A^{(n)} \quad \mathbf{U}_A^{(-n)} = -\mathbf{U}_A^{(n)} \quad \mathbf{Q}_B^{(-n)} = \mathbf{Q}_B^{(n)} \quad \mathbf{U}_B^{(-n)} = \mathbf{U}_B^{(n)}$$

Substituting these into Eq. (17) the bi-orthogonality relation for wave-pairs is expressed as in Eq. (18).

$$\left\langle \begin{pmatrix} \mathbf{U}_A^{(j)} \\ \mathbf{U}_B^{(j)} \\ \mathbf{Q}_B^{(j)} \\ \mathbf{Q}_A^{(j)} \end{pmatrix}, \left[\begin{pmatrix} \mathbf{Q}_B^{(n)} \\ \mathbf{Q}_A^{(n)} \\ -\mathbf{U}_A^{(n)} \\ -\mathbf{U}_B^{(n)} \end{pmatrix} \pm \begin{pmatrix} \mathbf{Q}_B^{(n)} \\ -\mathbf{Q}_A^{(n)} \\ \mathbf{U}_A^{(n)} \\ -\mathbf{U}_B^{(n)} \end{pmatrix} \right] \right\rangle = 0 \quad n^2 \neq j^2 \tag{18}$$

Now, consider either of the latter \pm cases we arrive at the bi-orthogonality relation formulated for wave-pairs. The upper in Eq. (19) is the + case and the lower the - case.

$$\begin{aligned}
\left\langle \begin{pmatrix} \mathbf{U}_A^{(j)} \\ \mathbf{U}_B^{(j)} \\ \mathbf{Q}_B^{(j)} \\ \mathbf{Q}_A^{(j)} \end{pmatrix}, 2 \begin{pmatrix} \mathbf{Q}_B^{(n)} \\ 0 \\ 0 \\ -\mathbf{U}_B^{(n)} \end{pmatrix} \right\rangle &\Rightarrow \left\langle \begin{pmatrix} \mathbf{U}_A^{(j)} \\ \mathbf{U}_B^{(j)} \\ \mathbf{Q}_B^{(n)} \\ \mathbf{Q}_A^{(n)} \end{pmatrix}, \begin{pmatrix} \mathbf{Q}_B^{(n)} \\ -\mathbf{U}_B^{(n)} \end{pmatrix} \right\rangle = 0 \\
& \left\langle \begin{pmatrix} \mathbf{U}_B^{(j)} \\ \mathbf{Q}_B^{(j)} \end{pmatrix}, \begin{pmatrix} \mathbf{Q}_A^{(n)} \\ -\mathbf{U}_A^{(n)} \end{pmatrix} \right\rangle = 0
\end{aligned} \tag{19}$$

Note that since the sign is arbitrary (discussed earlier) each relation can be obtained from the other by a simple index interchange. In conclusion, it is clear that each pair of \pm waves is bi-orthogonal to any other wave-pair. This simply means that the set of Class B functions $\begin{pmatrix} \mathbf{U}_B^{(\pm j)} \\ \mathbf{Q}_B^{(\pm j)} \end{pmatrix}$ is bi-orthogonal to the set of Class A functions $\begin{pmatrix} \mathbf{Q}_A^{(\pm n)} \\ -\mathbf{U}_A^{(\pm n)} \end{pmatrix}$, where $\pm j$ and $\pm n$ indicate wave-pairs.

Finally, the corresponding orthogonality relation is expressed as in Eq. (20), formulated in terms of its modal response.

$$\left\langle \begin{pmatrix} \mathbf{U}^{(j)} \\ \mathbf{Q}_A^{(j)} \end{pmatrix}, \begin{pmatrix} \mathbf{Q}_B^{(n)} \\ -\mathbf{U}_B^{(n)} \end{pmatrix} \right\rangle U^{(j)} U^{(n)} [f^{(j)}(x) f^{(n)}(x)]_{x=a}^{x=b} = 0 \quad n \neq j \quad (20)$$

4. Green's matrix

By definition Green's matrix is the general solution to the inhomogeneous problem with a point force/source (modelled as a delta-function) applied at an arbitrarily chosen excitation point, (ξ, r_0) , inside the domain under consideration, see e.g. [7, 8]. In this paper, a tailored modal Green's matrix is derived, which satisfy the interfacial conditions at the fluid-structure interface. Since Green's matrix is derived for each circumferential mode, ring sources distributed with the circumferential wavenumber are considered. From the reciprocity relation in Eq. (B.1) it is clear that there is a total of 5 fundamental loading conditions. For the fluid-filled shell the response to the load vector; $\mathbf{q}_m^{01} = [q_{1m}^{01}, q_{2m}^{01}, q_{3m}^{01}, T_m^{01}]^T = [-\delta(x - \xi), 0, 0, 0]^T$ constitutes the first row in Green's matrix, the second row is the response to; $\mathbf{q}_m^{02} = [0, -\delta(x - \xi), 0, 0]^T$, the third to; $\mathbf{q}_m^{03} = [0, 0, -\delta(x - \xi), 0]^T$, the fourth (bending moment) to; $\mathbf{q}_m^{04} = [0, 0, -\frac{\partial \delta(x - \xi)}{\partial \xi}, 0]^T$ and the fifth to an acoustic monopole given as; $\mathbf{q}_m^{05} = [0, 0, 0, -\frac{1}{r} \delta(x - \xi) \delta(r - r_0)]^T$, since the acoustic domain is continuous in r .

For linear boundary value problems as the one treated in this section the superposition principle in terms of the auxiliary Green's matrix is a strong tool in solving general forcing problems and, in particular, when introducing Boundary Integral Equations, see e.g. [9, 10]. The general response to an arbitrary load/source is retrieved through its convolution with Green's matrix as shown in Eq. (21) for the problem treated in this paper. Derivation of the properties of Green's matrix/function can be found in e.g. [7, 8].

$$\mathbf{u}_m(x, r) = \int_a^b \int_0^1 \mathbf{G}_m(x, \xi, r, r_0) \mathbf{q}_m(\xi, r_0) r_0 dr_0 d\xi \quad (21)$$

where $\mathbf{G}_m(x, \xi, r, r_0)$ is the kernel of the convolution (Green's matrix) and $\mathbf{u}_m(x, r)$ is the forced response to the arbitrary load/source, \mathbf{q}_m , formulated in (ξ, r_0) .

To obtain the general solution of the forced vibration problem (Green's matrix) the solution ansatz from Eq. (3) is expanded on its modes and the coordinate shift $\hat{x} = x - \xi$ is introduced. The shift ensures alignment of the origin with the excitation point, ξ , such that symmetry of the infinite waveguide (general solution) is retained. Due to the symmetry, the general solution adopts the Class properties of Eq. (7) also in the x -coordinate, where the content of the Classes are determined by the component loaded, see [29]. Note here that in this general set-up symmetry of each mode is not ensured since the relation between positive and negative going waves (wave-pairs) is yet to be

established. This relation is introduced in Sec. 4.3.

Now, using symmetry of the infinite waveguide the initial problem can, straightforwardly, be reformulated into a homogeneous problem with a set of both homogeneous and inhomogeneous boundary conditions at the excitation point, see e.g. [34]. This corresponds to dividing the shell into two semi-infinite segments separated at the excitation point. The set of boundary conditions constitute continuity in all variables across the two semi-infinite domains (homogeneous) except for a unit-jump in the loaded component (inhomogeneous), formulated as; $-\frac{1}{2}\text{sgn}(x - \xi)$, due to symmetry of the waveguide.

4.1. Derivation of modal amplitudes

Consider a radial point force applied on the shell wall with the circumferential wavenumber, m , and in accordance with the latter i.e. with a unit-jump and continuity in all other variables at $x \rightarrow \xi$. Since Class B functions, by definition, ensure continuity (even functions), the continuity conditions at $x \rightarrow \xi$ are formulated only for Class A functions. For these functions continuity is ensured only when passing zero at the excitation point and so the set of boundary conditions reduce to Eq. (22). Note that since Q_{3m} is loaded by an odd function in x and an even in k the components of the Classes of Eq. (7) interchange with respect to k but remain for x , while for a load in Q_{1m} the components interchange with respect to x but remain for k .

$$\begin{aligned}
 u_m^{03} &= \sum_{n=1}^{\infty} u_m^{03(n)} = 0 & w_m'^{03} &= \sum_{n=1}^{\infty} w_m'^{03(n)} = 0 \\
 Q_{2m}^{03} &= \sum_{n=1}^{\infty} Q_{2m}^{03(n)} = 0 & \vartheta_m^{03}(r) &= \sum_{n=1}^{\infty} \vartheta_m^{03(n)}(r) = 0 & x \rightarrow \xi & \quad (22) \\
 Q_{3m}^{03} &= \sum_{n=1}^{\infty} Q_{3m}^{03(n)} = -\frac{1}{2}\text{sgn}(x - \xi)
 \end{aligned}$$

where (x, ξ) is omitted as the equations are formulated at the boundary for $x \rightarrow \xi$ and 03 indicates that the unit-jump is applied in Q_{3m} – the third fundamental loading condition.

From Eq. (22) it appears that there are only five equations but infinitely many modal amplitudes to be determined. Conventionally, the number of waves are truncated to a finite, usually relatively low, number of waves (7-10 waves) and the remaining equations are found by averaging e.g. through Galerkin orthogonalisation, see [2]. Instead the bi-orthogonality relation can be used to decouple the system into modal equations similar to what has already been done for the circumferential modes.

Following [17] we multiply each of the five equations in Eq. (22) with its associated j^{th} modal force-/displacement and sum the conditions according to the bi-

orthogonality relation to arrive at Eq. (23).

$$\sum_{n=1}^{\infty} \left[\bar{Q}_{1m}^{(j)} u_m^{03(n)} + \mu \bar{Q}_{4m}^{(j)} w_m'^{03(n)} - i \frac{\rho}{\gamma^3 \mu \Omega} \int_0^1 \bar{p}_m^{(j)} \bar{\vartheta}_m^{03(n)} r dr - \bar{Q}_{2m}^{03(n)} \bar{v}_m^{(j)} - \bar{Q}_{3m}^{03(n)} \bar{w}_m^{(j)} \right] = \frac{1}{2} w_m^{(j)} \quad (23)$$

where (r) on the acoustic variables is omitted and further, only the right segment of the semi-infinite shell is considered for simplicity. Thus, for $x \rightarrow \xi$ with $x > \xi$ such that $\text{sgn}(x - \xi)$ and $\exp(k_m^{(n)}(x - \xi))$ approach 1, the equation may be written in terms of modal coefficients, see Eq. (24).

$$\sum_{n=1}^{\infty} \left[\bar{Q}_{1m}^{(j)} \bar{u}_m^{(n)} + \mu \bar{Q}_{4m}^{(j)} \bar{w}_m'^{(n)} - i \frac{\rho}{\gamma^3 \mu \Omega} \int_0^1 \bar{p}_m^{(j)} \bar{\vartheta}_m^{(n)} r dr - \bar{Q}_{2m}^{(n)} \bar{v}_m^{(j)} - \bar{Q}_{3m}^{(n)} \bar{w}_m^{(j)} \right] W_m^{03(n)} W_m^{03(j)} = \frac{1}{2} \bar{w}_m^{(j)} W_m^{03(n)} \quad (24)$$

Note here that only the modal amplitudes preserve the load index as the sum in square brackets is invariant to load and amplitude. Comparing this sum to Eq. (11) it is seen to contain the bi-orthogonality relation and is therefore denoted the modal relation, $\bar{R}_m^{(n,j)}$, defined as in Eq. (25), whereas its physical meaning is discussed in Sec. 6.3.

$$\bar{R}_m^{(n,j)} = \bar{Q}_{1m}^{(j)} \bar{u}_m^{(n)} + \mu \bar{Q}_{4m}^{(j)} \bar{w}_m'^{(n)} - i \frac{\rho}{\gamma^3 \mu \Omega} \int_0^1 \bar{p}_m^{(j)} \bar{\vartheta}_m^{(n)} r dr - \bar{Q}_{2m}^{(n)} \bar{v}_m^{(j)} - \bar{Q}_{3m}^{(n)} \bar{w}_m^{(j)} \quad (25)$$

where $\{ \bar{R}_m^{(n,j)} \mid n^2 \neq j^2 \} = \{0\}$

Now, Eq. (24) can be simplified by applying the modal relation in Eq. (25) in which it is stated that for $n^2 \neq j^2$ the waves are bi-orthogonal and the relation equates to zero. Thus, we arrive at Eq. (26).

$$\bar{R}_m^{(n,n)} W_m^{03(n)} = \left[\bar{Q}_{1m}^{(n)} \bar{u}_m^{(n)} + \mu \bar{Q}_{4m}^{(n)} \bar{w}_m'^{(n)} - i \frac{\rho}{\gamma^3 \mu \Omega} \int_0^1 \bar{p}_m^{(n)} \bar{\vartheta}_m^{(n)} r dr - \bar{Q}_{2m}^{(n)} \bar{v}_m^{(n)} - \bar{Q}_{3m}^{(n)} \bar{w}_m^{(n)} \right] W_m^{03(n)} = \frac{1}{2} \bar{w}_m^{(n)} \quad (26)$$

from which it is straightforward to solve explicitly for the modal amplitudes, see Eq. (27). In addition, we note from the derivation that n can be chosen freely such that we arrive at a set of uncoupled equations for $n \in \mathbb{N}$. Recall that $\bar{w}_m^{(n)} \equiv 1$ in this paper, see Eq. (4).

$$W_m^{03(n)} = \frac{1}{2} \frac{\bar{w}_m^{(n)}}{\bar{R}_m^{(n,n)}} \quad n \in \mathbb{N} \quad (27)$$

From the derivation it is seen that the problem of finding modal amplitudes can be decomposed into an explicit algebraic equation for each modal amplitude by means of

the bi-orthogonality relation. Remark that this decomposition method, using proper (bi-)orthogonality relations, is analogue to what has been done for the acoustic duct in [3], the elastic layer in [15, 16] and the beam, empty shell and helical spring in [17].

For the limit cases in Eq. (13) the load-independent modal relation, $\bar{R}_m^{(n,n)}$, from Eq. (25) reduce to Eq. (28). For the case of an acoustic duct the definition of $\bar{\phi}_m^{(n)}(r)$ is different than that of Eq. (6) and cannot be retrieved from the limits used in Eq. (13). See [3] for details.

$$\bar{R}_m^{(n,n)} = \bar{Q}_{1m}^{(n)} \bar{u}_m^{(n)} + \mu \bar{Q}_{4m}^{(n)} \bar{w}_m^{(n)} - \bar{Q}_{2m}^{(n)} \bar{v}_m^{(n)} - \bar{Q}_{3m}^{(n)} \bar{w}_m^{(n)} \quad (\text{Empty shell})$$

$$\bar{R}_0^{(n,n)} = \mu \bar{Q}_{4m=0}^{(n)} \bar{w}_0^{(n)} - \bar{Q}_{3m=0}^{(n)} \bar{w}_0^{(n)} = \frac{1}{6} \mu^2 k^{(n)3} \quad (\text{Bernoulli-Euler beam}) \quad (28)$$

$$\bar{R}_m^{(n,n)} = -i \frac{\rho}{\gamma^3 \mu \Omega} \int_0^1 \bar{p}_m^{(n)} \bar{\vartheta}_m^{(n)} r dr = \frac{\rho}{\gamma^2 \mu} k_m^{(n)} \int_0^1 J_m(\kappa_m^{(n)} r)^2 r dr \quad (\text{Acoustic duct})$$

Remark that $\bar{R}_m^{(n,n)}$ belongs to Class A by virtue of the product between odd/even functions such that the amplitudes in Eq. (27) are also Class A.

4.2. Green's matrix – Remaining loading conditions

To formulate Green's matrix for the complete set of fundamental loading conditions and thereby ensure compatibility with any arbitrary forcing condition the modal amplitudes for the remaining structural and acoustic fundamental loading conditions are derived following the procedure in Sec. 4.1. However, to get skew-symmetric/symmetric elements in Green's matrix the applied loads are scaled as shown in Eq. (29). Again we consider only the right-hand semi-infinite shell ($x \rightarrow \xi$ with $x > \xi$) and may therefore omit (x, ξ) . Note that the radial delta-function of the acoustic monopole cannot be reformulated further due to lack of symmetry.

$$Q_{1m}^{01} = -\frac{1}{2} \quad Q_{2m}^{02} = -\frac{1}{2} \quad Q_{4m}^{04} = -\frac{1}{2\mu} \quad \vartheta_m^{05}(r, r_0) = -\frac{1}{2r_0} \frac{\gamma^2 \mu}{\rho} \delta(r - r_0) \quad (29)$$

From these loading conditions the governing equation for the remaining modal amplitudes become

$$\begin{aligned} \bar{R}_m^{(n,n)} W_m^{01(n)} &= -\frac{1}{2} \bar{u}_m^{(n)} & \bar{R}_m^{(n,n)} W_m^{02(n)} &= \frac{1}{2} \bar{v}_m^{(n)} \\ \bar{R}_m^{(n,n)} W_m^{04(n)} &= -\frac{1}{2} \bar{w}_m^{(n)} & \bar{R}_m^{(n,n)} W_m^{05(n)} &= \frac{1}{2} \frac{i}{\gamma \Omega} \bar{p}_m^{(n)} \Big|_{r=r_0} \end{aligned} \quad (30)$$

By comparing Eq. (30) with Eq. (26) where only the right-hand-side change due to the generic property of $\bar{R}_m^{(n,n)}$ (independent of the applied load), it is seen that the amplitudes of any fundamental loading condition can be expressed in terms of any other fundamental loading condition by a simple modal scaling. This conveniently allow us to express the modal amplitudes in Eq. (30) via, for instance, the modal

amplitudes of the radial force, see Eq. (31), in which $\bar{w}_m^{(n)} \equiv 1$. Again, we note the Class properties of the amplitudes.

$$\begin{aligned} \text{Class A: } W_m^{03(n)} &= \frac{1}{2} \frac{\bar{w}_m^{(n)}}{\bar{R}_m^{(n,n)}} & W_m^{02(n)} &= \bar{v}_m^{(n)} \frac{W_m^{03(n)}}{\bar{w}_m^{(n)}} \\ W_m^{05(n)} &= \frac{i}{\gamma\Omega} \bar{p}_m^{(n)} \Big|_{r=r_0} \frac{W_m^{03(n)}}{\bar{w}_m^{(n)}} & &= -\bar{\phi}_m^{(n)} \Big|_{r=r_0} \frac{W_m^{03(n)}}{\bar{w}_m^{(n)}} \end{aligned} \quad (31)$$

$$\text{Class B: } W_m^{01(n)} = -\bar{u}_m^{(n)} \frac{W_m^{03(n)}}{\bar{w}_m^{(n)}} \quad W_m^{04(n)} = -\bar{w}_m^{\prime(n)} \frac{W_m^{03(n)}}{\bar{w}_m^{(n)}}$$

In this paper acoustic sources are of particular interest as accurate solutions for these loads are challenging to find as compared to the solution for structural loadings. Using the bi-orthogonality relation we can, following the latter procedure, easily derive the modal amplitudes directly for arbitrary acoustic sources and thereby obviate the convolution. Thus for an arbitrary acoustic source, $q(r)$, applied at ξ the modal amplitudes are given as in Eq. (32) for $x \rightarrow \xi$ with $x > \xi$.

$$\vartheta_m(r) = -\frac{1}{2}q(r) \quad \Rightarrow \quad W_m^{(n)} = i \frac{\rho}{\gamma^3 \mu \Omega} \frac{W_m^{03(n)}}{\bar{w}_m^{(n)}} \int_0^1 \bar{p}_m^{(n)}(r)q(r)rdr \quad (32)$$

where the amplitudes of the arbitrary source are also expressed through the amplitudes of a radial force as in Eq. (31).

Returning to the modal amplitudes in Eq. (31) with $\bar{w}_m^{(n)} \equiv 1$ Green's matrix can also be expressed via the amplitudes from a radial force, see Eq. (33).

$$\mathbf{G}_m(x, \xi, r, r_0) = \sum_{n=1}^{\infty} \mathbf{L}_m^{(n)}(r, r_0) W_m^{03(n)} \exp(k_m^{(n)}(x - \xi)) \quad (33)$$

where $\mathbf{L}_m^{(n)}(r, r_0)$ is the modal coefficient/amplitude scaling matrix shown in Eq. (34).

$$\mathbf{L}_m^{(n)}(r, r_0) = \mathbf{U}_m^{(n)}(r_0) \bar{\mathbf{U}}_m^{(n)T}(r) = \begin{pmatrix} -\bar{u}_m^{(n)} \\ \bar{v}_m^{(n)} \\ \bar{w}_m^{(n)} \\ -\bar{w}_m^{\prime(n)} \\ -\bar{\phi}_m^{(n)} \Big|_{r=r_0} \end{pmatrix} \begin{pmatrix} \bar{u}_m^{(n)} \\ \bar{v}_m^{(n)} \\ \bar{w}_m^{(n)} \\ \bar{w}_m^{\prime(n)} \\ \bar{\phi}_m^{(n)} \end{pmatrix}^T = \begin{bmatrix} -\bar{u}_m^{2(n)} & -\bar{u}_m^{(n)} \bar{v}_m^{(n)} & -\bar{u}_m^{(n)} \bar{w}_m^{(n)} & -\bar{u}_m^{(n)} \bar{w}_m^{\prime(n)} & -\bar{u}_m^{(n)} \bar{\phi}_m^{(n)} \\ -g_{12} & \bar{v}_m^{2(n)} & \bar{v}_m^{(n)} \bar{w}_m^{(n)} & \bar{v}_m^{(n)} \bar{w}_m^{\prime(n)} & \bar{v}_m^{(n)} \bar{\phi}_m^{(n)} \\ -g_{13} & g_{23} & \bar{w}_m^{2(n)} & \bar{w}_m^{(n)} \bar{w}_m^{\prime(n)} & \bar{w}_m^{(n)} \bar{\phi}_m^{(n)} \\ g_{14} & -g_{24} & -g_{34} & -\bar{w}_m^{2\prime(n)} & -\bar{w}_m^{\prime(n)} \bar{\phi}_m^{(n)} \\ g_{15} \Big|_{r=r_0} & -g_{25} \Big|_{r=r_0} & -g_{35} \Big|_{r=r_0} & g_{45} \Big|_{r=r_0} & -\bar{\phi}_m^{(n)} \Big|_{r=r_0} \bar{\phi}_m^{(n)} \end{bmatrix} \quad (34)$$

where $\mathbf{U}_m^{(n)}$ is the modal amplitude scaling vector defined from Eq. (31), $\bar{\mathbf{U}}_m^{(n)}$ is the modal coefficient vector and g_{nj} are elements of the $\mathbf{L}_m^{(n)}$ matrix indicating (skew-)symmetry in that g_{12} refers to another entry in the matrix i.e. $g_{12} = -\bar{u}_m^{(n)} \bar{v}_m^{(n)}$. Recall that $\bar{\phi}_m^{(n)}$ is a function of r .

From the coefficient/amplitude matrix in Eq. (34) it is seen that the scaling introduced in Eq. (29) gives rise to skew-symmetric and symmetric elements in Green's matrix according to the Class properties. This (skew-)symmetry of the matrix is, if substituted into the general framework of reciprocity, a manifestation of excitation and observation points being interchangeable. The immediate manifestation of the (skew-)symmetry of Green's matrix is, however, that forces and displacements are interchangeable for correct scaling of the load, meaning that applying a radial force and measuring axial displacement is identical to applying an axial force and measuring radial displacement. In particular, correct scaling applies to acoustic sources and bending loads whereas the scaling between other structural forces is unity. Finally, there may be other convenient scalings that are relevant depending on application but is, however, not pursued further here.

To analyse the near- and far-field distribution and energy exchange between transmission paths or generalise to finite/compound shells through the Boundary Integral Equations Method (BIEM), see e.g. [9, 10], the generalised forces associated with Green's matrix must be calculated. These generalised forces, \mathbf{Q}_m , are defined from the generalised displacements, \mathbf{G}_m in Eq. (33), through a differential operator, \mathcal{L}_m , as seen in Eq. (35). However, using the ansatz and introducing the modal coefficients of Eq. (5)–(6) \mathcal{L}_m becomes a simple transformation map such that \mathbf{Q}_m can be assembled similar to \mathbf{G}_m in Eq. (33).

$$\mathbf{Q}_m(x, \xi, r, r_0) = \mathcal{L}_m \mathbf{G}_m(x, \xi, r, r_0) \quad (35)$$

Thus, each row of \mathbf{G}_m and \mathbf{Q}_m , which constitute the Green's matrices, is associated with the response (and forces) to a set of external unit forces.

In conclusion, it is seen from the latter derivation that we only need to calculate the modal amplitudes for one fundamental loading condition from which we are able to formulate the complete Green's matrix using a simple modal scaling and an index interchange to provide an arbitrary number of amplitudes for the analysis. Through this method the formulation of Green's matrix becomes computationally cheap – even for an arbitrarily large number of waves, which implies that any desired accuracy of the solution can be obtained independent of source, frequency and/or circumferential wavenumber. This is discussed further in Sec. 6.

4.3. Decay and radiation conditions

The tailored Green's matrices introduced here does not yet satisfy decay and radiation conditions nor the solution for the left semi-infinite segment and the general solution is therefore incomplete. Following the same procedure for the left segment, $x < \xi$, it is easily seen from the derivation in Sec. 4.1 that to cope with both semi-infinite segments the amplitudes of Eq. (31) simply adopt the sign-function from Eq. (22).

To satisfy decay and radiation conditions only wavenumbers which decay away from the source and purely imaginary wavenumbers with positive group velocity,

$c_g = \frac{d\omega}{dk_i} > 0$, are chosen, see [11] for details. To satisfy these conditions for arbitrary x , only the wavenumbers for $x > \xi$ are introduced, while correctness of the wavenumbers for $x < \xi$ is ensured also by a sign-function such that $k_{<} = \text{sgn}(x - \xi)k_{>}$, where $k_{>}$ satisfy decay/radiation conditions. Here the sign-function establishes the correct relationship between negative and positive going waves (wave-pairs). In addition, it is also convenient to introduce the identity; $\text{sgn}(x - \xi)(x - \xi) = |x - \xi|$.

Introducing the latter conditions and identities to the Class variables in Eq. (7) it is, by virtue of their properties, given that only Class A functions adopt the sign-function such that, for instance, $\bar{R}_m^{(n,n)}$ becomes $\text{sgn}(x - \xi)\bar{R}_m^{(n,n)}$, $\bar{u}_m^{(n)}$ becomes $\text{sgn}(x - \xi)\bar{u}_m^{(n)}$ etc. Further, $\exp(k_m^{(n)} \text{sgn}(x - \xi)(x - \xi))$ becomes $\exp(k_m^{(n)} |x - \xi|)$ by virtue of the identity, which implies that $\mathbf{G}_m(x, \xi, r, r_0)$ becomes $\mathbf{G}_m(|x - \xi|, r, r_0)$. Thus, for the feasible solution the modal amplitudes in Eq. (31) are rewritten to Eq. (36) where we have used the definition $\bar{w}_m^{(n)} \equiv 1$.

$$\begin{aligned}
\text{Class A: } \quad W_m^{03(n)} &= \frac{1}{2} \frac{1}{\bar{R}_m^{(n,n)}} & W_m^{02(n)} &= \bar{v}_m^{(n)} W_m^{03(n)} \\
W_m^{05(n)} &= \frac{i}{\gamma\Omega} \bar{p}_m^{(n)} \Big|_{r=r_0} W_m^{03(n)} & & (36) \\
\text{Class B: } \quad W_m^{01(n)} &= -\text{sgn}(x - \xi)\bar{u}_m^{(n)} W_m^{03(n)} & W_m^{04(n)} &= -\text{sgn}(x - \xi)\bar{w}_m^{(n)} W_m^{03(n)}
\end{aligned}$$

Using these identities, the general solution (expansion on waves) ensures a generic solution for all loading conditions since the modal response has adopted the Class properties of Sec. 2.2 also in x , by virtue of the identity; $\text{sgn}(x - \xi)(x - \xi) = |x - \xi|$. In previous papers, see e.g. [2], a generic solution was ensured manually by choosing an appropriate ansatz specific to the loading condition.

With the versatile Green's matrices assembled using modal decomposition through the bi-orthogonality relation we may readily explore e.g. the energy flow for arbitrary sources/loads or the near-field transmission path analysis for ideal excitations using the total energy flow derived for general forcing in Appendix C and for Green's matrices in Eq. (37).

$$\begin{aligned}
N_m^{0F\Sigma}(x, \xi) &= \frac{\pi\chi_m}{2} \Omega \text{Im} \left(Q_{1m}^{0F} u_m^{0F*} + Q_{2m}^{0F} v_m^{0F*} \right. \\
&\quad \left. + Q_{3m}^{0F} w_m^{0F*} + \mu Q_{4m}^{0F} \bar{w}_m^{0F*} + i \frac{\rho}{\gamma^3 \mu \Omega} \int_0^1 \bar{p}_m^{0F*} \bar{\vartheta}_m^{0F} r dr \right)
\end{aligned}$$

\Updownarrow

$$\begin{aligned}
N_m^{0F\Sigma}(x, \xi) &= \frac{\pi\chi_m}{2} \Omega \sum_{n=1}^{\infty} \sum_{j=1}^{\infty} \text{Im} \left(\left[\bar{Q}_{1m}^{(n)} \bar{u}_m^{(j)*} + \bar{Q}_{2m}^{(n)} \bar{v}_m^{(j)*} + \bar{Q}_{3m}^{(n)} \bar{w}_m^{(j)*} \right. \right. \\
&\quad \left. \left. + \mu \bar{Q}_{4m}^{(n)} \bar{w}_m^{\prime(j)*} + i \frac{\rho}{\gamma^3 \mu \Omega} \int_0^1 \bar{p}_m^{(j)*} \bar{\vartheta}_m^{(n)} r dr \right] \right) & (37) \\
&\quad \times W_m^{0F(n)} W_m^{0F(j)*} \exp\left((k_m^{(n)} + k_m^{(j)*})|x - \xi|\right)
\end{aligned}$$

where $\chi_{m=0} = 2$, $\chi_{m \neq 0} = 1$ and each term defines the different transmission paths i.e. membrane paths, u, v (axial and membrane shear), flexure paths, w, w' (transverse shear and bending) and acoustic path, ϑ . See Appendix C for details.

The near-field analysis for an acoustic monopole ($0F = 05$) is seen in Fig. 2 for $f = 2\text{kHz}$, $m = 3$ and $M = 25$ waves retained in the expansion.

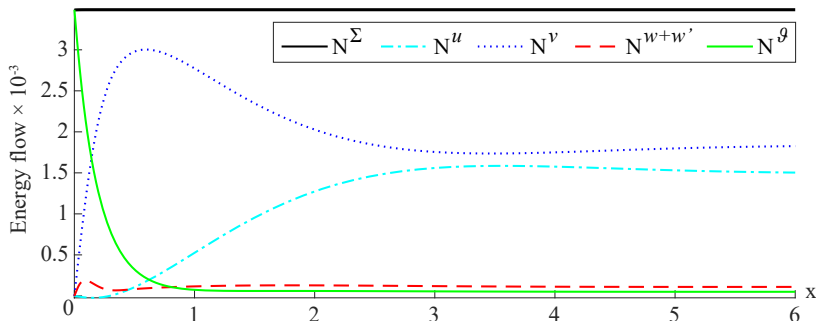


Fig. 2: Energy flow for an acoustic monopole at $f = 2\text{kHz}$, $m = 3$ and with $M = 25$ waves retained in the expansion. Notice the near- to far-field transition around $x \approx 5$. The case is chosen based on [2] and the scaling to dimensional quantities can be found in Appendix A.

As indicated in the figure the near-field analysis, in which the energy rapidly escapes from the fluid into membrane shear (torsional) energy in the shell wall, is considerably different than the far-field analysis in which the energy distributes almost equally between the axial and torsional components (only one propagating wave at this frequency). The transition between near- and far-field is seen to be around $x \approx 5$ (scaling to dimensional quantities is found in Appendix A). This case is chosen based on and validated against [2].

In the following, completeness and convergence of this new approach, as more waves are included in the expansion, is studied to ensure correctness and study accuracy of the Green's matrices.

5. Completeness and convergence of Green's matrices

The method of eigenfunction expansion as used in this paper is a subject widely explored in literature and is likely the most commonly used solution form for waveguide problems. Among others it has been successfully applied in both elastodynamics, [2, 6, 29, 35], acoustics, [3], and vibro-acoustics, [1–4, 6, 12]. The completeness of the solution to the linear problem considered here is ensured by virtue of the derivation through the variational principle which provides the complete set of basis functions (eigenfunctions and corresponding eigenvalues), see e.g. [7, 8, 36, 37] for details on completeness.

Convergence of general eigenfunction expansions for transcendental problems as considered here have been discussed in numerous papers e.g. [38–40] and applied mathematics books e.g. [7, 8, 37, 41]. With interest in these references we discuss con-

vergence of Green's matrices as more waves are included in the expansion in order to ensure correctness of the solution and understand its (possible) limitations in engineering applications. Related to these limitations is the discussion of the validity range of the linearised (acoustic) fluid model of an inviscid fluid. As known, see e.g. [42], the important parameter, which characterises the viscous effects in stationary fluid-structure interaction, is the frequency-dependent penetration depth. Roughly speaking, it specifies the thickness of a viscous boundary layer at the surface of a vibrating structure. The model of a thin elastic shell filled with an inviscid compressible fluid with no mean flow provides infinitely many evanescent waves, and their decay rate grows with the sequential number. As soon as a wave, predicted by this modelling, significantly decays within the distance equal to the penetration depth, the model of an inviscid acoustic medium becomes inadequate. Therefore, the convergence study within this model serves only to clarify mathematical limitations of the solution space, rather than physical limitations of the model.

The modal decomposition method used in e.g. [3, 15, 17], and presented here for the fluid-filled shell builds on decomposition of field variables as evident from the previous section. Upon decomposition each modal contribution becomes independent on the number of waves included in the expansion. This solution form is regarded as the strong (physical) form since the contribution of a specific mode should not change depending on the number of included waves as in the weak solution (integral average). Thus, using the strong form, convergence is achieved when continuity and unit-jump at $x \rightarrow \xi$ is satisfied and not when the contribution of each wave (amplitude) is converged (weak solution). This is discussed and illustrated further in Sec. 6.

Unfortunately, this solution form does not ensure monotonic convergence. This is, however, of no additional concern since the calculation of modal amplitudes by this method is computationally cheap. Hence the study of convergence becomes straightforward and is eased even further by the explicit formulation of the amplitudes which permit a strict mathematical study of convergence.

Particular complications in the convergence study are caused by acoustic sources as the associated solution must comply not only with a unit-jump in x but also with a delta-function in r . The unit-jump is, in general, of no significant concern as the (infinitely many) real-valued waves decay exponentially in x . This is, however, not the case for the delta-function in the radial direction as radial standing waves built up and thereby contribute 'harmonically' to the expansion on Bessel-functions. Hence decaying waves are needed to properly resemble the radial distribution of the acoustic variables in the near-field, making the acoustic domain more sensitive to evanescent waves.

5.1. Uniform convergence

In this convergence study the interest lies within uniform convergence of Green's matrix and its derivative(s) as solutions obeying uniform convergence have convenient properties such as term-wise differentiation and integration, see e.g. [7, 8, 37, 41].

This is important because the associated force matrix is derived from Green's matrix through a differential operator (Green's matrices), as seen in Eq. (35).

It is well-known from theory of wave propagation in infinite continuous waveguides that there is a finite number of propagating and attenuating waves (purely imaginary and complex wavenumbers in this paper – indicated by $i\mathbb{R}$ and \mathbb{C} , respectively), while there is an infinite number of decaying waves (real-valued wavenumbers indicated by \mathbb{R}), see e.g. [10, 43]. Thus, the expansion of the components of Green's matrix in Eq. (33) can be expressed on the form shown in Eq. (38), where n counts the number of propagating waves, j the number of attenuating waves and h the number of decaying waves such that $M = N + J + H$ is the number of waves included in the expansion. We note here that J is an even number since the attenuating waves exist in complex conjugated wave-pairs, see Fig. 1.

$$u_m(x, r) = \sum_n^N a_m^{(n)i\mathbb{R}} u_m^{(n)i\mathbb{R}}(x, r) + \sum_j^J a_m^{(j)\mathbb{C}} u_m^{(j)\mathbb{C}}(x, r) + \sum_h^H a_m^{(h)\mathbb{R}} u_m^{(h)\mathbb{R}}(x, r) \quad (38)$$

It is widely acknowledged that only propagating waves carry energy in the far-field and by virtue all propagating waves must be included in the expansion to ensure uniform convergence of the variables in the far-field. In the near-field, that is; around the excitation point, ξ , where decay of the exponents of attenuating and decaying waves have little effect, more waves are needed to recover the applied load and uncover the correct distribution of energy between alternative transmission paths. The pair(s) of complex conjugated attenuating waves ($-k_{\text{Re}} \pm k_{\text{Im}}$) usually contribute significantly and should therefore always be included in the expansion for near-field analysis. Hence, the study of convergence of Green's matrices reduce to the contribution of the infinite number of decaying waves.

Since the basis functions are chosen in accordance with the decay (and radiation) conditions the expansion on real-valued waves is continuous, bounded and a monotonic decreasing sequence in x . Thus, by Abel's test, see e.g. [7, 8], the structural components can be shown to converge uniformly everywhere only if the sequence of amplitudes, $\{a_m^{(n)}\}$, that is; modal coefficients times amplitudes, converge to zero – equivalent to near-field convergence. Note, however, that confer to the sign-function introduced by the loading in Eq. (22), the component with the applied unit-jump fails to be continuous at ξ , while all other variables will be continuous everywhere as they satisfy continuity in the limit ($M \rightarrow \infty$).

It can easily be shown for any structural component of Green's matrices that all sequences of $\{a_m^{(n)}\}$ are convergent for any loading (structural/acoustic), making them uniformly convergent. This can be observed by considering the limit of the amplitudes in Eq. (31) times the modal coefficients in Eq. (4)–(5) as the wavenumbers go towards those of the acoustic duct (zeros of the derivative of the Bessel-function). This is discussed further in Sec. 6.

The solution to the cylindrical wave equation is also continuous and bounded in the interval considered here ($r \in [0; 1]$), while for $r \in \mathbb{R}$ the solution is bounded only if $\kappa_m^{(n)} \in \mathbb{R}$. Since the Bessel-function is not a monotonic decreasing sequence

Abel's test fails and by further inspection it can be shown that the acoustic variables do not converge uniformly for any loading. For instance, it is seen from Fig. 3(a) that the amplitude sequence of the acoustic velocity, that is; $\bar{\vartheta}_m^{(n)} W_m^{(n)}$ from $\vartheta_m^{(n)} = \bar{\vartheta}_m^{(n)} W_m^{(n)} J_m(k_m^{(n)} r) \exp(k_m^{(n)} x)$, diverge for an acoustic monopole (as expected). However, as the acoustic energy redistribute between alternative transmission paths the profile of the acoustic variables smoothens rapidly away from the excitation point due to the decay in x . In general, the decay is faster than the divergence of the acoustic variables such that the profiles become sufficiently smooth and thereby uniformly convergent at some small distance, ε , away from the excitation point.

If instead we consider an integral representation of the acoustic variables equivalent to the average volumetric acoustic flow (or acoustic mass flow) it is easily verified that the amplitude sequence is convergent for all loadings, see Fig. 3(b). Thus, once again by Abel's test it is shown that this integral representation of the acoustic variables (r -independent) converge uniformly everywhere in x . The same can be observed for a dipole source (not treated here).

Fortunately, uniform convergence of the integral is sufficient for problems solved using Green's matrices as it implies that uniform convergence holds true, not only for all energy flow components, but also for the solution to arbitrary sources – provided that the arbitrary source is sufficiently smooth.

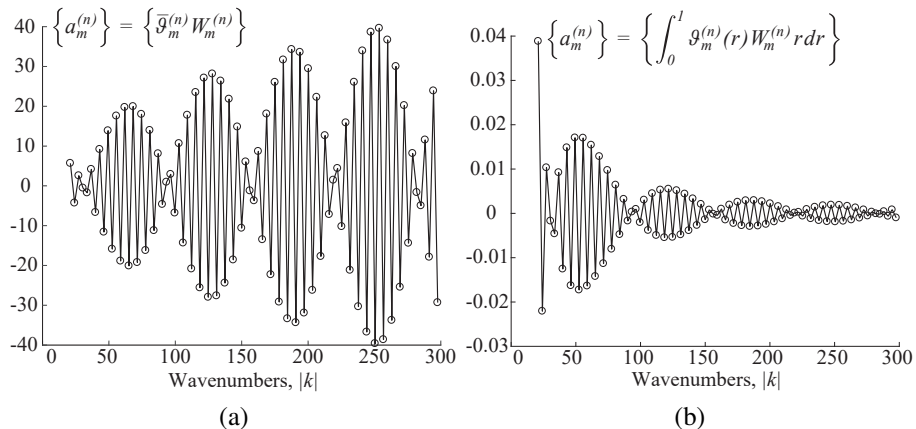


Fig. 3: Amplitude sequence for an applied acoustic monopole at $f = 2\text{kHz}$, $m = 3$, $r_0 = 0.95$. (a) Diverging amplitude sequence of the acoustic velocity (without Bessel-function) and (b) converging amplitude sequence of the average volumetric acoustic flow.

In conclusion, the structural variables as well as the integral representation of the acoustic variables converge uniformly everywhere i.e. $\{x \in \mathbb{R}\}$, except for the loaded variable (unit-jump) where uniform convergence holds true for $\{x \in \mathbb{R} \setminus \{\xi\}\}$. For the acoustic variables uniform convergence holds for $\{x \in \mathbb{R} \setminus \{\varepsilon\}, r \in [0; 1]\}$, where ε is some small region around the excitation point determined by the smoothness of the acoustic profile (decay rate).

5.2. Convergence rate

In particular, for eigenfunctions with equally (or almost equally) dispersed zeros e.g. harmonic- and Bessel-functions, convergence is, in general, slower than for functions with zeros concentrated at the ends of intervals, say Legendre or Chebyshev polynomials. Nonetheless, as only propagating waves (having purely imaginary wavenumbers) contribute harmonically to the expansion in x , convergence in the propagation direction may be achieved relatively fast. On the other hand, convergence in the acoustic domain may be slow as seen in Fig. 3.

The relative convergence rate between components of Green's matrices can be assessed considering the divergence/convergence rate of the modal coefficients as all components of Green's matrices are formulated with the same amplitude and spatial distribution by virtue of the formulation in terms of modal coefficients, see Eq. (33). First, it can easily be verified from Eq. (4) compared with Eq. (5) that the kinematic variables converge faster than the forces and the structural variables faster than the acoustic variables. Second, it can be shown by inspection of the amplitudes in Eq. (31) that for structural loadings all variables converge, in general, faster for membrane loads (axial and torsion) than for flexural loads – depending on frequency and circumferential wavenumber. This has the physical interpretation that flexural loads excite more fluid-originated waves than the membrane loads and thereby cause a stronger interaction between fluid and structure than what is observed for membrane loads.

Applying acoustic sources, especially dipole (not discussed here), gives an even slower convergence than the flexural loads and in addition the convergence depends heavily on the location of the applied delta-function, r_0 , as illustrated in Fig. 4. For the acoustic loads it translates also to a strong fluid-structure coupling and, in particular, to the sensitivity of a fluid-loading as it tends to excite more higher order waves than what is observed for structural loadings. This is mainly caused by the presence of standing waves in the radial direction and does indeed emphasise the importance of including the heavy fluid-loading format in deriving tailored Green's matrices.

From Fig. 4 it is easily seen that convergence of the applied source is faster for increasing r_0 . It is, on the other hand, more interesting to note that for each r_0 the solution has a number of (almost) converged points that are equally distributed with a specific number of waves. Even though it may be difficult to determine the first point of convergence it is easy to determine the remaining convergence points as the distance between is inversely proportional to the location of the source i.e. $M^{\text{pack}} = \frac{1}{r_0}$, as can be verified from Fig. 4. These equally spaced convergence points are controlled by what we denote a 'wave-pack' which is characterised by being (almost) self-equilibrating. This simple relation between the source location and size of the wave-pack arise from the dispersion of the zeros of the Bessel-function and emphasise the slow converging nature of such functions. Though the study of wave-packs is not considered further here there are still interesting aspects of this subject to be studied in future work, for instance, in relation to acceleration of convergence.

Nevertheless, the rate of convergence of Green's matrices is, in general, of no additional concern using this method since adding additional terms to the expansion is

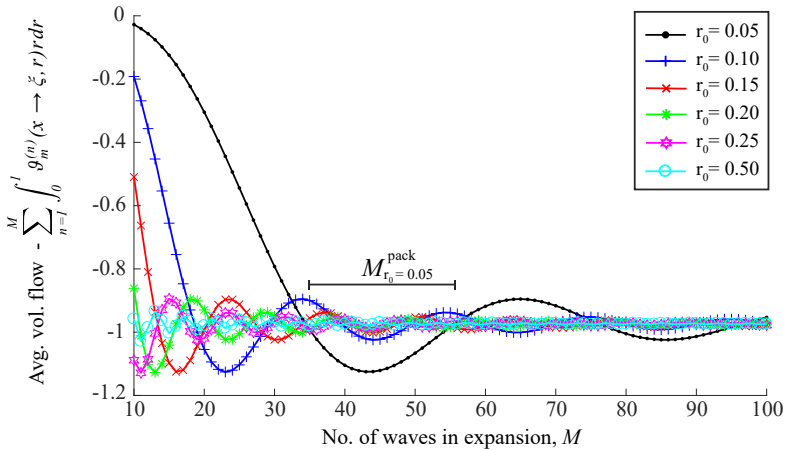


Fig. 4: Convergence of the average volumetric acoustic flow when an acoustic monopole is applied at different locations for $f = 2\text{kHz}$, $m = 3$ and $x \rightarrow \xi$. Convergence rate is seen to increase with increasing r_0 .

extremely computational cheap and further, as this method provides the correct modal contribution the feasible solution is considered to be the solution in which all relevant (non-zero) amplitudes are included. Thus, accelerating convergence is not straightforward but is, however, of great practical interest for successive calculations such as, for instance, energy flow calculations and application of the Boundary Integral Equations Method (BIEM) in order to ensure e.g. monotonic convergence or increase the computational efficiency. Nonetheless, taking advantage of the simple algebraic equations for the modal amplitudes in Eq. (36) there are ways of accelerating convergence, for instance, by rearranging terms according to their modal contribution (magnitude), considering wave-packs and their equivalent response or through alternative manipulations of Bessel-functions. This study is, however, a subject of future work.

6. Discussion

By virtue of the latter convergence study, limitations of the solution space have been defined and the near-field energy flow can now be studied freely using this method. This is done for acoustic mono- and dipoles in [13, 14]. In this section we strive, however, to highlight additional advantages, besides the explicit formulation of the modal amplitudes, of using modal decomposition as well as discuss the physical interpretation of the bi-orthogonality relation.

6.1. Unconverged and numerical inaccuracy of solutions

As discussed in the previous section a convergence study can be carried out straightforwardly. However, for practical engineering purposes such studies are rarely conducted, and the number of waves is rather chosen as a compromise between accuracy and computational time. Fortunately, unconverged results are, when using this method, visible directly in, for instance, the energy flow graphs as illustrated in Fig. 5.

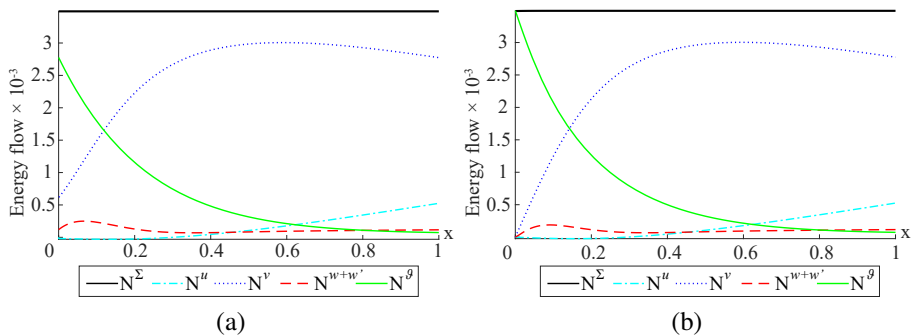


Fig. 5: Applied acoustic monopole at $f = 2\text{kHz}$, $m = 3$, $r_0 = 0.95$. (a) Unconverged energy flow for $M = 5$ and (b) converged energy flow for $M = 25$. The unconverged solution shows that the injected energy has leaked into non-loaded components at the excitation point ($\xi = 0$) such that continuity is not satisfied.

As seen the unconverged results show that the injected energy has leaked into non-loaded components at the excitation point ($\xi = 0$) and, therefore, continuity across this point is not satisfied. This is only related to the near-field solution as the far-field in Fig. 5(a) and (b) is converged when all propagating waves are included in the expansion, as discussed in Sec. 5.1. In addition, the total energy flow is seen to be constant also in the near-field which implies that only propagating waves contribute to the total energy flow as discussed in [1, 6] and explicitly shown in Sec. 6.3.

Fortunately, since convergence targets are known by virtue of the formulation this method immediately permits, by different means, error calculations such that the study of convergence becomes redundant upon application of the method. Thus, for any desired truncation of waves, M , we can calculate various relative errors that indicate the accuracy of the current solution. This is treated in Sec. 6.2.

Remark that no such indications are given when the problem is solved using the weak solution form because continuity and applied loads are strict conditions to be satisfied in the integral average formulation, see e.g. [2]. Hence, error predictions are not possible using the weak solution as the convergence targets are unknown such that monitoring convergence of amplitudes for increasing M is a necessity for approximating the accuracy of the solution.

Similar to the unconverged results lack of numerical accuracy of the solution can also be seen in the energy flow graphs, Fig. 6. In particular, the difference between the unconverged solution in Fig. 5(a) and the solution in Fig. 6 is the non-uniformity of the total energy in the near-field, where the total energy remains constant in the unconverged solution. The cause of this inaccuracy of the solution arise from insufficient precision of wavenumbers of the higher order decaying waves and is therefore a local effect only present in the close vicinity of the excitation point. Thus at relatively short distance from $\xi = 0$ the graphs of Fig. 5 and 6 become identical.

As will be discussed in detail in Sec. 6.3 and 6.4 these higher order waves does not satisfy the bi-orthogonality relation to the same degree as the lower order waves and does thereby introduce artificial energy into the total energy flow in Fig. 6 through the

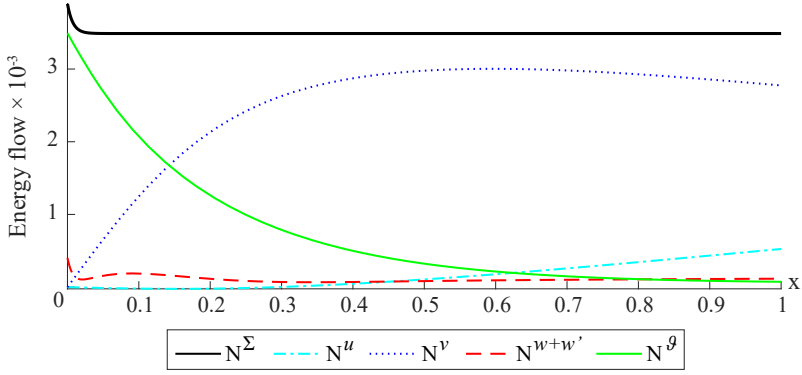


Fig. 6: Numerical inaccuracy errors caused by insufficient precision of wavenumbers of the higher order decaying waves. Applied monopole at $f = 2\text{kHz}$, $m = 3$, $r_0 = 0.95$ and $M = 50$.

cross-terms of the flexural components, making the solution appear unstable. From Sec. 6.3 it will also be clear that the total energy flow must always be constant when using this method as seen, for instance, for the unconverged solution in Fig. 5(a) and in effect non-uniformities may be perceived as measures of numerical inaccuracy of, in particular, the wavenumbers. The cause of insufficient precision of wavenumbers is anticipated to arise from the merging of zeros (wavenumbers) and poles in the dispersion equation which causes inadequate accuracy of the zeros.

Finally, notice that the three graphs in Fig. 5 and 6, which present the same case only with a different number of waves included in the expansion, highlight important accuracy features of the solution. These features are highlighted only by virtue of the modal decomposition method which makes them visible in the energy flow graphs but more importantly makes them measurable in terms of errors and accuracy.

6.2. Error calculations

Based on the results observed for unconverged solutions and wavenumber accuracy it is expedient to derive a set of error measures to predict the accuracy of the current solution. In what follows we, however, confine ourselves to consider only the unconverged solution and three particular error measures, though more can be defined: one measure for the applied load (volumetric flow for acoustic monopole), one for the applied energy flow (or power) and one for the continuity conditions. These error measures are all based on components that converge uniformly as discussed in Sec. 5.1, why the error calculations are considered in the framework of the supremum (maximum) norm, indicated by $\|\cdot\|_\infty$. In the following, the error calculations are presented only for an acoustic monopole but can be formulated for all load cases and reduce conveniently for structural loadings. Further, we consider only errors at the excitation point as $x \rightarrow \xi$ (the supremum norm).

For the acoustic monopole we consider the average volumetric flow (discussed in Sec. 5.1) as the acoustic variables themselves does not converge in the supremum

norm. The error in the prescribed flow can then be expressed as in Eq. (39), while the energy flow error is expressed as in Eq. (40). Recall, that for sufficiently smooth arbitrary loads the supremum norm/error of the acoustic variables can be evaluated directly since the convolution integral converge uniformly as discussed in Sec. 5.1.

$$\|\Delta\vartheta_m\|_\infty = \left| \int_0^1 [\vartheta_m - \hat{\vartheta}_m] r dr \right| = \left| -\frac{1}{2} \frac{\gamma^2 \mu}{\rho} - \int_0^1 \hat{\vartheta}_m r dr \right|$$

↓

$$|\vartheta_m^{\%}| = \frac{\|\Delta\vartheta_m\|_\infty}{\left| \int_0^1 \vartheta_m r dr \right|} = \left| 1 + \frac{2\rho}{\gamma^2 \mu} \int_0^1 \hat{\vartheta}_m r dr \right| \quad (39)$$

$$\begin{aligned} \|\Delta N_m^\vartheta\|_\infty &= |N_m^\vartheta - \hat{N}_m^\vartheta| = \frac{\pi \chi_m}{2} \frac{\rho}{\gamma^3 \mu} \operatorname{Re} \left(\int_0^1 \hat{p}_m^* \vartheta_m - \hat{p}_m^* \hat{\vartheta}_m r dr \right) \\ &= \frac{\pi \chi_m}{2} \frac{\rho}{\gamma^3 \mu} \operatorname{Re} \left(-\frac{1}{2} \frac{\gamma^2 \mu}{\rho} \hat{p}_m^*|_{r=r_0} - \int_0^1 \hat{p}_m^* \hat{\vartheta}_m r dr \right) \end{aligned} \quad (40)$$

↓

$$|N_m^{\% \vartheta}| = \frac{\|\Delta N_m^\vartheta\|_\infty}{|N_m^\vartheta|} = \operatorname{Re} \left(\left| 1 + \frac{2\rho}{\gamma^2 \mu \hat{p}_m^*|_{r=r_0}} \int_0^1 \hat{p}_m^* \hat{\vartheta}_m r dr \right| \right)$$

where (x, r) is omitted and $\hat{}$ indicates the truncated eigenfunction expansion. Note that variables without $\hat{}$ are known convergence targets.

On the other hand, deviations in continuity of energy flow can also be calculated. In this case the supremum norm is expressed as in Eq. (41).

$$\|N_m^C\|_\infty = \max \{ |N_m^u|, |N_m^v|, |N_m^w|, |N_m^{w'}| \} \quad \Rightarrow \quad |N_m^{\% C}| = \frac{\|N_m^C\|_\infty}{|N_m^\Sigma|} \quad (41)$$

where $\|N_m^C\|_\infty$ is the maximum value (at $x \rightarrow \xi$) of the non-loaded (continuity) energy flow components from Eq. (C.1) and N_m^Σ the total energy flow from Eq. (37) which according to Fig. 5 is correct even for unconverted solutions (when all propagating waves are included).

In accordance with Fig. 5(a), Eq. (41) gives the relative error between the maximum continuity jump (torsion – dashed blue) and the total energy flow (solid black), while Eq. (40) gives the relative error between the energy in the fluid (solid green) and the total energy flow approximated through the current expansion of \hat{p}_m . In the latter it may be expedient also to compared with the total energy as for the continuity error, however, the error measure becomes slightly more complex and the result is in general the same when considering acoustic sources. Finally, note that we can also calculate continuity errors of the Class A forces similar to that in Eq. (41) as well as capture numerical inaccuracy issues as that illustrated in Fig. 6.

In general, we note that force and continuity error(s) are more accurate since we know the convergence targets in advance as oppose to the (approximated) energy flow in Eq. (40), which may vary depending on the convergence of \hat{p}_m . In particular, errors based on forces alone are more conservative – especially for the acoustic variables. According to the discussion in Sec. 5 this is obvious as they converge slower than the energy components because the kinematic variables converge faster than the force variables. Further, as the variables does not converge monotonically we can not necessarily expect that a higher number of waves provide a smaller error as seen, for instance, from Fig. 4. However, if a set of wavenumbers are chosen according to the 'wave-packs' discussed in Sec. 5.2 a monotonic decrease of the errors may be observed. This also constitutes an interesting topic for future studies.

6.3. Relation between the total energy flow and $\bar{R}_m^{(n,j)}$

In the following we consider the total energy flow for the different loading conditions of Green's matrix (where the index $0F$ is omitted). In effect, the general formulation in Eq. (C.2) can be expanded in terms of modal coefficients as in Eq. (37) and/or in terms of modes (modal coefficients times amplitudes) as in Eq. (42).

$$N_m^\Sigma = \frac{\pi\chi_m}{2}\Omega \sum_{n=1}^{\infty} \sum_{j=1}^{\infty} \text{Im} \left(\left[\mathcal{Q}_{1m}^{(n)} u_m^{(j)*} + \mathcal{Q}_{2m}^{(n)} v_m^{(j)*} + \mathcal{Q}_{3m}^{(n)} w_m^{(j)*} + \mu \mathcal{Q}_{4m}^{(n)} w_m'^{(j)*} \right. \right. \\ \left. \left. + i \frac{\rho}{\gamma^3 \mu \Omega} \int_0^1 p_m^{(j)*} \vartheta_m^{(n)} r dr \right] \exp \left((k_m^{(n)} + k_m^{(j)*}) |x - \xi| \right) \right) \quad (42)$$

or by a convenient interchange of summation indices as in Eq. (43).

$$N_m^\Sigma = \frac{\pi\chi_m}{2}\Omega \sum_{n=1}^{\infty} \sum_{j=1}^{\infty} \text{Im} \left(\left[\mathcal{Q}_{1m}^{(j)} u_m^{(n)*} + \mu \mathcal{Q}_{4m}^{(j)} w_m'^{(n)*} \right] \exp \left((k_m^{(j)} + k_m^{(n)*}) |x - \xi| \right) \right. \\ \left. + \left[\mathcal{Q}_{2m}^{(n)} v_m^{(j)*} + \mathcal{Q}_{3m}^{(n)} w_m^{(j)*} + i \frac{\rho}{\gamma^3 \mu \Omega} \int_0^1 p_m^{(j)*} \vartheta_m^{(n)} r dr \right] \exp \left((k_m^{(n)} + k_m^{(j)*}) |x - \xi| \right) \right) \quad (43)$$

The structure of the total energy flow and the bi-orthogonality relation are similar and suggests a definite relation between the energy flow components and the components in the bi-orthogonality relation. In particular, we note from the structure of Eq. (37) the resemblance to $\bar{R}_m^{(n,j)}$, Eq. (25) – shown in Eq. (44) in terms of modes.

$$R_m^{(n,j)} = \bar{R}_m^{(n,j)} W_m^{(n)} W_m^{(j)} \quad n \neq j \\ = \mathcal{Q}_{1m}^{(j)} u_m^{(n)} + \mu \mathcal{Q}_{4m}^{(j)} w_m'^{(n)} - i \frac{\rho}{\gamma^3 \mu \Omega} \int_0^1 p_m^{(j)} \vartheta_m^{(n)} r dr - \mathcal{Q}_{2m}^{(n)} v_m^{(j)} - \mathcal{Q}_{3m}^{(n)} w_m^{(j)} = 0 \quad (44)$$

Note that since the decay and radiation conditions are satisfied for Green's matrix the restrictions on the bi-orthogonality relation reduce from $n^2 \neq j^2$ to $n \neq j$.

Now, utilising Class properties and the bi-orthogonality relation we can show that Eq. (43) is related to the imaginary part of Eq. (44) and further that the expression

for the total energy flow can be reduced significantly. To show this we first establish the domain and codomain (see e.g. [41]) of the modal forces/displacements (that is; modal coefficients times amplitudes) i.e. the output domain (codomain) of the modal forces/displacements for a given wavenumber (domain). This mapping is established straightforwardly considering the Class properties of the modal coefficients and amplitudes of Eq. (4)–(6) and (31), respectively. To generalise we consider in the following the domain and codomain of the modal Class A and B functions. Recall here that the content of the Classes depends on the loading condition (controlled by the amplitudes) as discussed in Sec. 4.2. As there are three wave types: propagating, attenuating and decaying (indicated with $i\mathbb{R}$, \mathbb{C}/\mathbb{C}^* and \mathbb{R} as in Eq. (38)), we consider, separately, for each of these domains the corresponding codomain. The Class A and B functions map from the domains $i\mathbb{R}$, \mathbb{R} , \mathbb{C}/\mathbb{C}^* to the codomains as defined in Eq. (45).

$$f^A(k_m^{(n)}) = f_m^{A(n)} : \begin{cases} i\mathbb{R} & \rightarrow & i\mathbb{R} \\ \mathbb{R} & \rightarrow & \mathbb{R} \\ \mathbb{C} & \rightarrow & \mathbb{C} \\ \mathbb{C}^* & \rightarrow & \mathbb{C}^* \end{cases} \quad f^B(k_m^{(n)}) = f_m^{B(n)} : \begin{cases} i\mathbb{R} & \rightarrow & \mathbb{R} \\ \mathbb{R} & \rightarrow & \mathbb{R} \\ \mathbb{C} & \rightarrow & \mathbb{C} \\ \mathbb{C}^* & \rightarrow & \mathbb{C}^* \end{cases} \quad (45)$$

where \mathbb{C}^* indicates the conjugated domain of \mathbb{C} such that the notation $\mathbb{C}^* \rightarrow \mathbb{C}^*$ implies that $f^{A/B}(k_m^{(n)*}) = f^{A/B}(k_m^{(n)})^*$. In addition, we note that the set of Class A functions are endomorphic (domain and codomain are similar), while the set of Class B functions for propagating waves maps from $i\mathbb{R}$ to \mathbb{R} , caused by the evenness of the Class B functions i.e. $(ik)^2 = (-ik)^2 = -k^2$. Further, it should be noted that as we contrast acoustic variables (pressure times velocity) with the structural (force times displacement) in Eq. (43) we need to multiply the codomains of ϑ by i . This is, however, compensated by the i on the fluid term in Eq. (43).

Returning to Eq. (44) and considering loading condition $0F = 02, 03, 05$ such that the components of index n in Eq. (44) belong to Class B functions we see from these maps that for propagating and decaying waves the codomain is real, while for attenuating waves conjugated pairs ($-k_{\text{Re}} \pm k_{\text{Im}}$) exist in both domain and codomain. Thus, applying the conjugated operator to the Class B components we can reformulate Eq. (44) to Eq. (46) which is then valid for $n^* \neq j$ instead. Recall the notation n^* refers to $k_m^{(n)*}$.

$$Q_{1m}^{(j)} u_m^{(n)*} + \mu Q_{4m}^{(j)} w_m'^{(n)*} = Q_{2m}^{(n)*} v_m^{(j)} + Q_{3m}^{(n)*} w_m^{(j)} + i \frac{\rho}{\gamma^3 \mu \Omega} \int_0^1 p_m^{(j)} \vartheta_m^{(n)*} r dr \quad n^* \neq j \quad (46)$$

Now, multiplying each side by $\exp((k_m^{(j)} + k_m^{(n)*})|x - \xi|)$ we get

$$\begin{aligned} & \left[Q_{1m}^{(j)} u_m^{(n)*} + \mu Q_{4m}^{(j)} w_m'^{(n)*} \right] \exp((k_m^{(j)} + k_m^{(n)*})|x - \xi|) = \\ & \left[Q_{2m}^{(n)*} v_m^{(j)} + Q_{3m}^{(n)*} w_m^{(j)} + i \frac{\rho}{\gamma^3 \mu \Omega} \int_0^1 p_m^{(j)} \vartheta_m^{(n)*} r dr \right] \exp((k_m^{(j)} + k_m^{(n)*})|x - \xi|) \end{aligned} \quad (47)$$

which reduce to Eq. (48) using the holomorphic properties of exponents and the integral i.e. $\int_0^1 p_m^{(j)} \vartheta_m^{(n)*} r dr = \left(\int_0^1 p_m^{(j)*} \vartheta_m^{(n)} r dr \right)^*$.

$$\begin{aligned} & \left[\mathcal{Q}_{1m}^{(j)} u_m^{(n)*} + \mu \mathcal{Q}_{4m}^{(j)} w_m'^{(n)*} \right] \exp\left((k_m^{(j)} + k_m^{(n)*})|x - \xi|\right) = \\ & \left[\mathcal{Q}_{2m}^{(n)} v_m^{(j)*} + \mathcal{Q}_{3m}^{(n)} w_m^{(j)*} + i \frac{\rho}{\gamma^3 \mu \Omega} \int_0^1 p_m^{(j)*} \vartheta_m^{(n)} r dr \right]^* \exp\left((k_m^{(j)*} + k_m^{(n)})|x - \xi|\right)^* \end{aligned} \quad (48)$$

Substituting Eq. (48) into Eq. (43) we immediately see that by addition of complex conjugated functions only real values preserve. From this we recognise that using only Class properties and the bi-orthogonality relation we have proven that cross-terms do not contribute with energy to the total energy flow since they are self-equilibrating. As these properties have previously (Sec. 3.2) been proven to be generic for symmetric waveguides we have proven that the total energy flow in symmetric waveguides is in fact a linear quantity obeying the principle of superposition.

Now, it is easy to show that $R_m^{(n,n)}$ is related to the total energy flow through its imaginary part (scaled by $\frac{\pi \chi_m}{2} \Omega$). As it has now been proven that the total energy flow in symmetric waveguides obey superposition it may be formulated as

$$\begin{aligned} N_m^\Sigma = \frac{\pi \chi_m}{2} \Omega \sum_{n=1}^{\infty} \text{Im} \left(\left[\mathcal{Q}_{1m}^{(n)} u_m^{(n)*} + \mathcal{Q}_{2m}^{(n)} v_m^{(n)*} + \mathcal{Q}_{3m}^{(n)} w_m^{(n)*} + \mu \mathcal{Q}_{4m}^{(n)} w_m'^{(n)*} \right. \right. \\ \left. \left. + i \frac{\rho}{\gamma^3 \mu \Omega} \int_0^1 p_m^{(n)*} \vartheta_m^{(n)} r dr \right] \exp\left((k_m^{(n)} + k_m^{(n)*})|x - \xi|\right) \right) \end{aligned} \quad (49)$$

Given that we only consider the imaginary part we see, using again the maps of Eq. (45), that the identities in Eq. (50) hold. Here index A and B refer to the Class properties of the functions (valid for $0F = 02, 03, 05$).

$$\begin{aligned} \text{Im}\left(\mathcal{Q}_{1m}^A u_m^{B*}\right) &= \text{Im}\left(\mathcal{Q}_{1m}^A\right) u_m^B & \text{Im}\left(\mathcal{Q}_{2m}^B v_m^{A*}\right) &= -\mathcal{Q}_{2m}^B \text{Im}\left(v_m^A\right) \\ \text{Im}\left(\mathcal{Q}_{3m}^B w_m^{A*}\right) &= -\mathcal{Q}_{3m}^B \text{Im}\left(w_m^A\right) & \text{Im}\left(\mathcal{Q}_{4m}^A w_m'^{B*}\right) &= \text{Im}\left(\mathcal{Q}_{4m}^A\right) w_m'^B \\ \text{Im}\left(p_m^{A*} \vartheta_m^B\right) &= -\text{Im}\left(p_m^A\right) \vartheta_m^B \end{aligned} \quad (50)$$

These identities are easily verified for decaying waves where all components are real and for propagating waves where Class B components are real and Class A components purely imaginary such that the conjugated may be replaced by a sign change. For attenuating waves, however, the identities do not hold but since they exist in conjugated wave-pairs in both domain and codomain the imaginary parts cancel and leaves only a real part when in the expansion. Thus, the attenuating waves are self-equilibrating as they carry energy of the same magnitude but in opposite direction and need therefore not be considered further here.

Hence the total energy in Eq. (49) reduces to Eq. (51) and can thereby be expressed

in terms of $R_m^{(n,n)}$, see Eq. (52).

$$N_m^\Sigma = \frac{\pi\chi_m}{2}\Omega \sum_{n=1}^{\infty} \text{Im} \left(\left[Q_{1m}^{(n)}u_m^{(n)} - Q_{2m}^{(n)}v_m^{(n)} - Q_{3m}^{(n)}w_m^{(n)} + \mu Q_{4m}^{(n)}w_m^{(n)} - i\frac{\rho}{\gamma^3\mu\Omega} \int_0^1 p_m^{(n)}\vartheta_m^{(n)}rdr \right] \exp\left((k_m^{(n)} + k_m^{(n)*})|x - \xi|\right) \right) \quad (51)$$

⇕

$$N_m^\Sigma = \frac{\pi\chi_m}{2}\Omega \sum_{n=1}^{\infty} \text{Im} \left(R_m^{(n,n)} \right) \exp\left((k_m^{(n)} + k_m^{(n)*})|x - \xi|\right) \quad (52)$$

where we clearly see the linearity of the total energy flow and further that the exponents become real-valued for any wavenumber due to the complex conjugated and may therefore be move outside the brackets. Again, we note that the attenuating wave-pair carry energy in opposite direction.

Now, to assess each wave types contribution to the total energy flow we define for the domains the corresponding codomains of $R_m^{(n,n)}$. These maps can easily be established from those in Eq. (45) since the product between even/odd functions is an odd function such that $R_m^{(n,n)}$ adopts the endomorphic properties of the Class A functions. Note, however, that this is true only when $n = j$ as indicated in Eq. (53).

$$R_m^{(n,n)} : \begin{cases} i\mathbb{R} & \rightarrow i\mathbb{R} \\ \mathbb{R} & \rightarrow \mathbb{R} \\ \mathbb{C} & \rightarrow \mathbb{C} \\ \mathbb{C}^* & \rightarrow \mathbb{C}^* \end{cases} \quad (53)$$

Using these maps, it is straightforward to see that decaying waves do not have an imaginary part and do thereby not contribute to the total energy flow while attenuating wave-pairs produce energy in opposite directions as already discussed. Thus, it is obvious that only propagating waves contribute to the total energy flow as discussed in [1, 6], however, not shown explicitly as in this paper. The total energy flow may then conveniently be reformulated to Eq. (54), where n counts only the propagating waves and the exponents become unity.

$$N_m^\Sigma = \frac{\pi\chi_m}{2}\Omega \text{Im} \left(\sum_{n=1}^N R_m^{(n,n)} \right) = \frac{\pi\chi_m}{2}\Omega \text{Im} \left(\sum_{n=1}^N \bar{R}_m^{(n,n)} \left(W_m^{(n)} \right)^2 \right) \quad (54)$$

This reformulation of the total energy flow emphasises that though the cross-terms may produce component-wise energy they produce a zero net energy. This simplification of the total energy flow is derived based on Class properties and the bi-orthogonality relation alone and is therefore generic for any symmetric waveguide as they retain both Class properties and bi-orthogonality relations as discussed in Sec. 3.2. Obviously, this can easily be derived also for loading condition $0F = 01,04$ as the indices are interchangeable and further, also for the general solution not satisfying

decay and radiation conditions.

As illustrated in e.g. Eq. (52), $R_m^{(n,n)}$ constitute the sum of modal energy of all transmission paths and includes both real and imaginary parts in which the imaginary part is authentic energy according to the definition in [43], and the real part may be perceived as pseudo-energy. Hence, $R_m^{(n,n)}$ is the total energy of each mode and may therefore be denoted the '*Total modal energy*'. In view of the latter it is appealing to also discuss $R_m^{(n,n)}$ in the framework of the governing equation for the modal amplitudes for a single point source in a homogeneous waveguide (Green's matrix) as derived in Eq. (31) and reprinted here ($0F = 03$).

$$\begin{aligned}
 R_m^{(n,n)} &= \bar{R}_m^{(n,n)} \left(W_m^{03(n)} \right)^2 \\
 &= \left[\bar{Q}_{1m}^{(n)} \bar{u}_m^{(n)} + \mu \bar{Q}_{4m}^{(n)} \bar{w}_m^{(n)} - \bar{Q}_{2m}^{(n)} \bar{v}_m^{(n)} - \bar{Q}_{3m}^{(n)} \bar{w}_m^{(n)} \right. \\
 &\quad \left. - i \frac{\rho}{\gamma^3 \mu \Omega} \int_0^1 \bar{P}_m^{(n)} \bar{\vartheta}_m^{(n)} r dr \right] \left(W_m^{03(n)} \right)^2 = \frac{1}{2} \bar{W}_m^{(n)} W_m^{03(n)}
 \end{aligned} \tag{55}$$

⇓

$$W_m^{03(n)} = \frac{1}{2} \frac{\bar{W}_m^{(n)}}{\bar{R}_m^{(n,n)}} \tag{56}$$

As seen from Eq. (55) the relation from which we derive the modal amplitudes constitutes a modal energy balance in which the '*Total modal energy*' conveyed through the structure (left-hand-side of Eq. (55)) balances the energy injected into that particular mode by external forcing (right-hand-side of Eq. (55)) such that only a unique choice of modal amplitudes satisfy the energy balance.

In conclusion, we note that since $R_m^{(n,n)}$ is formulated in terms of a real and imaginary part it always preserves both the correct phase and magnitude of each modal amplitude such as to ensure the correct contribution of energy of each mode, see Eq. (56). Further, it ensures the correctness of the Class properties and thereby correctness of the solution for all loading conditions. It is, however, important to note that there is found no direct relation between the real part of R_m (where $R_m = \sum_{n=1}^N R_m^{(n,n)}$) and the discarded real-part of the total energy flow but since $R_m^{(n,n)}$ preserves the correct magnitude and phase of the modal amplitudes we may regard $R_m^{(n,n)}$ as somewhat stronger than the total energy flow. Thus, formulating Eq. (55) using the total energy flow as defined in [43] will not provide the correct modal amplitudes.

Further, the interpretation of the energy balance in Eq. (55) suggests that a similar balance may be formulated for unsymmetric waveguides and is a subject of the ongoing work. As shown here we may expect that the relation is closely related to the total energy flow.

6.3.1. Alternative derivation using Eq. (42)

From the direct expansion in Eq. (42) the zero energy contribution of cross-terms is not immediately clear as this formulation has no immediate relation to the bi-orthogonality relation because the cross-energies retain an imaginary part. However,

as the relation between total energy flow and R_m from the previous section must of course also hold using this formulation, the cross-energy must be self-equilibrating when in the expansion. For consistency, we show using the formulation in Eq. (42) that the total energy flow is self-adjoint by showing that the cross-energy satisfy conjugated symmetry i.e. $N_m^{\Sigma(n,j)} = N_m^{\Sigma(j,n)*}$, which emphasize the self-equilibrating nature of the cross-terms. To show this we need just to prove that the relation in Eq. (57) holds.

$$\begin{aligned} & \left[\mathcal{Q}_{1m}^{(n)} u_m^{(j)*} + \mathcal{Q}_{2m}^{(n)} v_m^{(j)*} + \mathcal{Q}_{3m}^{(n)} w_m^{(j)*} + \mu \mathcal{Q}_{4m}^{(n)} w_m'^{(j)*} \right. \\ & \quad \left. + i \frac{\rho}{\gamma^3 \mu \Omega} \int_0^1 p_m^{(j)*} \vartheta_m^{(n)} r dr \right] \exp((k_m^{(n)} + k_m^{(j)*})|x - \xi|) = \\ & \left[\mathcal{Q}_{1m}^{(j)} u_m^{(n)*} + \mathcal{Q}_{2m}^{(j)} v_m^{(n)*} + \mathcal{Q}_{3m}^{(j)} w_m^{(n)*} + \mu \mathcal{Q}_{4m}^{(j)} w_m'^{(n)*} \right. \\ & \quad \left. + i \frac{\rho}{\gamma^3 \mu \Omega} \int_0^1 p_m^{(n)*} \vartheta_m^{(j)} r dr \right]^* \exp((k_m^{(j)} + k_m^{(n)*})|x - \xi|)^* \end{aligned} \quad (57)$$

Using again the holomorphic properties we get

$$\begin{aligned} & \mathcal{Q}_{1m}^{(n)} u_m^{(j)*} + \mathcal{Q}_{2m}^{(n)} v_m^{(j)*} + \mathcal{Q}_{3m}^{(n)} w_m^{(j)*} + \mu \mathcal{Q}_{4m}^{(n)} w_m'^{(j)*} + i \frac{\rho}{\gamma^3 \mu \Omega} \int_0^1 p_m^{(j)*} \vartheta_m^{(n)} r dr \\ & - \mathcal{Q}_{1m}^{(j)*} u_m^{(n)} - \mathcal{Q}_{2m}^{(j)*} v_m^{(n)} - \mathcal{Q}_{3m}^{(j)*} w_m^{(n)} - \mu \mathcal{Q}_{4m}^{(j)*} w_m'^{(n)} - i \frac{\rho}{\gamma^3 \mu \Omega} \int_0^1 p_m^{(n)} \vartheta_m^{(j)*} r dr = 0 \end{aligned} \quad (58)$$

⇕

$$\begin{aligned} & \mathcal{Q}_{1m}^{(n)} u_m^{(j)*} + \mu \mathcal{Q}_{4m}^{(n)} w_m'^{(j)*} - \mathcal{Q}_{2m}^{(j)*} v_m^{(n)} - \mathcal{Q}_{3m}^{(j)*} w_m^{(n)} - i \frac{\rho}{\gamma^3 \mu \Omega} \int_0^1 p_m^{(n)} \vartheta_m^{(j)*} r dr = \\ & \mathcal{Q}_{1m}^{(j)*} u_m^{(n)} + \mu \mathcal{Q}_{4m}^{(j)*} w_m'^{(n)} - \mathcal{Q}_{2m}^{(n)} v_m^{(j)*} - \mathcal{Q}_{3m}^{(n)} w_m^{(j)*} - i \frac{\rho}{\gamma^3 \mu \Omega} \int_0^1 p_m^{(j)*} \vartheta_m^{(n)} r dr \end{aligned} \quad (59)$$

Again we use the Class properties (and maps in Eq. (45)) to remove the conjugate operator on the left-hand-side of Eq. (59) (for $0F = 02, 03, 05$) and since we are only concerned with the cancelling of each cross-term with its self-adjoint counterpart ($n \neq j$) we note that the left-hand-side is zero by virtue of the bi-orthogonality relation. Thus, Eq. (59) reduce to Eq. (60) which may then be reformulated to Eq. (61).

$$\mathcal{Q}_{1m}^{(j)*} u_m^{(n)} + \mu \mathcal{Q}_{4m}^{(j)*} w_m'^{(n)} - \mathcal{Q}_{2m}^{(n)} v_m^{(j)*} - \mathcal{Q}_{3m}^{(n)} w_m^{(j)*} - i \frac{\rho}{\gamma^3 \mu \Omega} \int_0^1 p_m^{(j)*} \vartheta_m^{(n)} r dr = 0 \quad (60)$$

⇕

$$\left(\mathcal{Q}_{1m}^{(j)} u_m^{(n)*} + \mu \mathcal{Q}_{4m}^{(j)} w_m'^{(n)*} - \mathcal{Q}_{2m}^{(n)*} v_m^{(j)} - \mathcal{Q}_{3m}^{(n)*} w_m^{(j)} - i \frac{\rho}{\gamma^3 \mu \Omega} \int_0^1 p_m^{(j)} \vartheta_m^{(n)*} r dr \right)^* = 0 \quad (61)$$

The relation in brackets is similar to the left-hand-side of Eq. (59), in that the conjugated operator may be removed on the Class B functions and the equation is again zero by virtue of bi-orthogonality as the indices are interchangeable, see Sec. 3.1. Thus, the relation in Eq. (57) holds and the formulation in Eq. (42) is therefore self-adjoint, confirming that the cross-energy equilibrate and does not contribute to the total energy flow.

6.4. Discussion of cross-energy in the transmission paths

As discussed in Sec. 6.3 the total energy flow is produced by the principal values of propagating waves. However, the energy contribution to each of the physical transmission paths defined in Appendix C does not obey such simplifications. The contribution to energy in each transmission path by these cross-terms are discussed in the following with interest in the discussion of energy flow in evanescent waves for beams, [44], and the discussion of energy in shells, [6].

First, we generalise the study of energy flow in transmission paths by introducing a general modal energy flow component, denoted $\mathcal{N}_m^{TP(n,j)}$, in which we require that n always refer to Class A components and j always to Class B components. Hence, $\mathcal{N}_m^{TP(n,j)}$ (with TP omitted hereinafter) represents any given transmission path from Appendix C and is expanded as in Eq. (62) where $n \neq j$ constitutes the cross-terms and $n = j$ the principal values.

$$\mathcal{N}_m = \sum_{n=1}^{\infty} \sum_{j=1}^{\infty} \text{Im} \left(\mathcal{N}_m(k_m^{(n)}, k_m^{(j)}) \right) = \sum_{n=1}^{\infty} \sum_{j=1}^{\infty} \text{Im} \left(\mathcal{N}_m^{(n,j)} \right) \quad (62)$$

Now, to characterise the energy contribution of each cross-term to the transmission paths, $\mathcal{N}_m^{(n,j)}$, we study, initially, the most general case where $x \neq \xi$ by considering the domain/codomain (maps) as previously see e.g. Eq. (45) and (53). The maps are established straightforwardly using the Class maps from Eq. (45) and the simple map of exponents. From these maps it can easily be shown that when any index (n or j) is 'subjected' to a propagating wave cross-energy is produced no matter the origin of the corresponding wave (j or n , respectively) and the waves are said to interact in the sense that they produce cross-energy. On the other hand, evanescent waves (attenuating and decaying) do not interact in the sense of producing cross-energy because the imaginary part is either zero (decaying/decaying) or self-equilibrating (attenuating/attenuating or attenuating/decaying). Thus, in brief, we may characterise the contribution of cross-energy to the energy in each transmission path (for $x \neq \xi$) as

$$\begin{aligned} \left\{ \text{Im} \left(\mathcal{N}_m^{(n,j)} \right) \mid k_m^{(n)} \vee k_m^{(j)} \in i\mathbb{R} \right\} &\neq \{0\} &\Rightarrow &\text{Energy contribution} \\ \left\{ \text{Im} \left(\mathcal{N}_m^{(n,j)} \right) \mid k_m^{(n)}, k_m^{(j)} \notin i\mathbb{R} \right\} &= \{0\} &\Rightarrow &\text{No energy contribution} \end{aligned} \quad (63)$$

where evanescent waves 'interacting' with any other evanescent wave is regarded as non-contributing since they have either no imaginary part or exist in conjugated pairs and therefore produce a zero net energy flow in the expansion.

Now, by virtue of the energy contribution from the cross-terms, defined in Eq. (63), we can simplify the expansion of Eq. (62) to Eq. (64), where n counts propagating waves and δ_{jn} is Kronecker's delta.

$$\mathcal{N}_m = \sum_{n=1}^N \sum_{j=1}^{\infty} \text{Im} \left(\mathcal{N}_m^{(n,j)} + (1 - \delta_{jn}) \mathcal{N}_m^{(j,n)} \right) \quad (64)$$

As mentioned the energy contribution characterised in Eq. (63) may be perceived as the most general case, however, for the special case of $x \rightarrow \xi$ where the exponents goes to 1 for all cross-terms the contribution of cross-energy is reduced to half of those in Eq. (63). For this particular case where we consider the loaded cross-section it is interesting to note that only special configurations of waves interact and produce energy. When considering the cross-energy contribution to the transmission paths at the excitation point through the maps we see that only when a propagating wave is 'applied' in the Class A components (index n) does it produce energy with all other waves, while no energy is produced if the propagating wave is 'applied' in the Class B components (index j). In this special case we can say, in brief, that;

$$\begin{aligned} \left\{ \text{Im} \left(\mathcal{N}_m^{(n,j)} \right) \mid k_m^{(n)} \in i\mathbb{R} \right\} \neq \{0\} & \Rightarrow \text{Energy contribution} \\ \left\{ \text{Im} \left(\mathcal{N}_m^{(n,j)} \right) \mid k_m^{(n)} \notin i\mathbb{R} \right\} = \{0\} & \Rightarrow \text{No energy contribution} \end{aligned} \quad (65)$$

where we recall that n refer to Class A components as defined in Eq. (62). Note that at the excitation point the cross-energy balance the principal value(s) in the non-loaded transmission paths and in the loaded transmission path the energy sums to the total energy.

In conclusion, the maps in Eq. (45) permit the necessary knowledge to assess the generation of total energy flow and cross-energy flow in the different transmission paths. This conveniently allow us to simplify the total energy flow as well as the individual transmission path energy flow equations such as to improve the computational efficiency of these energy calculations. Again, this can easily be generalised to any waveguide for which the Class properties persist.

7. Conclusions

In this paper the tailored Green's matrices for an elastic cylindrical shell filled with an inviscid compressible fluid without mean flow in time-harmonic vibrations have been derived. The formulation of these matrices based on the canonical modal decomposition method has been facilitated by use of the specially derived orthogonality relations. These relations give explicit formulas for modal amplitudes and, therefore, allow for detailed convergence and error estimation studies. The main novel results presented in the paper are summarized as follows:

- The bi-orthogonality relation for the canonical model of the fluid-filled shell is derived and generalised to any symmetric waveguide. This derivation relies upon the division of all variables, defining the state of such a waveguide, into two classes having opposite oddness/evenness properties with respect to wavenumbers
- The completeness and convergence of Green's matrices for the fluid-filled shell is assessed
- The relation between the bi-orthogonality relation and total energy flow is derived and explained

- Simplified equations for the individual energy flow components are deduced by studying energy contributions from cross-terms (i.e. related to different wavenumbers) in the total energy flow

As mentioned above and discussed throughout the paper the present method to construct Green's matrices and analyse the energy flow is restricted to symmetric waveguides. However, as several significant advantages over the conventional solution have been discovered, it is relevant to explore the possibilities to generalise the method to unsymmetrical waveguides such as, for instance, the fluid-filled shell with mean flow or anisotropic shells. This task constitutes the subject of our on-going work.

Appendix A. Novozhilov-Gol'denweizer's shell theory and standard linear acoustics

The detailed derivation of the equations can be found in [2] and the equations are therefore only presented in brief here, however, formulated in non-dimensional form assuming time-harmonic vibrations. To reformulate the following equations and non-dimensional quantities into dimensional form the scaling shown in Eq. (A.1) must be applied.

$$\begin{aligned}
u_m^{(n)}(x, \theta) &= \frac{1}{R} \tilde{u}_m^{(n)}(x, \theta) & w_m^{(n)}(x, \theta) &= \frac{1}{R} \tilde{w}_m^{(n)}(x, \theta) \\
v_m^{(n)}(x, \theta) &= \frac{1}{R} \tilde{v}_m^{(n)}(x, \theta) & \phi_m^{(n)}(x, \theta, r) &= \frac{1}{R c_{fl}} \tilde{\phi}_m^{(n)}(x, \theta, r) \\
Q_{lm}^{(n)}(x, \theta) &= \frac{1 - \nu^2}{Eh} \tilde{Q}_{lm}^{(n)}(x, \theta) & \vartheta_m^{(n)}(x, \theta, r) &= \frac{1}{c_{fl}} \tilde{\vartheta}_m^{(n)}(x, \theta, r) \\
&& & \text{for } l = 1, 2, 3 \tag{A.1} \\
Q_{4m}^{(n)}(x, \theta) &= \frac{1 - \nu^2}{Eh^2} \tilde{Q}_{4m}^{(n)}(x, \theta) & p_m^{(n)}(x, \theta, r) &= \frac{1}{c_{fl}^2 \rho_{fl}} \tilde{p}_m^{(n)}(x, \theta, r) \\
q_{lm}^{(n)}(x, \theta) &= \frac{1 - \nu^2}{E} \tilde{q}_{lm}^{(n)}(x, \theta) & T_m^{(n)}(x, \theta, r) &= \frac{R}{c_{fl}} \tilde{T}_m^{(n)}(x, \theta, r) \\
&& & \text{for } l = 1, 2, 3
\end{aligned}$$

where the dimensional quantities are indicated by \sim and the non-dimensional quantities are given in Eq. (3) and (A.6).

From the action integral the governing equations for free vibrations of a fluid-filled shell are given in Eq. (A.2), the fluid's motion in cylindrical coordinates in Eq. (A.3)

and the continuity at the fluid-structure interface in Eq. (A.4).

$$\begin{aligned}
& -\frac{\partial^2 u}{\partial x^2} - \frac{1-\nu}{2} \frac{\partial^2 u}{\partial \theta^2} - \frac{1+\nu}{2} \frac{\partial^2 v}{\partial x \partial \theta} - \nu \frac{\partial w}{\partial x} - \Omega^2 u = -\frac{q_1}{\mu} \\
& -\frac{1+\nu}{2} \frac{\partial^2 u}{\partial x \partial \theta} - \frac{1-\nu}{2} \frac{\partial^2 v}{\partial x^2} - \frac{\partial^2 v}{\partial \theta^2} - \frac{\partial w}{\partial \theta} - \frac{2\mu^2(1-\nu)}{12} \frac{\partial^2 v}{\partial x^2} - \frac{\mu^2}{12} \frac{\partial^2 v}{\partial \theta^2} \\
& \quad + \frac{\mu^2}{12} \frac{\partial^3 w}{\partial \theta^3} + \frac{\mu^2(2-\nu)}{12} \frac{\partial^3 w}{\partial x^2 \partial \theta} - \Omega^2 v = -\frac{q_2}{\mu}
\end{aligned} \tag{A.2}$$

$$\begin{aligned}
& \nu \frac{\partial u}{\partial x} + \frac{\partial v}{\partial \theta} + w - \frac{\mu^2}{12} \frac{\partial^3 v}{\partial \theta^3} - \frac{\mu^2(2-\nu)}{12} \frac{\partial^3 v}{\partial x^2 \partial \theta} + \frac{\mu^2}{12} \frac{\partial^4 w}{\partial x^4} + \frac{2\mu^2}{12} \frac{\partial^4 w}{\partial x^2 \partial \theta^2} \\
& \quad + \frac{\mu^2}{12} \frac{\partial^4 w}{\partial \theta^4} - \Omega^2 w - i\Omega \frac{\rho}{\gamma\mu} \phi = -\frac{q_3}{\mu}
\end{aligned}$$

$$\frac{\partial^2 \phi}{\partial x^2} + \frac{\partial^2 \phi}{\partial r^2} + \frac{1}{r} \frac{\partial \phi}{\partial r} + \frac{1}{r^2} \frac{\partial^2 \phi}{\partial \theta^2} + \Omega^2 \gamma^2 \phi = -T \tag{A.3}$$

$$\left. \frac{\partial \phi}{\partial r} \right|_{r=1} = -i\Omega \gamma w \tag{A.4}$$

The generalised displacements (field variables) of Eq. (A.2)–(A.4) are associated with a set of generalised forces as illustrated in Eq. (A.5).

$$\begin{aligned}
Q_1(x, \theta) & \sim u(x, \theta) & Q_2(x, \theta) & \sim v(x, \theta) & Q_3(x, \theta) & \sim w(x, \theta) \\
Q_4(x, \theta) & \sim \frac{\partial w(x, \theta)}{\partial x} & p(x, \theta, r) & \sim \vartheta(x, \theta, r)
\end{aligned} \tag{A.5}$$

The generalised forces (with (x, θ, r) omitted) are also derived from the action integral, see Eq. (A.6).

$$\begin{aligned}
Q_1 & = \frac{\partial u}{\partial x} + \nu \frac{\partial v}{\partial \theta} + \nu w \\
Q_2 & = \frac{1-\nu}{2} \frac{\partial v}{\partial x} + \frac{1-\nu}{2} \frac{\partial u}{\partial \theta} + \frac{2\mu^2(1-\nu)}{12} \frac{\partial v}{\partial x} - \frac{2\mu^2(1-\nu)}{12} \frac{\partial^2 w}{\partial x \partial \theta} \\
Q_3 & = -\frac{\mu^2}{12} \left[\frac{\partial^3 w}{\partial x^3} + (2-\nu) \frac{\partial^3 w}{\partial x \partial \theta^2} - (2-\nu) \frac{\partial^2 v}{\partial x \partial \theta} \right] \\
Q_4 & = \frac{\mu}{12} \left[\frac{\partial^2 w}{\partial x^2} + \nu \frac{\partial^2 w}{\partial \theta^2} - \nu \frac{\partial v}{\partial \theta} \right] \\
p & = i\Omega \gamma \phi
\end{aligned} \tag{A.6}$$

where Q_l ($l = 1, \dots, 4$) is, respectively, the membrane axial force, membrane shear force (which produce a torsional moment), flexural transverse shear force, flexural axial bending moment and p is the acoustic pressure.

To solve the partial differential equations for free waves, i.e. $q_1 = q_2 = q_3 = T = 0$, we substitute the ansatz of Eq. (3) into the governing equations and arrive at the determinantal equation shown in Eq. (1) – also known as the dispersion equation. This equation is then solved for the axial wavenumbers to provide a set of eigenfunctions, from which the general solution can be assembled through the method of eigenfunction expansion. Note that the ansatz for the velocity potential is simplified from the general Hankel-function to the Bessel-function as the solution must be bounded at $r \rightarrow 0$.

Due to axi-symmetry of the cylindrical shell and orthogonality of the circumferential eigenfunctions, $\exp(-im\theta)$, the governing equation is uncoupled in the m -spectrum and the dispersion equation is solved at each circumferential wavenumber, $m \in \mathbb{Z}$ – indicated by the subscript. Each uncoupled dispersion equation contains, due to presence of a compressible fluid, an infinite number of roots (wavenumbers), $k_m^{(n)}$, associated with each frequency and circumferential wavenumber. Finally, due to the uncoupling of m , the general solution is also found for each circumferential wavenumber as an expansion on the wavenumbers, $k_m^{(n)}$ and the θ -dependence may therefore be omitted hereinafter. For further details, see e.g. [2].

Appendix B. Reciprocity relation

Following [2] we can also derive the reciprocity relation in non-dimensional form for an elastic fluid-filled cylindrical shell, see Eq. (B.1). This relation is valid for any two general solutions, n and j , and its dimensional form can be obtained by scaling with $\frac{EhR^2}{1-\nu^2}$.

$$\begin{aligned} & \left[Q_{1m}^{(n)}(x)u_m^{(j)}(x) + Q_{2m}^{(n)}(x)v_m^{(j)}(x) + Q_{3m}^{(n)}(x)w_m^{(j)}(x) + \mu Q_{4m}^{(n)}(x)w_m^{\prime(j)}(x) \right. \\ & \quad \left. + i \frac{\rho}{\gamma^3 \Omega \mu} \int_0^1 p_m^{(j)}(x, r) \vartheta_m^{(n)}(x, r) r dr \right]_{x=a}^{x=b} = \\ & \left[Q_{1m}^{(j)}(x)u_m^{(n)}(x) + Q_{2m}^{(j)}(x)v_m^{(n)}(x) + Q_{3m}^{(j)}(x)w_m^{(n)}(x) + \mu Q_{4m}^{(j)}(x)w_m^{\prime(n)}(x) \right. \\ & \quad \left. + i \frac{\rho}{\gamma^3 \Omega \mu} \int_0^1 p_m^{(n)}(x, r) \vartheta_m^{(j)}(x, r) r dr \right]_{x=a}^{x=b} \end{aligned} \quad (\text{B.1})$$

Appendix C. Energy flow

From the reciprocity relation in Appendix B we can generalise to the energy flow formulation which is valid for any general response, see e.g. [1, 2, 6, 43]. Following [2] and reformulating to non-dimensional form the individual energy flow components, which we associate with physical transmission paths, can be expressed in terms

of their generalised (non-dimensional) forces and displacements as seen in Eq. (C.1).

$$\begin{aligned}
N_m^u(x) &= \frac{\pi\chi_m}{2} \Omega \text{Im}(Q_{1m}u_m^*) \\
N_m^w(x) &= \frac{\pi\chi_m}{2} \Omega \text{Im}(Q_{3m}w_m^*) \\
N_m^\theta(x) &= \frac{\pi\chi_m}{2} \frac{\rho}{\gamma^3\mu} \int_0^1 \text{Re}(p_m^* \vartheta_m) r dr \\
N_m^v(x) &= \frac{\pi\chi_m}{2} \Omega \text{Im}(Q_{2m}v_m^*) \\
N_m^{w'}(x) &= \frac{\pi\chi_m}{2} \Omega \mu \text{Im}(Q_{4m}w_m'^*)
\end{aligned} \tag{C.1}$$

where * indicates the complex conjugated, $\chi_{m=0} = 2$ and $\chi_{m \neq 0} = 1$. According to the definitions in relation to Eq. (A.6), N^u , N^v , N^w and $N^{w'}$ constitutes the energy flow in the structural transmission paths, respectively, axial membrane, shear membrane (torsion), transverse shear and axial bending energy and N^θ is the energy flow in the acoustic transmission path.

The total energy flow is then defined as the summation of the energy flow of the individual transmission paths, see Eq. (C.2).

$$N_m^\Sigma(x) = \overbrace{N_m^u(x)}^{\text{Axial}} + \overbrace{N_m^v(x)}^{\text{Torsion}} + \overbrace{N_m^w(x) + N_m^{w'}(x)}^{\text{Flexural}} + \overbrace{N_m^\theta(x)}^{\text{Acoustic}} \tag{C.2}$$

where the dimensional energy flow is obtained by scaling the non-dimensional components with $\frac{EhR}{1-\nu^2} c_{str}$. Similarly, to the case of beam bending within Bernoulli-Euler theory, [43], the transverse shear and axial bending in the thin cylindrical shell constitutes the flexural transmission path.

Appendix C.1. Reformulation of the acoustic energy flow

From Eq. (C.1) it is seen that the structural energy flow components are calculated straightforwardly through algebraic equations. The acoustic energy flow is, on the other hand, an integral equation which is numerically cumbersome. Nonetheless, this integral equation can be reformulated to an algebraic equation as well using some mathematical manipulations and the analytical solution of Lommel's integral (Bessel products), see e.g. [18–20].

The definition of the acoustic energy flow in non-dimensional form is given as

$$N^\theta(x) = \frac{1}{2} \frac{\rho}{\gamma^3\mu} \text{Re} \left(\int_0^{2\pi} \int_0^1 p^* \vartheta r dr d\theta \right) \tag{C.3}$$

By decomposing the m -spectra, substituting the ansatz from Eq. (3) into Eq. (C.3) and utilising the holomorphic properties of the exponential- and Bessel-function i.e. $J_m(\kappa^{(j)}r)^* = J_m(\kappa^{*(j)}r)$, we arrive at Eq. (C.4). Note that the acoustic energy flow is not a linear quantity and thus the general solution (eigenfunction expansion) is considered.

$$N_m^\theta(x) = \frac{\pi\chi_m}{2} \frac{\rho}{\gamma^3\mu} \sum_{n=1}^{\infty} \sum_{j=1}^{\infty} \text{Re} \left(\hat{p}_m^{(j)*}(x) \hat{\vartheta}_m^{(n)}(x) \int_0^1 J_m(\kappa_m^{(n)}r) J_m(\kappa_m^{(j)*}r) r dr \right) \tag{C.4}$$

$$\text{where } \hat{\vartheta}_m^{(n)} = -i\Omega\gamma k_m^{(n)} \left[\frac{dJ_m(\kappa_m^{(n)} r)}{dr} \Big|_{r=1} \right]^{-1} W_m^{(n)} \exp(k_m^{(n)} x)$$

$$\hat{p}_m^{(j)} = \Omega^2 \gamma^2 \left[\frac{dJ_m(\kappa_m^{(j)} r)}{dr} \Big|_{r=1} \right]^{-1} W_m^{(j)} \exp(k_m^{(j)} x)$$

and the integral can be recognised as Lommel's integral which has an analytical solution, see e.g. [18–20].

Now, Eq. (C.4) can be rearranged into the convenient matrix form shown in Eq. (C.5).

$$N_m^\vartheta(x) = \frac{\pi\chi_m}{2} \frac{\rho}{\gamma^3 \mu} \sum \text{Re}(\hat{\mathbf{N}}_m(x) \mathbf{H}_m) \quad (\text{C.5})$$

$$\text{where } \hat{\mathbf{N}}_m(x) = \hat{\mathbf{p}}_m^*(x) \hat{\vartheta}_m^T(x), \quad \mathbf{H}_m = \int_0^1 \mathbf{J}_m(r) \mathbf{J}_m^{*T}(r) r dr$$

T is the transposed, $\hat{\mathbf{p}}$, $\hat{\vartheta}$ and \mathbf{J} are $M \times 1$ vectors of the modes of $\hat{p}_m^{(j)}$, $\hat{\vartheta}_m^{(n)}$ and $J_m(\kappa_m^{(n)} r)$ and M is the number of waves retained in the expansion. $\hat{\mathbf{N}}$ and \mathbf{H} are $M \times M$ matrices and \sum indicates the sum of all elements of the matrix.

In this matrix formulation we note that \mathbf{H}_m holds conjugated symmetry meaning that \mathbf{H}_m is Hermitian (self-adjoint) i.e. $\mathbf{H}_m^{ij} = \mathbf{H}_m^{ji*}$ which can be shown by applying the holomorphic properties of the Bessel-function and integral. This allow us, whether the integral is solved numerically or analytically, to reduce the number of computations of the cumbersome integral by $\left(\frac{1}{2} - \frac{1}{M^2}\right)$ which is approximately $\approx \frac{1}{2}$ for large M .

References

- [1] C. R. Fuller, F. J. Fahy, Characteristics of wave propagation and energy distributions in cylindrical elastic shells filled with fluid, *J. Sound and Vibration* 81(4) (1982) 501–518. doi:10.1016/0022-460X(82)90293-0.
- [2] S. V. Sorokin, J. B. Nielsen, N. Olhoff, Green's matrix and the boundary integral equation method for the analysis of vibration and energy flow in cylindrical shells with and without internal fluid, *J. Sound and Vibration* 271 (2004) 815–847. doi:10.1016/S0022-460X(03)00755-7.
- [3] S. V. Sorokin, A. V. Terentiev, Flow-induced vibrations of an elastic cylindrical shell conveying a compressible fluid, *J. Sound and Vibration* 296 (2006) 777–796. doi:10.1016/j.jsv.2006.03.028.
- [4] S. V. Sorokin, O. A. Ershova, Analysis of the energy transmission in compound cylindrical shells with and without internal heavy fluid loading by boundary integral equations and by Floquet theory, *J. Sound and Vibration* 291 (2006) 81–99. doi:10.1016/j.jsv.2005.05.031.
- [5] B. O. Olsen, Vibroacoustic power flow in infinite compliant pipes excited by mechanical forces and internal acoustic sources, Ph.D. thesis, University of Southampton, Institute of Sound and Vibration Research (2001).
- [6] G. Pavić, Vibrational energy flow in elastic circular cylindrical shells, *J. Sound and Vibration* 142 (1990) 293–310. doi:10.1016/0022-460X(90)90558-H.
- [7] T. Myint-U, L. Debnath, *Linear Partial Differential Equations for Scientists and Engineers*, 4th, Birkhäuser, 2007. doi:10.1007/978-0-8176-4560-1.
- [8] S. S. Bayin, *Mathematical methods in science and engineering*, 1st, Wiley, 2006.

- [9] G. C. Hsiao, W. L. Wendland, *Boundary Integral Equations*, 1st, Springer, 2008. doi:10.1007/978-3-540-68545-6.
- [10] F. Fahy, P. Gardonio, *Sound and Structural Vibration*, 2nd, Elsevier, 2007.
- [11] S. V. Sorokin, The Green's matrix and the boundary integral equations for analysis of time-harmonic dynamics of elastic helical springs, *J. Acoustical Society of America* 129 (2011) 1315–1323. doi:10.1121/1.3543985.
- [12] L. I. Slepyan, S. V. Sorokin, Analysis of structural-acoustic coupling problems by a two-level boundary integral method, part I: A general formulation and test problems, *J. Sound and Vibration* 184(2) (1995) 195–211. doi:10.1006/j.svi.1995.0312.
- [13] L. S. Ledet, S. V. Sorokin, J. B. Larsen, M. M. Lauridsen, Bi-orthogonality conditions for power flow analysis in fluid-loaded elastic cylindrical shells: Theory and applications, in: *5th International Conference on Noise and Vibration - Emerging Technologies (NOVEM)*, no. 51151, 2015.
- [14] L. S. Ledet, S. V. Sorokin, Vibro-acoustics of infinite and finite elastic fluid-filled cylindrical shells, *Procedia Engineering* 199 (2017) 1362–1367. doi:10.1016/j.proeng.2017.09.356.
- [15] B. Karp, Generation of symmetric Lamb waves by non-uniform excitations, *J. Sound and Vibration* 312 (2008) 195–209. doi:10.1016/j.jsv.2007.10.041.
- [16] Y. I. Bobrovnikskii, Orthogonality relations for Lamb waves, *Soviet Acoustical Physics* 18 (1973) 432–433.
- [17] S. V. Sorokin, On the bi-orthogonality conditions for multi-modal elastic waveguides, *J. Sound and Vibration* 332 (2013) 5606–5617. doi:10.1016/j.jsv.2013.05.011.
- [18] G. N. Watson, *A treatise on the theory of Bessel functions*, 2nd, Cambridge University Press, 1966.
- [19] M. Abramowitz, I. A. Stegun, *Handbook of mathematical functions with formulas, graphs, and mathematical tables*, 10th, Dover, New York, 1972.
- [20] C. H. Ziener, F. T. Kurz, L. R. Buschle, T. Kampf, Orthogonality, Lommel integrals and cross product zeros of linear combinations of Bessel functions, *SpringerPlus* 4:390. doi:10.1186/s40064-015-1142-0.
- [21] J. D. Achenbach, *Reciprocity in elastodynamics*, 2nd, Cambridge University Press, 2003. doi:10.1017/CB09780511550485.
- [22] L. I. Slepyan, Betty theorem and orthogonality relations for eigenfunctions, *Mechanics of Solids* 14(1) (1979) 74–77.
- [23] W. B. Fraser, Orthogonality relation for the Rayleigh-Lamb modes of vibration of a plate, *J. Acoustical Society of America* 59 (1976) 215–216. doi:10.1121/1.380851.
- [24] D. D. Zakharov, Orthogonality of 3d guided waves in viscoelastic laminates and far field evaluation to a local acoustic source, *J. Solids and Structures* 45 (2008) 1788–1803. doi:10.1016/j.jisolsstr.2007.10.025.
- [25] D. D. Zakharov, Generalized orthogonality relations for eigenfunctions in three-dimensional dynamic problem for an elastic layer (in Russian), *Mekhanika Tverdogo Tela* 6 (1988) 62–66.
- [26] B. G. Prakash, Generalised orthogonality relation for rectangular strips in elastodynamics, *J. Mechanics Research Communications* 5 (1978) 251–255. doi:10.1016/0093-6413(78)90019-8.
- [27] W. B. Fraser, An orthogonality relation for the modes of wave propagation in an elastic circular cylinder, *J. Sound and Vibration* 43 (1975) 568–571. doi:10.1016/0022-460X(75)90011-5.
- [28] R. D. Gregory, A note on bi-orthogonality relations for elastic cylinders of general cross section, *J. Elasticity* 13 (1983) 351–355. doi:10.1007/BF00043002.
- [29] D. J. Mead, Wave propagation and natural modes in periodic systems: II. multi-coupled systems, with and without damping, *J. Sound and Vibration* 40 (1975) 19–39. doi:10.1016/S0022-460X(75)80228-8.
- [30] C. R. Fuller, The effects of wall discontinuities on the propagation of flexural waves in cylindrical shells, *J. Sound and Vibration* 75(2) (1981) 207–228. doi:10.1016/0022-460X(81)90340-0.
- [31] R. Kumar, R. W. Stephens, Dispersion of flexural waves in circular cylindrical shells, *Proc. of the Royal Society of London* A329 (1972) 283–297. doi:10.1098/rspa.1972.0114.
- [32] B. R. Mace, E. Manconi, Wave motion and dispersion phenomena: Veering, locking and strong coupling effects, *J. Acoustic Society of America* 131(2) (2012) 1015–1028. doi:10.1121/1.3672647.
- [33] S. S. Rao, *Mechanical Vibrations*, 5th, Pearson, 2011.
- [34] K. F. Graff, *Wave motion in elastic solids*, 1st, Oxford University Press, 1975.
- [35] D. E. Budreck, J. H. Rose, Elastodynamic completeness relations for scattered wavefields, *SIAM J. Appl. Math.* 51 (6) (1991) 1568–1584. doi:10.1137/0151079.

- [36] E. Bai, A. Chen, A symplectic eigenfunction expansion approach for free vibration solutions of rectangular Kirchhoff plates, *J. Vibration and Control* 19(8) (2012) 1208–1215. doi:10.1177/1077546312448503.
- [37] E. Kreyszig, *Advanced Engineering Mathematics*, 10th, Wiley, 2011.
- [38] V. A. Il'in, Convergence of eigenfunction expansions at points of discontinuity of the coefficients of a differential operator, *Mathematical Notes of the Academy of Sciences of the USSR* 22 (1977) 870–882. doi:10.1007/BF01098352.
- [39] A. Rakhimov, On the uniform convergence of the eigenfunction expansions, *J. Physics: Conference Series* 435. doi:10.1088/1742-6596/435/1/012010.
- [40] L. Brandolini, L. Colzani, Localization and convergence of eigenfunction expansions, *J. Fourier Analysis and Applications* 5(5) (1999) 431–447. doi:10.1007/BF01261637.
- [41] W. R. Wade, *Introduction to Analysis*, 4th, Pearson, 2014.
- [42] A. A. Doinikov, Acoustic radiation pressure on a rigid sphere in a viscous fluid, *Proceedings: Mathematical and Physical Sciences* 447(1931) (1994) 447–466. doi:10.1098/rspa.1994.0150.
- [43] L. Cremer, M. Heckl, B. A. T. Petersson, *Structure-Borne Sound*, 3rd, Springer, 2005. doi:10.1007/b137728.
- [44] Y. I. Bobrovnikii, On the energy flow in evanescent waves [Letters to the editor], *J. Sound and Vibration* 152(1) (1992) 175–176. doi:10.1016/0022-460X(92)90073-7.

Paper B

On the application of the bi-orthogonality relations for
analysis of linear dynamical systems

Lasse S. Ledet & Sergey V. Sorokin

*Department of Materials and Production, Aalborg University,
Fibigerstraede 16, 9220 Aalborg East, Denmark*

Submitted to:
Journal of Sound and Vibration

© 2019 Elsevier Ltd. All rights reserved.
The layout has been revised.

On the application of the bi-orthogonality relations for analysis of linear dynamical systems

Lasse S. Ledet^a, Sergey V. Sorokin^a

^a*Department of Materials and Production, Aalborg University, Fibigerstraede 16, 9220 Aalborg, Denmark*

Abstract

The reciprocity and orthogonality relations are generally recognised as robust and convenient tools for solving a broad range of forced/free wave propagation and vibration problems in elastodynamics, acoustics and structural dynamics. Undeservedly, the more powerful bi-orthogonality relation remains relatively obscure in literature despite it has been known for many years, though mainly in the context of the forced Rayleigh-Lamb problem and recently also for shells and springs. The purpose of the paper is to promote the bi-orthogonality relation as the means not only to solve, in a surprisingly simple way, a much broader class of problems for semi-bounded domains in linear dynamics (e.g. waveguides), but also to find solutions to fully bounded problems. In addition, the bi-orthogonality relation reveals analytical closed form solutions for arbitrarily complicated waveguides under certain conditions. The usefulness of the bi-orthogonality relation, which may be applied in any realm of physics, is illustrated here using examples from waveguide theory, ranging from elementary 1D to advanced 3D composite waveguides.

Keywords:

Boundary Identity, Modal Projection, Boundary Integral Equations (BIE), Waveguides, Eigenfrequency analysis

1. Introduction

Solving linear boundary value problems is one of the core subjects of mathematical physics. These problems generally involve a set of equations for the domain (volume) and a set of equations for the bounding surfaces (boundary conditions). In stationary dynamics, whichever realm of physics is taken, these problems are either concerned with unbounded/semi-bounded domains, typically known as wave propagation analysis or with fully bounded domains, typically known as the analysis of formation of standing waves. In this paper, we consider how to efficiently solve fully bounded problems using symmetric semi-bounded domains (waveguides), where symmetry properties imply that eigenvalues (wavenumbers) exist in pairs such that $-k^{(n)} = k^{(-n)}$ (i.e. waves having identical properties but propagate/decay in opposite direction). This class of problems is dealt with in many realms of physics such as optics, acoustics, electromagnetics, seismics, quantum mechanics, structural dynamics etc.

The overwhelming majority of tools to solve these problems are essentially numerical, such as the Boundary Element (BE), Finite Element/Wave Finite Element

(FE/WFE), Wave Based (WB), Semi-Analytical Finite Element (SAFE), Spectral Element (SE), Scaled Boundary Finite Element (SBFE), Partial Wave Root Finding (PWRF), Pseudo-Spectral Collocation (PSC) and Thin layer (TLM) methods. The obvious advantage of these tools is the generality, which allows wave propagation analysis in compound, inhomogeneous arbitrarily shaped domains. However, this generality is achieved at the expense of an insight into the underlying physics of formation of propagating and standing waves. To retain this insight, one has to employ the analytical methods even if it narrows the range of problems to, say, canonically shaped piecewise homogeneous domains.

A valuable tool to attain insight into the underlying physics is the reciprocity theorem (or relation), which is very regularly explored both in theory and experiments, e.g. [1–3]. Application of reciprocity thus finds thousands of applications in literature to achieve both experimental, numerical and analytical advantages, see e.g. [2–8]. The pioneering work [4] presents the analytical reciprocity method in elastodynamics and illustrates its application to solve a broad range of problems in waveguide theory. The usefulness of the reciprocity relation becomes particularly appealing for semi-bounded domains in which the symmetry property is preserved. As proven in [9] the reciprocity relation for symmetric semi-bounded problems is composed of the pair of, indeed much stronger, bi-orthogonality relations. These have been used for finding analytical closed form solutions for a number of specific problems such as semi-infinite elastic layers, fluid-filled shells, helical springs, elastic strips etc., see e.g. [9–17]. Moreover, it was also proven rigorously in [9] that the physical properties of the constituents of the bi-orthogonality relation are explicitly related to the emanating energy. Despite their significant mathematical advantage and strong physical interpretation its application, oddly, appears only very occasionally in literature.

Our goal is here to promote the bi-orthogonality relation as an efficient tool to study the formation of standing waves in the fully bounded domain from the waves existing in its semi-bounded counterpart. Thus, our point of departure is the Boundary Integral Equations (BIE), in which the volume equations are eliminated, so that these boundary equations should be solved together with the boundary conditions. First, we employ the bi-orthogonality relation to resolve the BIE's into simple modal boundary identities and, second, use them to handle boundary conditions in a similar but less restrictive manner as compared with the general projection techniques in e.g. [18–22].

To illustrate the derivation and clarify the novelties we begin with general formulations and exemplify these using three structural/vibro-acoustic waveguide examples of diverse complexity, that is, both algebraic and transcendental problems, characterised by the waveguides' ability to carry waves i.e. a finite number of waves for an algebraic system and an infinite number for a transcendental system. The examples are, respectively, a classical Bernoulli-Euler beam (1D algebraic problem), a fluid-loaded membrane in the plane problem formulation (2D transcendental) and an elastic fluid-filled cylindrical shell (3D transcendental) – all presented in non-dimensional form (unless otherwise stated), all time-harmonic using $\exp(-i\omega t)$ and all with the preferred direction of propagation, x , so that the waveguide properties are defined by $\exp(kx)$ with $k \in \mathbb{C}$ (this implies uniformness of a waveguide in x -direction). Also

the latter waveguide allows propagation of helical (spinning) waves through $\exp(im\theta)$ with $m \in \mathbb{Z}$ (axi-symmetric). To solve the semi-bounded waveguide problems, we employ tailored Green's functions, which satisfy all continuity conditions in coordinates other than x . These Green's functions are found using the bi-orthogonality approach outlined in [9]. Further, the methodology and derivations presented here are generalised to accommodate uniform (in the above mentioned sense) symmetric problems of various complexity (as those treated in [9]). Finally, in relation to the BIE's, we use the notion of Somigliana's identity which may simply be perceived as a generalisation (or equivalent) to the Kirchhoff Integral in acoustics.

The structure of the paper is as follows: In Section 2 application of bi-orthogonality to convert the homogeneous BIE's to a modal boundary identity is illustrated. Section 3 is concerned with formulation of the boundary value problem using the boundary identity and modal projection of the boundary conditions. Then, in Section 4 we derive the associated boundary identity for the inhomogeneous problem. In Section 5 the boundary identity and modal projection method is discussed with respect to convergence and physical interpretation. Perspectives of the method are also discussed here. In Section 6 we conclude the findings and novelties of the paper and finally, technical details and derivations are relegated to Appendix.

2. Resolving Boundary Integral Equations by means of bi-orthogonality relations

When Green's function for an infinite waveguide is known it facilitates solving the subsequent boundary value problem for a 'finite' waveguide exposed to arbitrary boundary conditions. This approach is generally recognised as the Boundary Integral Equations Method. Through this section we illustrate how to resolve the Boundary Integral Equations into a simple and very convenient identity between modal amplitudes at the boundaries. We denote this identity the boundary identity. Conversion of the BIE's into boundary identities are enabled by bi-orthogonality relations which exist both for algebraic and transcendental problems. In general, the boundary identity holds for uniform symmetric waveguides of arbitrary complexity exposed to arbitrary boundary conditions at plane cross-sections orthogonal to the propagation direction.

2.1. Bi-orthogonality relations

In this paper we shall use bi-orthogonality relations (derived for unbounded problems) as a tool to analyse free and forced boundary value problems such as vibrations of bounded waveguides. All details of their derivations for problems governed by self-adjoint operators are presented in [23]. According to the latter reference the bi-orthogonality relations are expressed through the quantity $\bar{R}^{(n,j)}$, where n and j stand for any two eigenfunctions of the unbounded problem and thus, $\bar{R}^{(n,j)}$ holds the properties:

$$\begin{aligned} \bar{R}^{(n,j)} &= 0 \quad \text{for } n^2 \neq j^2 && \text{(Bi-orthogonality)} \\ \bar{R}^{(n,n)} &= \bar{R}^{(n,-n)} = -\bar{R}^{(-n,n)} = -\bar{R}^{(-n,-n)} \neq 0 && \text{(Class properties)} \end{aligned} \tag{1}$$

with $-n$ indicating the opposite eigenfunction of n i.e. $\exp(k^{(-n)}x) = \exp(-k^{(n)}x)$.

For the three examples considered here the bi-orthogonality relations may be derived as

$$\bar{R}^{(n,j)} = -\bar{Q}^{(n)}\bar{w}^{(j)} + \bar{M}^{(j)}\bar{\gamma}^{(n)} \quad (\text{Bernoulli-Euler beam}) \quad (2)$$

$$\bar{R}^{(n,j)} = -\bar{w}'^{(n)}\bar{w}^{(j)} + \alpha \int_0^1 \bar{\phi}'^{(n)}(z)\bar{\phi}^{(j)}(z)dz \quad (\text{Fluid-loaded membrane}) \quad (3)$$

$$\begin{aligned} \bar{R}_m^{(n,j)} = & \bar{Q}_{1m}^{(j)}\bar{u}_m^{(n)} + \mu\bar{Q}_{4m}^{(j)}\bar{w}_m'^{(n)} - \bar{Q}_{2m}^{(n)}\bar{v}_m^{(j)} - \bar{Q}_{3m}^{(n)}\bar{w}_m^{(j)} \\ & - i\frac{\rho}{\gamma^3\mu\Omega} \int_0^1 \bar{p}_m^{(j)}(r)\bar{\vartheta}_m^{(n)}(r)rdr \quad (\text{Fluid-filled shell}) \quad (4) \end{aligned}$$

where each of the corresponding state variables (Q , w , u etc.) are either even or odd functions of their eigenvalues (wavenumbers). These are denoted Class properties and the state variables may be divided into these groups as

	Bernoulli-Euler beam	Fluid-loaded membrane	Fluid-filled shell
Class A – odd:	$\{\bar{Q}, \bar{\gamma}\}$	$\{\bar{w}', \bar{\phi}'(z)\}$	$\{\bar{u}_m, \bar{Q}_{2m}, \bar{Q}_{3m}, \bar{w}_m', \bar{\vartheta}_m(r)\}$
Class B – even:	$\{\bar{M}, \bar{w}\}$	$\{\bar{w}, \bar{\phi}(z)\}$	$\{\bar{Q}_{1m}, \bar{v}_m, \bar{w}_m, \bar{Q}_{4m}, \bar{p}_m(r)\}$

(5)

The properties of the bi-orthogonality relation from Eq. (1) are invariant to the considered examples and, therefore, pivotal for the derivations throughout the paper. Detailed specification of the involved state variables (Q , w , u etc.) can be found in Appendix.

2.2. Resolving the BIE's

To resolve the BIE's we first formulate Somigliana's identity (from which the BIE's originate). Somigliana's identity constitutes the solution to the boundary value problem formulated by help of an auxiliary problem (Green's functions) and is thus based on a concept remote from the conventional eigenfunction expansion. However, the link between the general solution (eigenfunction expansion) and Somigliana's identity can be shown explicitly using bi-orthogonality. For completeness, this is shown in Appendix A. The subject of Somigliana's identity is standard and details are thus left to the literature, see e.g. [24, 25]. In the absence of external forcing Somigliana's identity may be expressed on the general form in Eq. (6) using the physical state vectors which are here composed as 'force' (\mathbf{Q}) and 'kinematic' (\mathbf{U}) state variables, though they may have other interpretations in other realms of physics.

$$U(X_0) = \langle \mathbf{U}(X, X_0), \mathbf{Q}(X) \rangle_{\partial V_X} - \langle \mathbf{Q}(X, X_0), \mathbf{U}(X) \rangle_{\partial V_X} \quad (6)$$

where \mathbf{Q}/\mathbf{U} may be vectors, X/X_0 multi-dimensional and the inner product imply integration in X over the surface of the bounding volume i.e. $\langle \cdot \rangle_{\partial V_X} \equiv \int_{\partial V_X} \cdot dS_X$ (with subscripts omitted in what follows). The variables depending only on the observation point, $\mathbf{Q}(X)/\mathbf{U}(X)$, constitutes the unknown functions of the boundary value problem and the variables depending also on the excitation point, $\mathbf{Q}(X, X_0)/\mathbf{U}(X, X_0)$, are known

force/kinematic Green's functions (satisfy radiation/decay conditions).

Now, to reduce the Boundary Integral Equations to invariant algebraic form we first formulate the BIE's from Somigliana's identity by letting the point, X_0 , move alternately towards the boundaries from inside the domain. Then we expand their kernels (Green's functions) in terms of their eigenfunctions and adopt similar expansions for the unknown boundary functions. Expanding on the eigenfunctions is very well-known but is usually of no significant advantage (if any). However, by use of the bi-orthogonality relation we resolve the integral (inner product) and arrive without much effort at the identities in Eq. (7). These identities describe the relation between modal amplitudes at different boundaries, $W_a^{(n)}/W_b^{(n)}$, for any wavenumber $k^{(n)}$ and since they are derived directly from the Boundary Integral Equations via Somigliana's identity it is natural to name them boundary identities. The boundary identities in this form are valid for any uniform symmetric waveguide with a preferred direction of propagation.

$$\begin{aligned} W_a^{(-n)} &= W_b^{(-n)} \exp(k^{(n)}|b - a|) \\ W_b^{(n)} &= W_a^{(n)} \exp(k^{(n)}|a - b|) \end{aligned} \quad \{n \in \mathbb{N} \mid n \neq 0\} \quad (7)$$

If convenient, they may also be expressed as one

$$W_b^{(n)} = W_a^{(n)} \exp(k^{(n)}|a - b|) \quad \{n \in \mathbb{Z} \mid n \neq 0\} \quad (8)$$

It is hardly surprising (see e.g. [4, 26]) that this is true for wave propagation in a semi-bounded waveguide, however, it is not immediately apparent that these identities persist for the fully bounded waveguide independent of the choice of boundary conditions and nature/complexity of the problem. This was, however, argued in [27] to be the case for the beam, while it was said in the same reference that for more complicated waveguides such boundary identities become cumbersome to derive, [27, p. 245, ll. 6-7]. Indeed, a rigorous proof hereof is hardly possible without use of the bi-orthogonality relation and does to the authors knowledge not exist in the literature. Identification and derivation of these boundary identities thus constitutes one of the main novelties of this paper.

Further, from the invariant form in Eq. (7) we find that dimensionality of the boundary value problem has reduced remarkably from the original formulation (3D) to boundary integral equations (2D) and finally into invariant algebraic 'point' modal equations (1D). Hence, the boundary identity demonstrates that the BIE's are invariant and defined fully by the eigenfunctions/-values themselves and therefore do not depend on any problem specific properties. This alone implies that the homogeneous Somigliana's identity is merely an identity between boundary amplitudes and eigenfunctions of a uniform waveguide rather than an identity between state variables of a specific problem – as we would expect for an eigenvalue (eigenfrequency) problem.

Example. To clarify derivation of the boundary identities we show here the details for a non-trivial example: a fluid-loaded membrane, which in the presence of a compressible fluid supports an infinite number of waves i.e. the solution to the wave propagation problem involves infinite eigenfunction expansions. Details of the problem formulation and all necessary preliminaries are presented in Appendix B.

Somigliana's identity for the fluid-loaded membrane involves two identities, which are expressed with Kronecker's delta, δ_{ij} , in Eq. (9) and without external forces.

$$\begin{aligned} \delta_{1F}w(\xi) + \delta_{2F}\alpha\phi(\xi, z_0) = & \quad F = 1, 2 \\ \left[w'(x)w^{0F}(x, \xi, z_0) - \alpha \int_0^1 \phi'(x, z)\phi^{0F}(x, \xi, z, z_0)dz \right. & \quad (9) \\ \left. - w'^{0F}(x, \xi, z_0)w(x) + \alpha \int_0^1 \phi'^{0F}(x, \xi, z, z_0)\phi(x, z)dz \right]_{x=a}^{x=b} \end{aligned}$$

where F denotes each Somigliana identity (corresponding to a fundamental loading condition) and for $F = 1$ (membrane load) the dependence upon z_0 vanishes completely because the membrane does not feature dependence on z , see details in Appendix B. To arrive at the boundary identities, we convert Somigliana's identity to modal form by expanding the unknown boundary functions on a basis similar to that of Green's functions i.e.

$$\begin{aligned} w(x) &= \sum_{j=-\infty}^{\infty} \bar{w}^{(j)}\psi^{(j)}(x) & w'(x) &= \sum_{j=-\infty}^{\infty} \bar{w}'^{(j)}\psi^{(j)}(x) \\ \phi(x, z) &= \sum_{j=-\infty}^{\infty} \bar{\phi}^{(j)}(z)\psi^{(j)}(x) & \phi'(x, z) &= \sum_{j=-\infty}^{\infty} \bar{\phi}'^{(j)}(z)\psi^{(j)}(x) \end{aligned} \quad (10)$$

where the modal coefficients are the same as those from Green's function in Eq. (B.5) and $\psi(x)$ some yet unknown modal transport functions which are closely related to the eigenfunctions. This choice of basis is eligible because the modal coefficients are derived from the governing (volume) equations and thus apply to both the waveguide and boundary value problem. Hence, at each cross-section the relation between state variables (in terms of modal coefficients) must persist. For the modal transport functions we introduce, at the boundaries $x = a$ and $x = b$, the modal boundary amplitudes

$$\psi^{(j)}(a) = W_a^{(j)} \quad \psi^{(j)}(b) = W_b^{(j)} \quad \psi^{(-j)}(a) = W_a^{(-j)} \quad \psi^{(-j)}(b) = W_b^{(-j)} \quad (11)$$

Now, substitute Eq. (10) and the Green's functions from Eq. (B.5) into Somigliana's identity, Eq. (9), and rearrange to get

$$\begin{aligned} \delta_{1F}w(\xi) + \delta_{2F}\alpha\phi(\xi, z_0) = & \quad F = 1, 2 \\ \sum_{n=1}^{\infty} \sum_{j=-\infty}^{\infty} \left[\left(\bar{w}'^{(j)}\bar{w}^{(n)} - \alpha \int_0^1 \bar{\phi}'^{(j)}(z)\bar{\phi}^{(n)}(z)dz \right) \right. & \quad (12) \\ \left. + \left(-\bar{w}'^{(n)}\bar{w}^{(j)} + \alpha \int_0^1 \bar{\phi}'^{(n)}(z)\bar{\phi}^{(j)}(z)dz \right) \text{sgn}(x - \xi) \right] & \\ \times \psi^{(j)}(x)W^{0F(n)}(z_0) \exp(k^{(n)}|x - \xi|) \Big|_{x=a}^{x=b} & \end{aligned}$$

where we immediately recognise the brackets as the quantity $\bar{R}^{(n,j)}$ from Eq. (3) and may thus express Eq. (12) as

$$\delta_{1F}W(\xi) + \delta_{2F}\alpha\phi(\xi, z_0) = \quad F = 1, 2$$

$$\sum_{n=1}^{\infty} \sum_{j=-\infty}^{\infty} \left[\bar{R}^{(n,j)} \text{sgn}(x - \xi) - \bar{R}^{(j,n)} \right] \psi^{(j)}(x) W^{0F(n)}(z_0) \exp(k^{(n)}|x - \xi|) \Big|_{x=a}^{x=b} \quad (13)$$

Convenient for this modal form is that the unknown functions, $\psi(x)$, have moved outside the integrals (which are all contained in $\bar{R}^{(n,j)}$). In the Boundary Element Method (BEM) the integrals are evaluated element-wise using a priori approximations of the unknown functions. Also recall from Appendix B that the Green's functions (index n) sum only over positive indices (wavenumbers) to satisfy radiation/decay conditions, while the unknown boundary functions sum over all indices (wavenumbers) as they are not restricted by these conditions.

Now, by using the bi-orthogonal property of $\bar{R}^{(n,j)}$ from Eq. (1) the inner summation may be cancelled by an index interchange such that Eq. (13) reduce to Eq. (14) and by using also the Class properties from Eq. (1) it reduces further to Eq. (15).

$$\delta_{1F}W(\xi) + \delta_{2F}\alpha\phi(\xi, z_0) =$$

$$\sum_{n=1}^{\infty} \left[\bar{R}^{(n,n)} \text{sgn}(x - \xi) - R^{(n,n)} \right] \psi^{(n)}(x) W^{0F(n)}(z_0) \exp(k^{(n)}|x - \xi|) \Big|_{x=a}^{x=b} \quad (14)$$

$$+ \left[\bar{R}^{(n,-n)} \text{sgn}(x - \xi) - R^{(-n,n)} \right] \psi^{(-n)}(x) W^{0F(n)}(z_0) \exp(k^{(n)}|x - \xi|) \Big|_{x=a}^{x=b}$$

↓

$$\delta_{1F}W(\xi) + \delta_{2F}\alpha\phi(\xi, z_0) =$$

$$\sum_{n=1}^{\infty} \left\{ [\text{sgn}(x - \xi) - 1] \psi^{(n)}(x) + [\text{sgn}(x - \xi) + 1] \psi^{(-n)}(x) \right\} \quad (15)$$

$$\times \bar{R}^{(n,n)} W^{0F(n)}(z_0) \exp(k^{(n)}|x - \xi|) \Big|_{x=a}^{x=b}$$

Expanding in terms of a and b while using the definitions in Eq. (11) we get

$$\delta_{1F}W(\xi) + \delta_{2F}\alpha\phi(\xi, z_0) = \quad (16)$$

$$\sum_{n=1}^{\infty} \left\{ [\text{sgn}(b - \xi) - 1] W_b^{(n)} + [\text{sgn}(b - \xi) + 1] W_b^{(-n)} \right\} \bar{R}^{(n,n)} W^{0F(n)}(z_0) \exp(k^{(n)}|b - \xi|)$$

$$- \left\{ [\text{sgn}(a - \xi) - 1] W_a^{(n)} + [\text{sgn}(a - \xi) + 1] W_a^{(-n)} \right\} \bar{R}^{(n,n)} W^{0F(n)}(z_0) \exp(k^{(n)}|a - \xi|)$$

As the BIE's are derived by letting the point ξ move to the boundaries from inside the domain we may suffice by considering only the interior domain of Somigliana's identity i.e. $b > \xi > a$, such that the sign functions become definite and the equation

simplifies to

$$\delta_{1F} w(\xi) + \delta_{2F} \alpha \phi(\xi, z_0) = \sum_{n=1}^{\infty} 2\bar{R}^{(n,n)} W^{0F(n)}(z_0) \left\{ W_b^{(-n)} \exp(k^{(n)}|b - \xi|) + W_a^{(n)} \exp(k^{(n)}|a - \xi|) \right\} \quad (17)$$

Expanding also the left-hand-side (lhs) using Eq. (10) we get

$$\begin{aligned} & \sum_{n=1}^{\infty} \delta_{1F} \left[\bar{w}^{(n)} \psi^{(n)}(\xi) + \bar{w}^{(-n)} \psi^{(-n)}(\xi) \right] + \sum_{n=1}^{\infty} \delta_{2F} \alpha \left[\bar{\phi}^{(n)}(z_0) \psi^{(n)}(\xi) + \bar{\phi}^{(-n)}(z_0) \psi^{(-n)}(\xi) \right] \\ & = \sum_{n=1}^{\infty} 2\bar{R}^{(n,n)} W^{0F(n)}(z_0) \left\{ W_b^{(-n)} \exp(k^{(n)}|b - \xi|) + W_a^{(n)} \exp(k^{(n)}|a - \xi|) \right\} \end{aligned} \quad (18)$$

Then, substitute the modal amplitudes, $W^{0F(n)}$, from Eq. (B.8) and Eq. (B.10) into the latter and use the Class properties on the lhs we get

$$\begin{aligned} \sum_{n=1}^{\infty} \bar{w}^{(n)} \left[\psi^{(n)}(\xi) + \psi^{(-n)}(\xi) \right] &= F = 1 \\ & \sum_{n=1}^{\infty} \bar{w}^{(n)} \left\{ W_b^{(-n)} \exp(k^{(n)}|b - \xi|) + W_a^{(n)} \exp(k^{(n)}|a - \xi|) \right\} \\ \sum_{n=1}^{\infty} \alpha \bar{\phi}^{(n)}(z_0) \left[\psi^{(n)}(\xi) + \psi^{(-n)}(\xi) \right] &= F = 2 \\ & \sum_{n=1}^{\infty} \alpha \bar{\phi}^{(n)}(z_0) \left\{ W_b^{(-n)} \exp(k^{(n)}|b - \xi|) + W_a^{(n)} \exp(k^{(n)}|a - \xi|) \right\} \end{aligned} \quad (19)$$

From this we immediately see that both Somigliana identities are satisfied only when Eq. (20) holds.

$$\begin{aligned} \psi^{(n)}(\xi) + \psi^{(-n)}(\xi) &= \\ & W_b^{(-n)} \exp(k^{(n)}|b - \xi|) + W_a^{(n)} \exp(k^{(n)}|a - \xi|) \quad \{n \in \mathbb{N} \mid n \neq 0\} \end{aligned} \quad (20)$$

It is then straightforward, from this invariant form of Somigliana's identity, to let ξ alternately tend towards the boundaries and use the boundary definitions for $\psi(x)$ from Eq. (11) to arrive at the novel boundary identities in Eq. (7). Remarkably, we see that the boundary integral equations have resolved to uncoupled modal identities, which simply says that in any finite waveguide (no matter the boundary conditions) a free wave of amplitude $W_a^{(n)}$ at $x = a$ arrives at $x = b$ as $W_b^{(-n)} = W_a^{(n)} \exp(k^{(n)}L)$ with $L = b - a$.

Naturally, the identities (7-8) are valid for any uniform symmetric waveguide with a preferred direction of wave propagation – also in any other realm of physics. Thus, following the latter simple algebraic steps it is easy to arrive at the same results for the beam and the fluid-filled shell through the Somigliana identities presented in Appendix C and Appendix D. ■

3. Eigenfrequency analysis using bi-orthogonality and boundary identities

When treating algebraic problems such as eigenfrequency analysis of a beam where the number of free waves (and their modal amplitudes) exactly matches the number of boundary conditions, construction and solution of the eigenfrequency equation emerges immediately. However, when transcendental problems are considered, the number of boundary conditions and modal amplitudes no longer match. In that case formulation of the eigenfrequency equation requires truncation of the eigenfunction expansion and alternative formulation of the eigenfrequency equation. Inherently, this leaves convergence of solutions as an important issue to be addressed.

In the framework of BIEM the eigenfrequency equation is typically constructed from the Boundary Integral Equations with boundary conditions already incorporated. Solutions to this problem are then usually sought by dividing the boundaries into elements and the Boundary Element Method emerges, [24, 25]. However, this procedure may be avoided and, therefore, the eigenfrequency analysis much simplified. Indeed, since the BIE's have been resolved to simple identities, Eq. (7), construction of the eigenfrequency equation is concerned only with the boundary conditions. Therefore, we convert the boundary conditions to their modal form and combine them into a scalar modal condition by means of the bi-orthogonality relation. From this we obtain a system of linear algebraic homogeneous equations with respect to the modal amplitudes. Equating its determinant to zero yields the eigenfrequency equation.

3.1. Eigenfrequency solution for arbitrary boundary conditions

Consider a transcendental waveguide characterised (as in Sec. 2) by sets of physical 'force' and 'kinematic' state variables, denoted, respectively, \mathbf{Q} and \mathbf{U} . If the waveguide is bounded at $X = a$ and $X = b$ the boundary conditions are given as

$$\mathbf{Q}(X_a) - \mathbf{Z}(X_a)\mathbf{U}(X_a) = \mathbf{0} \quad \mathbf{Q}(X_b) - \mathbf{Z}(X_b)\mathbf{U}(X_b) = \mathbf{0} \quad (21)$$

where \mathbf{Z} are the prescribed boundary values known as the (diagonal) impedance matrix and the subscript on $X_{a/b}$ indicate that the conditions apply at the respective boundaries. This leaves unknown continuous boundary functions to be determined. The conditions in Eq. (21) provide a finite number of equations but as the conditions must hold at every point on the continuous boundary the number of unknowns are infinite. Typically, these equations are solved together with the BIE's through the BEM. However, we have resolved the BIE's to identities and therefore we expand the unknown boundary functions onto their modes in the same way as in Sec. 2.2 using Eq. (10). As the boundary conditions are valid only at the respective boundaries we directly adopt the boundary definitions of $\psi(x)$ from Eq. (11) and obtain

$$\begin{aligned} \sum_{n=-\infty}^{\infty} [\bar{\mathbf{Q}}^{(n)}(X_a) - \mathbf{Z}(X_a)\bar{\mathbf{U}}^{(n)}(X_a)] W_a^{(n)} &= \mathbf{0} \\ \sum_{n=-\infty}^{\infty} [\bar{\mathbf{Q}}^{(n)}(X_b) - \mathbf{Z}(X_b)\bar{\mathbf{U}}^{(n)}(X_b)] W_b^{(n)} &= \mathbf{0} \end{aligned} \quad (22)$$

where the unknowns have transformed from boundary functions to modal amplitudes that may be taken outside the brackets. Then, we introduce the boundary identities to relate the equations at the different boundaries and as a result eliminate half the unknowns.

$$\begin{aligned} \sum_{n=1}^{\infty} \left[\bar{\mathbf{Q}}^{(n)}(X_a) - \mathbf{Z}(X_a) \bar{\mathbf{U}}^{(n)}(X_a) \right] \left(W_a^{(n)} + W_b^{(-n)} \exp(k^{(n)}|b-a|) \right) &= \mathbf{0} \\ \sum_{n=1}^{\infty} \left[\bar{\mathbf{Q}}^{(n)}(X_b) - \mathbf{Z}(X_b) \bar{\mathbf{U}}^{(n)}(X_b) \right] \left(W_b^{(-n)} + W_a^{(n)} \exp(k^{(n)}|a-b|) \right) &= \mathbf{0} \end{aligned} \quad (23)$$

Indeed, the choice of boundary identities is not unique, however, it is natural to choose them to compose a stable system i.e. using only decaying exponents as done here (given by the index definition, see Appendix B). Inherently, this makes the equation system well-conditioned.

Then, to formulate a consistent set of equations so that the truncation order may be chosen freely, the conditions at each boundary are projected into a scalar condition through the inner product with modal projection vectors, $\bar{\mathbf{C}}^{(j)}(X_{a/b})$, in which j is taken from an appropriate subset of the complete set of eigenfunctions – Explanation follows.

$$\begin{aligned} \sum_{n=1}^{\infty} \left\langle \left[\bar{\mathbf{Q}}^{(n)}(X_a) - \mathbf{Z}(X_a) \bar{\mathbf{U}}^{(n)}(X_a) \right], \bar{\mathbf{C}}^{(j)}(X_a) \right\rangle_a \left(W_a^{(n)} + W_b^{(-n)} \exp(k^{(n)}|b-a|) \right) &= 0 \\ \sum_{n=1}^{\infty} \left\langle \left[\bar{\mathbf{Q}}^{(n)}(X_b) - \mathbf{Z}(X_b) \bar{\mathbf{U}}^{(n)}(X_b) \right], \bar{\mathbf{C}}^{(j)}(X_b) \right\rangle_b \left(W_b^{(-n)} + W_a^{(n)} \exp(k^{(n)}|a-b|) \right) &= 0 \end{aligned} \quad (24)$$

for $\{j \in J \subset N \mid |J| = |\tilde{N}|\}$

where the inner product is defined over the prescribed boundaries at $X = a$ and b as indicated by the subscript. This methodology is similar to known projection methods such as Ritz' or Galerkin's method, but, different in that the modal projection vector, $\bar{\mathbf{C}}^{(j)}(X_{a/b})$, may be chosen freely i.e. as $\bar{\mathbf{Q}}^{(j)}$, $\bar{\mathbf{U}}^{(j)}$ or some combination thereof, given that each entry of $\bar{\mathbf{C}}$ corresponds to that of $\bar{\mathbf{Q}}/\bar{\mathbf{U}}$ (as dictated by the variational principle).

Now, as a virtue of the modal expansion the unknown modal amplitudes remain outside the inner product, making the problem a purely algebraic one. Formulation of the necessary algebraic equations is then done simply by taking j as modes of the complete set of eigenfunctions. In other words, if we define N to be the complete (infinite) set of eigenfunctions of the transcendental problem and \tilde{N} any appropriate (finite) truncated subset of N (necessary to obtain numerical solutions), then we construct the equations individually by taking j one-by-one from a subset J , where J is an arbitrary subset of N restricted to being of the same size as the truncated subset, \tilde{N} – as indicated in Eq. (24).

Example. For the fluid-loaded membrane the equation from (24) at $x = a$ becomes

$$\sum_{n=1}^{\tilde{N}} \left[\bar{w}'^{(n)} \bar{w}^{(j)} + \alpha \int_0^1 \bar{\phi}'^{(n)}(z) \bar{\phi}^{(j)}(z) dz \right. \\ \left. - Z_a^w \bar{w}^{(n)} \bar{w}^{(j)} - Z_a^\phi \alpha \int_0^1 \bar{\phi}^{(n)}(z) \bar{\phi}^{(j)}(z) dz \right] \left(W_a^{(n)} + W_b^{(-n)} \exp(k^{(n)}|b-a|) \right) = 0 \quad \{j \in J \subset N \mid |J| = |\tilde{N}|\} \quad (25)$$

and similar for $x = b$ (not shown). Here the necessary truncation order $\tilde{N} \subset N$ is introduced and $\bar{\mathbf{C}}^{(j)}(X_a)$ has been taken as $\bar{\mathbf{C}}^{(j)}(z) = [\bar{w}^{(j)}, \alpha \bar{\phi}^{(j)}(z)]^T$. The superscript on Z indicates the impedance type e.g. w the impedance between shear force and transverse displacement. Technical details of the example may be found in Appendix B.

Then formulation of the equation system is simply done by taking J as a subset of N of size \tilde{N} and formulate each equation on modal form based on this subset i.e. $j \in J$ – as indicated in Eq. (25). From this we get a $2\tilde{N}$ -system composed directly from the boundary conditions, thus avoiding technicalities of BIE's, Transfer matrices and other methods. It should now indeed also be clear that the problem is a purely algebraic one because the square brackets can be evaluated straightforwardly (analytically or numerically).

Obviously, this method applies also to inherently algebraic problems such as the beam. Even in this case when N is finite ($N = \{-2, -1, 1, 2\}$) the choice of J and $\bar{\mathbf{C}}^{(j)}$ is still not unique. Despite some choices may be favourable the exact solution emerges for any choice, obviously. Formulation of the equation system for the beam with $\bar{\mathbf{C}}^{(j)} = \bar{\mathbf{U}}^{(j)} = [\bar{w}^{(j)}, \bar{\gamma}^{(j)}]^T$ is shown in Eq. (26).

$$\sum_{n=1}^{\tilde{N}=2} \left[\bar{Q}^{(n)} \bar{w}^{(j)} + \bar{M}^{(n)} \bar{\gamma}^{(j)} - Z_a^w \bar{w}^{(n)} \bar{w}^{(j)} - Z_a^\gamma \bar{\gamma}^{(n)} \bar{\gamma}^{(j)} \right] \\ \times \left(W_a^{(n)} + W_b^{(-n)} \exp(k^{(n)}|b-a|) \right) = 0 \quad j \in J = \{-1, 2\} \\ \sum_{n=1}^{\tilde{N}=2} \left[\bar{Q}^{(n)} \bar{w}^{(j)} + \bar{M}^{(n)} \bar{\gamma}^{(j)} - Z_b^w \bar{w}^{(n)} \bar{w}^{(j)} - Z_b^\gamma \bar{\gamma}^{(n)} \bar{\gamma}^{(j)} \right] \\ \times \left(W_b^{(-n)} + W_a^{(n)} \exp(k^{(n)}|a-b|) \right) = 0 \quad j \in J = \{1, -2\} \quad (26)$$

where we have chosen independent sets of J for each equation. This choice is free and may also be chosen as, for instance, $J = \{-1, 1\}$ or $\{1, 2\}$ etc. ■

As already indicated by the examples the subsets J and \tilde{N} may be chosen completely arbitrary (provided they are of the same size) and independent i.e. independent of each other and independent at each boundary. In much the same way the projection vector may be chosen arbitrarily (in the framework of the variational principle) and independent at each boundary. Interestingly, this free choice of subsets and projection vectors allow tailoring to accelerate convergence and as we shall see shortly, great advantage can be achieved for some special cases, for which explicit closed form solutions emerge – even for transcendental problems.

This method is enabled by the existence of bi-orthogonality of free waves (modes) and we denote it: 'The modal projection method'. Promotion of this novel method constitutes also one of the goals of this paper.

3.2. Eigenfrequency solution for Class consistent boundary conditions

The structure of the Class A/B properties and the bi-orthogonality relation enables identification of two special cases for which proper choice of projection vector(s) reveals an analytical closed form solution of the otherwise complicated eigenvalue problem. The special cases are concerned with homogeneous conditions at each boundary which are consistent with the Class properties and therefore we denote them 'Class consistent boundary conditions'. The first special case is when the boundary conditions at each boundary are the same and prescribed according to either the Class A or Class B state variables. The second case is when the boundary conditions are prescribed as a mixture i.e. Class A at one boundary and Class B at the other. For an elementary beam problem, these boundary conditions are known as simply supported (pinned) and irrotationally sliding ends. The significance of these boundary conditions has been stressed in [28], where they were used to determine relations between eigenfrequencies and the stop/pass band properties of periodic structures.

Example – Eigenfrequency equations. First, consider the elementary Bernoulli-Euler beam with Class A boundary conditions applied at both ends i.e. $Q(a) = Q(b) = \gamma(a) = \gamma(b) = 0$. This problem is a classical text book example and it is therefore no surprise that the eigenfrequency equation is on the well-known canonical form of Eq. (27) with the length $L = b - a$.

$$\sinh(kL) = 0 \Rightarrow k = 0 \quad \sin(kL) = 0 \Rightarrow k = \frac{q\pi}{L} \quad \{q \in \mathbb{Z}\} \quad (27)$$

Similarly, it should be no surprise that we obtain the same result when the boundary conditions are prescribed in accordance with Class B components. However, it may come as quite a surprise that we obtain the very same result also for the fluid-loaded membrane and fluid-filled shell when exposed to their corresponding Class consistent boundary conditions. For these transcendental problems the solution is indeed not straightforward nor obvious and is to the authors knowledge not found in literature.

To show that this result holds also for the transcendental problems we follow the modal projection method outlined in the previous section with some additional manipulations. For the fluid-loaded membrane the Class A consistent boundary conditions are: $w'(a) = \phi'(a) = w'(b) = \phi'(b) = 0$. Then following Sec. 3.1 we expand the boundary conditions in terms of eigenfunctions and, this time, before applying the boundary identities, project the boundary conditions into the scalar condition through the inner product with $\bar{\mathbf{C}}^{(j)}$. The choice of $\bar{\mathbf{C}}^{(j)}$ is important and we choose it in accordance with the bi-orthogonality relation such that we exactly assemble $\bar{R}^{(n,j)}$ at the boundaries. Thus taking $\bar{\mathbf{C}}^{(j)}(z) = [-\bar{w}^{(j)}, \alpha \bar{\phi}^{(j)}(z)]^T$ and recalling that the inner prod-

uct applies to the respective boundaries we get

$$\begin{aligned} \sum_{n=-\infty}^{\infty} \left[-\bar{w}'^{(n)} \bar{w}^{(j)} + \alpha \int_0^1 \bar{\phi}'^{(n)}(z) \bar{\phi}^{(j)}(z) dz \right] W_a^{(n)} &= 0 \\ \sum_{n=-\infty}^{\infty} \left[-\bar{w}'^{(n)} \bar{w}^{(j)} + \alpha \int_0^1 \bar{\phi}'^{(n)}(z) \bar{\phi}^{(j)}(z) dz \right] W_b^{(n)} &= 0 \end{aligned} \quad (28)$$

where we immediately recognise the square brackets as the quantity $\bar{R}^{(n,j)}$ from Eq. (3) so that we may rewrite to

$$\sum_{n=-\infty}^{\infty} \bar{R}^{(n,j)} W_a^{(n)} = 0 \qquad \sum_{n=-\infty}^{\infty} \bar{R}^{(n,j)} W_b^{(n)} = 0 \quad (29)$$

This problem can now be solved straight-away following the procedure in Sec. 3.1 by applying the boundary identities and set up the necessary equations one-by-one from $j \in J$. However, for Class consistent boundary conditions we may continue and manipulate the equations above to get a completely factorised system. Therefore we multiply the condition at $x = a$ by $W_a^{(j)}$ and subtract it from that at $x = b$ multiplied by $W_b^{(j)}$ so that we get

$$\sum_{n=-\infty}^{\infty} \bar{R}^{(n,j)} \left(W_b^{(n)} W_b^{(j)} - W_a^{(n)} W_a^{(j)} \right) = 0 \quad (30)$$

Now, if we take j to be a positive going wave, n (positive index), and employ the bi-orthogonality properties of $\bar{R}^{(n,j)}$ we get

$$\begin{aligned} \bar{R}^{(n,n)} \left(W_b^{(n)} W_b^{(n)} - W_a^{(n)} W_a^{(n)} \right) + \\ \bar{R}^{(-n,n)} \left(W_b^{(-n)} W_b^{(n)} - W_a^{(-n)} W_a^{(n)} \right) = 0 \quad \{n \in \mathbb{N} \mid n \neq 0\} \end{aligned} \quad (31)$$

Then we apply the boundary identities to transform $W_b^{(n)}$ into $W_a^{(n)}$ and further use the Class properties of $\bar{R}^{(n,j)}$ to get Eq. (33).

$$\begin{aligned} \bar{R}^{(n,n)} W_a^{(n)} W_a^{(n)} \left(\exp(k^{(n)}|b-a|) \exp(k^{(n)}|b-a|) - 1 \right) + \\ \bar{R}^{(-n,n)} W_a^{(-n)} W_a^{(n)} \left(\exp(k^{(n)}|b-a|) \exp(k^{(-n)}|b-a|) - 1 \right) = 0 \quad \{n \in \mathbb{N} \mid n \neq 0\} \end{aligned} \quad (32)$$

\Downarrow

$$\bar{R}^{(n,n)} W_a^{(n)} W_a^{(n)} \left(\exp(2k^{(n)}|b-a|) - 1 \right) = 0 \quad \{n \in \mathbb{N} \mid n \neq 0\} \quad (33)$$

Similar for $j = -n$ we get by proper choice of boundary identities (transforming $W_a^{(n)}$ into $W_b^{(n)}$)

$$\bar{R}^{(n,n)} W_b^{(-n)} W_b^{(-n)} \left(\exp(2k^{(n)}|b-a|) - 1 \right) = 0 \quad \{n \in \mathbb{N} \mid n \neq 0\} \quad (34)$$

Thus, for each wavenumber the otherwise coupled eigenfrequency equation has fully decoupled into modal equations from which it is immediately clear that the eigenfrequencies are produced only by propagating waves i.e. when $k^{(n)}$ is purely imaginary.

From this we straightforwardly deduce the canonical eigenfrequency equation from Eq. (27). This result is for transcendental problems hardly possible to obtain without the bi-orthogonality relation. Further, it also becomes clear that the positive and negative going waves behave identically and in fact, due to factorisation, we see from Eq. (34) that the eigenmodes' standing waves are constructed solely from identical but opposite freely propagating waves i.e. $\exp(k^{(n)}x) - \exp(k^{(-n)}x) = 0 \Leftrightarrow \exp(2k^{(n)}x) - 1 = 0$, as prescribed by the phase closure principle, [29].

In particular, the decoupled equations expressed on matrix form, Eq. (35) (with the condensed notation, e^x , used), are surprising even for the beam since the matrix is no longer fully populated as is the case for conventional BIEM/BEM. This, indeed, provides an insight into the formation of the eigenfrequency spectrum.

$$\begin{bmatrix} \ddots & 0 & 0 & 0 \\ 0 & e^{2k^{(n)}|b-a|} - 1 & 0 & 0 \\ 0 & 0 & e^{2k^{(n)}|b-a|} - 1 & 0 \\ 0 & 0 & 0 & \ddots \end{bmatrix} \begin{pmatrix} \vdots \\ W_a^{(n)} \\ W_b^{(-n)} \\ \vdots \end{pmatrix} = 0 \quad (35)$$

On the other hand, for mixed conditions (Class B at one end and Class A at the other) factorisation is achieved by choosing $\bar{\mathbf{C}}^{(j)}$ independent at each end, corresponding to the prescribed boundary conditions. Again it is no surprise that for the beam we arrive at the eigenfrequency equation in Eq. (36). However, it can be shown (following the previous steps) to hold for any uniform symmetric waveguide with a preferred propagation direction, which is again not obvious.

$$\cosh(kL) = 0 \quad \cos(kL) = 0 \quad \Rightarrow \quad k = \frac{(2q-1)\pi}{2L} \quad \{q \in \mathbb{Z}\} \quad (36)$$

To arrive at this we have added rather than subtracted in Eq. (30), a fact arising from derivation of the bi-orthogonality relation, [9].

In more general terms we can write the decoupled eigenfrequency equations for the two special cases on factorised form, see Eq. (37) for Class A or B (A/B) at both ends and Eq. (38) for mixed conditions.

$$\prod_{n=1}^{\tilde{N}} (e^{2k^{(n)}L} - 1)^2 = 0 \quad \prod_{n=1}^{\tilde{N}} (e^{2k^{(n)}L} + 1)^2 = 0 \quad (37, 38)$$

which is the exact closed form solution when the 'truncated' subset, \tilde{N} , includes all propagating waves in either positive or negative direction – even for complicated transcendental waveguides. Thus, determining the truncation order for these special cases becomes trivial and convergence of solutions becomes irrelevant. ■

Example – Relation between eigenfrequency equation and dispersion diagram. For the beam example the solutions to the latter eigenfrequency equations are found readily by substitution of $k = i\frac{q\pi}{L}$ and $k = i\frac{(2q-1)\pi}{2L}$ found from Eq. (27) and (36) (or equivalently Eq. (37) and (38)) into the dispersion equation such that we get (in dimensional form) the eigenfrequencies, ω .

$$\omega_{A/B} = \left(\frac{q\pi}{L}\right)^2 cr_g \quad \omega_{Mixed} = \left(\frac{(2q-1)\pi}{2L}\right)^2 cr_g \quad (39, 40)$$

The eigenfrequency equation in (39) is remarkably similar to the dispersion equation and in fact by taking L as half a wavelength, $L = \frac{q\pi}{k}$, we immediately recover the dispersion relation. Likewise, since both Eq. (27) and (36) are formulated for wavenumbers they may indeed be plotted directly into the dispersion diagram as horizontal lines such that their intersections with the dispersion curves constitute the eigenfrequency spectrum. This is shown in Fig. 1 for a hollow cylindrical beam, where the dimensional parameters have been chosen for illustrative purposes only – explaining also the large eigenfrequencies.

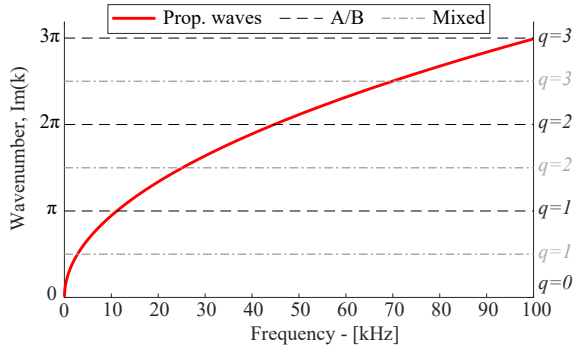


Fig. 1: Dispersion diagram for a hollow cylindrical PTFE polymer (Teflon) Bernoulli-Euler beam with the dimensional properties: $R = 75$ mm, $h = 7.5$ mm, $E = 300$ MPa, $\rho = 2100$ kg m⁻³ and $L = r_g = 1$. The intersection of the horizontal lines with the propagating wave branch constitutes eigenfrequencies for Class A/B boundary conditions (dashed) and for mixed conditions (dash-dot).

As the results of Eq. (37) and (38) have been proven to be valid also for the transcendental problems we may for the fluid-loaded membrane with Class A/B consistent boundary conditions write the eigenfrequency equation as Eq. (41) by simple substitution of $k = i\frac{q\pi}{L}$ into the dispersion equation from Eq. (B.2).

$$\left(i\frac{q\pi}{L}\right)^2 + \Omega_{qn}^2 \alpha \beta - \frac{\Omega_{qn}^2 \alpha \cos\left(\sqrt{\Omega_{qn}^2 + \left(i\frac{q\pi}{L}\right)^2}\right)}{\sqrt{\Omega_{qn}^2 + \left(i\frac{q\pi}{L}\right)^2} \sin\left(\sqrt{\Omega_{qn}^2 + \left(i\frac{q\pi}{L}\right)^2}\right)} = 0 \quad (41)$$

for $\{n, q \in \mathbb{Z} \mid n \neq 0\}$

This gives the eigenfrequency spectra Ω_{qn} where n is the sequential number of branches of propagating waves and q is the sequential number of eigenfrequencies in this spectrum. This generation of the spectra is readily exemplified by the second Timoshenko spectrum, see for instance [30], that is, each propagating wave, n , generates an eigenfrequency spectrum with the wavenumbers $k = i\frac{q\pi}{L}$, $q \in \mathbb{Z}$.

Computation of the eigenfrequencies then become a trivial task, as Eq. (41) may easily be converted to a polynomial form with an arbitrarily high accuracy by means

of e.g. the finite product method, see [31–33]. Again, eigenfrequencies may also be found graphically from the dispersion diagram as intersection of the horizontal lines at $k = i\frac{q\pi}{L}$ with the propagating wave branches. This is shown in Fig. 2.

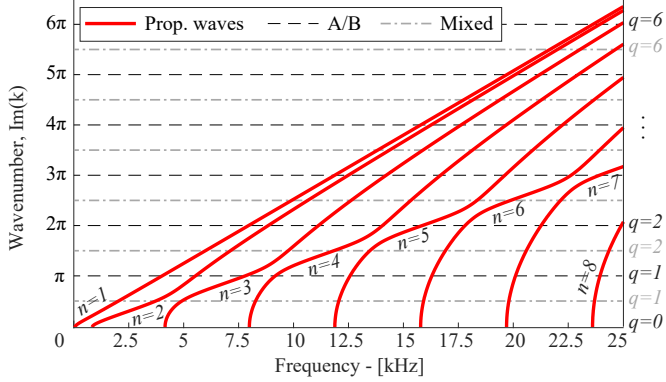


Fig. 2: Dispersion diagram for a fluid-loaded membrane with non-dimensional parameters: $\alpha = 0.113$, $\beta = 2.218$ and $L = 1$ – corresponding to, for instance, a rubber-membrane loaded by air with the properties: $T = 54.3 \text{ kN m}^{-1}$, $\rho_{str} = 800 \text{ kg m}^{-3}$, $h_0 = 0.147 \text{ mm}$, $H = 43.29 \text{ mm}$, $\rho_{fl} = 1.225 \text{ kg m}^{-3}$, $c_{fl} = 340 \text{ m s}^{-1}$, $L = H$. The intersection of the horizontal lines with each propagating wave branch defines the eigenfrequency spectra Ω_{qn} at fixed n for Class A/B boundary conditions (dashed) and for mixed conditions (dash-dot).

Similarly, we may substitute into the dispersion equation for the fluid-filled shell and use the finite product method to find eigenfrequencies, but as this equation becomes too extensive to show here we shall settle with the graphical representation in Fig. 3. To factorise the equations for the fluid-filled shell we choose for Class A consistent boundary conditions $\tilde{\mathbf{C}}^{(j)}(X_{a/b})$ as $\tilde{\mathbf{C}}^{(j)}(r) = [\bar{Q}_{1m}^{(j)}, \mu\bar{Q}_{4m}^{(j)}, -\bar{v}_m^{(j)}, -\bar{w}_m^{(j)}, -i\frac{\rho}{\gamma^3\mu\Omega}\bar{p}_m^{(j)}(r)]^T$ and so forth for mixed conditions.

In particular, for the ‘thickness-resonant’ modes (i.e. eigenfrequencies of uniform transverse motion of the layer/shell) one sets $q = 0$ in Eq. (27) and in case of the fluid-loaded membrane obtain the canonical Eq. (42), which also conveniently defines the cut-on frequencies.

$$\Omega_{0n}\beta - \frac{\cos(\Omega_{0n})}{\sin(\Omega_{0n})} = 0 \quad \{n \in \mathbb{Z} \mid n \neq 0\} \quad (42)$$

From this reservation we note that for symmetric ‘finite’ waveguides bounded by Class A/B conditions the fundamental (first order) modes ($q = 0$) defines the cut-on frequencies of the infinite waveguide. Hence, we find that for a symmetric ‘finite’ waveguide constrained by Class A/B conditions, the fundamental frequencies will not depend on the length of the waveguide. For some advanced problems this observation may lead to convenient methods for retrieving cut-on frequencies.

Likewise, we can just as easily obtain the eigenfrequency equation for mixed Class A and B boundary conditions by substituting $k = i\frac{(2q-1)\pi}{2L}$ into the dispersion equa-

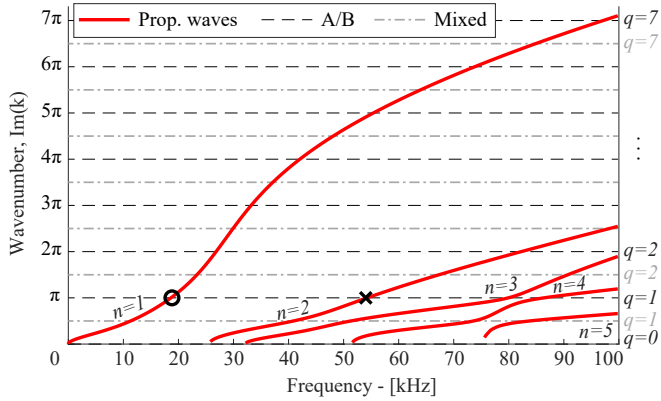


Fig. 3: Dispersion diagram for a fluid-filled shell vibrating in bending mode ($m = 1$) with non-dimensional parameters: $\rho = 0.1282$, $\gamma = 3.7773$, $\mu = 0.0175$ and $L = 1$ – corresponding to, for instance, a water-filled steel-shell with the properties: $E = 210$ GPa, $\nu = 0.3$, $\rho_{str} = 7800$ kg m $^{-3}$, $R = 20$ mm, $h = 0.35$ mm, $\rho_{fl} = 1000$ kg m $^{-3}$, $c_{fl} = 1440$ m s $^{-1}$ and $L = R$. The intersection of the horizontal lines with each propagating wave branch defines the eigenfrequency spectra Ω_{qn} at fixed n for Class A/B boundary conditions (dashed) and for mixed conditions (dash-dot).

tion, or, equivalently, plot them as horizontal lines in the dispersion diagram – also shown in Fig. 2 and 3 with dash-dot lines. ■

3.2.1. Concluding remarks

The simplicity of solving eigenfrequency problems with Class consistent boundary conditions becomes analogue to the analysis of free vibrations of a multi degree-of-freedom mechanical system exposed to initial conditions, which excite a specific eigenmode, see [34].

In the case illustrated in Fig. 3 the eigenfrequency of ≈ 20 kHz (indicated by circle) corresponds to a standing wave generated by a pair of identical waves propagating in opposite direction. This eigenfrequency is characterised solely by the first branch of the dispersion diagram, while all other propagating and evanescent waves (not shown) remain inactive. Thus, there are no modal interaction or mode conversion at the boundaries and the eigenmodes become of simple sinusoidal shapes. Similar, the pair of propagating waves characterised by the second branch produce, on their own, a standing wave at $f \approx 55$ kHz (indicated by cross) and so forth.

For Class inconsistent boundary conditions, on the other hand, we cannot factorise the equation system because we cannot assemble $\bar{R}^{(n,j)}$ in full at the boundaries. Physically, this means that mode interaction and conversion happens at the boundaries and so the eigenmodes will be a mixture of multiple modes of the waveguide in which case truncation order and convergence is to be addressed.

4. Forcing problems and their boundary identities

From the derivation of Somigliana’s identity, see e.g. [35], we find that it is straightforward to include the forcing term which constitutes the particular solution

and thus superimpose directly to the homogeneous Somigliana identity from Eq. (6), see Eq. (43). Then, by linearity of the inner products, all operations of Sec. 2 and 3 remain valid, also in the case of forcing problems. By the latter argument we follow the steps from Sec. 2.2 for the particular solution to reduce Eq. (43) to what we shall denote the inhomogeneous boundary identities in Eq. (44).

$$U(X_0) = \langle \mathbf{U}(X, X_0), \mathbf{Q}(X) \rangle_{\partial V_X} - \langle \mathbf{Q}(X, X_0), \mathbf{U}(X) \rangle_{\partial V_X} + \langle \mathbf{q}(X), \mathbf{U}_V(X, X_0) \rangle_V \quad (43)$$

$$\begin{aligned} W_a^{(-n)} &= W_b^{(-n)} \exp(k^{(n)}|b - a|) \\ &+ \frac{1}{2\bar{R}^{(n,n)}} \int_V [\mathbf{q}(X) \cdot \bar{\mathbf{U}}_V^{(n)}(X)] \exp(k^{(n)}|x - a|) dV \quad \{n \in \mathbb{N} \mid n \neq 0\} \\ W_b^{(n)} &= W_a^{(n)} \exp(k^{(n)}|a - b|) \\ &+ \frac{1}{2\bar{R}^{(n,n)}} \int_V [\mathbf{q}(X) \cdot \bar{\mathbf{U}}_V^{(n)}(X)] \exp(k^{(n)}|x - b|) dV \quad \{n \in \mathbb{Z} \mid n \neq 0\} \end{aligned} \quad (44)$$

where the latter inhomogeneous boundary identity may also be taken as the general one valid for all \pm wavenumbers (as indicated). Here $\mathbf{U}_V(X, X_0)$ is the kernel of the volume integral (Green's functions for the field variables), which may, for some problems, differ from the kernel (Green's functions) of the surface integral. $\bar{\mathbf{U}}_V$ is the associated modal coefficients introduced in Sec. 2 and $\mathbf{q}(X)$ the external forcing.

We see here that as soon as the inhomogeneous boundary value problem is considered the identities preserve the physical properties of the problem (contained in \bar{R} and $\bar{\mathbf{U}}_V$). Likewise, we note that the inhomogeneous part evaluates to a constant and thus constitutes nothing but a right-hand-side to the equation system. Then, solving the inhomogeneous boundary value problem using the inhomogeneous boundary identity follows directly from the method outlined in Sec. 3, nevertheless, with a non-zero right-hand-side, so that the solution is found by inversion. Again, for Class consistent boundary conditions we may employ bi-orthogonality to factorise and find closed form solutions to the problem.

Finally, the physical interpretation of the inhomogeneous boundary identity follows directly from the homogeneous identity discussed in Sec. 2, with the inhomogeneous part found to be remarkably similar to the modal amplitudes derived in Appendix B and [9]. Hence the physical interpretation follows directly from there (elaborated in [9]).

Example. To clarify the derivation of the inhomogeneous boundary identities we show here the details for the non-trivial fluid-loaded membrane example. As discussed with Eq. (43) we may depart directly from Eq. (19) by adding the forcing term with $\mathbf{U}_V(X, X_0) = \sum_{n=1}^{\infty} [\bar{w}^{(n)}, \bar{\phi}^{(n)}(z)]^T W^{OF(n)}(z_0) \exp(k^{(n)}|x - \xi|)$ and $\mathbf{q}(X) =$

$[-q^w(x), \alpha q^\phi(x, z)]^T$, to get

$$\begin{aligned}
\sum_{n=1}^{\infty} \bar{w}^{(n)} [\psi^{(n)}(\xi) + \psi^{(-n)}(\xi)] &= \\
\sum_{n=1}^{\infty} \bar{w}^{(n)} \{ W_b^{(-n)} \exp(k^{(n)}|b - \xi|) + W_a^{(n)} \exp(k^{(n)}|a - \xi|) \} &+ \\
\sum_{n=1}^{\infty} W^{01(n)} \int_V [-q^w(x) \bar{w}^{(n)} + \alpha q^\phi(x, z) \bar{\phi}^{(n)}(z)] \exp(k^{(n)}|x - \xi|) dV & \\
\sum_{n=1}^{\infty} \alpha \bar{\phi}^{(n)}(z_0) [\psi^{(n)}(\xi) + \psi^{(-n)}(\xi)] &= \tag{45} \\
\sum_{n=1}^{\infty} \alpha \bar{\phi}^{(n)}(z_0) \{ W_b^{(-n)} \exp(k^{(n)}|b - \xi|) + W_a^{(n)} \exp(k^{(n)}|a - \xi|) \} &+ \\
\sum_{n=1}^{\infty} W^{02(n)}(z_0) \int_V [-q^w(x) \bar{w}^{(n)} + \alpha q^\phi(x, z) \bar{\phi}^{(n)}(z)] \exp(k^{(n)}|x - \xi|) dV &
\end{aligned}$$

and by introducing the modal amplitudes from Eq. (B.8) and (B.10) we get

$$\begin{aligned}
\sum_{n=1}^{\infty} \bar{w}^{(n)} [\psi^{(n)}(\xi) + \psi^{(-n)}(\xi)] &= \\
\sum_{n=1}^{\infty} \bar{w}^{(n)} \{ W_b^{(-n)} \exp(k^{(n)}|b - \xi|) + W_a^{(n)} \exp(k^{(n)}|a - \xi|) \} &+ \\
\sum_{n=1}^{\infty} \bar{w}^{(n)} \frac{1}{2\bar{R}^{(n,n)}} \int_V [-q^w(x) \bar{w}^{(n)} + \alpha q^\phi(x, z) \bar{\phi}^{(n)}(z)] \exp(k^{(n)}|x - \xi|) dV & \\
\sum_{n=1}^{\infty} \alpha \bar{\phi}^{(n)}(z_0) [\psi^{(n)}(\xi) + \psi^{(-n)}(\xi)] &= \tag{46} \\
\sum_{n=1}^{\infty} \alpha \bar{\phi}^{(n)}(z_0) \{ W_b^{(-n)} \exp(k^{(n)}|b - \xi|) + W_a^{(n)} \exp(k^{(n)}|a - \xi|) \} &+ \\
\sum_{n=1}^{\infty} \alpha \bar{\phi}^{(n)}(z_0) \frac{1}{2\bar{R}^{(n,n)}} \int_V [-q^w(x) \bar{w}^{(n)} + \alpha q^\phi(x, z) \bar{\phi}^{(n)}(z)] \exp(k^{(n)}|x - \xi|) dV &
\end{aligned}$$

from which it is clear that both equations are satisfied only when

$$\begin{aligned}
\psi^{(n)}(\xi) + \psi^{(-n)}(\xi) &= W_b^{(-n)} \exp(k^{(n)}|b - \xi|) + W_a^{(n)} \exp(k^{(n)}|a - \xi|) \\
&+ \frac{1}{2\bar{R}^{(n,n)}} \int_V [-q^w(x) \bar{w}^{(n)} + \alpha q^\phi(x, z) \bar{\phi}^{(n)}(z)] \exp(k^{(n)}|x - \xi|) dV \tag{47}
\end{aligned}$$

which is similar to Eq. (20), nonetheless, with an inhomogeneous part. Then let ξ alternately tend towards the boundaries a and b (as prescribed by the BIE's) and use the

boundary definitions from Eq. (11) to arrive at the boundary identities from Eq. (44) – written here explicitly for the fluid-loaded membrane.

$$W_a^{(-n)} = W_b^{(-n)} \exp(k^{(n)}|b - a|) \quad \{n \in \mathbb{N} \mid n \neq 0\}$$

$$+ \frac{1}{2\bar{R}^{(n,n)}} \int_V [-q^w(x)\bar{w}^{(n)} + \alpha q^\phi(x, z)\bar{\phi}^{(n)}] \exp(k^{(n)}|x - a|) dV \quad (48)$$

$$W_b^{(n)} = W_a^{(n)} \exp(k^{(n)}|a - b|) \quad \{n \in \mathbb{Z} \mid n \neq 0\}$$

$$+ \frac{1}{2\bar{R}^{(n,n)}} \int_V [-q^w(x)\bar{w}^{(n)} + \alpha q^\phi(x, z)\bar{\phi}^{(n)}] \exp(k^{(n)}|x - b|) dV \quad (49)$$

Similarly, we may follow these simple algebraic steps and easily arrive at the same result for the beam and fluid-filled shell, nevertheless, with a different external force vector (see Appendix C and Appendix D) and corresponding Green's functions. Hence, changes only apply to the square bracket as also indicated by the general formulation in Eq. (44).

To clarify the interpretation of the inhomogeneous identities we may apply a simple load, say, a transverse point force on the membrane at some section, c , prescribed as $q^w(x) = -\delta(x - c)$ and observe that the identity reduce to

$$W_b^{(n)} = W_a^{(n)} \exp(k^{(n)}|a - b|) + \frac{1}{2} \frac{\bar{w}^{(n)}}{\bar{R}^{(n,n)}} \exp(k^{(n)}|c - b|) \quad \{n \in \mathbb{Z} \mid n \neq 0\} \quad (50)$$

This essentially emphasise that the inhomogeneous part is obviously nothing but a superposition of the modal contribution of the external force to the homogeneous identity. ■

5. Discussion

Here we discuss in more detail the boundary identities and the modal projection method. From this discussion several interesting topics of future research have emerged.

5.1. The boundary identity

Though the boundary identity may, to some, be perceived as obvious, it has to the best of the authors knowledge been proved rigorously here for the first time in literature. It has been derived in Sec. 2 for a bounded homogeneous symmetric problem and in Sec. 4 for the corresponding inhomogeneous problem. The derivation is valid for uniform symmetric waveguides with a preferred direction of propagation and relies only on the existence of bi-orthogonality, which fortunately holds for any such problem, as discussed in [9]. In view of the derivation of these identities an alternative classification of state vectors, which differs from the common definition based on their physical interpretation i.e. force and kinematic state vectors, see Eq. (51), may be proposed. Instead the state vectors may conveniently be arranged according to the bi-orthogonality relation i.e. in terms of their mathematical properties, see Eq. (52), such that their inner product gives directly the quantity $R^{(n,j)}$. In doing so the derivation of the boundary identity in Sec. 2 and Sec. 4 and the analytical closed form solution in Sec. 3.2 will appear immediately.

Example. For the fluid-filled shell this corresponds to changing from the classical definition in Eq. (51) to the definition via bi-orthogonality in Eq. (52).

$$\begin{aligned}\mathbf{Q}(X) &= [Q_{1m}(x), Q_{2m}(x), Q_{3m}(x), Q_{4m}(x), \vartheta_m(x, r)]^T \\ \mathbf{U}(X) &= [u_m(x), v_m(x), w_m(x), w'_m(x), p_m(x, r)]^T\end{aligned}\quad (51)$$

⇓

$$\begin{aligned}\mathbf{C}_A(X) &= \left[u_m(x), -Q_{2m}(x), -Q_{3m}(x), w'_m(x), -\frac{1}{\gamma} \vartheta_m(x, r) \right]^T \\ \mathbf{C}_B(X) &= \left[Q_{1m}(x), v_m(x), w_m(x), \mu Q_{4m}(x), i \frac{\rho}{\gamma^2 \mu \Omega} p_m(x, r) \right]^T\end{aligned}\quad (52)$$

where the composition in Eq. (52) should be obvious from $\bar{R}^{(n,j)}$ in Eq. (4). ■

Furthermore, interpretation of the boundary identity suggests that the relationship between the wave amplitudes at the various stations for the semi-bounded waveguide is also perfectly valid for the amplitudes at physical boundaries regardless of the boundary conditions. Thus, we may conclude that the homogeneous BIE's conceal just a unique identity between individual modal boundary amplitudes rather than being a virtue of a specific problem. Only when the inhomogeneous boundary identity is considered does the identity rely on physical properties of the problem but does otherwise apply the same way.

In the context of vibration analysis this means that the eigenfrequency spectrum is formed by co-existence (superposition) of all positive/negative and propagating/evanescent waves more than by reflection thereof. In effect, the formulation of reflection matrices become redundant. The very same reservation was made by Mace in [27] with the words: “For simple cases it is a straightforward procedure to write relationships between the wave amplitudes at the various stations on the beam and manipulate these equations to obtain the solution.” . . . “In more complex situations writing the relations between wave amplitudes at different stations directly is a cumbersome procedure. It is easier, especially when numerical solutions are sought, to extend the use of reflection matrices and proceed as follows.” – [27, pp. 244-245], who then continued with reflection matrices in the absence of generalised boundary identities.

Remarkably it is, that we arrive at the same modal identity regardless of which problem and Somigliana identity (loading condition $0F$) is taken. Effectively, it makes formulation of BIE's equally redundant as the formulation of Transfer Matrices. In view of this, it is also worth mentioning that the boundary identities are in no way restricted to structural dynamics, acoustics or vibro-acoustics and their generality to ever more complicated problems have huge potential for finding solutions to such transcendental boundary value problems in linear dynamics.

Finally, the boundary identities establish a direct link between the methods typically applied for analysis of linear dynamical systems and in fact, it is straightforward to recover any of these methods by rather simple algebraic manipulations of the

boundary identity. This is illustrated in Appendix A where Somigliana's identities are rewritten to the form leading to the modal Transfer Matrix Method (TMM).

5.2. *The modal projection method*

In this section the discussion is concerned with and relevant only for the transcendental problems i.e. when the eigenfunction expansions (solution) are infinite. In the modal projection method we convert the physical boundary conditions to their modal form and take full advantage of the structure of state vectors shown in Eq. (52) to formulate a scalar boundary condition. Here our projection basis, $\tilde{\mathbf{C}}^{(j)}$, is taken in accordance with the variational principle so that it may be composed freely from the kinematic/force state variables – preferably as the $\mathbf{C}_{A/B}$ -vectors from Eq. (52). Notably, its components need not satisfy kinematic boundary conditions as in the canonical Ritz and Galerkin methods. By this novel formulation of the eigenvalue problem the nature of convergence of field and state variables differs from conventional techniques such as the Finite Element Method (FEM) and BEM and requires attention when it comes to solving transcendental problems. The modal projection method builds on the very same principle as elaborated in [9] and therefore the study of convergence is here also concerned with how the field and state variables converge at the boundaries.

Since boundary conditions are projected into a scalar modal condition each individual boundary condition in Eq. (21) is no longer ensured for any truncation order. In the aforementioned conventional techniques the boundary conditions are ensured at any truncation order as they are usually condensed out of the equation system from the outset. In this case an unconverged solution manifests itself as only satisfying the governing PDE's in an integral average sense. Convergence is then ensured in the limit as the number of elements is increased.

For the modal projection method, on the other hand, converged solutions are found as those for which each individual boundary condition of Eq. (21) is satisfied, while unconverged solutions can be interpreted as the solution (for example, an eigenfrequency spectrum) to another set of boundary conditions (determined by the truncation order), because the field and state variables have not yet converged on the boundaries. Nevertheless, the governing PDE's are satisfied for any truncation order. In other words, at any truncation order a set of boundary conditions emerges for which the spectrum of eigenfrequencies (solution) is indeed exact. Thus, for a set of arbitrarily prescribed boundary conditions any truncated solution will be the solution to a similar but not identical set of boundary conditions, while in the limit we find, of course, the spectrum to the prescribed ones. Then, by recovering the components of $\mathbf{Z}_{\text{approx}}$ from the boundary values for a given truncation order and comparing them with the prescribed boundary values, \mathbf{Z} , the accuracy of the solution can be instantaneously characterised by exact error measures. This is possible because the prescribed boundary values, \mathbf{Z} , have become definite targets of convergence and we thus obtain instant measures of convergence. An elaboration on the error measures can be found in [9]. For the conventional techniques no similar error measures can be derived, so that convergence is customarily traced by gradually increasing the truncation order.

In summary, the modal projection method promotes correctness of waves' participation to the solution rather than correctness of the boundary conditions. It means

that the prescribed boundary values are achieved only when all waves relevant to the spectrum of eigenfrequencies are retained. This makes the modal projection method less restrictive yet somewhat more physically meaningful as compared with other projection methods.

Another convenient advantage of the projection method over the conventional BIEM/BEM is the size of the equation system. As just discussed, the size of the equation system for the projection method depends fully on how each wave contributes to the given spectrum of eigenfrequencies i.e. for some boundary conditions decaying waves contribute whereas for others only the propagating waves do, as demonstrated in Sec. 3.2. In the BIEM/BEM framework, on the other hand, the minimum number of equations that a system can attain is indeed equal to twice the number of boundary conditions. For the fluid-loaded membrane this becomes an 8-by-8 system and for the fluid-filled shell a 20-by-20 system regardless the type of boundary conditions. For the Class consistent case, however, it was just shown in Sec. 3.2 that a single equation defines the exact eigenfrequency spectrum for both the fluid-loaded membrane and fluid-filled shell. Further, in the FE formulation the number of equations usually increase much beyond the latter as this formulation is based on volume discretisation.

5.3. Perspectives on future studies

Inspired by the latter discussion we formulate here just a few of the interesting future research questions that have emerged:

- As mentioned in the introduction, a variety of numerical tools are available for analysis of symmetric waveguides. The standard output of such an analysis is wavenumbers and related mode shapes. Since bi-orthogonality is a generic property of these waveguides, the quantity $\bar{R}^{(n,j)}$ and the composition of Class consistent boundary conditions may be retrieved by any of these tools. Then the numerically obtained dispersion diagrams may be used to straightforwardly solve the subsequent problems ranging from forced response and energy flow of the infinite waveguide to forced response and eigenfrequency analysis of the finite one.

In our opinion, the advantages that can be achieved by the method highlighted in this paper fully justifies the effort of their incorporation in a Finite Element environment, for example, in the framework of Wave-Finite Element. The analytical solutions presented in this paper may then be used as validation examples for the numerical tools.

- Though derivation of bi-orthogonality relies heavily on the symmetry of a waveguide its physical interpretation suggests that its generalised counterpart should exist also for unsymmetric problems. Derivation in this framework may require alternative methods but it is nonetheless hypothesised that such relations can be found. This hypothesis is further supported by the interpretation of the boundary identity stating that waves transfer individually between boundaries. This should indeed persist for unsymmetric linear waveguides.

In addition, the boundary identity and projection method is yet confined to uniform symmetric waveguides with a preferred direction of propagation (in any realm of physics). However, it is expected that by appropriate generalisation of the steps in Sec. 2 and 3 they may be adjusted to multi-directional waveguides.

- In experimental vibration analysis the boundary conditions usually constitute one of the largest uncertainties, yet they seem to affect radically the observed spectrum, causing discrepancies between experiments and mathematical models. Since the convergence properties of the modal projection method suggests an exact solution (to similar boundary conditions) for any truncation order, this method may be used together with the discrepancies to characterise the actual boundary impedances of the experimental set-up using much the same techniques as for source characterisation. In the same way these discrepancies are likely to reveal which waves are difficult to constrain and may thus hint towards 'ideal' boundary conditions recommended for testing in order to minimise uncertainties in boundary conditions.

6. Conclusions

In this paper we have demonstrated that the bi-orthogonality relations are equally efficient for solving both infinite waveguide and boundary value problems. Moreover, the method demonstrated apply equally to problems in any other realm of physics. The novel results are summarised as follows:

- The modal decomposition and direct application of bi-orthogonality to Somigliana's identity resolve the Boundary Integral Equations into a simple boundary identity between individual modal amplitudes at different boundaries. This holds for both homogeneous and inhomogeneous problems and immediately obviates commonly used methods such as BIEM, Transfer Matrix Method, wave-based methods etc. As suggested in earlier literature, [27], we find that application of boundary identities superseded alternative methods.
- The modal projection method condenses all boundary conditions into a modal scalar condition. Then, enabled by the boundary identities, a well-posed equation system is formulated directly from the boundary conditions.
- Enabled by the bi-orthogonality relation two special sets of boundary conditions (Class consistent) are identified. For these Class consistent boundary conditions, the eigenfrequency equation emerges from the dispersion equation no matter the complexity of the problem.
- For Class inconsistent boundary conditions the modal projection formulation suggests that free waves (eigenvalues) compose the prescribed boundary conditions only in the limit. It means that for any (unconverged) truncation order the solution is exact, however, to a set of boundary conditions similar but not identical to the prescribed ones. Thus, clearly defined error measures may be used to assess the instant state of convergence (as discussed in Sec. 5.2).

- Based on the bi-orthogonality relation, boundary identity and modal projection method an alternative composition of the state vectors, defined by the mathematical rather than the physical properties of their components, has emerged.

In conclusion, we hope that the demonstration here and in [9, 23] of the advantages of the bi-orthogonality approach over traditional methods inspire other researches to commence to the subject.

Appendix A. From Somigliana's identity to eigenfunction expansion

As the problems considered here are linear they must obviously obey uniqueness of solution so that, for any two solution methods to be exact, they must be identical. The direct link between the eigenfunction expansion and Somigliana's identity is however not immediately clear as Somigliana's identity originates from a different concept and so the proof of their equivalence becomes somewhat challenging. As discussed in Sec. 2 Somigliana's identity constitutes the solution to the boundary value problem and so we need to show its equivalence with the general eigenfunction expansion.

The challenging step here is to reduce the inner product to its invariant form. This can, however, be done straightforwardly using the bi-orthogonality relation as shown in Sec. 2. Thus, for the fluid-loaded membrane example we may take Eq. (19) directly as starting point. Let us consider, first, loading condition 01 with the left-hand-side in unexpanded form. Then, we apply the boundary identities transforming $W_b^{(-n)}$ to $W_a^{(-n)}$, use $k^{(-n)} = -k^{(n)}$ and consider only the interior ($b > \xi > a$) so that we may eventually dissolve the module and rewrite to

$$w(\xi) = \sum_{n=1}^{\infty} \bar{w}^{(n)} \left\{ W_a^{(-n)} \exp(k^{(-n)}|a-b|) \exp(k^{(n)}|b-\xi|) + W_a^{(n)} \exp(k^{(n)}|a-\xi| \right\} \quad (\text{A.1})$$

$$= \sum_{n=1}^{\infty} \bar{w}^{(n)} \left\{ W_a^{(-n)} \exp(k^{(-n)}|a-\xi|) + W_a^{(n)} \exp(k^{(n)}|a-\xi| \right\} \quad (\text{A.2})$$

$$= \sum_{n=-\infty}^{\infty} \bar{w}^{(n)} W_a^{(n)} \exp(k^{(n)}[\xi-a]) = \sum_{n=-\infty}^{\infty} \bar{w}^{(n)} W_b^{(n)} \exp(k^{(n)}[\xi-b]) \quad (\text{A.3})$$

which is exactly the complete eigenfunction expansion solving the governing equation, however, transformed into ξ with an arbitrary choice of origin. Note also from Eq. (A.2) to (A.3) that we have used the Class properties of $\bar{w}^{(n)}$. Likewise, we see that we recover the boundary identities by letting ξ to either a or b . Similarly, for loading condition 02 we get

$$\begin{aligned} \phi(\xi, z_0) &= \sum_{n=-\infty}^{\infty} \bar{\phi}^{(n)}(z_0) W_a^{(n)} \exp(k^{(n)}[\xi-a]) \\ &= \sum_{n=-\infty}^{\infty} \frac{i\Omega}{\kappa^{(n)} \sin(\kappa^{(n)})} \cos(\kappa^{(n)} z_0) W_a^{(n)} \exp(k^{(n)}[\xi-a]) \end{aligned} \quad (\text{A.4})$$

So, in view of the latter proof of equivalence, we may conclude that the boundary identities (and bi-orthogonality relation) indeed constitute the direct link between these methods, making them, essentially, interchangeable.

Appendix B. Fluid-loaded membrane

The fluid-loaded membrane in the plane problem formulation is a two-dimensional vibro-acoustic (infinite) waveguide which consists of a layer of acoustic medium bounded at one side by a rigid baffle and at the other side by a membrane, see Fig. B.4. Though the waveguide has a preferred direction of propagation, x , the fluid layer depends on the z -coordinate (as indicated in the figure), implying that the dispersion equation becomes transcendental. In the formulation of Somigliana's identity we have two fundamental loading conditions: 01 a point force acting on the membrane at (ξ) and 02 an acoustic source in the fluid at (ξ, z_0) . Note, as mentioned in Sec. 1, that we employ tailored Green's functions i.e. satisfying the continuity and baffle conditions in z .

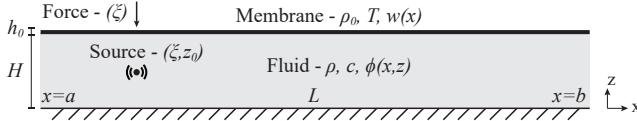


Fig. B.4: Sketch of the fluid-loaded membrane illustrating source/force locations, geometry and material properties.

Appendix B.1. Reciprocity and bi-orthogonality relations

The time-harmonic problem ($\exp(-i\omega t)$ omitted) is formulated in the non-dimensional form (with H as length scale) through the velocity potential, ϕ , and transverse displacement, w .

$$\frac{\partial^2 \phi(x, z)}{\partial x^2} + \frac{\partial^2 \phi(x, z)}{\partial z^2} + \Omega^2 \phi(x, z) = 0 \quad (\text{Wave equation})$$

$$\frac{d^2 w(x)}{dx^2} + \Omega^2 \alpha \beta w(x) + i \Omega \alpha \phi(x, z) = 0 \quad (\text{Membrane})$$

$$\left. \frac{\partial \phi(x, z)}{\partial z} \right|_{z=0} = 0 \quad (\text{Rigid baffle}) \quad \left. \frac{\partial \phi(x, z)}{\partial z} \right|_{z=1} = -i \Omega w(x) \quad (\text{Continuity})$$

The solution ansatz to this problem is on the form

$$w^{(n)}(x) = W^{(n)} \exp(k^{(n)} x) \quad \phi^{(n)}(x, z) = \Phi^{(n)} \cos(\kappa^{(n)} z) \exp(k^{(n)} x) \quad (\text{B.1})$$

and by substitution into the governing equation the transcendental dispersion equation in Eq. (B.2) emerges. Thus, this waveguide supports an infinite number of waves (eigenfunctions) i.e. $\{n \in \mathbb{Z} \mid n \neq 0\}$ where $n = 0$ is not an eligible index.

$$k^2 + \Omega^2 \alpha \beta - \frac{\Omega^2 \alpha \cos(\kappa)}{\kappa \sin(\kappa)} = 0 \quad (\text{B.2})$$

with the frequency parameter introduced as $\Omega = \frac{\omega H}{c}$, the non-dimensional axial wavenumber as $k = \frac{k_{dim}}{H}$ and the transverse wavenumber as $\kappa = \sqrt{\Omega^2 + k^2}$. Furthermore, the non-dimensional parameters α and β are: $\alpha = \frac{\rho c^2 H}{T}$ and $\beta = \frac{\rho_0 h_0}{\rho H}$, where c is the sound speed in the fluid, ρ and ρ_0 , respectively, the fluid and membrane density, H and h_0 its thickness and T the membrane tension, see Fig. B.4. The parameter α then characterises the stiffness ratio and β the inertia ratio between the components of the waveguide. From the ansatz we see that the wavenumbers of negative real part and positive imaginary part describe, respectively, waves decaying/propagating in the positive direction of the x -coordinate, hence, a positive index.

The scaled kinematic and force state variables (vectors) associated with this problem are, respectively, $[w(x), \phi(x, z)]^T$ (displacement and velocity potential – proportional to pressure) and $[\frac{d}{dx}w(x), \frac{d}{dx}\phi(x, z)]^T \equiv [w'(x), \phi'(x, z)]^T$ (force and velocity). The modal coefficients interrelating the state variables ($\bar{\mathbf{Q}}$ and $\bar{\mathbf{U}}$) are defined by scaling the amplitudes of the ansatz with $W^{(n)}$ such that

$$\begin{aligned} \bar{w}^{(n)} &= 1 & \bar{\phi}^{(n)}(z) &= \frac{i\Omega}{\kappa^{(n)} \sin(\kappa^{(n)})} \cos(\kappa^{(n)}z) \\ \bar{w}'^{(n)} &= k^{(n)} \bar{w}^{(n)} & \bar{\phi}'^{(n)}(z) &= k^{(n)} \bar{\phi}^{(n)}(z) \end{aligned} \quad (\text{B.3})$$

from which the Class properties of Eq. (5) are immediately deduced. From these state variables the reciprocity relation may be derived as

$$\begin{aligned} \left[w'^{(j)}(x)w^{(n)}(x) - \alpha \int_0^1 \phi'^{(j)}(x, z)\phi^{(n)}(x, z)dz \right. \\ \left. - w'^{(n)}(x)w^{(j)}(x) + \alpha \int_0^1 \phi'^{(n)}(x, z)\phi^{(j)}(x, z)dz \right]_{x=a}^{x=b} = 0 \end{aligned} \quad (\text{B.4})$$

and following [9] the associated bi-orthogonality relation is derived as in Eq. (3).

Appendix B.2. Formulation of Green's functions – Forcing problem

The composition of Green's functions includes the response of the waveguide to the two fundamental loading conditions characterised by delta functions in the right-hand-side of the governing equation. In both cases, Green's functions are formulated by expansion on free waves, see Eq. (B.5), and must satisfy the radiation/decay conditions. For symmetric waveguides the inhomogeneous problem may conveniently be reformulated to two semi-infinite homogeneous problems with inhomogeneous boundary conditions, see e.g. [9, 17, 36]. Writing out the solution for each segment of the membrane ($x > \xi$ and $x < \xi$) it is easily verified that the general solution for the

state variables for both segments may be written using the module.

$$\begin{aligned}
w^{0F}(x, \xi, z_0) &= \sum_{n=1}^{\infty} \bar{w}^{(n)} W^{0F(n)}(z_0) \exp(k^{(n)}|x - \xi|) \\
\phi^{0F}(x, \xi, z, z_0) &= \sum_{n=1}^{\infty} \bar{\phi}^{(n)}(z) W^{0F(n)}(z_0) \exp(k^{(n)}|x - \xi|) \\
w'^{0F}(x, \xi, z_0) &= \operatorname{sgn}(x - \xi) \sum_{n=1}^{\infty} \bar{w}'^{(n)} W^{0F(n)}(z_0) \exp(k^{(n)}|x - \xi|) \\
\phi'^{0F}(x, \xi, z, z_0) &= \operatorname{sgn}(x - \xi) \sum_{n=1}^{\infty} \bar{\phi}'^{(n)}(z) W^{0F(n)}(z_0) \exp(k^{(n)}|x - \xi|)
\end{aligned} \tag{B.5}$$

with summation only over positive indices to satisfy radiation and decay conditions (by definition of index notation in Appendix B.1). Note that $W^{0F(n)}$ is only a function of the source location, z_0 , for some $0F$. Further, in the general solution we note that the purpose of the module and accompanying sign function is to ensure the correct propagation/decay away from the source and so the sign function is merely to be viewed as a 'logical-type' operator and is therefore not subject to differentiation, see [9] for details. This holds for any symmetric problem.

Details of the derivation of modal amplitudes using bi-orthogonality are shown in [9] and thus presented only in brief here. In case of a mechanical excitation the loading conditions (equation system) are

$$\begin{aligned}
w'^{01}(x, \xi) &= \operatorname{sgn}(x - \xi) \sum_{n=1}^{\infty} \bar{w}'^{(n)} W^{01(n)} = -\frac{1}{2} \operatorname{sgn}(x - \xi) \\
&\hspace{15em} \text{at } x = \xi \pm |\varepsilon|, \quad \varepsilon \rightarrow 0 \tag{B.6} \\
\phi'^{01}(x, \xi, z) &= \operatorname{sgn}(x - \xi) \sum_{n=1}^{\infty} \bar{\phi}'^{(n)}(z) W^{01(n)} = 0
\end{aligned}$$

Then following [9] we multiply each condition in Eq. (B.6) with its counterpart (from the reciprocity relation) of index j and summarise according to the bi-orthogonality relation to get

$$\sum_{n=1}^{\infty} \left[-\bar{w}'^{(n)} \bar{w}^{(j)} + \alpha \int_0^1 \bar{\phi}'^{(n)}(z) \bar{\phi}^{(j)}(z) dz \right] W^{01(n)} = \sum_{n=1}^{\infty} \bar{R}^{(n,j)} W^{01(n)} = \frac{1}{2} \bar{w}^{(j)} \tag{B.7}$$

for $\{j \in \mathbb{Z} \mid j \neq 0\}$

with $\bar{R}^{(n,j)}$ given in Eq. (3) or explicitly in Eq. (B.8). Then due to bi-orthogonality the summation vanishes and each modal amplitude may be found individually as

$$\begin{aligned}
W^{01(n)} &= \frac{\bar{w}^{(n)}}{2\bar{R}^{(n,n)}} \quad \{n \in \mathbb{Z} \mid n \neq 0\} \\
\text{with } \bar{R}^{(n,n)} &= -k^{(n)} \left[1 + \frac{\alpha \Omega^2}{\kappa^{2(n)} \sin^2(\kappa^{(n)})} \int_0^1 \cos^2(\kappa^{(n)} z) dz \right]
\end{aligned} \tag{B.8}$$

For the acoustic excitation the forcing problem is formulated as follows

$$\begin{aligned} w'^{02}(x, \xi, z_0) &= \operatorname{sgn}(x - \xi) \sum_{n=1}^{\infty} \bar{w}'^{(n)} W^{02(n)}(z_0) = 0 & \text{at } x = \xi \pm |\varepsilon|, \varepsilon \rightarrow 0 \\ \phi'^{02}(x, \xi, z, z_0) &= \operatorname{sgn}(x - \xi) \sum_{n=1}^{\infty} \bar{\phi}'^{(n)}(z) W^{02(n)}(z_0) = \frac{1}{2} \operatorname{sgn}(x - \xi) \delta(z - z_0) \end{aligned} \quad (\text{B.9})$$

and following the same procedure the modal amplitudes are found as

$$W^{02(n)}(z_0) = \frac{1}{2} \frac{\alpha \bar{\phi}^{(n)}(z_0)}{\bar{R}^{(n,n)}} = \frac{1}{2} \frac{i\alpha\Omega \cos(\kappa^{(n)} z_0)}{\bar{R}^{(n,n)} \kappa^{(n)} \sin(\kappa^{(n)})} \quad \{n \in \mathbb{Z} \mid n \neq 0\} \quad (\text{B.10})$$

where the amplitude, obviously, features dependence upon location of the acoustic source, z_0 . Then following [35] the two Somigliana's identities may be expressed as in Eq. (B.11) with external forces, q .

$$\begin{aligned} \delta_{1F} w(\xi) + \delta_{2F} \alpha \phi(\xi, z_0) &= & F = 1, 2 \\ \int_a^b \left[-q^w(x) w^{0F}(x, \xi, z_0) + \alpha \int_0^1 q^\phi(x, z) \phi^{0F}(x, \xi, z, z_0) dz \right] dx + \\ & \left[w'(x) w^{0F}(x, \xi, z_0) - \alpha \int_0^1 \phi'(x, z) \phi^{0F}(x, \xi, z, z_0) dz \right. \\ & \left. - w'^{0F}(x, \xi, z_0) w(x) + \alpha \int_0^1 \phi'^{0F}(x, \xi, z, z_0) \phi(x, z) dz \right]_{x=a}^{x=b} \end{aligned} \quad (\text{B.11})$$

Appendix C. Bernoulli-Euler beam

Time-harmonic wave propagation in a Bernoulli-Euler beam is indeed an elementary problem found in many text books. Therefore we have left the specific details to the literature and in particular to [17] where the bi-orthogonality relations have been used to solve the beam problem. The beam is characterised by the shear force and moment i.e. the force state variables $\mathbf{Q}(X) = [Q(x), M(x)]^T$ and the kinematic state variables $\mathbf{U}(X) = [w(x), \gamma(x)]^T$ i.e. displacement and rotation. As shown in [17] the bi-orthogonality relation is easily derived as in Eq. (2).

To formulate Somigliana's identities Green's functions should be derived. Green's functions represent here the response (states) of the infinite beam to, respectively, 01 a point force and 02 a point moment. The derivations of Green's functions may be found in, for instance, [17]. Then, following [35] the two Somigliana identities are formulated as in Eq. (C.1) with external forces, q .

$$\begin{aligned} \delta_{1F} w(\xi) + \delta_{2F} \gamma(\xi) &= \int_a^b q^w(x) w^{0F}(x, \xi) dx + & F = 1, 2 \\ & \left[Q(x) w^{0F}(x, \xi) + M(x) \gamma^{0F}(x, \xi) - Q^{0F}(x, \xi) w(x) - M^{0F}(x, \xi) \gamma(x) \right]_{x=a}^{x=b} \end{aligned} \quad (\text{C.1})$$

From Somigliana's identities the conventional boundary (integral) equations are derived straightforwardly by letting ξ alternately tend towards the boundaries from inside the domain. Then, following the derivation in Sec. 2 it is straightforward to substitute the Green's functions into Eq. (C.1), use the bi-orthogonality from Eq. (2) and arrive at the boundary identities.

Appendix D. Fluid-filled shell

The elastic fluid-filled cylindrical shell characterised by an internal acoustic medium and a Kirchhoff-Love type surrounding shell constitutes a three-dimensional vibroacoustic waveguide. This particular problem, depicted in Fig. D.5, is comparable with the fluid-loaded membrane by being also transcendental in nature but is otherwise more complicated as it allows for propagation of helical (spinning) waves in the preferred propagation direction. Details beyond those shown here can be found in [9] where this specific problem is considered.

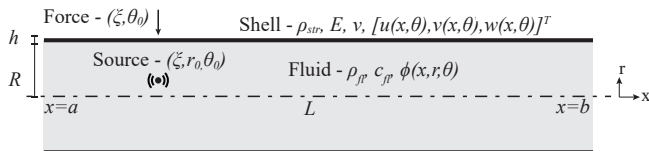


Fig. D.5: Sketch of the fluid-filled shell illustrating source/force locations, geometry and material properties.

For this problem we exploit also the axial symmetry which allows decomposition into circumferential wavenumbers, $m \in \mathbb{Z}$, and we may thus consider each m -spectra individually (indicated by subscript m) so that (θ) may be omitted. Hence, the axial wavenumbers, $k_m^{(n)}$, depend on the circumferential modes as defined by the dispersion equation. For this waveguide there is a total of 10 state variables (five forces and five kinematic) and five Somigliana identities. The five forces constitute axial, tangential, transverse, bending moment and velocity and the five kinematic axial, tangential, transverse, rotation and pressure, see Eq. (51). The Somigliana identities associated with this problem can be found in [37] or adapted to the terminology of [9]

in Eq. (D.1).

$$\begin{aligned}
& \delta_{1F}u_m(\xi) + \delta_{2F}v_m(\xi) + \delta_{2F}w_m(\xi) + \delta_{4F}w'_m(\xi) + \delta_{5F}i\frac{1}{\gamma\Omega}p_m(\xi, r_0) = \\
& \left[Q_{1m}(x)u_m^{0F}(x, \xi) + Q_{2m}(x)v_m^{0F}(x, \xi) + Q_{3m}(x)w_m^{0F}(x, \xi) \right. \\
& \quad \left. + \mu Q_{4m}(x)w_m^{0F}(x, \xi) + i\frac{\rho}{\gamma^3\mu\Omega} \int_0^1 p_m^{(0F)}(x, \xi, r)\vartheta_m(x, r)rd r \right] \Bigg|_{x=a}^{x=b} \\
& - \left[Q_{1m}^{0F}(x, \xi)u_m(x) + Q_{2m}^{0F}(x, \xi)v_m(x) + Q_{3m}^{0F}(x, \xi)w_m(x) \right. \\
& \quad \left. + \mu Q_{4m}^{0F}(x, \xi)w'_m(x) + i\frac{\rho}{\gamma^3\mu\Omega} \int_0^1 p_m(x, r)\vartheta_m^{(0F)}(x, \xi, r)rd r \right] \Bigg|_{x=a}^{x=b} \quad (D.1) \\
& + \int_a^b \left[q_{1m}(x)u_m^{0F}(x, \xi) + q_{2m}(x)v_m^{0F}(x, \xi) \right. \\
& \quad \left. + q_{3m}(x)w_m^{0F}(x, \xi) + i\frac{\rho}{\gamma^3\Omega} \int_0^1 T_m(x, r)p_m^{0F}(x, \xi, r)rd r \right] dx \\
& \qquad \qquad \qquad \text{for } F = 1, \dots, 5
\end{aligned}$$

with the external forces, q/T , included. As for the fluid-loaded membrane Green's functions also depend on the source location, r_0 , for some loading conditions, $0F$ – not indicated here.

References

- [1] H. Phan, Y. Cho, J. D. Achenbach, Verification of surface wave solutions obtained by the reciprocity theorem, *Ultrasonics* 54 (7) (2014) 1891–1894. doi : 10.1016/j.ultras.2014.05.003.
- [2] J. Matthews, F. Battista, D. Sánchez, P. Samuelsson, H. Linke, Experimental verification of reciprocity relations in quantum thermoelectric transport, *Phys. Rev. B - Condens. Matter Mater. Phys.* 90 (16) (2014) 1–6. doi : 10.1103/PhysRevB.90.165428.
- [3] J. D. Achenbach, Application of the reciprocity theorem to analyze ultrasound generated by high-intensity surface heating of elastic bodies, *J. Therm. Stress.* 30 (8) (2007) 841–853. doi : 10.1080/01495730701462782.
- [4] J. D. Achenbach, *Reciprocity in Elastodynamics*, Cambridge University Press, 2003. doi : 10.1017/CB09780511550485.
- [5] C. G. Panagiotopoulos, Reciprocal theorems in structural dynamics including initial conditions, *Earthq. Eng. Struct. Dyn.* 35 (5) (2006) 653–656. doi : 10.1002/eqe.538.
- [6] R. J. Potton, Reciprocity in optics, *Reports Prog. Phys.* 67 (5) (2004) 717–754. doi : 10.1088/0034-4885/67/5/R03.
- [7] R. G. Payton, An application of the dynamic Betti-Rayleigh reciprocal theorem to moving-point loads in elastic media, *Q. Appl. Math.* 21 (4) (1964) 299–313.
- [8] L. Knopoff, A. F. Gangi, Seismic reciprocity, *Geophysics* 24 (4) (1959) 681–691.
- [9] L. S. Ledet, S. V. Sorokin, Bi-orthogonality relations for fluid-filled elastic cylindrical shells: Theory, generalisations and application to construct tailored Green's matrices, *J. Sound Vib.* 417 (2018) 315–340. doi : 10.1016/j.jsv.2017.12.010.
- [10] P. N. Shankar, On the use of biorthogonality relations in the solution of some boundary value problems for the biharmonic equation, *Curr. Sci.* 85 (7) (2003) 975–979.
- [11] B. Karp, Generation of symmetric Lamb waves by non-uniform excitations, *J. Sound Vib.* 312 (2008) 195–209. doi : 10.1016/j.jsv.2007.10.041.
- [12] B. G. Prakash, Generalized orthogonality relation for rectangular strips in elastodynamics, *Mech. Res. Commun.* 5 (5) (1978) 251–255. doi : 10.1016/0093-6413(78)90019-8.

- [13] V. Pagneux, A. Maurel, Lamb Wave Propagation in Inhomogeneous Elastic Waveguides, *Proc. Math. Phys. Eng. Sci.* 458 (2024) (2002) 1913–1930. doi:10.1098/rspa.2001.0950.
- [14] W. B. Fraser, An orthogonality relation for the modes of wave propagation in an elastic circular cylinder, *J. Sound Vib.* 43 (3) (1975) 568–571. doi:10.1016/0022-460X(75)90011-5.
- [15] W. B. Fraser, Orthogonality relation for the Rayleigh-Lamb modes of vibration of a plate, *J. Acoust. Soc. Am.* 59 (1) (1976) 215–216. doi:10.1121/1.380851.
- [16] R. D. Gregory, A note on bi-orthogonality relations for elastic cylinders of general cross section, *J. Elast.* 13 (3) (1983) 351–355. doi:10.1007/BF00043002.
- [17] S. V. Sorokin, On the bi-orthogonality conditions for multi-modal elastic waveguides, *J. Sound Vib.* 332 (21) (2013) 5606–5617. doi:10.1016/j.jsv.2013.05.011.
- [18] C. L. Dym, I. H. Shames, *Solid Mechanics - A Variational Approach*, augmented Edition, Springer, 2013. doi:10.1007/978-1-4614-6034-3.
- [19] D. Gottlieb, S. A. Orszag, *Numerical Analysis of Spectral Methods: Theory and Applications*, SIAM, 1977. doi:10.1137/1.9781611970425.
- [20] J. S. Hesthaven, S. Gottlieb, D. Gottlieb, *Spectral Methods for Time-Dependent Problems*, 1st Edition, Cambridge University Press, 2007. doi:10.1017/CB09780511618352.
- [21] J. Shen, L.-I. Wang, T. Tang, *Spectral Methods: Algorithms, Analysis and Applications*, Springer, 2011. doi:10.1007/978-3-540-71041-7.
- [22] L. N. Trefethen, *Approximation Theory and Approximation Practice*, SIAM, 2013.
- [23] L. S. Ledet, S. V. Sorokin, (Bi)-orthogonality relation for eigenfunctions of self-adjoint operators, *R. Soc. Philos. Trans. A* doi:10.1098/rsta.2019.0112.
- [24] G. C. Hsiao, W. L. Wendland, *Boundary Integral Equations*, Vol. 164, Springer, 2008. doi:10.1007/978-3-540-68545-6.
- [25] S. Rjasanow, O. Steinbach, *The Fast Solution of Boundary Integral Equations*, Springer, 2007. doi:10.1007/0-387-34042-4.
- [26] L. Cremer, M. Heckl, B. A. Petersson, *Structure-Borne Sound*, 3rd Edition, Springer, 2005. doi:10.1007/b137728.
- [27] B. R. Mace, Wave reflection and transmission in beams, *J. Sound Vib.* 97 (2) (1984) 237–246. doi:10.1016/0022-460X(84)90320-1.
- [28] D. J. Mead, Wave propagation and natural modes in periodic systems: II. Multi-coupled systems, with and without damping, *J. Sound Vib.* 40 (1) (1975) 19–39. doi:10.1016/S0022-460X(75)80228-8.
- [29] D. J. Mead, Waves and modes in finite beams: Application of the phase-closure principle, *J. Sound Vib.* 171 (5) (1994) 695–702. doi:10.1006/jsvi.1994.1150.
- [30] N. G. Stephen, The second spectrum of Timoshenko beam theory - Further assessment, *J. Sound Vib.* 292 (2006) 372–389. doi:10.1016/j.jsv.2005.08.003.
- [31] C. J. Chapman, S. V. Sorokin, The finite-product method in the theory of waves and stability, *Proc. R. Soc. A Math. Phys. Eng. Sci.* 466 (2010) 471–491. doi:10.1098/rspa.2009.0255.
- [32] C. J. Chapman, An asymptotic decoupling method for waves in layered media, *Proc. R. Soc. A* 469. doi:10.1098/rspa.2012.0659.
- [33] E. Manconi, S. V. Sorokin, On the effect of damping on dispersion curves in plates, *Int. J. Solids Struct.* 50 (2013) 1966–1973. doi:10.1016/j.ijsolstr.2013.02.016.
- [34] S. S. Rao, *Mechanical Vibrations*, 5th Edition, Prentice, 2011.
- [35] S. V. Sorokin, J. B. Nielsen, N. Olhoff, J. B. Larsen, N. Olhoff, Green’s matrix and the boundary integral equation method for the analysis of vibration and energy flow in cylindrical shells with and without internal fluid loading, *J. Sound Vib.* 271 (2004) 815–847. doi:10.1016/S0022-460X(03)00755-7.
- [36] K. Graff, *Wave motion in elastic solids*, 1st Edition, Oxford University Press, 1975.
- [37] L. S. Ledet, S. V. Sorokin, Vibro-acoustics of infinite and finite elastic fluid-filled cylindrical shells, *Procedia Eng.* 199 (2017) 1362–1367. doi:10.1016/j.proeng.2017.09.356.

Paper C

(Bi)-orthogonality relation for eigenfunctions of
self-adjoint operators

Lasse S. Ledet & Sergey V. Sorokin

*Department of Materials and Production, Aalborg University,
Fibigerstraede 16, 9220 Aalborg East, Denmark*

Published in:

Philosophical Transactions of the Royal Society A
doi:10.1098/rsta.2019.0112

© 2019 The Royal Society Publishing. All rights reserved.
The layout has been revised.

(Bi)-orthogonality relation for eigenfunctions of self-adjoint operators

Lasse S. Ledet^a, Sergey V. Sorokin^a

^a*Department of Materials and Production, Aalborg University, Fibigerstraede 16, 9220 Aalborg, Denmark*

Abstract

The bi-orthogonality relation for eigenfunctions of self-adjoint operators is derived. Its composition is explained in view of the structure of a characteristic equation and of the energy flow components. Application of the bi-orthogonality relation for solving forcing problems is generalised and the connection between the bi-orthogonality relation and the virtual wave method is highlighted. Technicalities are illustrated in a non-trivial example of propagation of free/forced cylindrical waves in a thin elastic plate under heavy fluid loading.

Keywords:

Bi-orthogonality relation, Reciprocity relation, Self-adjoint operator, Fluid-loaded plate, Energy flow

1. Introduction

Modelling of dynamic phenomena in structured media requires use of a versatile 'toolbox' of various concepts and methods. We elaborate hereafter on the usefulness of the bi-orthogonality relation, which is readily available from the reciprocity theorem, to solve both the inhomogeneous and the eigenvalue problems for self-adjoint operators. An operator of this type emerges relatively often in many realms of physics, for instance, in linear dynamics of electromagnetics, optics, quantum mechanics, seismics, elastodynamics, vibro-acoustics etc.

An excellent historical overview of development and application of the reciprocity theorem (also known as the Betty theorem) in physics is presented in the canonical text [1, pp. 1-4]. This text also gives an exhaustive account of the problems in elastodynamics, which may conveniently be solved by the so-called virtual wave method originated from the reciprocity relation. The book [1], however, has not been our only inspiration to revisit the reciprocity relation and the closely linked orthogonality and bi-orthogonality relations. The orthogonality relations for Lamb waves have been derived in [2, 3], and the bi-orthogonality relations have been used to find the forced response of an elastic layer in [4, 5]. In a similar way (bi)-orthogonality for wave modes in cylindrical shells have been derived in e.g. [6, 7]. L. I. Slepyan [8] generalised these relations for a broad range of linear problems in dynamics in general, and the recent papers [9, 10] illustrate their usefulness in structural dynamics and vibro-acoustics.

In what follows, we advance further and formulate the bi-orthogonality relations for eigenfunctions of self-adjoint operators, not necessarily emerging from elastodynamics. According to Mikhlin [11] differential operators derived from the variational principle are on this form. Furthermore, we apply these relations to solve, in cylindrical coordinates, a problem of wave propagation in a thin elastic plate under heavy fluid loading. Solution of this non-trivial problem highlights several important and very useful properties of the bi-orthogonality relation, which, to the best of our knowledge, have not yet been identified and discussed.

To conclude the introduction, we clarify the terminology adopted hereafter. We define the reciprocity relation as stated in [1, p. 3, 2nd paragraph]. The orthogonality relation is defined as the reciprocity specialised for any pair of free waves (eigenvalues) as stated in [1, p. 73, Eq. (5.2.8)] for the Bernoulli-Euler beam and in [2, Eq. (7)] for the canonical Rayleigh-Lamb problem. Then the bi-orthogonality relation is defined as stated in [9, Eq. (6)] for the Bernoulli-Euler beam, in [10, Eq. (12)] for a fluid-filled cylindrical shell and in [4, Eq. (19)] for the Rayleigh-Lamb problem. It should be observed, however, that in [1] the same relation written in the form of Eq. (9.4.23) on p. 152 is referred to as the orthogonality of Rayleigh-Lamb modes. This ambiguity of definitions of the orthogonality relation and the bi-orthogonality relation in the literature should be kept in mind.

Each section of the paper begins with a general formulation and derivation of the proposed method followed by a non-trivial vibro-acoustic example, thus relating the rather general mathematics to actual physics problems.

2. Generalisation of bi-orthogonality relations

As highlighted in the introduction the bi-orthogonality relation proves powerful for solving problems in waveguide theory, see e.g. [4, 6, 9, 10]. In these problems an important and much practically relevant issue is the assessment of energy flow in the waveguide. Quite often calculation of energy flow is a tedious task. However, as shown in [4, 10] a use of bi-orthogonality dramatically simplifies this calculation. Common for the specific problems considered in the latter references is that preferred directions of wave propagation exist (i.e. extend to infinity). For the fluid-filled shell treated in [10] the preferred direction of propagation is axially and in the example of the fluid-loaded plate considered in this paper, it is the radial direction. Thus, we may treat any surface with the normal coinciding with this direction (a cross-section at $x = a$ for the fluid-filled shell and a cylinder at $r = r_0$ for the fluid-loaded plate) as a hypothetical boundary on which there are no prescribed boundary values of state variables. As we shall generalise here to cover self-adjoint operators we denote such boundaries as empty, implying simply that there is nothing prescribed on them.

Now, suppose that V is a volume with ∂V_m empty boundaries and $\partial V_m^c = \partial V \setminus \partial V_m$ physical boundaries with prescribed boundary values. Suppose that

$$Lu = 0 \quad \text{on } V \tag{1}$$

where L is a linear self-adjoint system of partial differential equations (PDE) acting on the vectorial field, u , where u constitute eigenfunctions with associated eigenvalues, λ , and which satisfy boundary conditions on ∂V_m^c , see [11]. The eigenvalues are found from the characteristic equation which is on the form

$$f(\lambda^2) = 0 \quad (2)$$

i.e. formulated in even powers of the eigenvalues, λ . Thus, the eigenvalues are grouped in pairs of $\pm\lambda^{(\pm n)}$, implying the index notation $\lambda^{(-n)} = -\lambda^{(n)}$. For self-adjoint L we may write the self-adjoint condition in Eq. (3) following e.g. [8, 12].

$$\langle Lu^{(n)}, u^{(j)} \rangle_V = \langle Lu^{(j)}, u^{(n)} \rangle_V \quad (3)$$

i.e. taking the inner product over the volume and with $u^{(n)}$ and $u^{(j)}$ being any two solutions (eigenfunctions) to Eq. (1). Then employing 'by parts integration' on Eq. (3) and noting that boundary conditions on ∂V_m^c are fulfilled, the self-adjoint condition reduces to the relation in Eq. (4).

$$\langle \mathcal{L}q^{(n)}, q^{(j)} \rangle_{\partial V_m} - \langle \mathcal{L}q^{(j)}, q^{(n)} \rangle_{\partial V_m} = 0 \quad (4)$$

where the differential operator, \mathcal{L} , emerges directly from partial integration. The partition into $\mathcal{L}q^{(n)}$ and $q^{(n)}$ corresponds to standard formulation of state variables e.g. generalised forces, $\mathbf{Q}^{(n)} = \mathcal{L}q^{(n)}$ and the generalised displacements, $\mathbf{U}^{(n)} = q^{(n)}$. When the operator L is harmonic, $q^{(n)} = u^{(n)}$ and, therefore, $\mathcal{L}q^{(n)} = \mathcal{L}u^{(n)}$. When the problem formulation involves a bi-harmonic operator (as in the example we consider in Sec. 2.1) $q^{(n)}$ includes $u^{(n)}$ and $\nabla u^{(n)}$. Accordingly, $\mathcal{L}q^{(n)}$ includes high-order derivatives i.e. $\nabla^2 u^{(n)}$ and $\nabla(\nabla^2 u^{(n)})$. Moreover, the state variables $\mathcal{L}q^{(n)}/q^{(n)}$ are not necessarily equal to their counterparts, for instance, derived from the variational principle. However, from [11, 13] we find that the energy flow is not affected by these differences, see Remark 2.3.

Since L is self-adjoint the relation in Eq. (4) with the state variables, $\mathcal{L}q^{(n)}$ and $q^{(n)}$, may be much simplified due to cancellations of common terms in $\langle \mathcal{L}q^{(n)}, q^{(j)} \rangle_{\partial V_m}$ and $\langle \mathcal{L}q^{(j)}, q^{(n)} \rangle_{\partial V_m}$. These cancellations are case-sensitive and will be illustrated in the example to follow. The remaining terms in $\mathcal{L}q$ and q may be called essential. Then two groups of functions denoted: $C_A^{(n/j)}, C_B^{(n/j)}$, are formed from these essential terms as functions having odd (Class A) and even (Class B) properties of their expansion coefficients with respect to the eigenvalues. Thus, each group consists of parts of $\mathcal{L}q$ and q . Definitions of Class functions and essential parts are elaborated in [10] and in the example in Sec. 2.1. It can again be shown that only the essential part is necessary to construct the energy flow, see e.g. [13] or Sec. 4. Now, using the Class functions, Eq. (4) may be written as

$$\langle C_A^{(j)}, C_B^{(n)} \rangle_{\partial V_m} = \langle C_A^{(n)}, C_B^{(j)} \rangle_{\partial V_m} \quad \Leftrightarrow \quad R^{(j,n)} - R^{(n,j)} = 0 \quad (5)$$

$$\text{with} \quad R^{(j,n)} = \langle C_A^{(j)}, C_B^{(n)} \rangle_{\partial V_m} \quad \wedge \quad R^{(n,j)} = \langle C_A^{(n)}, C_B^{(j)} \rangle_{\partial V_m} \quad (6)$$

which is simply a reduced form of Eq. (4) and thus holds also for all n and j over all boundaries in ∂V_m . However, we see from either of the two formulations that when $n = j$ the relation is identically satisfied independent of the boundary ∂V_m . Similarly, as suggested in [1] and illustrated in the following example, we can show that when $n^2 \neq j^2$, Eq. (5) can be satisfied only if $R^{(n,j)}$ and $R^{(j,n)}$ vanish independently and therefore also independent of the boundary. Thus, $R^{(n,j)}$ and $R^{(j,n)}$ must obey the bi-orthogonal relation in Eq. (7).

$$R^{(n,j)} = R^{(j,n)} = 0 \quad n^2 \neq j^2 \quad (7)$$

For the case $n = -j$ we can, however, not show that the relation in Eq. (5) is satisfied independent of the boundary. This is illustrated in the example. Returning to Eq. (4) it is then clear that only the case $n = -j$ does not vanish independent of the boundary. Fortunately, this proves useful for solving forcing problems of such type and moreover it proves particularly meaningful from a physical viewpoint as also emphasised by the 'virtual wave' method introduced for elastodynamics in [1].

The proof of bi-orthogonality, Eq. (7), is straightforward in Cartesian coordinates following for example [6] or [10]. However, in other cases such as, for instance, in cylindrical and spherical coordinates an alternative approach should be taken. In the following example, this is done by showing explicitly that the bi-orthogonality relation, Eq. (7), can be converted to a linear combination of characteristic equations, Eq. (2), for the involved eigenfunctions.

2.1. Example: Free cylindrical waves in a fluid-loaded plate

Let us consider the time harmonic waves ($\exp(-i\omega t)$) in an r -infinite plate loaded by an inviscid compressible fluid of finite depth, see Fig. 1.

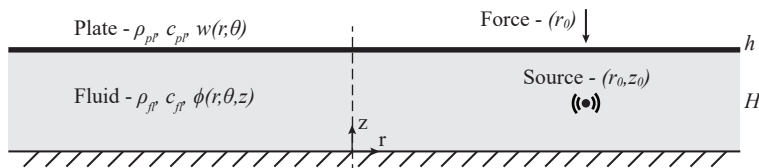


Fig. 1: Sketch of r -infinite fluid-loaded plate in cylindrical coordinates.

This vibro-acoustic problem is governed by the canonical PDE's for the radial displacement, w , and velocity potential, ϕ , in Eq. (8)-(11), see e.g. [14, 15].

$$\frac{\beta^2 \mu^3}{\rho} \nabla^4 w(r, \theta) - \frac{\mu}{\rho} \Omega^2 w(r, \theta) - i\Omega \phi(r, \theta, z)|_{z=1} = 0 \quad (8)$$

$$\nabla^2 \phi(r, \theta, z) + \Omega^2 \phi(r, \theta, z) = 0 \quad (9)$$

$$\nabla \phi(r, \theta, z) \cdot n|_{z=0} = -\frac{\partial \phi(r, \theta, z)}{\partial z} \Big|_{z=0} = 0 \quad (10)$$

$$\nabla \phi(r, \theta, z) \cdot n|_{z=1} = \frac{\partial \phi(r, \theta, z)}{\partial z} \Big|_{z=1} = -i\Omega w(r, \theta) \quad (11)$$

The length scale is chosen as H and the non-dimensional parameters are

$$\Omega^2 = \frac{\omega^2 H^2}{c_{fl}^2} \quad \beta = \frac{c_{pl}}{c_{fl}} \quad \mu = \frac{h}{H} \quad \rho = \frac{\rho_{fl}}{\rho_{pl}} \quad (12)$$

Omitting technicalities, the solution to this problem is given as

$$w(r, \theta) = \bar{w} W H_m^{(1)}(kr) \cos(m\theta) \quad \phi(r, \theta, z) = \bar{\phi}(z) W H_m^{(1)}(kr) \cos(m\theta) \quad (13)$$

with W as the modal amplitude. Then the modal coefficients become

$$\bar{w} = 1 \quad \wedge \quad \bar{\phi}(z) = i \frac{\Omega \cos(\kappa z)}{\kappa \sin(\kappa)} \quad \text{with} \quad \kappa^2 = \Omega^2 - k^2 \quad (14)$$

The transcendental dispersion relation is

$$k^4 + \frac{\rho}{\beta^2 \mu^3} \frac{\Omega^2 \cos(\kappa)}{\kappa \sin(\kappa)} - \left(\frac{\Omega}{\beta \mu} \right)^2 = 0 \quad (15)$$

This relation is invariant to the choice of coordinates and is thus the same in Cartesian coordinates.

Then take the inner product of Eq. (8) for eigenfunction $w^{(n)}$ with the solution $w^{(j)}$ and similar Eq. (9) for eigenfunction $\phi^{(n)}$ with solution $\phi^{(j)}$ – omitting the (r, θ, z) -dependencies hereafter. Carrying out full by parts integration and superimposing the two equations we arrive at

$$\begin{aligned} & \left\langle \nabla^4 w^{(n)} w^{(j)} - \frac{\Omega^2}{\beta^2 \mu^2} w^{(n)} w^{(j)} + \frac{\rho}{\beta^2 \mu^3} \left[\nabla^2 \phi^{(n)} \phi^{(j)} + \Omega^2 \phi^{(n)} \phi^{(j)} \right] \right\rangle_V - i \frac{\rho}{\beta^2 \mu^3} \Omega \left\langle \phi^{(n)} w^{(j)} \right\rangle_{\partial V, z=1} \\ & = \left\langle \nabla \left(\nabla^2 w^{(n)} \right) w^{(j)} - \nabla \left(\nabla^2 w^{(j)} \right) w^{(n)} + \left(\nabla^2 w^{(j)} \right) \nabla w^{(n)} - \left(\nabla^2 w^{(n)} \right) \nabla w^{(j)} \right\rangle_{\partial V} \\ & \quad + \frac{\rho}{\beta^2 \mu^3} \left\langle \nabla \phi^{(n)} \phi^{(j)} - \nabla \phi^{(j)} \phi^{(n)} \right\rangle_{\partial V} - i \frac{\rho}{\beta^2 \mu^3} \Omega \left\langle \phi^{(n)} w^{(j)} \right\rangle_{\partial V, z=1} \\ & \quad + \left\langle \nabla^4 w^{(j)} w^{(n)} - \frac{\Omega^2}{\beta^2 \mu^2} w^{(n)} w^{(j)} + \frac{\rho}{\beta^2 \mu^3} \left[\nabla^2 \phi^{(j)} \phi^{(n)} + \Omega^2 \phi^{(n)} \phi^{(j)} \right] \right\rangle_V \end{aligned} \quad (16)$$

where the scalar product implied by the inner product has already been carried out. The inner products over the fluid and plate then imply only integration with: $dV_{fl} = r dr d\theta dz$, $dV_{pl} = r dr d\theta$ and so forth for the surfaces. $\partial V, z = 1$ indicates the surface/interface at $z = 1$.

Then using Eq. (8) and (9) the inner product over the volume vanishes, leaving only the boundary terms. As mentioned in Sec. 2 the boundary terms correspond to the standard formulation of generalised forces and displacements. Introducing these as

$$\gamma^{(n)} = \nabla w^{(n)} \quad \tilde{M}^{(n)} = \nabla^2 w^{(n)} \quad \tilde{Q}^{(n)} = \nabla \left(\nabla^2 w^{(n)} \right) \quad p^{(n)} = i \Omega \phi^{(n)} \quad v^{(n)} = \nabla \phi^{(n)} \quad (17)$$

we may rewrite the self-adjoint condition to

$$\begin{aligned} & \left\langle \tilde{Q}^{(n)} w^{(j)} - \tilde{Q}^{(j)} w^{(n)} + \tilde{M}^{(j)} \gamma^{(n)} - \tilde{M}^{(n)} \gamma^{(j)} - i \frac{\rho}{\beta^2 \mu^3 \Omega} \left[v^{(n)} p^{(j)} - v^{(j)} p^{(n)} \right] \right\rangle_{\partial V} \\ & \quad - \frac{\rho}{\beta^2 \mu^3} \left\langle p^{(n)} w^{(j)} + p^{(j)} w^{(n)} \right\rangle_{\partial V, z=1} = 0 \end{aligned} \quad (18)$$

where \tilde{M} and \tilde{Q} originate from bending moment and shear force, γ is rotation angle and p and v are pressure and fluid velocity. Recall that though \tilde{Q} , γ and v are vectors, see Eq. (17), the inner product imply a scalar equation since the surface integral imply projection with the surface normal i.e. $\cdot n ds$.

As already discussed, the condition in Eq. (18) is identically satisfied on ∂V_m^c by the boundary conditions. In this case, the integrals at $\theta = 0, 2\pi$ are eliminated due to periodicity and the integrals at $z = 0, 1$ due to the boundary/continuity conditions in Eq. (10)–(11). This leaves only the unbounded direction with normal $n = [\pm 1, 0, 0]^T$. Since the fluid-loaded plate extends to infinity in r we take the definite integral over some hypothetical cylindrical surface, $r = r_0$, making this boundary, essentially, an empty one and so the eigenfunctions themselves are bound to obey the remaining relation in Eq. (19). This relation is typically known as the reciprocity relation and corresponds to Eq. (4).

$$\int_0^{2\pi} \left\{ \tilde{Q}^{(n)} w^{(j)} - \tilde{Q}^{(j)} w^{(n)} + \tilde{M}^{(j)} \gamma^{(n)} - \tilde{M}^{(n)} \gamma^{(j)} - i \frac{\rho}{\beta^2 \mu^3 \Omega} \int_0^1 [v^{(n)} p^{(j)} - v^{(j)} p^{(n)}] dz \right\} r d\theta \Big|_{r=a}^{r=r_0} = 0 \quad (19)$$

where we have changed notation to the explicit integral form and in this case let $a \rightarrow 0$. The forces/displacements from Eq. (17) ($\mathcal{L}q^{(n)}/q^{(n)}$ from Eq. (4)) in the unbounded direction (omitting amplitudes and $\cos(m\theta)$) are

$$\begin{aligned} w^{(n)} &= H_m^{(1)}(k^{(n)}r) & \gamma^{(n)} &= -k^{(n)} H_{m+1}^{(1)}(k^{(n)}r) + \frac{m}{r} H_m^{(1)}(k^{(n)}r) \\ \tilde{M}^{(n)} &= k^{2(n)} H_m^{(1)}(k^{(n)}r) & \tilde{Q}^{(n)} &= k^{3(n)} H_{m+1}^{(1)}(k^{(n)}r) + k^{2(n)} \frac{m}{r} H_m^{(1)}(k^{(n)}r) \\ p^{(n)} &= i\Omega \bar{\phi}^{(n)}(z) H_m^{(1)}(k^{(n)}r) & v^{(n)} &= \bar{\phi}^{(n)}(z) \left(-k^{(n)} H_{m+1}^{(1)}(k^{(n)}r) + \frac{m}{r} H_m^{(1)}(k^{(n)}r) \right) \end{aligned} \quad (20)$$

These forces/displacements may be simplified to only the first terms by noting that the second terms of γ , \tilde{Q} and v cancel within the reciprocity relation, Eq. (19). Take for instance $\tilde{Q}^{(n)} w^{(j)} - \tilde{M}^{(n)} \gamma^{(j)}$ we get

$$\begin{aligned} \tilde{Q}^{(n)} w^{(j)} - \tilde{M}^{(n)} \gamma^{(j)} &= \left[k^{3(n)} H_{m+1}^{(1)}(k^{(n)}r) + k^{2(n)} \frac{m}{r} H_m^{(1)}(k^{(n)}r) \right] H_m^{(1)}(k^{(j)}r) \\ &\quad - k^{2(n)} H_m^{(1)}(k^{(n)}r) \left[-k^{(j)} H_{m+1}^{(1)}(k^{(j)}r) + \frac{m}{r} H_m^{(1)}(k^{(j)}r) \right] \\ &= k^{3(n)} H_{m+1}^{(1)}(k^{(n)}r) H_m^{(1)}(k^{(j)}r) + k^{2(n)} k^{(j)} H_m^{(1)}(k^{(n)}r) H_{m+1}^{(1)}(k^{(j)}r) \end{aligned} \quad (21)$$

and similar for $v^{(n)} p^{(j)} - v^{(j)} p^{(n)}$. Thus, the essential part of the forces/displacements (represented without accents in the following) corresponding to C_A/C_B from Eq. (5)

are

$$\begin{aligned}
w^{(n)} &= \bar{w}^{(n)} H_m^{(1)}(k^{(n)} r) &= H_m^{(1)}(k^{(n)} r) \\
\gamma^{(n)} &= \bar{\gamma}^{(n)} H_{m+1}^{(1)}(k^{(n)} r) &= -k^{(n)} H_{m+1}^{(1)}(k^{(n)} r) \\
M^{(n)} &= \bar{M}^{(n)} H_m^{(1)}(k^{(n)} r) &= k^{2(n)} H_m^{(1)}(k^{(n)} r) \\
Q^{(n)} &= \bar{Q}^{(n)} H_{m+1}^{(1)}(k^{(n)} r) &= k^{3(n)} H_{m+1}^{(1)}(k^{(n)} r) \\
p^{(n)} &= \bar{p}^{(n)} H_m^{(1)}(k^{(n)} r) &= i\Omega \bar{\phi}^{(n)}(z) H_m^{(1)}(k^{(n)} r) \\
v^{(n)} &= \bar{v}^{(n)} H_{m+1}^{(1)}(k^{(n)} r) &= -\bar{\phi}^{(n)}(z) k^{(n)} H_{m+1}^{(1)}(k^{(n)} r)
\end{aligned} \tag{22}$$

For this particular formulation of forces/displacements we immediately find that the modal coefficients obey the Class properties defined in [10] i.e. being either odd (C_A) or even (C_B) with respect to the eigenvalues, $k^{(n)}$. Thus,

$$\text{Class A – odd: } \{\gamma, Q, v(z)\} \qquad \text{Class B – even: } \{w, M, p(z)\} \tag{23}$$

Substituting the essential variables into the reciprocity relation we get Eq. (24) when having performed the circumferential integration. This corresponds to the reduced form in Eq. (5).

$$\left[\bar{R}^{(n,j)} H_m^{(1)}(k^{(j)} r) H_{m+1}^{(1)}(k^{(n)} r) - \bar{R}^{(j,n)} H_m^{(1)}(k^{(n)} r) H_{m+1}^{(1)}(k^{(j)} r) \right] r \Big|_{r=a}^{r=r_0} = 0 \tag{24}$$

\Downarrow

$$\left[R^{(n,j)} - R^{(j,n)} \right] \Big|_{r=a}^{r=r_0} = 0 \tag{25}$$

with

$$R^{(n,j)} = \bar{R}^{(n,j)} H_m^{(1)}(k^{(j)} r) H_{m+1}^{(1)}(k^{(n)} r) r \tag{26}$$

$$\bar{R}^{(n,j)} = \bar{Q}^{(n)} \bar{w}^{(j)} + \bar{M}^{(j)} \bar{\gamma}^{(n)} - i \frac{\rho}{\beta^2 \mu^3 \Omega} \int_0^1 \bar{v}^{(n)} \bar{p}^{(j)} dz \tag{27}$$

Then, expanding $\bar{R}^{(n,j)}$ in full we arrive, after some algebraic manipulations, on the form

$$\bar{R}^{(n,j)} = \frac{k^{(n)}}{k^{2(j)} - k^{2(n)}} \left[k^{4(j)} - k^{4(n)} + \frac{\Omega^2 \rho}{\beta^2 \mu^3} \left(\frac{\cos(\kappa^{(j)})}{\kappa^{(j)} \sin(\kappa^{(j)})} - \frac{\cos(\kappa^{(n)})}{\kappa^{(n)} \sin(\kappa^{(n)})} \right) \right] \tag{28}$$

where we recognise the square bracket as the dispersion relation, Eq. (15), formulated for $k^{(n)}$ subtracted from the dispersion relation for $k^{(j)}$. Then, by the factor in front, it becomes clear that $\bar{R}^{(n,j)} = 0$ only when $n^2 \neq j^2$. This immediately proves that $R^{(n,j)}$, Eq. (26), also obeys bi-orthogonality as stated in Eq. (7) and furthermore independent of which empty boundary ($r = a$ or $r = r_0$) we consider.

Continue further and expand the inner part of Eq. (25) we arrive after some algebraic

manipulations at

$$R^{(n,j)} - R^{(j,n)} = \frac{\left[H_m^{(1)}(k^{(j)}r) H_{m+1}^{(1)}(k^{(n)}r) k^{(n)}r - H_m^{(1)}(k^{(n)}r) H_{m+1}^{(1)}(k^{(j)}r) k^{(j)}r \right]}{k^{(j)} - k^{(n)}} \quad (29)$$

$$\frac{1}{(k^{(j)} + k^{(n)})} \left[k^{4(j)} - k^{4(n)} + \frac{\Omega^2 \rho}{\beta^2 \mu^3} \left(\frac{\cos(\kappa^{(j)})}{\kappa^{(j)} \sin(\kappa^{(j)})} - \frac{\cos(\kappa^{(n)})}{\kappa^{(n)} \sin(\kappa^{(n)})} \right) \right]$$

which emphasise that this is zero if $n \neq -j$ again independent of which boundary we consider. Note, however, for the case when $n = -j$, $H_m^{(1)}(k^{(-n)}r)$ must be taken as $H_m^{(2)}(k^{(n)}r)$ and the expression in square brackets can be identified as the Wronskian. This essentially makes the relation $R^{(-n,n)} - R^{(n,-n)}$ invariant to r , yet not zero at a specific boundary, say, $r = r_0$. Similar results for the Rayleigh-Lamb problem in polar coordinates are presented in [1, p. 155]. Before proceeding with the applications of bi-orthogonality we make the following remarks.

Remark 2.1. As $R^{(n,j)}$ and $\bar{R}^{(n,j)}$ constitute a linear combination of dispersion relations they are, as the dispersion relation itself, indeed invariant to the choice of coordinate system. This implies that when using $R^{(n,j)}$ and $\bar{R}^{(n,j)}$ (bi-orthogonality) to solve forcing problems the solution appears in its strong form. This is not immediately obvious since reciprocity is generally perceived as a method to solve a problem in its weak form.

Remark 2.2. Bi-orthogonality and thus invariance of Eq. (19) becomes obvious only when using the correct (essential) formulation of forces/displacements from Eq. (22). In the Cartesian formulation they appear immediately whereas for problems in cylindrical and spherical coordinates the correct formulation appears in a non-trivial way.

Remark 2.3. The forces whether from Eq. (20) or (22) are different from the conventional definition of forces in classical literature, derived in e.g. [16, p. 283, Eq. (192)], which is again different from those derived from the variational principle shown in Eq. (30), see e.g. [12]. Most notably, the Poisson's ratio is absent in \bar{M} and \bar{Q} . Despite this ambiguity it is easy to show that the energy flow in a free wave using the essential forces is exactly the same as the energy flow using the classical ones, see e.g. Sec. 4, Fig. 3. This appears from the definition of energy flow in [13, Sec. 2.5] which is derived directly from the equations of motion, in which Poisson's ratio is also absent. The same was also suggested by Mikhlin in [11, p. 169, Eq. (7)].

$$Q_r = \frac{\partial^3 w(x, \theta)}{\partial r^3} + \frac{1}{r} \frac{\partial^2 w(x, \theta)}{\partial r^2} - \frac{1}{r^2} \frac{\partial w(x, \theta)}{\partial r} + \frac{(2 - \nu)}{r^2} \frac{\partial^3 w(x, \theta)}{\partial \theta^2 \partial r} - \frac{(3 - \nu)}{r^3} \frac{\partial^2 w(x, \theta)}{\partial \theta^2} \quad (30)$$

$$M_r = \frac{\partial^2 w(x, \theta)}{\partial r^2} + \nu \left(\frac{1}{r} \frac{\partial w(x, \theta)}{\partial r} + \frac{1}{r^2} \frac{\partial^2 w(x, \theta)}{\partial \theta^2} \right)$$

The difference between the various forces and moments from Eq. (20), (30) and (22) are shown in Fig. 2. As the main difference (Poisson's ratio) appears only in the plate

the real and imaginary part of the forces/moments are shown for the simple case when $\rho \rightarrow 0$ – corresponding to an ‘in-vacuo’ plate. Note from the figure that the moments from Eq. (20) and (22) fully align.

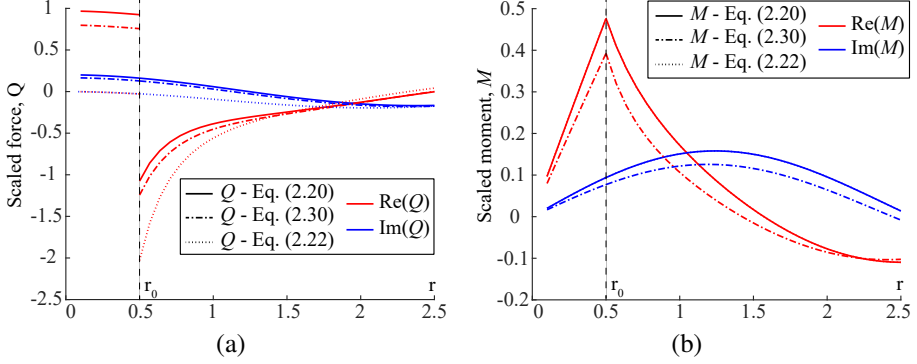


Fig. 2: Different definitions of forces (a) and moments (b) as a function r for an applied force at $r_0 = 0.5$. Only the plate is considered and the non-dimensional parameters are: $\rho = 0, \beta = 3.7773, \mu = 0.1, \nu = 0.3, \Omega = 2.2$ and $m = 1$. Note that the solid and dotted lines fully align in (b).

3. Application of bi-orthogonality to solve forcing problems

In this section we consider the following problem

$$Lu = f \quad \text{on } V \quad (31)$$

which is simply Eq. (1) with a non-zero right-hand-side (rhs). Then u is the entire (infinite) eigenfunction expansion, $u = \sum_{j=-\infty}^{\infty} u^{(j)}$, where $u^{(j)}$ is a known eigenfunction with a yet unknown amplitude. For transcendental problems the solutions are rather difficult to find. However, the bi-orthogonality relation dramatically simplifies the procedure. To show this we follow Sec. 2 and formulate the self-adjoint condition with $u^{(n)}$ where $u^{(n)}$ is an individual eigenfunction satisfying the homogeneous equation. In the presence of empty boundaries this simplifies to the inhomogeneous reciprocity relation

$$\langle \mathcal{L}q, q^{(n)} \rangle_{\partial V_m} - \langle \mathcal{L}q^{(n)}, q \rangle_{\partial V_m} = \langle f, u^{(n)} \rangle_V \quad (32)$$

which may be rearranged in terms of Class functions to get

$$\langle C_A, C_B^{(n)} \rangle_{\partial V_m} - \langle C_A^{(n)}, C_B \rangle_{\partial V_m} = \langle f, u^{(n)} \rangle_V \quad (33)$$

\Leftrightarrow

$$\sum_{j=-\infty}^{\infty} \left[\langle C_A^{(j)}, C_B^{(n)} \rangle_{\partial V_m} - \langle C_A^{(n)}, C_B^{(j)} \rangle_{\partial V_m} \right] = \langle f, u^{(n)} \rangle_V \quad (34)$$

Then, confer to Sec. 2 bi-orthogonality (and the trivial case, $n = j$) ensures that on a particular empty boundary in ∂V_m , say ∂V_n , the left-hand-side (lhs) of Eq. (34) is

non-zero only when $n = -j$ and we arrive at the modal equation in Eq. (35) valid for $n \in \mathbb{N}$.

$$\langle \mathcal{C}_A^{(-n)}, \mathcal{C}_B^{(n)} \rangle_{\partial V_n} - \langle \mathcal{C}_A^{(n)}, \mathcal{C}_B^{(-n)} \rangle_{\partial V_n} = \langle f, u^{(n)} \rangle_V \quad n \in \mathbb{N} \quad (35)$$

Pulling out the unknown amplitudes and introducing the following notation

$$\langle \mathcal{C}_A^{(j)}, \mathcal{C}_B^{(n)} \rangle_{\partial V_n} = R^{(j,n)} = U^{(j)} U^{(n)} \hat{R}^{(j,n)} \quad \wedge \quad u^{(n)} = U^{(n)} \hat{u}^{(n)} \quad (36)$$

we get

$$U^{(-n)} = \frac{\langle f, \hat{u}^{(n)} \rangle_V}{\hat{R}^{(-n,n)} - \hat{R}^{(n,-n)}} \quad \wedge \quad U^{(n)} = -\frac{\langle f, \hat{u}^{(-n)} \rangle_V}{\hat{R}^{(-n,n)} - \hat{R}^{(n,-n)}} \quad n \in \mathbb{N} \quad (37)$$

where the latter equation is obtained using instead $Lu^{(-n)} = 0$ in the self-adjoint condition. Thus, we have found algebraic solutions for the amplitude of each eigenfunction individually and hence independent of each other. In elastodynamics, this result formulates the 'virtual wave' method, [1].

3.1. Example: Forcing of a fluid-loaded plate in cylindrical coordinates

Given the details in the example in Sec. 2.1 it follows from the derivation in Sec. 3 that we may find the modal amplitudes directly using Eq. (37). For simplicity we consider the Green's function, first, for a structural excitation (indicated ⁰¹) by a unit 'ring' force at some circumference $r = r_0$ (see Fig. 1). This corresponds to a non-zero right-hand-side in Eq. (8), while keeping the right-hand-side of Eq. (9) zero. Thus, the force is formulated as: $f = \left[\frac{1}{r} \delta(r - r_0) \cos(m\theta) \exp(-i\omega t), 0 \right]^T$ - omitting, however, $\cos(m\theta) \exp(-i\omega t)$ in what follows. Green's function needs also to satisfy radiation conditions (propagation towards infinity), decay conditions at $r \rightarrow \infty$ and be bounded at $r = 0$. To ensure this, the admissible Bessel (eigen-)functions should be selected as presented in the table.

Free waves	Type	$r < r_0$	$r > r_0$
$k \in \mathbb{R}, k > 0$	Propagating	$J_m(kr)$	$H_m^{(1)}(kr)$
$ik \in \mathbb{R}, k > 0$	Attenuating	$I_m(kr)$	$K_m(kr)$

First, we consider the propagating waves by taking only purely real valued wavenumbers, say, $k^{(n)} \in \mathbb{R}$ and substitute into Eq. (37) with $\hat{u}^{(n)} = \left[\hat{v}^{(n)}(r), \hat{\phi}^{(n)}(r, z) \right]^T$. Then, we take the inner product over the surface $r = r_0$ and straightforwardly arrive at the modal amplitudes

$$W^{01(n)} = -\frac{J_m(k^{(n)} r_0)}{\bar{R}^{(n,n)} \left(J_{m+1}(k^{(n)} r_0) H_m^{(1)}(k^{(n)} r_0) - J_m(k^{(n)} r_0) H_{m+1}^{(1)}(k^{(n)} r_0) \right)} \quad (38)$$

in which we recognize the bracket in the denominator to be the Wronskian which simplifies to: $\frac{2i}{\pi k^{(n)} r_0}$, so that Eq. (38) may be reduced to

$$W^{01(n)} = i \frac{\pi k^{(n)} J_m(k^{(n)} r_0)}{2 \bar{R}^{(n,n)}} \quad k^{(n)} \in \mathbb{R} \quad (39)$$

and similar for the attenuating waves. Next, let us consider an acoustic source (indicated ⁰²) corresponding to a non-zero right-hand-side in Eq. (9). The source corresponding to a 'ring' monopole is: $f = \left[0, \frac{1}{r}\delta(r-r_0)\delta(z-z_0)\cos(m\theta)\exp(-i\omega t)\right]^T$ – omitting again $\cos(m\theta)\exp(-i\omega t)$. Then, for the propagating waves with wavenumber $k^{(n)} \in \mathbb{R}$, it is obvious from Eq. (37) that only the numerator changes and so, using the modal coefficients in Eq. (14), we find the amplitudes as

$$W^{02(n)} = i\bar{\phi}^{(n)}(z_0)\frac{\pi k^{(n)}J_m(k^{(n)}r_0)}{2\bar{R}^{(n,n)}} = \bar{\phi}^{(n)}(z_0)W^{01(n)} \quad k^{(n)} \in \mathbb{R} \quad (40)$$

For both cases we arrive at an algebraic expression in which the integrals may be evaluated analytically. Furthermore, the invariance of $\bar{R}^{(n,j)}$, discussed in Sec. 2.1 and Remark 2.1, immediately suggests that the modal amplitudes are found within the strong formulation of the forcing problem.

4. Energy flow

As mentioned in Sec. 2 the energy conveyed by an individual free wave is determined only by the essential state variables. For the inhomogeneous case we may show this following [13]. First we formulate the inhomogeneous reciprocity relation as in Sec. 3, however, in this case with known amplitudes for the eigenfunctions $C_A^{(j)}$ and $C_B^{(j)}$. Thus, we may depart directly from Eq. (35) in which bi-orthogonality have already been used. If we consider stationary dynamics with non-dimensional frequency, $\exp(-i\Omega t)$, we may multiply Eq. (35) with $-i\Omega$ and get

$$\langle C_A^{(-n)}, -i\Omega C_B^{(n)} \rangle_{\partial V_n} - \langle -i\Omega C_A^{(n)}, C_B^{(-n)} \rangle_{\partial V_n} = \langle f, -i\Omega u^{(n)} \rangle_V \quad (41)$$

Considering only the physical energy produced by the real part of the state variables as in [13] the relation becomes

$$\langle \text{Re}(C_A^{(-n)}), \text{Re}(-i\Omega C_B^{(n)}) \rangle_{\partial V_n} - \langle \text{Re}(-i\Omega C_A^{(n)}), \text{Re}(C_B^{(-n)}) \rangle_{\partial V_n} = \langle \text{Re}(f), \text{Re}(-i\Omega u^{(n)}) \rangle_V \quad (42)$$

↓

$$\Omega \langle \text{Re}(C_A^{(-n)}), \text{Im}(C_B^{(n)}) \rangle_{\partial V_n} - \Omega \langle \text{Im}(C_A^{(n)}), \text{Re}(C_B^{(-n)}) \rangle_{\partial V_n} = \Omega \langle \text{Re}(f), \text{Im}(u^{(n)}) \rangle_V$$

Then it follows directly from [13] that the equation may be reduced to

$$N^{(n)} = -\frac{\Omega}{2}\text{Im}\left(\langle C_A^{(n)*}, C_B^{(-n)} \rangle_{\partial V_n} - \langle C_A^{(-n)}, C_B^{(n)*} \rangle_{\partial V_n}\right) = \frac{\Omega}{2}\text{Im}\left(\langle f, u^{(n)*} \rangle_V\right) \quad (43)$$

Considering the rhs we observe that this is exactly the energy injected through the eigenfunction, $u^{(n)}$, as defined in [13]. Then, the left-hand-side must indeed represent the fraction of the total energy flow transported by the same eigenfunction. As observed in [10] for a fluid-filled shell, this proves linearity of the energy flow implying that all cross terms cancel and thus produce no net flow of energy.

Likewise, it is easy to arrive also at Eq. (44) using Eq. (32) as starting point (without employing bi-orthogonality).

$$N^{(n)} = -\frac{\Omega}{4} \text{Im} \left(\langle \mathcal{L}q^{(n)*}, q \rangle_{\partial V_n} - \langle \mathcal{L}q, q^{(n)*} \rangle_{\partial V_n} \right) \quad (44)$$

$$= -\frac{\Omega}{4} \sum_{j=-\infty}^{\infty} \text{Im} \left(\langle \mathcal{L}q^{(n)*}, q^{(j)} \rangle_{\partial V_n} - \langle \mathcal{L}q^{(j)}, q^{(n)*} \rangle_{\partial V_n} \right) \quad (45)$$

Thus proving that the fraction of total energy flow conveyed by the eigenfunction $u^{(n)}$ is the same no matter if we use the direct form of the forces/displacements ($\mathcal{L}q/q$) or just their essential parts (C_A/C_B). However, note that only when using the essential forces/displacements does the energy reduce to the linear form in Eq. (43).

Returning to Eq. (43) it can be shown following the example in [10] that $N^{(n)}$ from Eq. (43) (or (44)) is the same as

$$N^{(n)} = \frac{\Omega}{2} \text{Im} \left(\langle C_A^{(n)}, C_B^{(n)*} \rangle_{\partial V_n} \right) \quad (46)$$

$$= -\frac{\Omega}{2} \text{Im} \left(R^{(-n,n)} - R^{(n,-n)} \right) \quad (47)$$

where the former is exactly the definition of energy flow from [13] (however reduced to linear form) and the latter, essentially, the imaginary part of Eq. (35). Then by linearity of the energy flow it is obvious that the total energy flow (with known amplitudes associated with each eigenfunction) may be expressed as Eq. (48).

$$N^\Sigma = \frac{1}{2} \Omega \sum_{n=1}^{\infty} \text{Im} \left(\langle C_A^{(n)}, C_B^{(n)*} \rangle_{\partial V_n} \right) = -\frac{1}{2} \Omega \sum_{n=1}^{\infty} \text{Im} \left(R^{(-n,n)} - R^{(n,-n)} \right) \quad (48)$$

Moreover, following [10], only some products of eigenfunctions in Eq. (48) contribute to the energy flow. In the theory of waveguides these energy conveying terms are produced by propagating waves. Thus, the infinite sum reduces to a finite one

$$N^\Sigma = -\frac{1}{2} \Omega \text{Im} \sum_{n=1}^N \left(R^{(-n,n)} - R^{(n,-n)} \right) \quad (49)$$

where n counts only the energy conveying terms.

Indeed the latter emphasise the fact that the reciprocity relation, Eq. (4), bi-orthogonality relation, Eq. (5) and inhomogeneous relation, Eq. (33), all constitute an energy balance between the transmitted and accumulated energy. As suggested in Sec. 3 this energy balance reduce to modal form thanks to bi-orthogonality and essentially each amplitude may be found algebraically from a modal energy balance. Further,

Remark 4.1. *We may conclude that the left-hand-side of Eq. (41) may be perceived as more general than the expression from [13]:*

$$N^\Sigma = -\frac{1}{2} \text{Re} \left(\langle \mathcal{L}q, \dot{q}^* \rangle_{\partial V_n} \right) \quad (50)$$

This can be argued since $R^{(-n,n)} - R^{(n,-n)}$ is essential in the derivation of modal amplitudes and thus preserves both correct real and imaginary parts. Correctness of both real and imaginary parts is not guaranteed from the former definition.

4.1. Example: Energy flow in a fluid-loaded plate in cylindrical coordinates

For the example treated in Sec. 3.1 it is easy to show that Eq. (46) holds. Confer to Eq. (49) only the propagating waves contribute to the energy flow, which in this case is easily shown following [10]. In this example it reduces to considering only the Bessel/Hankel functions. Thus we proceed considering only the Bessel/Hankel functions (justified by the proportionality sign) using the short notation: $H_{m+1}^{(1)}(k^{(n)}r) = H_{m+1}^{(1)}$, $J_m(k^{(n)}r) = J_m$ etc. Then for each propagating wave, $k^{(n)} \in \mathbb{R}$, we find by help of the table in Sec. 3.1 and the Wronskian that Eq. (43), (46) and (47) reduce, respectively, to

$$\begin{aligned} N^{(n)} &= -\frac{\Omega}{2} \operatorname{Im} \left(\left\langle C_A^{(n)*}, C_B^{(-n)} \right\rangle_{\partial V_n} - \left\langle C_A^{(-n)}, C_B^{(n)*} \right\rangle_{\partial V_n} \right) \\ &\propto \operatorname{Im} \left(H_{m+1}^{(2)} J_m - J_{m+1} H_m^{(2)} \right) r = \frac{2}{\pi k^{(n)}} \end{aligned} \quad (51)$$

$$\begin{aligned} N^{(n)} &= \frac{\Omega}{2} \operatorname{Im} \left(\left\langle C_A^{(n)}, C_B^{(n)*} \right\rangle_{\partial V_n} \right) \\ &\propto -\operatorname{Im} \left(H_{m+1}^{(1)} H_m^{(2)} r \right) = -\operatorname{Im} \left(J_{m+1} J_m + Y_{m+1} Y_m + i [J_m Y_{m+1} - J_{m+1} Y_m] \right) r = \frac{2}{\pi k^{(n)}} \end{aligned} \quad (52)$$

$$N^{(n)} = -\frac{\Omega}{2} \operatorname{Im} \left(R^{(-n,n)} - R^{(n,-n)} \right) \propto \operatorname{Im} \left(J_{m+1} H_m^{(1)} - H_{m+1}^{(1)} J_m \right) r = \frac{2}{\pi k^{(n)}} \quad (53)$$

Comparing Eq. (52) and (53) we see, as noted in Remark 4.1, that correctness of both real and imaginary part is not guaranteed by the definition in [13]. Furthermore, we note that the Wronskian ensures that the expressions become invariant in r as expected for conservative systems where the energy flow must be conserved at any station of the waveguide. The same can easily be shown to hold also in Cartesian coordinates.

This is also illustrated in Fig. 3 where the total energy flow is shown using the definition from [13], Eq. (50), with the forces/displacements from, respectively, Eq. (20) and (30) and the novel definition from Eq. (49) with the essential forces/displacements. Thus, Fig. 3 presents the total energy flow computed using three alternative definitions of the forces/moments from Fig. 2 and hence supports Remark 2.3. In the figure we see that only for the energy definition from Eq. (49) are both the real and imaginary parts invariant. The same is true for the formulations in Eq. (43) and (44), whereas Eq. (46) and (50) preserves only invariant imaginary parts. This is essential to assemble the invariant energy balance from which the amplitudes are derived and thus supports Remark 4.1. Finally, remark that the novel definition of energy flow from Eq. (49) gives the same result for any of the definitions of state variables shown in Fig. 2 – corresponding to the dotted line in Fig. 3.

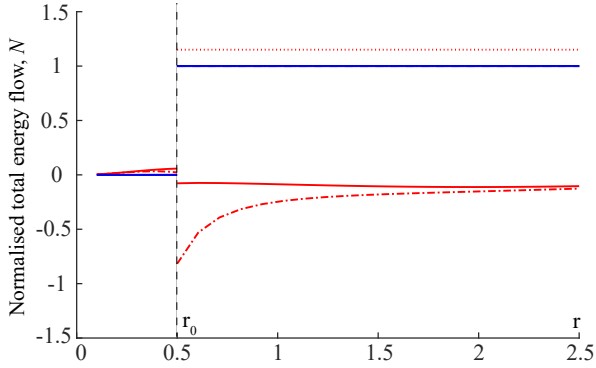


Fig. 3: Total energy flow (blue) using Eq. (50), [13], with the forces/displacements from Eq. (20) and (30) and the definition from Eq. (49) with the essential forces/displacements (all coincident). Red is the complementary real part using Eq. (50) with Eq. (20) (solid) and (30) (dash-dot) and using Eq. (49) with Eq. (22) (dotted). Non-dimensional parameters are similar to Fig. 2 but with $\rho = 0.1282$ i.e. fluid-load included. The solution involves only the propagating waves: $k = 1.9095$ and $k = 2.7931$ – corresponding to the far field solution.

An explicit formula for the total energy flow in the waveguide from the example in Sec. 3.1 with loading condition 01 is found simply by writing out Eq. (49). With integration in θ performed this becomes

$$N^\Sigma = -\chi_m \frac{\pi}{2} \Omega \sum_{n=1}^N \text{Im} \left(W^{01(n)} W^{01(-n)} \bar{R}^{(n,n)} \right) \quad (54)$$

$$\times \left[J_{m+1}(k^{(n)}r) H_m^{(1)}(k^{(n)}r) - J_m(k^{(n)}r) H_{m+1}^{(1)}(k^{(n)}r) \right] r$$

$$= -\chi_m \frac{\pi}{2} \Omega \sum_{n=1}^N \text{Im} \left(\frac{2i}{\pi k^{(n)}} W^{01(n)} W^{01(-n)} \bar{R}^{(n,n)} \right) \quad (55)$$

$$= -\chi_m \frac{\pi}{2} \Omega \sum_{n=1}^N \text{Re} \left(\frac{\pi k^{(n)} J_m(k^{(n)}r_0) H_m^{(1)}(k^{(n)}r_0)}{2 \bar{R}^{(n,n)}} \right)$$

where $\chi_{m=0} = 2, \chi_{m \neq 0} = 1$. Note again that when expressed via Eq. (49) the Wronskian ensures conservation of energy. In Cartesian coordinates this is ensured immediately by $R^{(-n,n)}$ since $\exp(k^{(-n)}x) \exp(k^{(n)}x) = 1$.

5. Perspectives on bi-orthogonality relations

The advantages of employing the bi-orthogonality relation are indeed remarkable in the theory of unbounded waveguides – whether in elastodynamics, vibro-acoustics, optics, electromagnetics, etc. Typically, it is also of interest to proceed and study the response or eigenfrequencies of ‘finite’ waveguides. When given the solution to the unbounded waveguide problem this is conveniently done using the method of Boundary Integral Equations (BIE). The essence of this method is the reciprocity between the problem at hand and an auxiliary problem chosen such that its solution has a simple

analytical form. Such a solution is referred to as the Green's tensor, matrix or function – depending on the dimensionality and complexity of the domain under consideration. Since derivation of BIE's is so much similar to derivation of the bi-orthogonality relation, it is reasonable to suggest that bi-orthogonality may find equally powerful applications in the BIE-method. In the derivation of BIE's we should employ the forcing problem from Sec. 3 (Green's function) as the auxiliary problem to solve the fully bounded one, just as we used the homogeneous problem from Sec. 2 to solve the forcing problem in Sec. 3. In particular, since the fully bounded problem may be expanded on the same eigenfunctions as the auxiliary problem (and solved with additional boundary conditions) the BIE's reduce entirely to identities between the relevant stations of the finite waveguide. Then the integral problem involving the BIE's may be reduced to a purely algebraic problem involving only the boundary conditions. Assembling boundary equations for 'primitive' components of a fluid-loaded thin-walled structure into a hierarchy of simultaneous equations proposed by L. I. Slepyan and co-workers [17] is relevant to this concept. For some special sets of boundary conditions the problem factorise completely into canonical eigenfrequency equations.

6. Conclusion

The novel results obtained in this paper are summarised as follows:

- The bi-orthogonality relation for any two distinct eigenfunctions exists in any problem governed by a self-adjoint operator and it may be obtained as a linear combination of characteristic equations for associated eigenvalues. Therefore, its form is invariant to the choice of coordinate system
- The bi-orthogonality relation involves only essential components of state variables
- By means of the bi-orthogonality relation, in forcing problems governed by a self-adjoint operator, the modal amplitudes are determined independently upon each other. Therefore, the virtual wave method may be reliably used for solving any problem of this type
- The bi-orthogonality relation in the waveguide theory provides a simple and robust way to compute energy flow regardless the amount of propagating waves

References

- [1] J. D. Achenbach, Reciprocity in elastodynamics, 2nd, Cambridge University Press, 2003. doi : 10.1017/CB09780511550485.
- [2] Y. I. Bobrovnikii, Orthogonality relations for Lamb waves, Soviet Acoustical Physics 18 (1973) 432–433.
- [3] W. B. Fraser, Orthogonality relation for the Rayleigh-Lamb modes of vibration of a plate, J. Acoustical Society of America 59 (1976) 215–216. doi : 10.1121/1.410103.
- [4] B. Karp, Generation of symmetric Lamb waves by non-uniform excitations, J. Sound and Vibration 312 (2008) 195–209. doi : 10.1016/j.jsv.2007.10.041.
- [5] R. D. Gregory, I. Gladwell, The Generation of Waves in a Semi-Infinite Plate by a Smooth Oscillating Piston, J. Appl. Mech. 51 (4) (1984) 787–791. doi : 10.1115/1.3167725.
- [6] R. D. Gregory, A note on bi-orthogonality relations for elastic cylinders of general cross section, J. Elasticity 13 (1983) 351–355. doi : 10.1007/BF00043002.

- [7] W. B. Fraser, An orthogonality relation for the modes of wave propagation in an elastic circular cylinder, *J. Sound and Vibration* 43 (1975) 568–571. doi:10.1016/0022-460X(75)90011-5.
- [8] L. I. Slepyan, Betty Theorem and Orthogonality Relations for Eigenfunctions, *Mech. Solids* 14(1) (1979) 74–77.
- [9] S. V. Sorokin, On the bi-orthogonality conditions for multi-modal elastic waveguides, *J. Sound and Vibration* 332 (2013) 5606–5617. doi:10.1016/j.jsv.2013.05.011.
- [10] L. S. Ledet, S. V. Sorokin, Bi-orthogonality relations for fluid-filled elastic cylindrical shells: Theory, generalisations and application to construct tailored green’s matrices, *J. Sound and Vibration* 417 (2018) 315–340. doi:10.1016/j.jsv.2017.12.010.
- [11] S. G. Mikhlin, *Variatsionnye metody v matematicheskoy fizike* (in Russian), 2nd, Moscow Nauka, 1970.
- [12] C. L. Dym, I. H. Shames, *Solid Mechanics - A Variational Approach*, Aug., Springer, 2013. doi:10.1007/978-1-4614-6034-3.
- [13] L. Cremer, M. Heckl, B. A. T. Petersson, *Structure-Borne Sound*, 3rd, Springer, 2005. doi:10.1007/b137728.
- [14] M. C. Junger, D. Feit, *Sound, structures, and their interaction*, Vol. 225, MIT press Cambridge, MA, 1986.
- [15] F. Fahy, P. Gardonio, *Sound and Structural Vibration*, 2nd, Elsevier, 2007.
- [16] S. Timoshenko, S. Woinowsky-Krieger, *Theory of plates and shells*, 2nd, McGraw Hill, 1959.
- [17] L. I. Slepyan, S. V. Sorokin, Analysis of structural-acoustic coupling problems by a two-level boundary integral equations method. part 1. a general formulation and test problems, *J. Sound and Vibration* 184(2) (1995) 195–212. doi:10.1006/jsvi.1995.0312.

Paper D

Using the Finite Product Method for solving eigenvalue problems formulated in cylindrical coordinates

Lasse S. Ledet & Sergey V. Sorokin

*Department of Materials and Production, Aalborg University,
Fibigerstraede 16, 9220 Aalborg East, Denmark*

To be published in:

Journal of Physics: Conference Series

As part of the 13th Intl. Conf. on Recent Advances in Structural Dynamics (RASD),
15-17 April 2019, Lyon

© 2019 IOP Publishing Ltd.
The layout has been revised.

Using the Finite Product Method for solving eigenvalue problems formulated in cylindrical coordinates

Lasse S. Ledet^a, Sergey V. Sorokin^a

^a*Department of Materials and Production, Aalborg University, Fibigerstraede 16, 9220 Aalborg, Denmark*

Abstract

Analysis of free/forced wave propagation in multi-layered structures and structures under heavy fluid loading constitute classical problems of fluid-structure interaction. These waveguides and many similar ones support infinitely many waves and, in some cases, e.g. at high-frequency excitations or in near-field analysis it is necessary to account for a large number of them. Finding the dispersion curves from these transcendental dispersion equations is not a trivial task due to their ill-conditioned/unstable nature as well as numerical algorithms' ability to solve transcendental equations. These issues can, however, be circumvented by using the Finite Product Method (FPM). The FPM is generic and has been used to solve dispersion equations of homogeneous waveguides derived in Cartesian coordinates with sine/cosine functions. However, it is yet to be formulated in cylindrical coordinates when Bessel functions are involved in the dispersion equations. We focus in this paper on extending the method to the cylindrical problems and compound waveguides, illustrated here by a fluid-filled cylindrical shell. The great advantage of the FPM is that it reduces the transcendental dispersion equation to a polynomial equation easily solved by numerical algorithms but more importantly it delivers only authentic roots of the dispersion equation i.e. no spurious roots as often encountered when using Taylor approximations etc.

1. Introduction

The eigenvalue problems formulated in cylindrical coordinates condense to solving transcendental characteristic equations containing Bessel functions. These characteristic equations may be written on the general form;

$$h(\Omega, k, m) - g(\Omega, k, m) \frac{G_m[\kappa(\Omega, k)]}{G'_m[\kappa(\Omega, k)]} = 0 \quad (1)$$

where h and g are some functions containing the physical properties of the problem, G_m any Bessel function and G'_m its derivative. In general, Ω , k and m are unknown parameters. This equation, presented here in a rather general format, encloses a wide variety of challenging physical and engineering problems, conveniently formulated in cylindrical coordinates, see e.g. [1–4]. A broad range of these problems are concerned with waveguides in various realms of physics such as; acoustics, optics, electromagnetics and structural dynamics, so that the characteristic equation, Eq. (1), encounters

the meaning of a dispersion equation for a waveguide supporting an infinite number of waves.

To analyse performance of a waveguide the (Ω, k) -dispersion diagram is needed. Thus, we need to find the solutions, k , to the dispersion equation as a function of Ω . However, since such an equation system often evolve from interacting fields of different nature (compound waveguides) e.g. vibro-acoustics or electromagnetics (essentially rigid/compliant), finding (or approximating) these roots is not a trivial task as discussed in [5]. Various methods to accommodate this exist, such as Wave Based (WB), Semi-Analytical Finite Element (SAFE), Partial Wave Root Finding (PWRF), Pseudo-spectral Collocation (PSC) methods etc. In engineering applications, the preferred choice is the methods based on geometrical discretisation into elements such as the Wave Finite Element (WFE) or Spectral Element (SE) method, see e.g. [6, 7]. In particular, these methods are suitable for retrieving dispersion diagrams for complicated waveguides but require CAD models for element discretisation. However, when the dispersion equation is on analytical form as in Eq. (1), approximations are nevertheless necessary, either as a substitute for the exact equation or as input to find the exact solutions. Some of the most used approximations are polynomials such as Chebyshev or Taylor series, where the former is good but tends to mask the physical nature and analytical structure of the problem, [5], while the latter offers a poor accuracy and introduce spurious roots, [5]. In light of these drawbacks the Finite Product Method (FPM) developed in [5] was proposed as a powerful alternative. Several benefits of this method can be listed from [5], for instance, it offers arbitrarily high accuracy at negligible expense, introduce no spurious roots and preserves the physical nature of the problem at hand – but most important: It is surprisingly simple. Further, the FPM also exhibits strengths similar to the Chebyshev polynomials by escaping Runge’s Phenomenon.

However, the FPM is yet to be developed for problems formulated in cylindrical coordinates as well as for compound waveguides and, given its advantages, this is the obvious objective of this paper. As an example to illustrate the formulation of the FPM for solving Eq. (1) we consider wave propagation in a conservative elastic fluid-filled cylindrical shell (using $\exp[kx - im\theta - i\omega t]$) in which case Eq. (1) encounters the interpretation of a dispersion equation, the Bessel functions become of first kind and order $m \in \mathbb{Z}$ where m constitutes circumferential modes, $k \in \mathbb{C}$ are axial wavenumbers, $\Omega \in \mathbb{R}$ (conservative) is the frequency parameter, $G'_m(\kappa) = J'_m(\kappa) = \frac{1}{\kappa} \left. \frac{dJ_m(\kappa r)}{dr} \right|_{r=1} = \frac{dJ_m(\kappa)}{d\kappa}$ and

$$g(\Omega, k, m) = \frac{\alpha(\Omega)}{\kappa(\Omega, k)} f_1(\Omega, k, m) \quad h(\Omega, k, m) = f_2(\Omega, k, m) \quad (2)$$

$$\text{where } \kappa(\Omega, k) = \sqrt{k^2 + \Omega^2 \gamma^2} \quad \wedge \quad \alpha(\Omega) = \frac{\rho}{\mu} \Omega^2$$

all formulated in their non-dimensional form (unless otherwise stated). Here κ is the radial wavenumber, $f_2 = 0$ corresponds to the dispersion equation for the in vacuo shell, $G_m(\kappa) \rightarrow J_m(\kappa) = 0$ to the soft baffle dispersion equation (pressure release) and $G'_m(\kappa) \rightarrow J'_m(\kappa) = 0$ to the rigid baffle dispersion equation. Since f_1 and f_2 are

rather cumbersome for this problem they are not presented here but can be deduced from e.g. [3, 4]. For the example used in this paper we use the non-dimensional parameters; $\mu = 0.0175$, $\rho = 0.128$, $\gamma = 3.7773$, corresponding to e.g. a water-filled steel shell. Here μ is the thickness-to-radius ratio, ρ the fluid-to-structure density ratio and γ the structure-to-fluid sound speed ratio, see e.g. [3, 4] for details.

2. The Finite Product Method for problems involving Bessel functions

To formulate the shell problem in the framework of FPM we follow [5] and introduce, first, an equivalent infinite product formulation of the transcendental terms (Bessel functions). This form is standard and can be found in e.g. [1, 8, 9] as

$$J_m(\kappa) = \frac{\left(\frac{\kappa}{2}\right)^m}{\Gamma(m+1)} \prod_{n=1}^{\infty} \left[1 - \frac{\kappa^2}{j_{m,n}^2}\right] = \frac{\left(\frac{\kappa}{2}\right)^m}{\Gamma(m+1)} \prod_{n=1}^{N_1} \left[1 - \frac{\kappa^2}{j_{m,n}^2}\right] \prod_{n=N_1+1}^{\infty} \left[1 - \frac{\kappa^2}{j_{m,n}^2}\right] \quad (3)$$

$$J'_m(\kappa) = \frac{\left(\frac{\kappa}{2}\right)^{m-1}}{2\Gamma(m)} \prod_{n=1}^{\infty} \left[1 - \frac{\kappa^2}{j_{m,n}^2}\right] = \frac{\left(\frac{\kappa}{2}\right)^{m-1}}{2\Gamma(m)} \prod_{n=1}^{N_2} \left[1 - \frac{\kappa^2}{j_{m,n}^2}\right] \prod_{n=N_2+1}^{\infty} \left[1 - \frac{\kappa^2}{j_{m,n}^2}\right], \quad m \neq 0 \quad (4)$$

where $j_{m,n}$ and $j'_{m,n}$ are the zeros of the transcendental functions, also found in e.g. [8, 9] and is otherwise standard in most mathematical software. Further, we split the product into a finite and an infinite one characterised by the approximation order $(N_1, N_2) \in \mathbb{N}$. Note that Eq. (4) holds only for $m \neq 0$ as indicated, however, at $m = 0$ we use instead the identity: $J'_0(\kappa) = -J_1(\kappa)$, so that Eq. (3) applies.

Then, following [5] we may write the infinite product in terms of a so-called gamma-conversion factor (converting Bessel functions to polynomials), which constitutes an amplitude modulation of the Bessel approximation. However, since there are no explicit form of the zeros of the Bessel function, one needs to apply approximate asymptotic zeros so that the conversion factor is accurate only up to some power, p : $\mathcal{O}\left(\frac{1}{N^p}\right)$. This was shown in [1] for $p = 1$ with the asymptotic zeros from Eq. (5).

$$\begin{aligned} j_{m,n} &= \tilde{j}_{m,n} + \mathcal{O}\left(\frac{1}{N}\right) = \left(n + \frac{1}{2}m - \frac{1}{4}\right)\pi + \mathcal{O}\left(\frac{1}{N}\right) \\ j'_{m,n} &= \tilde{j}'_{m,n} + \mathcal{O}\left(\frac{1}{N}\right) = \left(n + \frac{1}{2}m - \frac{3}{4}\right)\pi + \mathcal{O}\left(\frac{1}{N}\right) = \tilde{j}_{m,n} - \frac{1}{2}\pi + \mathcal{O}\left(\frac{1}{N}\right) \end{aligned} \quad (5)$$

where we see that the asymptotic zeros corresponds to a shifted sine/cosine dispersion and so they follow; $\tilde{j}'_{m,n} = \tilde{j}_{m,n} - \frac{1}{2}\pi = \tilde{j}_{m-1,n}$ and incidentally $\tilde{j}'_{m,n+1} = \tilde{j}_{m+1,n}$. Also, as given in e.g. [8, 9], the actual zeros interlace as

$$\begin{aligned} j_{m,n} < j_{m+1,n} < j_{m,n+1} \quad \text{and} \quad j'_{m,n} < j'_{m+1,n} < j'_{m,n+1} \\ j'_{m,n} < j_{m,n} < j'_{m,n+1} < j_{m,n+1} \end{aligned} \quad (6)$$

Obviously, we may always improve this approximation taking increasing asymptotic orders of p . However, as the essential part of the FPM is that the conversion factors of

$J_m(\kappa)$ and $J'_m(\kappa)$ cancel almost exactly for proper choice of N_1 and N_2 , increasing the accuracy is indeed redundant. As in [5] this cancellation and corresponding choice of N_1/N_2 can be found using e.g. Stirling's approximation, but as this choice is more or less obvious from Eq. (3) and (4) using (5) or (6) we take it for granted until returning to it in Sec. 3 and use the approximation order $(N_1, N_2) = (N_1, N_1 + 1)$. Thus, to get the finite products, $\tilde{J}_m(\kappa)$ and $\tilde{J}'_m(\kappa)$, we simply discard the transcendental terms and replace the Bessel functions with their FP-approximations in Eq. (7), assuming N_1 large enough that the approximation remains good in some region of the real/complex (Ω, k) -space.

$$\tilde{J}_m(\kappa) = \frac{\left(\frac{\kappa}{2}\right)^m}{\Gamma(m+1)} \prod_{n=1}^{N_1} \left[1 - \frac{\kappa^2}{J_{m,n}^2} \right] \quad \tilde{J}'_m(\kappa) = \frac{\left(\frac{\kappa}{2}\right)^{m-1}}{2\Gamma(m)} \prod_{n=1}^{N_2} \left[1 - \frac{\kappa^2}{J_{m,n}'^2} \right] \quad (7)$$

with $\tilde{J}_m(\kappa) \equiv 1$ and $\tilde{J}'_m(\kappa) \equiv 1$ for $N_1 = N_2 = 0$. In contrast to Taylor approximations, the FPM requires no derivatives, nor does it introduce spurious zeros. Further, Runge's phenomenon cancels (by way of the fraction, see e.g. Fig. 3) as in Chebyshev polynomials, yet it preserves the physical nature of the equation system. In essence, the FPM is extremely simple in that we use only an equivalent infinite product representation of the transcendental terms (available in literature), introduce the approximation order (N_1, N_2) , discard the transcendental part of the product formulation and find the relation between the approximation orders to ensure correct limit behaviour. As we shall see in Sec. 3 finding the approximation orders are equally simple.

In Fig. 1 dispersion diagrams for different approximation orders $(N_1, N_1 + 1)$ are shown for a water-filled steel shell in bending ($m = 1$). From the figures we find that even for low order approximations the dispersion curves are surprisingly accurate in a fairly large region of the real/complex (Ω, k) -space bounded approximately by $\Omega = \frac{J_{m,N_2}}{\gamma} \approx \frac{(N_1 + \frac{3}{4})\pi}{\gamma}$ and $k = J'_{m,N_2} \approx \left(N_1 + \frac{3}{4}\right)\pi$ for the cases shown here ($m = 1$). This is discussed further in Sec. 3. Fortunately, as seen from the dimensional frequency scale on figure (e,f) this constitutes a large accuracy range for waveguide problems. Note also from figure (f) that a real-branch of the dispersion diagram is not captured at all, explained by a too low approximation order since the branch originates from J'_{m,N_2+1} .

3. Accuracy analysis and discussion

Proper relation between N_1 and N_2 may be found from a Stirling approximation and/or a limit study to ensure the asymptotic behaviour. However, by using just the distribution of zeros from Eq. (6) the relation appears directly from the fraction of the finite products in Eq. (8).

$$\frac{\tilde{J}_m(\kappa)}{\tilde{J}'_m(\kappa)} = \frac{\left(\frac{\kappa}{2}\right)^m}{\Gamma(m+1)} \prod_{n=1}^{N_1} \left[1 - \frac{\kappa^2}{J_{m,n}^2} \right] = \frac{\kappa}{m} \frac{\prod_{n=1}^{N_1} \left[1 - \frac{\kappa^2}{J_{m,n}^2} \right]}{\prod_{n=1}^{N_2} \left[1 - \frac{\kappa^2}{J_{m,n}'^2} \right]} \cong \frac{\kappa}{m} \frac{\prod_{n=1}^{N_1} \left[1 - \left(\frac{\kappa}{J_{m,n}}\right)^2 \right]}{\prod_{n=1}^{N_2} \left[1 - \left(\frac{\kappa}{J_{m,n}' - \frac{1}{2}\pi}\right)^2 \right]} \quad (8)$$

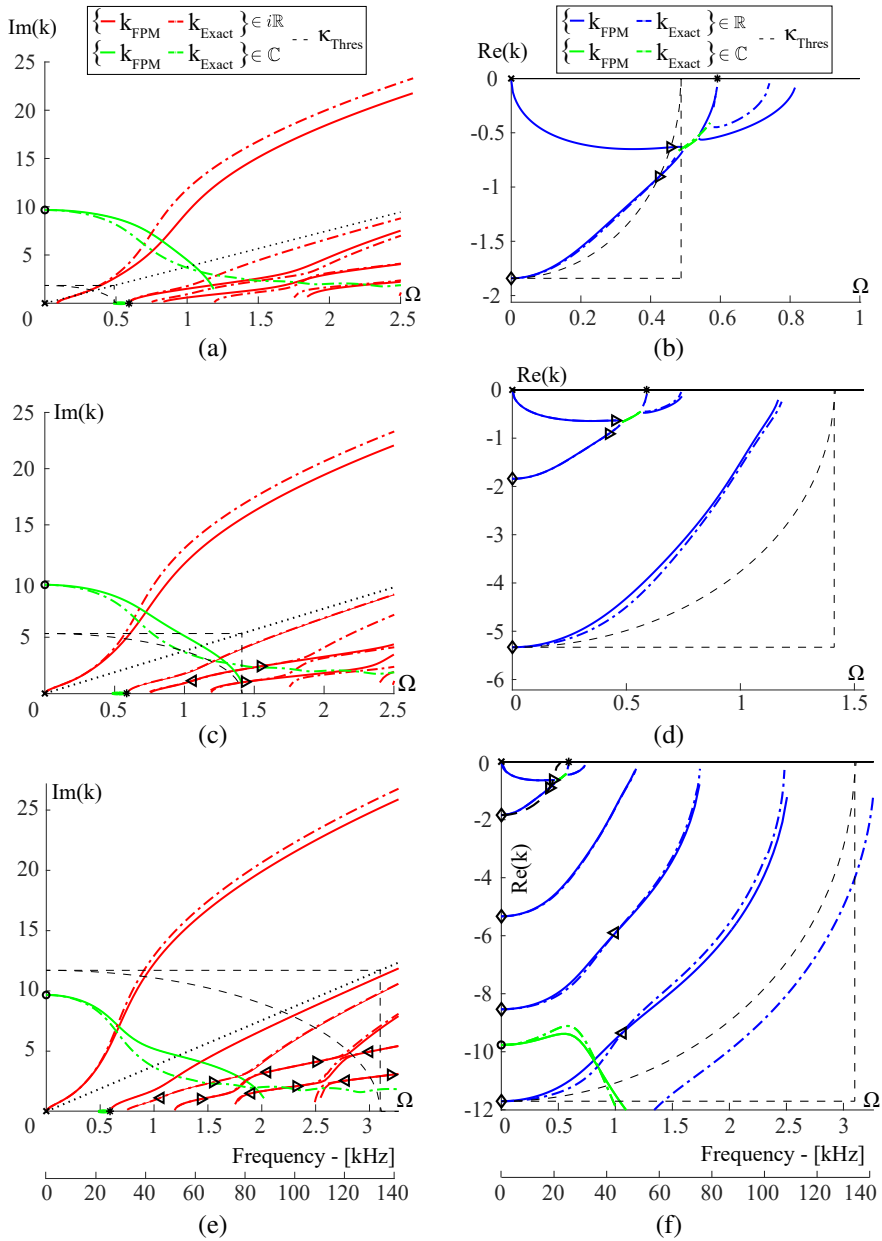


Fig. 1: A comparison between the exact and the FPM dispersion diagrams for a fluid-filled shell vibrating in bending ($m = 1$). Left figures show imaginary parts (propagating waves), right shows real parts with approximation orders (0,1) for (a,b), (1,2) for (c,d) and (3,4) for (e,f). Grid points according to Sec. 3 are shown and $i\mathbb{R}$ indicate purely imaginary wavenumbers.

Then using Eq. (6) we see from Eq. (8) that the fraction is led by its zero $j_{m,n}$ (or $\tilde{j}_{m,n}$) for fixed n (seen explicitly using the first order asymptotic zeros, last in Eq. (8)). This leaves only two obvious choices; either $N_1 = N_2$, (fraction lead by zero, $j_{m,n}$) or $N_2 = N_1 + 1$ (fraction lead by pole, $j'_{m,n}$). From this we may also deduce a conservative validity range for $k \in \mathbb{R}$ based on the last zero included i.e. $|\kappa| \leq \max\{|j_{m,N_1}|, |j'_{m,N_2}|\}$ corresponding to

$$\begin{aligned} |\kappa| \leq j_{m,N_1} &= \left(N_1 + \frac{1}{2}m - \frac{1}{4}\right)\pi + \mathcal{O}\left(\frac{1}{N}\right) & \text{for } N_2 = N_1 \\ |\kappa| \leq j'_{m,N_1+1} &= \left(N_1 + \frac{1}{2}m + \frac{1}{4}\right)\pi + \mathcal{O}\left(\frac{1}{N}\right) & \text{for } N_2 = N_1 + 1 \end{aligned} \quad (9)$$

For $|\kappa| > \max\{|j_{m,N_1}|, |j'_{m,N_2}|\}$ the FP-fraction in Eq. (8) diverges rapidly from the exact, see Fig. 3b. Hence, the threshold of Eq. (9) constitute the arc in the (Ω, k) -space, seen in Fig. 1 as κ_{Thres} i.e. $k(\Omega) = \sqrt{\max\{|j_{m,N_1}|, |j'_{m,N_2}|\}^2 - \gamma^2\Omega^2}$. Though the validity range for $k \in i\mathbb{R}$ (purely imaginary) extends beyond this as seen from Fig. 1 we may use Eq. (9) also as a conservative range for the complex domain.

For any other choice of approximation order, zeros (and poles) are 'left out' resulting in the approximation being no better than $\min\{j_{m,N_1}, j'_{m,N_2}\}$ since Eq. (8) will diverge significantly already in this region as a consequence of the amplitude modulation. Then by the same argument all zeros up to the chosen approximation order should obviously be included. In general, the approximation order should be chosen as all zeros, r_n and q_n , up to an arbitrarily chosen truncation in the sorted set of zeros:

$$\{\dots, r_{N_1}, q_{N_2}, r_{N_1+1}, \dots\} \quad \text{where } \dots < r_{N_1} < q_{N_2} < r_{N_1+1} < \dots \quad (10)$$

corresponding to a lead of either q_{N_2} or r_{N_1+1} . Indeed this corresponds to $N_2 = N_1$ and $N_2 = N_1 + 1$ for the shell and using this generalisation it is easy from Eq. (5) to show, for some hypothetical fraction $\frac{J_{m+2}(k)}{J_m(k)}$, that the proper relation between N_1/N_2 is either $N_2 = N_1 + 1$ or $N_2 = N_1 + 2$.

Returning to the shell example, the two choices are in general equally good, in that, taking $N_2 = N_1 + 1$ the validity range of κ extends by $\frac{1}{2}\pi + \mathcal{O}\left(\frac{1}{N}\right)$, however, at the expense of an increase in the polynomial order of power two. Thus, we cannot immediately argue one choice over the other as this depends on the problem at hand. Though both choices are good and equally valid we wish to find the best choice. To do so we study the nature of the problem. From this we find that f_2 is quartic in k^2 and f_1 quadratic, so that from the dispersion equation in Eq. (11)

$$\frac{f_1(\Omega, k, m)}{f_2(\Omega, k, m)} = \frac{\mu}{\rho\Omega^2} \kappa(\Omega, k) \frac{J'_m[\kappa(\Omega, k)]}{J_m[\kappa(\Omega, k)]} \quad (11)$$

we get that $\frac{f_1}{f_2} = \mathcal{O}\left(\frac{1}{k^4}\right) \rightarrow 0$ as $k \rightarrow \infty$. Hence, $J'_m[\kappa(\Omega, k)]$ must tend to zero for $k \rightarrow \infty$ and we may conclude that $\kappa \rightarrow j'_{m,n}$ so that the asymptotic solution for k becomes:

$k_0 \cong \sqrt{j_{m,n}^2 - \Omega^2 \gamma^2}$. For this reason it is indeed favourable to have $j'_{m,n}$ in the lead, since we, besides increasing the approximation order, capture also another branch of the dispersion equation. This, along with the asymptotic behaviour, is easily seen from Fig. 2 at $\Omega = 0$ where new branches depart only from $j'_{m,n}$. For the waveguide considered, it means that higher order waves converge towards the rigid duct waves, as discussed in [3] and therefore the higher order waves do not notice the compliance of the shell. For more details on this specific problem attention should be drawn to e.g. [3, 4].

3.1. Grid points

The FP-approximation of the dispersion equation is concerned only with approximation of the transcendental terms and therefore we indeed have a number of solutions (denoted grid points) for which the solution of the approximate dispersion equation belongs to the solution set of the exact one. The grid points are readily available from Eq. (1) (with the transcendental functions replaced by their FP-approximations) when each term is simultaneously zero. In general, this gives the four cases:

$$\begin{aligned} 1) \quad & h(\Omega, k, m) = g(\Omega, k, m) = 0 & 2) \quad & h(\Omega, k, m) = G_m[\kappa(\Omega, k)] = 0 \\ 3) \quad & g(\Omega, k, m) = G'_m[\kappa(\Omega, k)] = 0 & 4) \quad & G_m[\kappa(\Omega, k)] = G'_m[\kappa(\Omega, k)] = 0 \end{aligned}$$

in which not all cases necessarily hold in the real/complex (Ω, k) -space. In terms of the fluid-filled shell this translates, by way of the definitions in Eq. (2), to nine cases:

1. (✗) $\Omega = \kappa = 0 \Rightarrow (\Omega, k) = (0, 0)$
2. (○) $\Omega = f_2(\Omega, k, m) = 0 \Rightarrow (\Omega, k) = (0, f_2(m, k, 0) = 0)$ – Structure originated stationary wavenumbers (corresponds to the in vacuo shell)
3. (◇) $\Omega = \tilde{J}'_m(\kappa) = 0 \Rightarrow (\Omega, k) = (0, \pm j'_{m,n})$ – Fluid originated stationary wavenumbers (corresponds to the rigid duct)
4. (◄) $f_2(\Omega, k, m) = \tilde{J}_m(\kappa) = 0 \Rightarrow (\Omega, k) = \left(f_2 \left(\Omega, \sqrt{j_{m,n}^2 - \gamma^2 \Omega^2}, m \right) = 0, \sqrt{j_{m,n}^2 - \gamma^2 \Omega^2} \right)$ – ‘Periodic’ grid points governed by structure (structure acts as soft baffle)
5. (►) $f_1(\Omega, k, m) = \tilde{J}'_m(\kappa) = 0 \Rightarrow (\Omega, k) = \left(f_1 \left(\Omega, \sqrt{j_{m,n}^2 - \gamma^2 \Omega^2}, m \right) = 0, \sqrt{j_{m,n}^2 - \gamma^2 \Omega^2} \right)$ – ‘Periodic’ grid points governed by rigid baffle (structure acts as rigid baffle)
6. (*) $f_2(\Omega, k, m) = f_1(\Omega, k, m) = 0$ – Cut-on of structure originated wave
7. (+) $\kappa = f_1(\Omega, k, m) = 0 \Rightarrow (\Omega, k) = (f_1(\Omega, i\gamma\Omega, m) = 0, i\gamma\Omega)$ – Solutions belong to the $\Omega \in \mathbb{C}$ -space
8. (⋯) $\kappa = \tilde{J}_m(\kappa) = 0 \Rightarrow \tilde{J}_m(0) = 0 \Rightarrow (\Omega, k) = (\Omega, i\gamma\Omega)$ for $m \neq 0$
9. (□) $\tilde{J}'_m(\kappa) = \tilde{J}_m(\kappa) = 0 \Rightarrow (\Omega, k) = (\Omega, i\gamma\Omega)$ for $m \neq \{0, 1\}$

From these cases we effortlessly find the grid points shown in Fig. 1 and 2 plotted with symbols corresponding to those above. The colours indicate whether the cases are feasible (green) or infeasible (red). In particular, case 8 and 9 both originate from

$J'_m(\kappa)$ (Eq. (2)) and constitute in fact spurious roots as a consequence of rearranging the dispersion equation (true both for exact and FP-dispersion equation), while case 7 belongs to the complex Ω -space and is thus invalid for conservative systems where $(\Omega, k) \in (\mathbb{R}, \mathbb{C})$. From case 2 and 3 we see that only at the stationary frequency ($\Omega = 0$) is all fluid and structural waves fully uncoupled simultaneously and behave respectively as a rigid duct and an empty shell. Case 6 gives only the cut-on for the second structural wave. In addition, note that the grid points of case 3-5 depends on the approximation order meaning that all fluid governed wave branches attain grid points lying on, respectively: $k_3 = \pm j'_{m,n}$, $k_4(\Omega) = \sqrt{j_{m,n}^2 - \gamma^2 \Omega^2}$ and $k_5(\Omega) = \sqrt{j_{m,n}^2 - \gamma^2 \Omega^2}$.

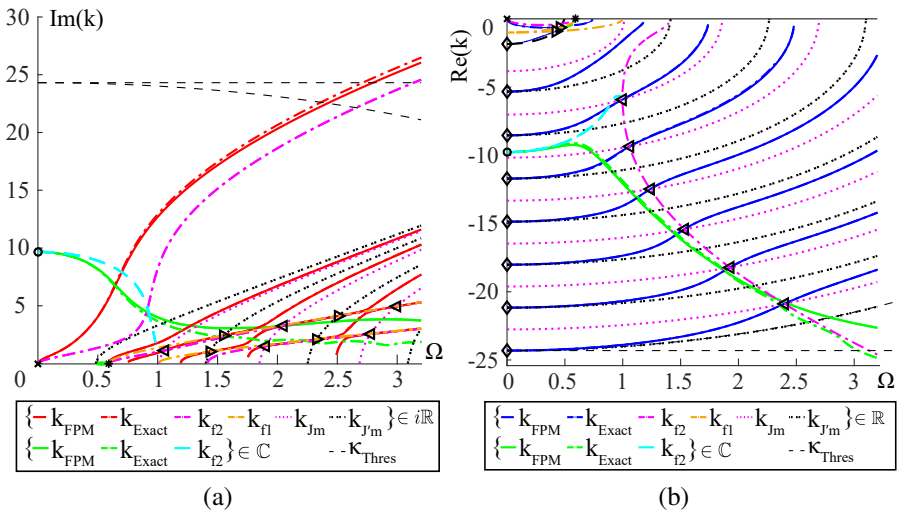


Fig. 2: Comparison of dispersion diagrams with grid points (case 8 discarded). Included are the terms from Eq. (2) corresponding to exact, FP-approximation $(N_1, N_2) = (7, 8)$, in vacuo shell, rigid duct and soft baffle dispersion diagrams and f_1 . For higher order waves the dispersion curves of the exact and FPM are inseparable by eye. (a) Imaginary part (propagating waves) (b) real part.

Note from the figure that the 'periodic' grid points appear exactly when the soft baffle and 'in vacuo' shell branches intersect (move in phase) and when f_1 intersects with the rigid duct branches, which eventually also becomes in-phase 'movement' of structure and fluid. In addition, we note that when a dispersion curve veers away (introduced in [10]) in the presence of veering (or cut-on) of others it 'looses' the ability to attain future grid points, yet it remains surprisingly accurate. For compound waveguides this veering appears in the transition zone for a wave being structure to becoming fluid governed – clear from Eq. (11) by the limit behaviour of the dispersion equation. Effectively, a veering wave branch becomes fluid governed and so the wave of the compound waveguide is bounded always by its two extremes, respectively, the waves in a rigid and soft baffle, as seen from the figure. This ensures on its own a high accuracy range for these wave branches and does in fact improve as $\Omega \rightarrow \infty$ since the

asymptotes of these waves converge (compound, soft and rigid baffle).

3.2. Accuracy

Though we have already discussed the choice of N_1/N_2 as well as a simple accuracy limit, Eq. (9), we shall discuss here rather brief, following [5], other convenient properties of the FPM and FP-fraction, causing the accuracy range to extend beyond the conservative one based on the fraction itself, Eq. (9). First, consider the discarded fraction, Eq. (12).

$$\frac{\prod_{n=N_1+1}^{\infty} \left[1 - \left(\frac{\kappa}{j_{m,n}} \right)^2 \right]}{\prod_{n=N_2+1}^{\infty} \left[1 - \left(\frac{\kappa}{j_{m,n}} \right)^2 \right]} \cong \frac{\prod_{n=N_1+1}^{\infty} \left[1 - \left(\frac{\kappa}{j_{m,n}} \right)^2 \right]}{\prod_{n=N_2+1}^{\infty} \left[1 - \left(\frac{\kappa}{j_{m,n} - \frac{1}{2}\pi} \right)^2 \right]} \cong 1 \quad (12)$$

Obviously, the FP-approximations require this fraction to be close to one ($\cong 1$) for the finite product to be a good approximation. From the equation and the chosen approximation order it is obvious that the product tends monotonically to 1 for any fixed κ as $N_1, N_2 \rightarrow \infty$. Similar for κ from $\max\{|j_{m,N_1}|, |j'_{m,N_2}|\}$ to 0 the fraction is uniform meaning that the product tends monotonically to 1 for any approximation order as $\kappa \rightarrow 0$. This is seen from Fig. 3(a) showing Eq. (12) approximated using Gamma functions and the asymptotic zeros from Eq. (5) following [1]. However, as discussed in [5] (and supported by the figure) this error measure does not fully comprehend the excellent accuracy obtained by the FP dispersion equation. For one, it does not capture the grid points which indeed belongs to the exact solution set. On the other hand, it was argued in [5] that a proper error measure is to consider the difference in tangents of the dispersion curves at the grid points. This fact appear fairly obvious from the approximation methodology, find details in [5, Sec. 4], and as it is a generic property it therefore also applies immediately to cylindrical problems. Do, however, note that for compound waveguides this measure does likely not explain properly the accuracy of the wave branches after veering (as the grid points are 'lost'), which is nonetheless explained with Fig. 2.

Now, instead of reproducing these results we consider the FP-fraction plotted in Fig. 3(b) from which we see that Runge's phenomenon cancels almost exactly in the presence of the Bessel fraction so that the amplitude modulation in the FP-approximations vanish. As a consequence this ensures that the validity range extends beyond the simplified on in Eq. (9) and in effect makes the FPM particularly powerful in the presence of fractions. By this simple consideration we may safely extend the accuracy range from the arc in Eq. (9) to the entire square

$$\begin{aligned} |\Omega, k| \leq j_{m,N_1} &= \left(N_1 + \frac{1}{2}m - \frac{1}{4} \right) \pi + \mathcal{O}\left(\frac{1}{N}\right) \quad \text{for } N_2 = N_1 \\ |\Omega, k| \leq j'_{m,N_1+1} &= \left(N_1 + \frac{1}{2}m + \frac{1}{4} \right) \pi + \mathcal{O}\left(\frac{1}{N}\right) \quad \text{for } N_2 = N_1 + 1 \end{aligned} \quad (13)$$

As seen from Fig. 2 this proves well for propagating and decaying waves (real and imaginary), while the attenuating waves (complex) seem to require higher approximation orders.

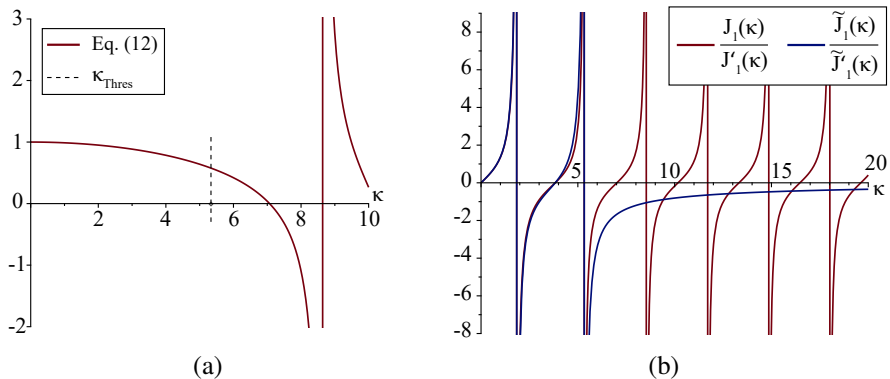


Fig. 3: (a) Infinite fraction of Eq. (12) plotted for $(N_1, N_2) = (1, 2)$ and (b) Bessel fraction from Eq. (1) plotted together with the $(N_1, N_2) = (1, 2)$ FP-fraction, Eq. (8).

Finally, as suggested by the figures, the validity range may in some cases, as for the fluid-filled shell, extend significantly beyond the simplified measures deduced here. Indeed better estimates may be derived for specific problems following the methodology in [5], however, those derived here are generic and based alone on the last zero included in the finite products, which is directly related to the approximation order.

4. Conclusion

In this paper we have developed and illustrated the Finite Product Method for problems formulated in cylindrical coordinates and exemplified it using a conservative time-harmonic elastic cylindrical fluid-filled shell. The strength of the FPM is that it introduces no spurious roots but most importantly: It is extremely simple. Essentially, in the FPM, we simply replace the transcendental terms with their equivalent infinite products (available in literature), truncate the products to finite ones and determine proper approximation orders based on the sorted set of roots of the original transcendental terms. In addition, a region of high accuracy for all wave branches is defined directly from the chosen approximation order.

Given the simplicity and excellent accuracy of the FPM it is a particularly powerful tool in the realm of waveguide theory and because of its generality and simplicity, it is easily extended to more complicated dispersion equations such as e.g. multi-layered compound waveguides, either in the format of circular plates or layered shells. Also, the example presented here is indeed not restricted to integer m , hence pipes/profiles of open cross-section can also be studied straightforwardly using the FPM.

Acknowledgments

A special thanks to Professor C. J. Chapman from Keele University for helpful discussions and comments.

References

- [1] A. D. Rawlins, The method of finite-product extraction and an application to Wiener-Hopf theory, *J. Appl. Math.* 77 (4) (2012) 590–602. [doi:10.1093/imamat/hxr043](https://doi.org/10.1093/imamat/hxr043).
- [2] L. J. Landau, Ratios of Bessel Functions and Roots of $\alpha J_\nu(x) + xJ'_\nu(x) = 0$, *J. Math. Anal. Appl.* 240 (1999) 174–204. [doi:10.1006/jmaa.1999.6608](https://doi.org/10.1006/jmaa.1999.6608).
- [3] L. S. Ledet, S. V. Sorokin, Bi-orthogonality relations for fluid-filled elastic cylindrical shells: Theory, generalisations and application to construct tailored Green's matrices, *J. Sound Vib.* 417 (2018) 315–340. [doi:10.1016/j.jsv.2017.12.010](https://doi.org/10.1016/j.jsv.2017.12.010).
- [4] S. V. Sorokin, J. B. Nielsen, N. Olhoff, J. B. Larsen, N. Olhoff, Green's matrix and the boundary integral equation method for the analysis of vibration and energy flow in cylindrical shells with and without internal fluid loading, *J. Sound Vib.* 271 (3-5) (2004) 815–847. [doi:10.1016/S0022-460X\(03\)00755-7](https://doi.org/10.1016/S0022-460X(03)00755-7).
- [5] C. J. Chapman, S. V. Sorokin, The finite-product method in the theory of waves and stability, *Proc. R. Soc. A Math. Phys. Eng. Sci.* 466 (2114) (2010) 471–491. [doi:10.1098/rspa.2009.0255](https://doi.org/10.1098/rspa.2009.0255).
- [6] B. F. Shorr, *The Wave Finite Element Method*, Springer, 2004. [doi:10.1007/978-3-540-44579-1](https://doi.org/10.1007/978-3-540-44579-1).
- [7] S. Gopalakrishnan, A. Chakraborty, D. R. Mahapatra, *Spectral Finite Element Method*, Springer, 2008. [doi:10.1007/978-1-84628-356-7](https://doi.org/10.1007/978-1-84628-356-7).
- [8] M. Abramowitz, I. A. Stegun, *Handbook of Mathematical Functions*, New York: Dover, 1964. [doi:10.1115/1.3625776](https://doi.org/10.1115/1.3625776).
- [9] F. W. Olver, D. W. Lozier, R. F. Boisvert, C. W. Clark, *NIST Handbook of Mathematical Functions*, Cambridge University Press, 2010.
- [10] B. R. Mace, E. Manconi, Wave motion and dispersion phenomena: Veering, locking and strong coupling effects, *J. Acoust. Soc. Am.* 131 (2) (2012) 1015–1028. [doi:10.1121/1.3672647](https://doi.org/10.1121/1.3672647).

Paper E

Wave propagation in helically orthotropic elastic
cylindrical shells and lattices

Sergey V. Sorokin^b, Elisabetta Manconi^a, Lasse S. Ledet^b &
Rinaldo Garziera^a

^a *Dipartimento di Ingegneria e Architettura, Università degli Studi di Parma,
Viale delle Scienze 181/A, 43100 Parma, Italy*

^b *Department of Materials and Production, Aalborg University,
Fibigerstraede 16, 9220 Aalborg East, Denmark*

Published in:
International Journal of Solids and Structures, Vol. 170, pp. 11–21, 2019
doi:10.1016/j.ijsolstr.2019.04.031

© 2019 Elsevier Ltd. All rights reserved.
The layout has been revised.

Wave propagation in helically orthotropic elastic cylindrical shells and lattices

S. V. Sorokin^b, E. Manconi^{*a}, L. S. Ledet^b, R. Garziera^a

^a*Dipartimento di Ingegneria e Architettura, Università degli Studi di Parma, Viale delle Scienze 181/A, 43100 Parma, Italy*

^b*Department of Materials and Production, Aalborg University, Fibigerstraede 16, 9220 Aalborg, Denmark*

Abstract

A use of orthotropic materials such as fibre-reinforced composites can introduce enhanced vibro-acoustic performance of cylindrical structures that are not feasible when an isotropic material is used. In this paper, free and forced wave propagation in cylindrical structures with helically orthotropic material properties is analysed to demonstrate these effects. Two models, a thin cylindrical shell and a cylindrical beam lattice, are considered and two methods, an analytical method of the thin shell theory and a numerical Wave Finite Element method, are used. For both models, the symmetry breaking effect concerned with the location of dispersion curves is captured by means of these methods and explained. The influence of the helix angle and of the material parameters on the location of dispersion curves is investigated. The Green's matrix is formulated for rotating forces and the forcing problems are solved to highlight some unusual waveguide properties of the helically orthotropic cylindrical structures. The results are discussed in view of a possible application for control of energy flow in piping systems exposed to rotating excitation.

Keywords:

Helical structures, Wave propagation, Dispersion curves, Green's matrix, Rotating forces, Energy flow

1. Introduction

Wave propagation in helical waveguides has been a subject of interest for a long time, see e.g. [1], and, as for many other research subjects, many original and interesting studies and applications can be found in the literature. Due to difficulties in solving partial differential equations for helical structures, in recent years there has been an increased interest in numerical methods for the analysis of wave propagation in helical waveguides, in particular, due to developments in structural health monitoring techniques. Dispersion curves in helical springs were obtained in [2] applying an asymptotic analysis and then the dominant balance method. Natural frequencies in helical springs were calculated in [3] using a dynamic stiffness method, while vibrations were studied in [4] applying a pseudo-spectral method and in [5] using the Green's matrix the Boundary Integral Method. Several numerical methods based on Finite Element discretisation have been also proposed, each one showing some advantages or

disadvantages with respect to the other. Vibration of helical springs with non-uniform ends was studied in [6] using a hybrid Wave Finite Element method. In [7] a Semi Analytical Finite Element method, based on translational invariance of curved waveguides, was presented, while in [8] dispersion curves were obtained based on the Scaled Boundary Finite Element. A Spectral Finite Element method was also recently applied for investigation of wave propagation in a piezoelectric helical waveguide, [9].

Wave propagation in elastic cylindrical shells has been studied in numerous publications. The vast majority of those are concerned with shells made of an isotropic material. Orthotropic shells have been considered in much fewer publications and the principal directions of tensor of elastic constants are customarily taken as coinciding with the cylindrical system of coordinates. It has been shown that all qualitative features of dispersion curves known for isotropic shells are preserved with some quantitative changes in magnitudes of cut-on frequencies, which, obviously, become dependent upon the ratio of elastic moduli in principal directions. A detailed survey of the literature on wave propagation in an orthotropic elastic shell lies beyond the scope of this paper, but the state-of-the-art in this area can be found in [10]. Recent advances in this area are highlighted in [11].

The technology of manufacturing elastic pipes (cylindrical shells) for some technical applications, however, is such that the principal directions of the tensor of elastic constants are turned at a certain angle α to the cylindrical system of coordinates. This angle is kept constant along the length of a pipe so that fibres in a ply are helically wound at the cylindrical surface. Often, an orthotropic cylindrical shell is made of many plies and the pitch angle for consecutive plies is switched to the opposite. By these means, the principal directions of elastic properties become aligned with the cylindrical coordinate system. In the cases, when an odd number of plies is used, and this number is small, the pitch angle affects the waveguide properties of the shell. Rather surprisingly, just a few publications dealing with helical waves and helically orthotropic cylindrical shells have been found by the authors. Specifically, helical waves in an isotropic elastic cylindrical shell have been considered in [12]. In this reference, the circumferential wave number has been treated as not necessarily integral, and, depending upon a chosen direction of propagation of the helical wave, the dispersion equation has different solutions. References [13, 14] are concerned with the wave propagation in a helically orthotropic cylindrical shell. However, most of the results of wave propagation analysis presented in these references are obtained for the axisymmetric wave. Bending vibrations are considered only for 'semi-infinite' shells. Therefore, we conclude that, to the best of our knowledge, propagation of non-axisymmetric waves in elastic cylindrical shells with helical orthotropy has not yet been properly analysed and this task constitutes the research goal and the novelty of this paper. Furthermore, in various technical applications, thin elastic cylindrical shells (pipes) are exposed to time-harmonic rotating forces. We are unaware of any publications dealing with the analysis of energy flow generated by such forces in a helically orthotropic shell and consider such an analysis as yet another aspect of novelty of our work.

The paper is structured as follows. Section 2 is concerned with the analytical model of wave propagation in a thin helically orthotropic cylindrical shell. In Section

3, this model is validated firstly by comparison of the dispersion diagrams with those presented in [11] for a 'conventional' orthotropic shell. Second, the Wave Finite Element model is used for numerical analysis of wave propagation in a structure with helical geometry, [15], and an agreement between numerical and analytical results is demonstrated. Section 3 also presents parametric studies of free waves in helically orthotropic cylindrical shells. In Section 4, a lattice beam model featuring the helical pattern is analysed to confirm the results obtained in the previous section. The Green's matrix for a cylindrical shell with helical orthotropy is derived and used for analysis of the energy flow generated by a rotating force in Section 5. Novel findings of the paper are summarised in Section 6.

2. The analytical model of propagation of spinning waves in a thin helically orthotropic elastic cylindrical shell

The governing equations of time-harmonic dynamics of a thin elastic cylindrical shell in the cylindrical coordinates (x, r, θ) , with time-dependence taken as $\exp(-i\omega t)$ and this multiplier being omitted, are written following Novozhilov-Gol'denweizer theory [16, 17]:

$$\begin{aligned} \frac{\partial N_x(x, \theta)}{\partial x} + \frac{1}{R} \frac{\partial S_{x\theta}(x, \theta)}{\partial \theta} + \rho h \omega^2 u(x, \theta) &= -q_x \\ \frac{1}{R} \frac{\partial N_\theta(x, \theta)}{\partial \theta} + \frac{\partial S_{x\theta}(x, \theta)}{\partial x} + \frac{1}{R^2} \frac{\partial M_\theta(x, \theta)}{\partial \theta} + \frac{2}{R} \frac{\partial H_{x\theta}(x, \theta)}{\partial x} + \rho h \omega^2 v(x, \theta) &= -q_\theta \quad (1) \\ -\frac{1}{R} N_\theta(x, \theta) + \frac{\partial^2 M_x(x, \theta)}{\partial x^2} + \frac{2}{R} \frac{\partial^2 H_{x\theta}(x, \theta)}{\partial x \partial \theta} + \frac{1}{R^2} \frac{\partial^2 M_\theta(x, \theta)}{\partial \theta^2} + \rho h \omega^2 w(x, \theta) &= -q_r \end{aligned}$$

The components of deformation in the cylindrical coordinates are

$$\begin{aligned} \varepsilon_x &= \frac{\partial u(x, \theta)}{\partial x}, \quad \varepsilon_\theta = \frac{1}{R} \frac{\partial v(x, \theta)}{\partial \theta} + \frac{w(x, \theta)}{R}, \quad \varepsilon_{x\theta} = \frac{1}{2} \left(\frac{1}{R} \frac{\partial u(x, \theta)}{\partial \theta} + \frac{\partial v(x, \theta)}{\partial x} \right) \\ \kappa_x &= -\frac{\partial^2 w(x, \theta)}{\partial x^2}, \quad \kappa_\theta = -\frac{1}{R^2} \frac{\partial^2 w(x, \theta)}{\partial \theta^2} + \frac{1}{R^2} \frac{\partial v(x, \theta)}{\partial \theta} \\ \kappa_{x\theta} &= -\frac{1}{R} \frac{\partial^2 w(x, \theta)}{\partial x \partial \theta} + \frac{1}{R} \frac{\partial v(x, \theta)}{\partial x} \end{aligned} \quad (2)$$

The principal directions of orthotropy of the shell's material are turned by the angle α to the in-plane coordinates (x, θ) and constitute another orthogonal system (y, ψ) , so that x coincides with y and θ coincides with ψ when $\alpha = 0$. It is convenient to write Hooke's law in the system (y, ψ) , see [18, p. 55, Eq. (14.13)] (note the inverted indices in notations for Poisson's ratio):

$$\begin{aligned} N_y &= \frac{E_1 h}{1 - \nu_{21} \nu_{12}} \left(\varepsilon_y + \nu_{12} \frac{E_2}{E_1} \varepsilon_\psi \right), \quad N_\psi = \frac{E_2 h}{1 - \nu_{21} \nu_{12}} \left(\nu_{12} \varepsilon_y + \varepsilon_\psi \right) \\ M_y &= \frac{E_1 h^3}{12(1 - \nu_{21} \nu_{12})} \left(\kappa_y + \nu_{12} \frac{E_2}{E_1} \kappa_\psi \right), \quad M_\psi = \frac{E_2 h^3}{12(1 - \nu_{21} \nu_{12})} \left(\nu_{12} \kappa_y + \kappa_\psi \right) \quad (3) \\ S_{y\psi} &= 2G_e \varepsilon_{y\psi}, \quad H_{y\psi} = \frac{G_e h^3}{6} \kappa_{y\psi} \end{aligned}$$

The relations between components of deformation in these systems of coordinates are (see [19, p. 74, Eqs. (2.72–2.73)]):

$$\begin{aligned}
\varepsilon_y &= \varepsilon_x \cos^2(\alpha) + \varepsilon_\theta \sin^2(\alpha) + 2\varepsilon_{x\theta} \cos(\alpha) \sin(\alpha) \\
\varepsilon_\psi &= \varepsilon_x \sin^2(\alpha) + \varepsilon_\theta \cos^2(\alpha) - 2\varepsilon_{x\theta} \cos(\alpha) \sin(\alpha) \\
\varepsilon_{y\psi} &= -\varepsilon_x \cos(\alpha) \sin(\alpha) + \varepsilon_\theta \cos(\alpha) \sin(\alpha) + \varepsilon_{x\theta} (\cos^2(\alpha) - \sin^2(\alpha)) \\
\kappa_y &= \kappa_x \cos^2(\alpha) + \kappa_\theta \sin^2(\alpha) + 2\kappa_{x\theta} \cos(\alpha) \sin(\alpha) \\
\kappa_\psi &= \kappa_x \sin^2(\alpha) + \kappa_\theta \cos^2(\alpha) - 2\kappa_{x\theta} \cos(\alpha) \sin(\alpha) \\
\kappa_{y\psi} &= -\kappa_x \cos(\alpha) \sin(\alpha) + \kappa_\theta \cos(\alpha) \sin(\alpha) + \kappa_{x\theta} (\cos^2(\alpha) - \sin^2(\alpha))
\end{aligned} \tag{4}$$

Respectively, the forces and moments in the (y, ψ) system are related to their counterparts in the (x, θ) coordinates as follows:

$$\begin{aligned}
N_y &= N_x \cos^2(\alpha) + N_\theta \sin^2(\alpha) + 2S_{x\theta} \cos(\alpha) \sin(\alpha) \\
N_\psi &= N_x \sin^2(\alpha) + N_\theta \cos^2(\alpha) - 2S_{x\theta} \cos(\alpha) \sin(\alpha) \\
S_{y\psi} &= -N_x \cos(\alpha) \sin(\alpha) + N_\theta \cos(\alpha) \sin(\alpha) + S_{x\theta} (\cos^2(\alpha) - \sin^2(\alpha)) \\
M_y &= M_x \cos^2(\alpha) + M_\theta \sin^2(\alpha) + 2H_{x\theta} \cos(\alpha) \sin(\alpha) \\
M_\psi &= M_x \sin^2(\alpha) + M_\theta \cos^2(\alpha) - 2H_{x\theta} \cos(\alpha) \sin(\alpha) \\
H_{y\psi} &= -M_x \cos(\alpha) \sin(\alpha) + M_\theta \cos(\alpha) \sin(\alpha) + H_{x\theta} (\cos^2(\alpha) - \sin^2(\alpha))
\end{aligned} \tag{5}$$

Eq. (2), (4) and (5) are substituted to the constitutive Eq. (3) and solved for $N_x, N_\theta, S_{x\theta}$ and $M_x, M_\theta, H_{x\theta}$. By these means, the forces and moments in cylindrical coordinates (x, θ) are expressed via displacements and their derivatives in the same system, while the Hooke's law has been formulated in helical coordinates (y, ψ) , see [18, p. 62, Eq. (16.2)] or [19, p. 77, Eqs. (2.84–2.85)]. Eventually, the forces and moments are substituted to Eq. (1) to yield the governing equations of wave motion in an infinite cylindrical shell with helical orthotropy in coordinates (x, θ) . These equations are very cumbersome, and, therefore, not presented here. The derivation has been done in the analytical form using the symbolic manipulator *Mathematica*. It has been checked by the same means that setting $\alpha = 0$ gives conventional equations for an orthotropic cylindrical shell with the principal directions coinciding with the coordinate axes. Setting elastic moduli to their values for an isotropic material gives equations for an isotropic shell for any value of α .

This system of differential equations allows solution in the form

$$\begin{aligned}
u(x, \theta) &= U \exp(ikx + im\theta) \\
v(x, \theta) &= V \exp(ikx + im\theta) \\
w(x, \theta) &= W \exp(ikx + im\theta)
\end{aligned} \tag{6}$$

Substitution of Eq. (6) into the governing equations and equating to zero the determinant of the system of linear algebraic equations with respect to the amplitudes (U, V, W) yields the dispersion equation in the polynomial form. The polynomial is

of sixth order in the frequency parameter and of eighth order in the wavenumber. As soon as $\alpha \neq 0$ it contains both even and odd powers of the wavenumber, which suggests a difference between the characteristics of waves travelling along the shell in opposite directions.

In Eq. (6), the integral circumferential wavenumber m may be both positive and negative. With the time-dependence in the form $\exp(-i\omega t)$, positive wavenumbers k found from the dispersion equation for a positive m describe waves travelling in the positive direction of the shell's axis and rotating clockwise. If a negative circumferential wavenumber is plugged in the dispersion equation, then positive wavenumbers describe waves travelling in the positive direction of the shell's axis and rotating anti-clockwise. It should also be noted that the conventional solution, which describes waves travelling without rotation along the axis of an orthotropic shell i.e.

$$\begin{aligned} u(x, \theta) &= U \exp(ikx) \cos(m\theta) \\ v(x, \theta) &= V \exp(ikx) \sin(m\theta) \\ w(x, \theta) &= W \exp(ikx) \cos(m\theta) \end{aligned} \quad (7)$$

does not allow separation of trigonometric functions in the governing equations. This separation is recovered, when either the elastic parameters describe the isotropic shell, or $\alpha = 0$. Therefore, we conclude that 'standing in the circumferential direction' waves cannot propagate in an orthotropic cylindrical shell with $\alpha \neq 0$. On the other hand, solution in the form of Eq. (6) for an isotropic cylindrical shell allows separation of exponents in the circumferential coordinate in the governing equations at any α . The resulting dispersion equation remains the same as when the conventional form of solution of Eq. (7) is used. It means that the properties of spinning and 'standing in the circumferential direction' waves are the same as for an isotropic cylindrical shell. It is well-known and reported in classical texts on the dynamics of these shells.

3. Dispersion diagrams: Validation and discussion

In this section, the model introduced in the previous section is verified, and waveguide characteristics of cylindrical shells with helically orthotropic material properties are discussed. In the following, dispersion diagrams are plotted in the non-dimensional form with $k = k_{\text{dim}}R$ and $\Omega = \omega R \sqrt{\frac{\rho(1-\nu_{12}\nu_{21})}{E_1}}$.

3.1. Verification of the analytical model of an orthotropic cylindrical shell

We begin with a validation of the model of an orthotropic shell for the case when principal directions of orthotropy coincide with the cylindrical coordinates, i.e. when $\alpha = 0$. The parameters of a shell are taken as in [11, p. 25, Eq. (8)]: $E_x = E_1 = 207\text{GPa}$, $E_\theta = E_2 = 5\text{GPa}$, $G_{x\theta} = G_{12} = 2.6\text{GPa}$, $\nu_{x\theta} = \nu_{12} = 0.25$ (and thus $\nu_{21} = 0.006$), $\frac{h}{R} = 0.1$ and $m = 2$.

The branches corresponding to propagating waves (purely real wavenumbers) and to evanescent waves (purely imaginary wavenumbers) are marked dark blue and red (in this order). The real parts of complex wavenumbers of attenuated waves are

marked light blue, and their imaginary parts are marked magenta. In [11, Fig. 1] only purely real wavenumbers are presented. Fig. 1 in this paper provides a more detailed dispersion diagram, in which purely imaginary and complex-valued wavenumbers are also shown. There is a perfect agreement between characteristics of propagating waves in these two Figures; as an example, the cut-on frequencies are exactly the same: $\Omega_{\text{cut-on},1} = 0.012026$, $\Omega_{\text{cut-on},2} = 0.22415$, $\Omega_{\text{cut-on},3} = 0.34789$. In the case $\alpha = 0$, the dispersion equation contains only even powers of the wavenumber and features the symmetry of the dispersion diagram with respect to the frequency axis. Therefore, the common practice to show only its upper part, i.e. $\text{Re}[k] \geq 0$, $\text{Im}[k] \geq 0$ is followed in Fig. 1.

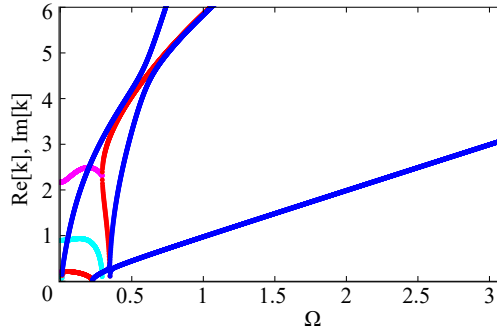


Fig. 1: Verification in comparison with Fig. 1 from [11].

As soon as $\alpha \neq 0$, the symmetry is broken. This is illustrated in Fig. 2 for a shell with the same parameters as in the previous case, but with $\alpha = \frac{\pi}{6}$. The colours are used in the same way as in Fig. 1. It is more convenient to present the dispersion diagram in 3D as is done in Fig. 2(b).

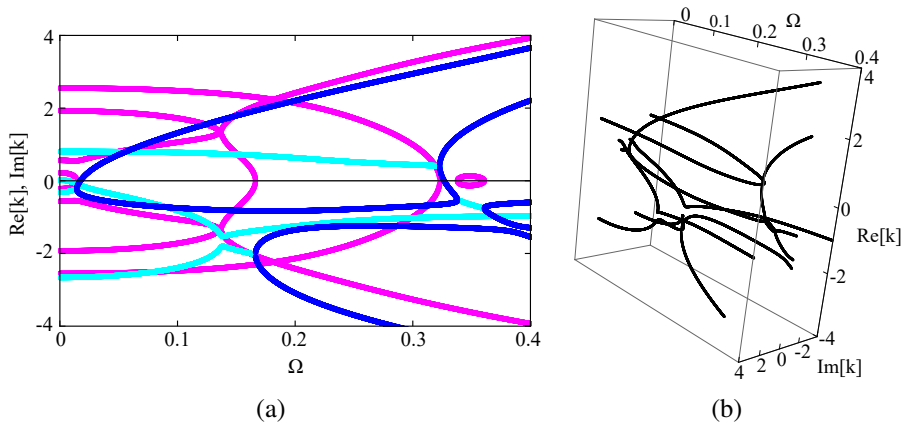


Fig. 2: (a) dispersion diagram for the shell with the same parameters as in [11] and $\alpha = \frac{\pi}{6}$ (b) 3D representation of the dispersion diagram.

This diagram features the classical veering effect in the frequency range $0.135 < \Omega <$

0.145 and the classical locking effect in the frequency range $0.34 < \Omega < 0.36$, see [20, 21], but more importantly, it shows the unevenness of frequency-dependence of wavenumbers, which describe waves moving with anti-clockwise rotation in the positive and negative directions of the axial coordinate. It manifests itself as the non-symmetry of the location of dispersion curves with respect to the plane $\text{Re}[k] = 0$. On the other hand, it is straightforward to check that there is symmetry with respect to this plane between the dispersion curves for $(m = 2, \alpha = \frac{\pi}{6})$ and the dispersion curves for $(m = 2, \alpha = -\frac{\pi}{6})$.

Likewise, the symmetry is preserved for the dispersion curves plotted for $(m = 2, \alpha = \frac{\pi}{6})$ and $(m = -2, \alpha = \frac{\pi}{6})$. This is readily explained by the simple observation that the waves travelling in the positive direction of the x -axis and rotating anti-clockwise are identical to the waves travelling in the negative direction of the x -axis and rotating clockwise and vice-versa (if this rotation is viewed from the same point).

3.2. Comparison of results obtained by means of the analytical model and the wave finite element method

The results, presented in the previous sub-section, have conclusively validated the analytical model of an orthotropic cylindrical shell in the case when the principal directions of orthotropy coincide with the axes of coordinates. Since no references, which present dispersion diagrams for an orthotropic shell with $\alpha \neq 0$, have been found we choose to validate this model for a helically orthotropic shell by calculations of wavenumbers by means of the Wave Finite Element method as presented in [15].

A pipe with thickness $h = 0.01\text{m}$ and mean radius $R = 0.2\text{m}$ (that gives $\frac{h}{R} = 0.05$) is considered. Material properties are: $E_x = E_1 = 28.89\text{GPa}$, $E_\theta = E_2 = 9.63\text{GPa}$, $G_{x\theta} = G_{12} = 4.128\text{GPa}$, $\nu_{x\theta} = \nu_{12} = 0.06$ (this implies that $\nu_{\theta x} = \nu_{21} = 0.02$), $\rho = 1389\text{kg/m}^3$. The angle is $\alpha = \frac{\pi}{6}$. To apply the WFE approach the FE model of a small periodic segment of the pipe of length $L_x = L_y = 0.002\text{m}$ is discretised using 5 solid elements; this model allows to obtain accurate results up to high frequency [15].

We note that the analytical model in Sec. 2 is based on the classical thin shell theory, whereas the finite element model is constructed by means of 3D solid elements in the framework of the commercially available software ANSYS. Therefore, the agreement between results obtained by the use of these so profoundly different models should be regarded as the strong indication of the correctness of both. However, some discrepancies are likely to occur due to the difference between modelling methods. The results are presented in Tab. 1 for two circumferential wavenumbers and two excitation frequencies. As seen from this Table, the differences are small and should be attributed to the difference in formulations of constitutive relations in the finite element and analytical models. The detailed convergence studies and comparison of validity ranges of the models do not constitute the goal of this paper. We just note that the closeness of the wavenumbers to each other suggests that both models are applicable for the analysis of wave propagation in helically orthotropic cylindrical shells.

As already mentioned, the remarkable feature of these results is the unevenness of purely real wavenumbers (those corresponding to travelling waves) presented in the

Analytical, $m = -1, \bar{\omega} = 0.1$	-2.0088	1.5403	24.71±23.94i	-24.71±23.94i	0.32±1.52i
WFEM, $m = -1, \bar{\omega} = 0.1$	-2.0596	1.6294	25.69±25.34i	-25.69±25.34i	0.21±1.62i
Analytical, $m = -1, \bar{\omega} = 0.6$	-7.6834	5.0445	22.08±21.58i	-19.15±21.61i	1.31±1.70i
WFEM, $m = -1, \bar{\omega} = 0.6$	-7.6445	4.8194	23.35±22.93i	-19.47±23.06i	1.21±2.21i
Analytical, $m = -2, \bar{\omega} = 0.1$	-3.1665	2.5961	25.24±24.83i	-19.46±25.18i	0.35±2.71i
WFEM, $m = -2, \bar{\omega} = 0.1$	-3.1300	2.7207	26.53±26.32i	-19.26±26.79i	0.30±2.89i
Analytical, $m = -2, \bar{\omega} = 0.6$	-12.2693	8.3454	22.27±22.83i	-16.79±23.65i	2.33±5.05i
WFEM, $m = -2, \bar{\omega} = 0.6$	-12.1535	8.0039	24.01±24.16i	-16.65±25.13i	2.09±5.88i

Tab. 1: Wavenumbers in m^{-1} . Frequency is scaled as $\bar{\omega} = \frac{\omega}{\Omega_{\text{ring}}}$, $\Omega_{\text{ring}} = \frac{1}{R} \sqrt{\frac{E_1}{\rho(1-\nu_{12}\nu_{21})}}$.

first two columns of the Table. In what follows in this section, we briefly explore the influence of geometry and material parameters on the location of dispersion curves by means of the analytical model. It is a straightforward matter to show that the dispersion polynomial at the 'breathing mode' $m = 0$ does not contain odd powers of the wavenumber for any α regardless the helical orthotropy. The difference between wave propagation in a general helically orthotropic cylindrical shell and an orthotropic shell with $\alpha = 0$ is the coupling of purely torsional and longitudinal-flexural axisymmetric deformation. In what follows, we do not elaborate on this issue and do not consider this mode any further. On the other hand, the performance of a helically orthotropic shell at any other circumferential wavenumber is qualitatively the same. Therefore, we restrict our subsequent analysis to the case $m = 1$.

3.3. The influence of the geometry parameter α

In Fig. 3(a), the non-dimensional parameters are chosen as $\frac{E_2}{E_1} = 8$, $\nu_{12} = 0.3$, $\frac{G_{12}}{E_1} = 0.35$, $\frac{h}{R} = 0.05$. Black curves are plotted for $\alpha = 0$ blue ones for $\alpha = \frac{\pi}{2}$ and red ones for $\alpha = \frac{\pi}{4}$.

To begin with, it should be noted that the dispersion diagram is shown in the range of complex-valued wavenumbers, in which not all eight branches can be seen. In particular, when $\alpha = \frac{\pi}{2}$, the two curves chopped at $\text{Im}[k] = \pm 1$ may be traced to the plane $\Omega = 0$ in a broader window ($\text{Re}[k], \text{Im}[k]$). Only four branches are located within this range of ($\text{Re}[k], \text{Im}[k]$) at $\alpha = 0$ and $\alpha = \frac{\pi}{4}$. Naturally, at $\alpha = 0$ and $\alpha = \frac{\pi}{2}$ the dispersion diagrams are perfectly symmetric with respect to $\text{Re}[k] = 0$ plane, and the second propagating wave cuts on in the standard 'divergence-type' manner at $k = 0$, $\Omega_{\text{cut-on},2} = n \sqrt{\frac{G_{12}}{E_1}} = 0.5916$. This value of cut-on frequency is obtained analytically, and it is the same for both $\alpha = 0$ and $\alpha = \frac{\pi}{2}$. For $\alpha = \frac{\pi}{4}$, the scenario of this cut-on is different, and it is of 'flutter-type', which is well-known in the theory of elastic waves in layers and thin shells. As seen from Fig. 3, the transformation of two attenuated waves to two propagating ones occurs at $\Omega \approx 0.4152$, $k \approx 0.2264$ and the lower branch in the frequency range $0.4152 \leq \Omega \leq 0.4693$ describes the anomalous (or negative energy) wave, which has the positive phase velocity $c_{\text{phase}} > 0$ and negative group velocity $c_{\text{group}} < 0$. Remarkably, in the analogous symmetric waveguides (say, the second branch of symmetric waves in the Rayleigh-Lamb problem, see [22, p. 151, Fig. 5.072]) such waves exist in pairs, whereas here, due to the symmetry break, this wave does not have a counterpart of similar properties. In Fig. 3, the other branch emerging from $\Omega \approx 0.4152$, $k \approx 0.2264$ has both $c_{\text{phase}} > 0$, $c_{\text{group}} > 0$. This result is

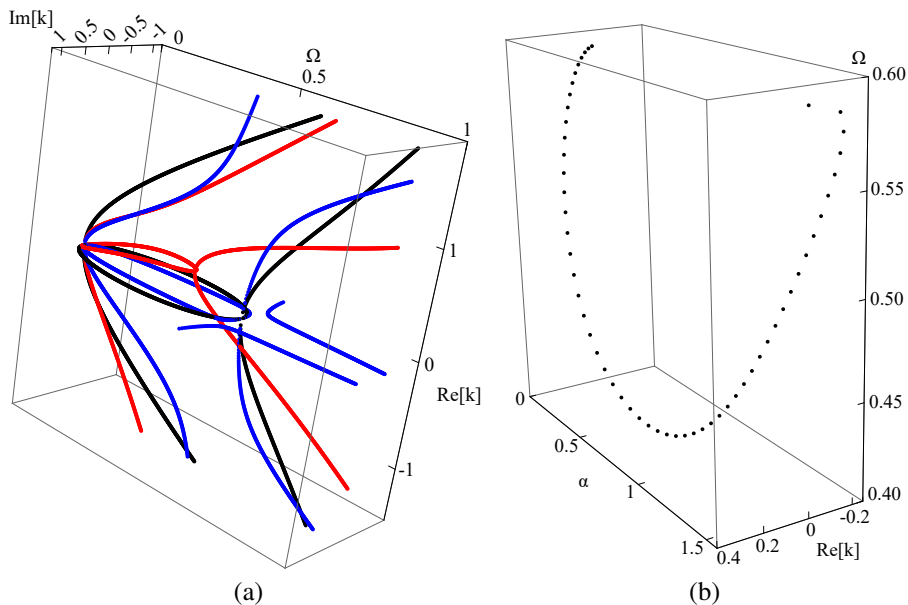


Fig. 3: (a) dispersion diagram for $\alpha = 0$ (black), $\alpha = \frac{\pi}{4}$ (red), $\alpha = \frac{\pi}{2}$ (blue); (b) the second cut-on frequency and associated purely real wavenumber, at which the group velocity is zero versus the orthotropy angle.

interesting on its own, but it also has some implications regarding solving the forcing problems in general and constructing the Green's matrix in particular. An elaboration on this important issue is presented in Sec. 5. The evolution of the cut-on frequency for $0 < \alpha < \frac{\pi}{2}$ is illustrated in Fig. 3(b). Effectively, this figure presents a dependence of the position of a point (Ω_0, k_0) in the $(\Omega, \text{Re}[k])$ -plane, at which $c_{\text{group}} = 0$, upon the angle α . As seen (also from Fig. 3), $\Omega_0 = \Omega_{\text{cut-on},2}$, $k_0 = 0$ at both extreme values $\alpha = 0$ and $\alpha = \frac{\pi}{2}$. The dependence of (Ω_0, k_0) upon the angle α is not monotonic and, for the given parameters of orthotropy, the angle $\alpha = \frac{\pi}{4}$ does not appear to be the one, at which the dispersion diagram is maximally distorted. Fig. 3(b) shows that the second wave at $\alpha \approx 1.0755$ cuts-on when $k_0 = 0$. However, this does not mean that the whole dispersion diagram recovers symmetry, see Fig. 4.

In this figure, all branches of the dispersion diagram are plotted. Despite conventional 'divergence' type generation of the second propagating waves, the diagram is lacking symmetry with respect to $\text{Re}[k] = 0$ plane. In the considered frequency range, there are two waves propagating in the negative direction of the axial coordinate that do not experience any transformations. The situation is different with waves travelling in the positive direction: at around $\Omega = 0.78$ two propagating waves cut on. One of these waves interacts with the first propagating wave in the 'veering' manner, see [20], and, due to 'repelling', interacts with the second branch in the 'locking' manner. Therefore, in the frequency range $0.815 \leq \Omega \leq 0.931$ this waveguide supports four waves with positive phase velocity. Two of these waves have negative group velocity. This result has a potential for tailoring the waveguide properties of helically orthotropic cylindrical shells and, as already mentioned, is considered in Sec. 5, where

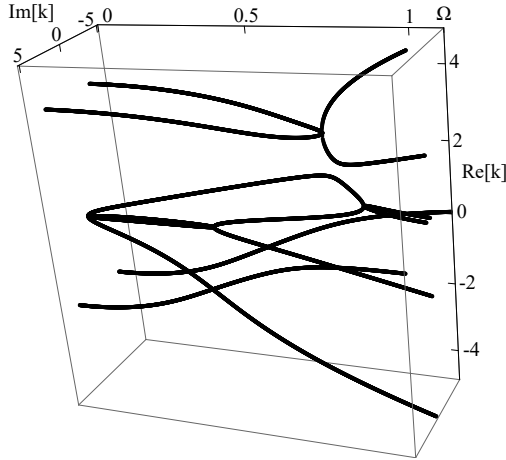


Fig. 4: Dispersion diagram for $\alpha \approx 1.0755$.

the problem of excitation of elastic waves in a shell by a rotating force is solved.

3.4. The influence of the parameters of orthotropy

Obviously, the parameters of orthotropy strongly affect the location of dispersion curves, and variation of the angle α adds one more dimension to the space of parameters. Therefore, the analysis reported in this subsection is purely illustrative and highlights the influence of the stiffness ratios $\frac{E_2}{E_1}$ and $\frac{G_{12}}{E_1}$ with other ones being fixed to the values used in Sec. 3.2: $\nu_{12} = 0.3$, $\frac{h}{R} = 0.05$. In addition, $\alpha = \frac{\pi}{4}$. It is important to observe the limitations on the values of the parameter $\frac{E_2}{E_1}$, see [10]. For $\nu_{12} = 0.3$, the limitation is $\frac{E_2}{E_1} < 11$. In Fig. 5(a), the influence of this parameter is illustrated for $\frac{G_{12}}{E_1} = 0.35$. As expected, the reverse change in the ratio $\frac{E_2}{E_1}$ tends the diagram in the opposite directions. The quantitative differences between the case $\frac{E_2}{E_1} = 8$ and $\frac{E_2}{E_1} = \frac{1}{8}$ are explained by, firstly, the scaling of the frequency parameter with E_1 in both cases and, secondly, by fixation of $\nu_{12} = 0.3$.

Fully reversed choice of parameters gives the dispersion diagram 'mirrored' with respect to the plane $\text{Re}[k] = 0$. The dispersion diagram is recovered completely if, in addition to the rescaling of the frequency parameter and fixing ν_{21} , the circumferential wavenumber is set to be $m = -1$. In Fig. 5(b), the dependence on the position of a point (Ω_0, k_0) in the $(\Omega, \text{Re}[k])$ -plane, at which $c_{\text{group}} = 0$, upon the ratio $\frac{E_2}{E_1}$ is illustrated. Finally, we illustrate the influence of the shear stiffness parameter $\frac{G_{12}}{E_1}$ in Fig. 6 with other ones being fixed to the values used in Sec. 3.3: $\nu_{12} = 0.3$, $\frac{E_2}{E_1} = 8$, $\frac{h}{R} = 0.05$, $\alpha = \frac{\pi}{4}$. This parameter also strongly influences the location of dispersion curves and triggers veering and locking interaction phenomena.

To conclude this brief analysis of dispersion diagrams of cylindrical shell with the helical orthotropy, we notice that the symmetry of dispersion curves remains preserved with respect to the $\text{Im}[k] = 0$ plane. In other words, the complex-valued and purely

imaginary roots exist only in complex conjugate pairs simply because the dispersion polynomial has purely real coefficients in the absence of damping.

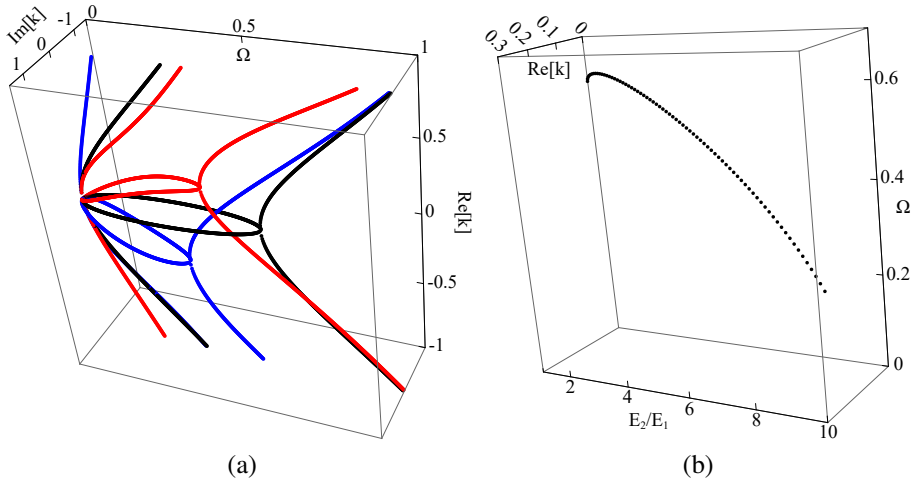


Fig. 5: (a) dispersion diagrams for $\frac{E_2}{E_1} = 1$ (black), $\frac{E_2}{E_1} = 8$ (red), $\frac{E_2}{E_1} = \frac{1}{8}$ (blue); (b) the second cut-on frequency and associated purely real wavenumber versus $\frac{E_2}{E_1}$.

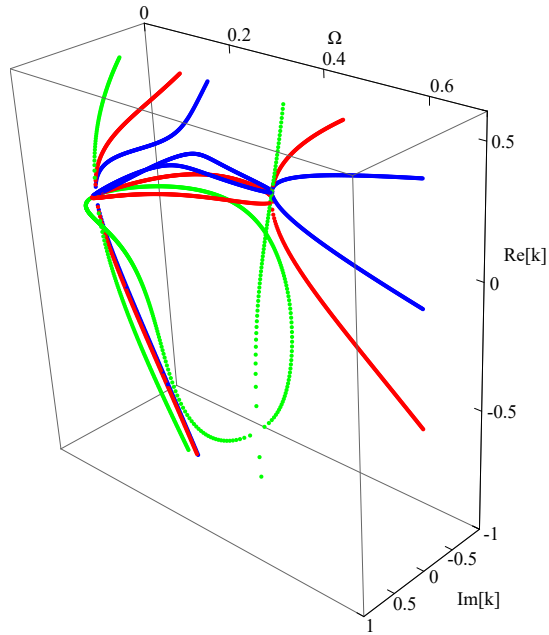


Fig. 6: Dispersion diagram for $\frac{G_{12}}{E_1} = 0.35$ (red), $\frac{G_{12}}{E_1} = 3.5$ (green) and $\frac{G_{12}}{E_1} = 0.035$ (blue).

4. Waves in a cylindrical beam lattice with helical pattern

As shown in the previous section, wave propagation in a helically orthotropic cylindrical shell is different depending upon the direction of propagation. Mathematically, it manifests itself as the presence of both even and odd powers of the wavenumber in the dispersion equation. On the other hand, as is well-known, the dispersion equation for a helical spring contains only even powers of the wavenumber and, therefore, there is symmetry in the waveguide properties of an isolated helical fibre. It is realistic to assume that a helically orthotropic cylindrical shell is made of a fibre-reinforced composite, which consists of a large number of identical helical fibres uniformly embedded into a relatively soft matrix. A simplified discrete model of a shell may then be set up as a lattice of beam elements forming helical fibres with the matrix between them being modelled as discrete beams of lower stiffness.

In this section complex dispersion curves of an orthotropic lattice structure with helical pattern are shown. Lattice structures have been extensively studied due to their application in many engineering fields, see e.g. [23], and the investigation and optimisation of their properties is still the subject of many recent studies. As an example, homogenisation of a two-dimensional lattice has been presented in [24], directionality behaviour of lattices has been investigated in [25], while in [26] stress waves in two-dimensional periodic lattices has been studied.

Floquet and Bloch analysis of a unit cell are particularly useful to investigate the behaviour of beam lattice structures, and the WFE method [15] can be straightforwardly applied to these structures. Although the interest here is not in the bandgap formation of the lattice, see e.g. [27], these can be also easily investigated using the present approach. Fig. 7 shows a schematic representation of the helical lattice considered, together with the skew periodic unit cell used for the WFE discretisation, [15]. The latter is modelled using beam elements with six degrees of freedom per node: displacements and rotations in the x , y and z directions. Orthotropy is assumed such that Young's modulus in the y direction is three times those in the helical direction, that is: $\frac{E_y}{E_{x'}} = 3$. The radius of the cylinder is 0.2m and 250 cells are considered around the circumference; the beam cross section is square 0.01×0.01 m, and the helix angle is $\alpha = \frac{\pi}{4}$.

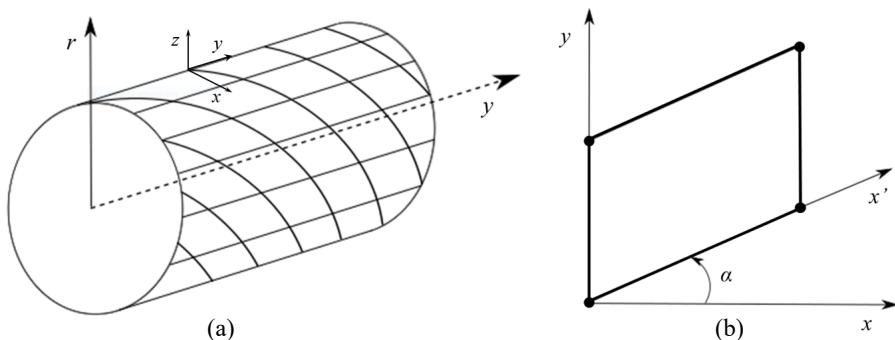


Fig. 7: (a) schematic representation of the cylindrical beam lattice with helical pattern; (b) the skew periodic unit cell.

The estimation of the differences between the orthotropic cylindrical lattice, viz. rectangular periodic cell, and the orthotropic cylindrical helical lattice, viz. skew periodic cell, is shown in Fig. 8, where the real valued dispersion curves for the first circumferential mode are compared. Dispersion curves are plotted using the same non-dimensional parameters as in Sec. 3. For the orthotropic cylindrical lattice, it can be seen that the curves show symmetry with respect to $\text{Re}[k] = 0$ i.e. wavenumbers occur in pairs $\pm k$ and waves propagating in positive and negative axial direction have the same characteristics in terms of wavenumbers and wavemodes. It can also be noticed that quasi-extensional wave modes (the second branch in the plot) propagate below $\Omega = 1$. As the frequency increases, the structure starts to be less stiff in the radial direction, the extensional wave mode changes in the behaviour due to the transverse motion of the cross-section, and a higher order mode starts propagating close to $\Omega = 1$ as expected.

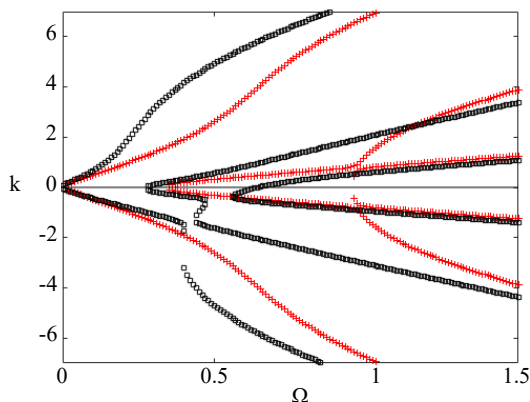


Fig. 8: Comparison between the real-valued dispersion curves for the cylindrical beam lattice, first circumferential mode $m = 1$: +++ orthotropic cylindrical lattice (rectangular cell); □□□ orthotropic helical cylindrical lattice (skew cell).

The figure shows clearly that the presence of the helical orthotropy highly affects the waves propagating in the lattice, which leads to changes in the cut-on frequencies and in the wave propagation properties as described in the previous sections i.e. the symmetry of dispersion curves no longer holds and waves propagate differently in positive and negative direction provided that the helical angle is different from 0 and $\frac{\pi}{2}$. Complex dispersion curves and some of the wavemodes for the orthotropic helical lattice are shown in Fig. 9.

5. Formulation of Green's matrix and energy flow analysis

The analytical model formulated in Sec. 2 may readily be used for analysis of forced response of a cylindrical shell with helical orthotropy. The convenient tool to handle arbitrary excitation conditions is the Green's matrix. Since the studies of free spinning waves have demonstrated their unusual properties of non-symmetry, formulation of Green's matrix is particularly interesting for rotating forces, which are typical

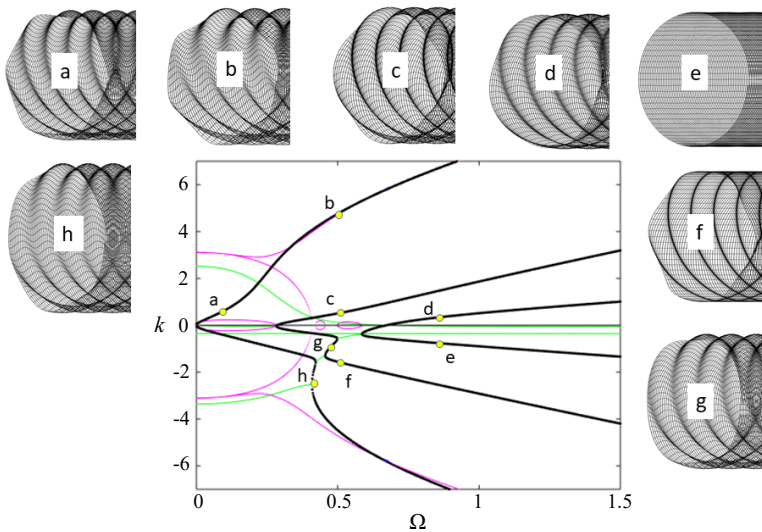


Fig. 9: Complex dispersion curves for the helical orthotropic cylindrical beam lattice, first circumferential mode $m = 1$: — propagating waves; — evanescent waves; — complex waves (note that complex waves occur as a pair of complex conjugated waves, and only one is shown here). The surrounding figures show the corresponding wave modes.

for various technical applications, such as water-supplying pipes equipped with centrifugal pumps, wind turbines and other rotating machinery.

5.1. The loading cases

We consider time-harmonic, $\exp(-i\omega t)$, external forces of unit amplitude concentrated in the axial direction (i.e. applied at the cross-section $x = x_0$) and rotating in the circumferential direction:

$$q_m^{F(n)}(x - x_0, \theta) = \delta(x - x_0) \exp(im\theta) \quad n = 1, 2, 3, 4 \quad (8)$$

Forcing at each circumferential wavenumber may be considered individually, and the four loading cases, $n = 1, 2, 3, 4$, in Eq. (8) correspond to the action of an axial force, circumferential force, radial force and axial bending moment, respectively. Explicit formulas for these forces in the case of isotropic cylindrical shells are well-known and may be found, for instance, in [28]. However, in the case of helical orthotropy, the closed form analytical expressions become cumbersome and so we do not reproduce them here.

The derivation of Green's matrix is based on the modal decomposition on free waves. For an orthotropic cylindrical shell with the principal directions of orthotropy coinciding with cylindrical coordinates (i.e. for a symmetric waveguide), it is sufficient to formulate four loading conditions. These conditions, see [28], ensure symmetry of the wave propagation pattern to the left and to the right of the loaded cross-section $x = x_0$. Respectively, four wavenumbers k_j ($j = 1, 2, 3, 4$), each of which satisfies radiation/decay conditions, are used and the solution ansatz for the radial

displacement with the loading case $q_m^{F(n)}(x - x_0, \theta)$ has the form:

$$w_m^{F(n)}(x - x_0) = \sum_{j=1}^4 A_{mj}^{(n)} \exp(ik_j|x - x_0|)$$

All other state variables (generalised forces and displacements) are expressed in the closed analytical form via amplitudes $A_{mj}^{(n)}$ and wavenumbers k_j using the modal coefficients, for instance,

$$Q_{m1}^{F(n)}(x - x_0) = \sum_{j=1}^4 M_{m1j} A_{mj}^{(n)} \exp(ik_j|x - x_0|)$$

see details in [28].

As soon as the symmetry is broken (the helical orthotropy is considered), all eight wavenumbers should be involved in the formulation of Green's matrix and eight conditions at the loaded cross-section $x = x_0$ should be formulated. Specifically, each component of the displacement vector and three forces are continuous, while the remaining force experiences a unit jump. For the loading case 3 (rotating radial force) at $X_0 = 0$ these conditions are:

$$\begin{aligned} u_{m+}^{F(3)}(0) &= u_{m-}^{F(3)}(0) & v_{m+}^{F(3)}(0) &= v_{m-}^{F(3)}(0) \\ w_{m+}^{F(3)}(0) &= w_{m-}^{F(3)}(0) & \gamma_{m+}^{F(3)}(0) &= \gamma_{m-}^{F(3)}(0) \\ Q_{m1+}^{F(3)}(0) &= Q_{m1-}^{F(3)}(0) & Q_{m2+}^{F(3)}(0) &= Q_{m2-}^{F(3)}(0) \\ Q_{m4+}^{F(3)}(0) &= Q_{m4-}^{F(3)}(0) & Q_{m3+}^{F(3)}(0) &= Q_{m3-}^{F(3)}(0) + 1 \end{aligned} \quad (9)$$

Modal decomposition of the forced response in the region $x < x_0$ is done using free waves with wavenumbers which have $\text{Im}[k_j^-] < 0$, ($j = 1, 2, 3, 4$) and, if $\text{Im}[k_j^-] = 0$ using $\frac{d\omega}{dk_j^-} < 0$:

$$w_{m-}^{F(n)}(x - x_0) = \sum_{j=1}^4 A_{mj-}^{(n)} \exp(ik_j^-(x - x_0))$$

In the region $x > x_0$, wavenumbers with $\text{Im}[k_j^+] > 0$ and, if $\text{Im}[k_j^+] = 0$, with $\frac{d\omega}{dk_j^+} > 0$ are used:

$$w_{m+}^{F(n)}(x - x_0) = \sum_{j=1}^4 A_{mj+}^{(n)} \exp(ik_j^+(x - x_0))$$

As soon as $\alpha = 0$ or $\alpha = \frac{\pi}{2}$, wavenumbers satisfy the condition $k_j^- = -k_j^+$. Then the symmetry is recovered and the Green's matrix for rotating forces acquires the form known for the isotropic cylindrical shell.

5.2. The energy flow

The scaled energy flow through a cross-section of the shell is formulated as, see [28–30]:

$$N_{m+}^{(n)} = \frac{1}{2} \text{Re} \left\{ Q_{m1+}^{F(n)}(x) [i\Omega u_{m+}^{F(n)}(x)]^* + Q_{m2+}^{F(n)}(x) [i\Omega v_{m+}^{F(n)}(x)]^* \right. \\ \left. + Q_{m3+}^{F(n)}(x) [i\Omega w_{m+}^{F(n)}(x)]^* + Q_{m4+}^{F(n)}(x) [i\Omega \gamma_{m+}^{F(n)}(x)]^* \right\} \quad x > x_0 \quad (10a)$$

$$N_{m-}^{(n)} = \frac{1}{2} \text{Re} \left\{ Q_{m1-}^{F(n)}(x) [i\Omega u_{m-}^{F(n)}(x)]^* + Q_{m2-}^{F(n)}(x) [i\Omega v_{m-}^{F(n)}(x)]^* \right. \\ \left. + Q_{m3-}^{F(n)}(x) [i\Omega w_{m-}^{F(n)}(x)]^* + Q_{m4-}^{F(n)}(x) [i\Omega \gamma_{m-}^{F(n)}(x)]^* \right\} \quad x < x_0 \quad (10b)$$

In an orthotropic case, when $\alpha = 0$ or $\alpha = \frac{\pi}{2}$, any force defined as Eq. (8) generates, similarly to an isotropic shell, the same energy flow in the regions $x < x_0$ and $x > x_0$ i.e. $N_{m-}^{(n)} = N_{m+}^{(n)}$. As soon as $\alpha \neq 0$, the energy input is not split into equal shares between these regions. This effect, introduced by the helical orthotropy, may be utilised to control the transmission of vibro-acoustic energy generated by rotating forces in various piping systems.

We illustrate this effect for an orthotropic shell with the parameters used in Sec. 3.3: $\nu_{12} = 0.3$, $\frac{E_2}{E_1} = 8$, $\frac{h}{R} = 0.05$, $\frac{G_{12}}{E_1} = 0.35$. We consider a rotating radial force ($n = 3$) of unit amplitude with $m = 1$ at the excitation frequency $\Omega = 0.4$. The scaled energy flow as a function of the angle α is shown in Fig. 10, where α is measured in degrees and varies from $\alpha = 0^\circ$ to $\alpha = 45^\circ$ with the step of 1° . To explain peaks in the energy input at the angles $\alpha \approx 6^\circ$ and $\alpha \approx 16^\circ$ it is necessary to address the dependence of purely real wavenumbers upon α at the frequency $\Omega = 0.4$, see Fig. 11.

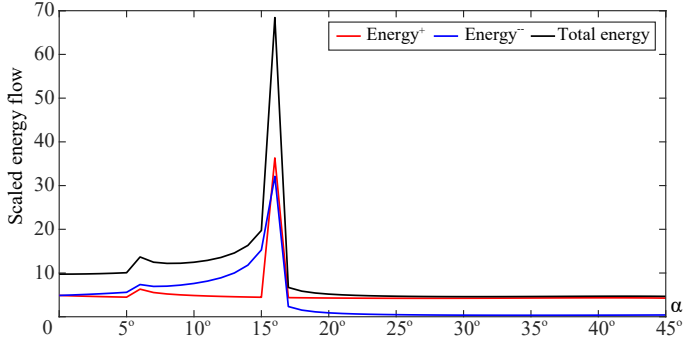


Fig. 10: The energy flow in a helically orthotropic cylindrical shell.

When $\alpha \leq 6^\circ$, there is only one pair of propagating waves, which have almost the same absolute values of purely real wavenumbers. Therefore, there is little difference in the energy flow in the positive and negative direction. This can be seen in Fig. 12(a), where the contributions to energy flow are presented versus the axial coordinate for $\alpha = 3^\circ$. It can also be noticed that a second pair of propagating waves emerges at $\approx 6^\circ$ (notably, not at the $k = 0$ axis, but rather following the condition $\frac{d\omega}{dk} = 0$, attained when $k^+ = k^- \neq 0$). Their wavenumbers are pronouncedly different (first, in magnitude and, when $\alpha > 8^\circ$, in sign) and, therefore, a preferred direction of energy flow

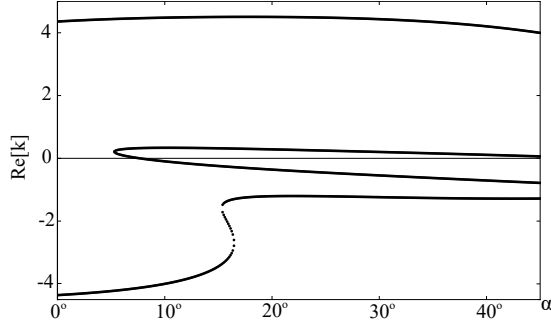


Fig. 11: The purely real wavenumbers at $\Omega = 0.4$ as functions of the orthotropy angle α .

(the negative direction of the axial coordinate) emerges. Partition of energy flow for $\alpha = 12^\circ$ is illustrated in Fig. 12(b). The waveguide properties of the shell are transformed again at $\alpha \approx 15^\circ$. As seen in Fig. 11, a pair of propagating waves emerges (cuts on) and the lower branch (the 'anomalous' one characterised by the inequality $\frac{\omega}{k} \frac{d\omega}{dk} < 0$) 'collides' with the branch coming from $\alpha = 0^\circ$ and this pair transforms back (cuts off) to attenuated waves. After this transformation, the preferred direction of the energy flow is reversed, as seen in Fig. 10. The partition of energy flow at $\alpha = 18^\circ$ is shown in Fig. 12(c). As seen in Fig. 11, the structure of dispersion curves remains unchanged up to $\alpha = 45^\circ$. For consistency, the contributions to energy flow at $\alpha = 45^\circ$ are presented in Fig. 12(d). In Fig. 12, each of the four components of the energy flow from Eq. (10) is presented separately:

$$\begin{aligned}
 N_{m=1}^u &= \frac{1}{2} \operatorname{Re} \left\{ \mathcal{Q}_{11\pm}^{F(3)}(x) \left[i\Omega u_{1\pm}^{F(3)}(x) \right]^* \right\} & N_{m=1}^v &= \frac{1}{2} \operatorname{Re} \left\{ \mathcal{Q}_{12\pm}^{F(3)}(x) \left[i\Omega v_{1\pm}^{F(3)}(x) \right]^* \right\} \\
 N_{m=1}^w &= \frac{1}{2} \operatorname{Re} \left\{ \mathcal{Q}_{13\pm}^{F(3)}(x) \left[i\Omega w_{1\pm}^{F(3)}(x) \right]^* \right\} & N_{m=1}^\gamma &= \frac{1}{2} \operatorname{Re} \left\{ \mathcal{Q}_{14\pm}^{F(3)}(x) \left[i\Omega \gamma_{1\pm}^{F(3)}(x) \right]^* \right\}
 \end{aligned}$$

Detailed analysis of the energy distribution between alternative transmission paths illustrated in Fig. 12(a)–(d) lies beyond the scope of this paper, but two remarks should be made. First, the energy input of the radial force is distributed to all transmission paths already at the loaded cross-section, whereas in the isotropic shell and in the cases $\alpha = 0$ and $\alpha = \frac{\pi}{2}$ the energy is pumped only to the directly excited path at $x = x_0$, and is redistributed in the near field. Second, the energy distribution between alternative transmission paths is not the same in the regions $x < x_0$ and $x > x_0$.

The features of the energy transmission are sensitive to the material parameters of the shell and to the excitation conditions. Therefore, optimisation of material layout in order to control energy flow generated by a given rotating force is plausible and may be much beneficial in various applications, for instance, for water-supplying pipes equipped with centrifugal pumps operated at constant speed.

6. Conclusions

Elastic wave propagation in helically orthotropic cylindrical shells and in helical lattices is studied using an analytical approach and a Wave Finite Element model. Both

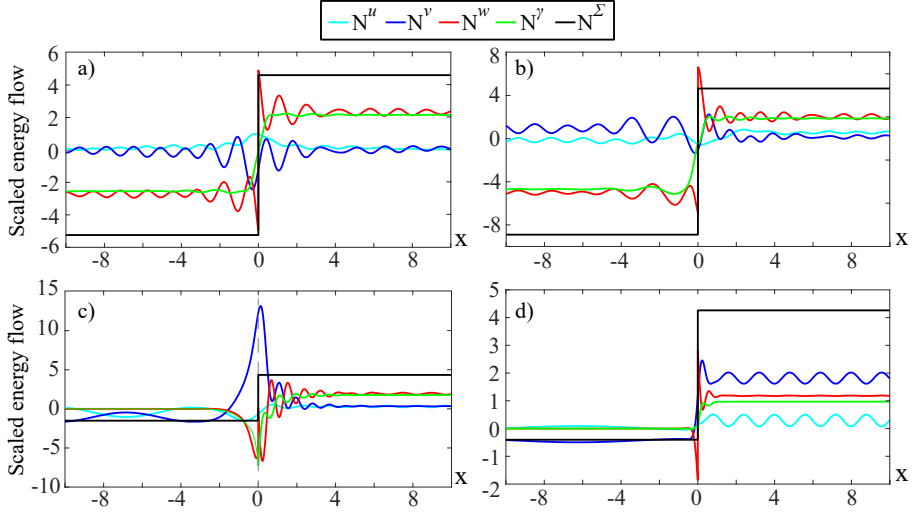


Fig. 12: Partition of the energy flow between alternative paths at $\Omega = 0.4$. (a) $\alpha = 3^\circ$, (b) $\alpha = 12^\circ$, (c) $\alpha = 18^\circ$, (d) $\alpha = 45^\circ$.

methods are very efficient in terms of computational cost, theoretical understanding of the wave characteristics and utilisation of the model for parametric studies. Results obtained by these methods are in a good agreement with each other, and contain the following aspects of novelty:

1. The analysis of propagation of free waves demonstrates that the symmetry in the location of dispersion curves for an orthotropic cylindrical shell with respect to the $\text{Re}[k] = 0$ plane breaks as soon as the angle α between the principal directions of orthotropy and the cylindrical coordinates depart from its extreme values $\alpha = 0$ and $\alpha = \frac{\pi}{2}$. Mathematically, it is explained by the simple fact that the polynomial dispersion equation contains both odd and even powers of the wavenumber. However, the symmetry of dispersion curves for an orthotropic cylindrical shell with respect to the $\text{Im}[k] = 0$ plane is preserved at any α , because the coefficients in the polynomial dispersion equation are purely real so that it may have only complex conjugated roots. As soon as the orthotropy angle acquires the limit values of the pitch angle $\alpha = 0$ or $\alpha = \frac{\pi}{2}$ the odd powers vanish, and the symmetry with respect to the $\text{Re}[k] = 0$ plane is recovered. The odd powers also vanish for an arbitrary α if the elastic parameters describe an isotropic material of the shell. Exactly the same features of the location of dispersion curves are detected for a helical lattice;
2. The non-symmetry of dispersion diagrams with respect to the $\text{Re}[k] = 0$ plane is significant for applications, where a cylindrical shell is exposed to the excitation by a rotating force. Solutions of forcing problems in these excitation conditions show that the angle of orientation of principal directions of orthotropy strongly influences partition of the energy flow in the positive and the negative direction of the axial coordinate as well as the energy distribution between alternative transmission paths in each direction. Therefore, the helical orthotropy may be

used as a novel efficient tool to tailor the waveguide properties of cylindrical shells in the prescribed direction of wave propagation and, therefore, to control energy flow in piping systems at prescribed excitation frequencies.

References

- [1] D. Pearson, Dynamic behaviour of helical springs, *Shock Vib. Dig.* 20 (1988) 3–9. doi:10.1177/058310248802000703.
- [2] S. Sorokin, Linear dynamics of elastic helical springs: asymptotic analysis of wave propagation, *Proc. R. Soc. A Math. Phys. Eng. Sci.* 465 (2009) 1513–1537. doi:10.1098/rspa.2008.0468.
- [3] J. Lee, D. J. Thompson, Dynamic stiffness formulation, free vibration and wave motion of helical springs, *J. Sound Vib.* 239 (2001) 297–320. doi:10.1006/jsvi.2000.3169.
- [4] J. Lee, Free vibration analysis of non-cylindrical helical springs by the pseudospectral method, *J. Sound Vib.* 302 (2007) 185–196. doi:10.1016/j.jsv.2007.04.017.
- [5] S. V. Sorokin, The Green’s matrix and the boundary integral equations for analysis of time-harmonic dynamics of elastic helical springs, *J. Acoust. Soc. Am.* 129 (2011) 1315–1323. doi:10.1121/1.3543985.
- [6] J. M. Renno, B. R. Mace, Vibration modelling of helical springs with non-uniform ends, *J. Sound Vib.* 331 (2012) 2809–2823. doi:10.1016/j.jsv.2012.01.036.
- [7] F. Treysède, Elastic waves in helical waveguides, *Wave Motion* 45 (2008) 457–470. doi:10.1016/j.wavemoti.2007.09.004.
- [8] Y. Liu, Q. Han, C. Li, H. Huang, Numerical investigation of dispersion relations for helical waveguides using the Scaled Boundary Finite Element method, *J. Sound Vib.* 333 (2014) 1991–2002. doi:10.1016/j.jsv.2013.11.041.
- [9] Y. Liang, Y. Li, Y. Liu, Q. Han, D. Liu, Investigation of wave propagation in piezoelectric helical waveguides with the spectral finite element method, *Compos. Part B Eng.* 160 (2019) 205–216. doi:10.1016/j.compositesb.2018.09.083.
- [10] Z. C. Xi, G. R. Liu, K. Y. Lam, H. M. Shang, Dispersion and characteristic surfaces of waves in laminated composite circular cylindrical shells, *J. Acoust. Soc. Am.* 108 (2000) 2179–2186. doi:10.1121/1.1316093.
- [11] J. Kaplunov, A. Nobili, A robust approach for analysing dispersion of elastic waves in an orthotropic cylindrical shell, *J. Sound Vib.* 401 (2017) 23–35. doi:10.1016/j.jsv.2017.04.028.
- [12] V. V. Tyutekin, Helical waves of an elastic cylindrical shell, *Acoust. Phys.* 50 (3) (2004) 331–336. doi:10.1134/1.1739495.
- [13] I. A. Panfilov, Y. A. Ustinov, A study of harmonic fluctuations hollow the cylinder with screw anisotropy on the basis of three-dimensional equations of elasticity theory (in Russian), *Vladikavkazskij Mat. Zhurnal* 13 (2011) 35–44.
- [14] I. A. Panfilov, Y. A. Ustinov, Harmonic vibrations and waves in a cylindrical helically anisotropic shell, *Mech. Solids* 47 (2012) 195–204. doi:10.3103/s0025654412020069.
- [15] E. Manconi, S. Sorokin, R. Garziera, A. Sjøe-knudsen, Wave Motion and Stop-Bands in Pipes with Helical Characteristics Using Wave Finite Element Analysis, *J. Appl. Comput. Mech.* 4 (2018) 420–428. doi:10.22055/JACM.2018.24930.1218.
- [16] V. V. Novozhilov, *The theory of thin shells*, P. Noordhoff Ltd, 1959.
- [17] A. L. Gol’denweizer, V. B. Lidskij, P. E. Tovstik, *Free Vibration of Thin Elastic Shells* (in Russian), Nauka, Moskva, 1979.
- [18] S. A. Ambartsumjan, *Theory of Anisotropic Shells* (in Russian), FizMATGiz, Moscow, 1961.
- [19] R. M. Jones, *Mechanics of Composite Materials*, Taylor & Francis, 1999.
- [20] B. R. Mace, E. Manconi, Wave motion and dispersion phenomena: Veering, locking and strong coupling effects, *J. Acoust. Soc. Am.* 131 (2012) 1015–1028. doi:10.1121/1.3672647.
- [21] E. Manconi, B. Mace, Veering and Strong Coupling Effects in Structural Dynamics, *J. Vib. Acoust.* 139 (2017) Article 021009. doi:10.1115/1.4035109.
- [22] R. D. Mindlin, *An Introduction to the Mathematical Theory of Vibrations of Elastic Plates*, World Scientific, Singapore, 2006. doi:10.2307/3608805.
- [23] L. Gibson, M. Ashby, *Cellular solids: structure and properties*, Cambridge University Press, 1997. doi:10.1017/CB09781139878326.

- [24] S. Gonella, M. Ruzzene, Homogenization and equivalent in-plane properties of two-dimensional periodic lattices, *Int. J. Solids Struct.* 45 (2008) 2897–2915. doi:10.1016/j.ijsolstr.2008.01.002.
- [25] S. M. Jeong, M. Ruzzene, Analysis of Vibration and Wave Propagation in Cylindrical Grid-Like Structures, *Shock Vib.* 11 (2004) 311–331. doi:10.1155/2004/629240.
- [26] F. Casadei, J. J. Rimoli, Anisotropy-induced broadband stress wave steering in periodic lattices, *Int. J. Solids Struct.* 50 (2013) 1402–1414. doi:10.1016/j.ijsolstr.2013.01.015.
- [27] P. G. Martinsson, A. B. Movchan, Vibrations of lattice structures and phononic band gaps, *Q. J. Mech. Appl. Math.* 56 (2003) 45–64. doi:10.1093/qjmam/56.1.45.
- [28] S. V. Sorokin, J. B. Nielsen, N. Olhoff, J. B. Larsen, N. Olhoff, Green’s matrix and the boundary integral equation method for the analysis of vibration and energy flow in cylindrical shells with and without internal fluid loading, *J. Sound Vib.* 271 (2004) 815–847. doi:10.1016/S0022-460X(03)00755-7.
- [29] G. Pavic, Vibroacoustical energy flow through straight pipes, *J. Sound Vib.* 154 (3) (1992) 411–429. doi:10.1016/0022-460X(92)90776-T.
- [30] M. B. Xu, W. H. Zhang, Vibrational power flow input and transmission in a circular cylindrical shell filled with fluid, *J. Sound Vib.* 234 (2000) 387–403. doi:10.1006/jsvi.1999.2880.

Paper F

Experimental analysis, simulation and decomposition of
vibrations in not perfectly axi-symmetric pipes

Lasse S. Ledet^{a,b}, Sergey V. Sorokin^a & Jan Balle Larsen^b

^a *Department of Materials and Production, Aalborg University,
Fibigerstraede 16, 9220 Aalborg East, Denmark*

^b *Sound and Vibration Laboratory, Grundfos Holding A/S,
Poul Due Jensens Vej 7, 8850 Bjerringbro, Denmark*

Published in:

NAFEMS Proceedings

As part of the NAFEMS World Congress (NWC17),
11-14 June 2017, Stockholm

Available: https://www.nafems.org/publications/resource_center/nwc17_481/.

[Accessed 08 May 2019]

© 2017 NAFEMS Ltd. All rights reserved.
The layout has been revised.

Experimental analysis, simulation and decomposition of vibrations in not perfectly axi-symmetric pipes

Lasse S. Ledet^{a,b}, Sergey V. Sorokin^a, Jan B. Larsen^b

^a*Department of Materials and Production, Aalborg University, Fibigerstraede 16, 9220 Aalborg, Denmark*

^b*Sound and Vibration Centre, Grundfos Holding A/S, Poul Due Jensens vej 7, 8850 Bjerringbro, Denmark*

Abstract

In this paper we consider experimental analysis of vibrations in pipes and pipelines, its decomposition into modal response and comparison with mathematical models. The decomposition into modes is useful in many engineering disciplines to obtain additional physical knowledge without additional effort. In general, decomposition is possible for any structure that is uniform, axi-symmetric and obeys linearity, which, fortunately, holds true for many engineering problems. Decomposition is widely used in, for instance, vibro-acoustics, electromagnetics and/or mechanics and is important in view of, for instance, suppression of vibrations or emitted noise, as some modes may be critical from the viewpoint of vibrations and others from the viewpoint of noise. In particular, the subject of decomposition becomes increasingly more important for larger and more compliant structures since resonances of the higher order modes tend towards the lower frequencies. On the other hand, if the structure is not perfectly axi-symmetric, for instance, due to inhomogeneous material properties, shape imperfections (e.g. weldings or damages) or experimental sources of error (e.g. misplacement of transducers), the circumferential modes mix up and cause what is typically known as modal leakage. Specifically, each spectrum to be decoupled becomes contaminated by spurious response (resonances), belonging to other decoupled spectrums. As a result, the decomposed spectra become inconclusive and the valuable insight of decoupling is lost. In this paper, however, we are concerned with how to cope with these issues of modal leakage and retain the valuable insight – even for structures with significant modal leakage – without demands for any additional data or experimental work. Thus, the methods developed here are based purely on new approaches to data processing. First, the main cause of modal leakage is studied mathematically by means of model disturbances i.e. a sensitivity study. From this study two strong methods used to enhance transparency to modal leakage are deduced. The first method is used for mode separation such as to permit modal characterisation of each resonance, whereas the second is used in comparison with mathematical models such as to avoid ambiguous conclusions in model validation. Lastly, the discussion is extended to the general aspect of spectral leakage in terms of aliasing.

1. Introduction

In many branches of engineering and science decomposition of measured response is widely used to gain superior physical knowledge of the system or component at hand. Decomposition is widely used in, for instance, electromagnetics to decompose the fluctuating force density field, see e.g. [1, 2] or in vibro-acoustics to decompose the response of a pipe into cross-sectional modes – known as modal response, see e.g. [3, 4]. In particular, the interest of this paper is the study of decomposition of uniform axi-symmetric structures in vibro-acoustics. This is important in view of, for instance, suppression of vibrations or emitted sound, as some modes are critical from the viewpoint of vibrations, while others are critical from the viewpoint of noise.

In [3] a convenient decomposition method, which allows for a reduction of the number of measurement points from N to $N/2 + 1$, was developed. This work was used and elaborated further in the PhD Thesis in [4] in which the decomposition of experimental results was studied with special emphasis on reducing modal leakage for comparison with mathematical models. Moreover, decomposition becomes increasingly more important for larger pipe diameters since this, in general, lowers the so-called cut-on frequency of the higher order modes as will be discussed in Sec. 2, see e.g. [5, 6].

In almost all practical cases the data set (e.g. experimental results) to be decomposed will be contaminated with leakage errors caused by, for instance, inhomogeneous material properties, shape imperfections (e.g. weldings or damages) or experimental sources of error e.g. due to misplacement and/or imprecise transducers etc. which will cause the modes to mix up and become inseparable. This is known as modal leakage since the response originating from other modes leak into spectrums to which they do not belong. As a result, the decomposed spectrum becomes inconclusive and the knowledge gained by decoupling is lost.

A typical example of modal leakage is shown in Fig. 1 for the modal response of the fifth mode ($m = 4$) from vibration measurements on an empty thin-walled pipe. Here three different decomposition methods are compared. From the figure we immediately locate at least nine resonances (peaks) in the graph, while mathematical analysis reveals only five resonances in the spectrum from 0 – 1600Hz with the first resonance located around 1215Hz. Does this then mean that we have a poor model? Or rather that the experimental data is contaminated with errors? As it turns out, the ambiguity is caused by modal leakage from the measurements. This can immediately be seen from the cut-on frequency of this mode, since no resonances can exist below this frequency, see e.g. [5]. In addition, validation of mathematical models is usually also obscured when compared with leakage contaminated experiments, as seen in Fig. 2. Thus, it is clear that we need stronger tools to separate authentic modes from spurious and to compare model with experiments such as to avoid ambiguous conclusions in both mode characterisation and model validation.

The structure of the paper is as follows: Section 2 serves as to shortly present the preliminaries of the area of vibro-acoustics of pipes, their vibration modes and decomposition as well as briefly summarise the experimental procedure. In Section 3

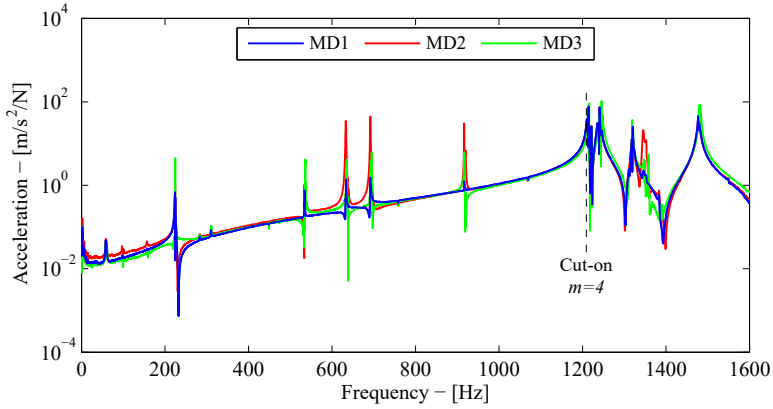


Fig. 1: Typical measured response decomposed by three different methods all showing significant modal leakage. Results are retrieved from decomposed vibration measurements on an empty pipe at $m = 4$ – discussed further in Sec. 2.

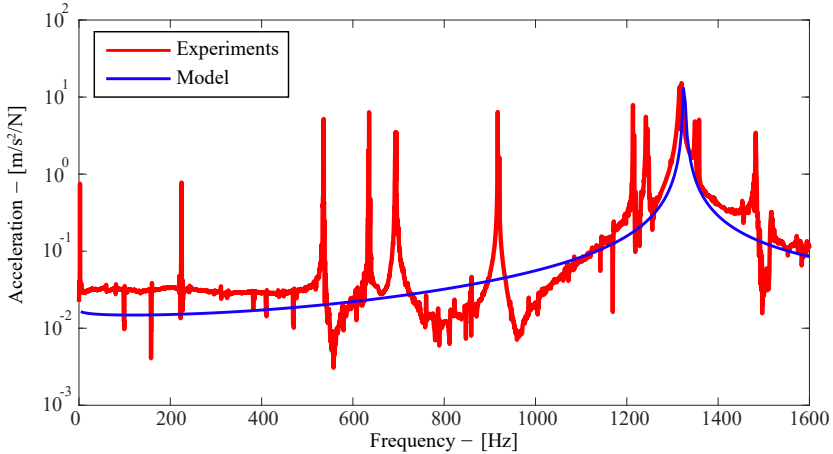


Fig. 2: Decomposed response (red) compared to modal response from a mathematical model (blue) at $m = 1$. The validity of the model is inconclusive.

the main cause of modal leakage is studied through sensitivities in a mathematical model. Section 4 presents a straightforward method to distinguish and characterise the circumferential modes of each resonance – in spite of significant modal leakage. Section 4 also presents a generic method to make leakage transparent in validation of mathematical models. Section 5 is devoted to discuss, in more general terms, other aspects of modal leakage. Section 6 concludes the paper and Appendix briefly summarises the experiments.

2. Preliminaries

As mentioned in Sec. 1 this paper is concerned with ways of retrieving detailed physical knowledge through post-processing of measured data and therefore emphasis

will be on experimental data, whereas details of the mathematical model etc. may be found in the provided references. Thus, to keep emphasis on data processing we restrict ourselves to vibration measurements on a simple empty pipe of the dimensions presented in Tab. A.1 in appendix. Nevertheless, the problem is still closely related to Multiphysics in the sense that the methodologies developed here are generic and therefore directly applicable to many Multiphysics problems, for instance, in vibro-acoustics, electromagnetics and/or mechanics.

Alternatively, we could also consider the fluid-filled pipe. However, as this is indeed associated with many more sources of error from an experimental viewpoint a significant effort is required to reduce these and thus emphasis will be led away from the actual scope of this paper. In fact, as will be obvious later, the methods developed require only that the test specimen obey linearity, is uniform and quasi axi-symmetric. Fortunately, this holds true for many classical problems in engineering and science.

The mathematical model used in this paper is formulated in the framework of Novozhilov–Gol’denvejzer’s shell theory for uniform axi-symmetric thin shells, [7]. The model is expressed via a set of Partial Differential Equations (PDE) that are decoupled into circumferential modes, m , and solved assuming time-harmonic vibrations. The solution is obtained through the method of Green’s matrix and is found analytically by means of bi-orthogonality relations and Boundary Integral Equations (BIE) with unit loads applied, [8] – equivalent to the Boundary Element Method (BEM). Further details concerning the model and its validity may be found in e.g. [9–12].

In this shell theory the solution to the governing PDE’s, when assuming time-harmonic vibrations (linearity), can be decomposed into distinct circumferential vibration modes by virtue of the axi-symmetry and orthogonality of the trigonometric functions solving this linear problem. The deformation shapes of the circumference of the first four modes ($m = 0, 1, 2, 3$) are presented in Fig. 3.

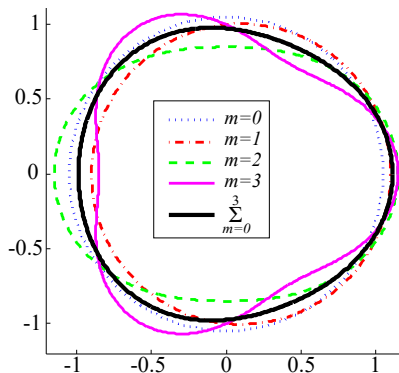


Fig. 3: Illustration of a general cross-sectional response (black) decomposed into its circumferential modes.

Thus, the general response (displacement) of the pipe may be expressed as an expansion on all circumferential modes, as seen in Eq. (1).

$$w(x, \theta, t) = \sum_{m=0}^{\infty} W_m(x, t) \cos(m\theta) \quad m \in \mathbb{Z} \quad (1)$$

where $w(x, \theta, t)$ is the radial response at the axial distance x , at time t and $W_m(x, t)$ is the amplitudes of each circumferential mode. These modes are the circumferential vibration modes and are not to be confused with neither the resonances (shown in Fig. 1) nor with the axial modes. For instance, the second mode ($m = 1$ – red in Fig. 3) is the bending mode of the pipe i.e. horizontal (or vertical) translation of the entire cross-section.

When assuming time-harmonic vibrations ($\exp(-i\omega t)$) the accelerations follow directly from Eq. (1) as:

$$\frac{\partial^2 w(x, \theta, t)}{\partial t^2} = -\omega^2 w(x, \theta, t) \quad (2)$$

where ω is the angular frequency and i is the complex operator. Note that since vibrations are typically measured in accelerations, the notation; amplitudes, refers to accelerations in what follows.

The circumferential modes shown in Fig. 3 are each associated with a characteristic frequency at which the first wave of that specific mode starts to propagate through the pipe and therefore convey energy. This characteristic frequency is known as the cut-on frequency and since all waves below this frequency are evanescent, no resonances of this specific mode can exist here, [5]. Furthermore, the cut-on frequency is characterised only by the mechanical and cross-sectional properties of the pipe, which implies that no matter the length of the pipe, modal resonances cannot exist below this frequency. However, for changing cross-sectional properties e.g. increasing radius (or decreasing thickness) both the cut-on frequency and resonances decrease.

2.1. Experimental procedure

A description of the experimental set-up, equipment and specifications of the test specimen can be found in appendix, whereas the experimental procedure is briefly presented here.

To decompose into modal response we need N equidistant measurements around the circumference of the pipe. In general, this can be done by four different methods, see e.g. [3, 4]. These methods are, ideally, identical but have individual disadvantages/advantages from the viewpoint of the experimental procedure.

MD1 Attach all, N , transducers equidistantly around the circumference. Perform a single measurement with any arbitrary excitation point – choose a few to avoid stationary points.

Pros: All points are measured in a single measurement

Cons: Increased added mass effects and N transducers needed

- MD2** Assume perfect symmetry in measurements and measure only on half the pipe, [3].
Pros: Only $N/2 + 1$ transducers/measurements needed (accelerometer 1–6 in Fig. A.9)
Cons: Rely fully on skew-/symmetry of the measurements and is therefore more sensitive to imperfections/misplacement
- MD3** Attach a single transducer and excite the structure at any arbitrary excitation point. Move the excitation point equidistantly around the circumference and continue to get the N measurements.
Pros: Reduced added mass effects and only one transducer with a fixed position is needed (application dependent)
Cons: N measurements needed
- MD4** Use the reciprocity theorem for **MD3** (applicable for linear systems) and keep a fixed excitation point, while moving the transducer equidistantly around the circumference.
Pros: Reduced added mass effects and excitation point fixed (application dependent)
Cons: N measurements needed and transducers need be attached/reattached between each measurement

Note: **MD2** applies also to **MD3** and **MD4**.

To investigate the strength of these methods with respect to leakage the methods MD1-3 are investigated in this paper.

2.2. Modal decomposition

The decomposition into modal response can be done in several ways provided that we have a number of N equidistant measurements around the circumference. To avoid aliasing N must be chosen specifically to the frequency spectrum of interest as discussed in Sec. 5.

For continuous functions decomposition is done by the integral weighting method known as Galerkin's orthogonalisation. This is for this specific case, however, equivalent to the (inverse) Fourier Transformation as defined in Eq. (3). For N equidistant measurement points Eq. (3) reform to the Discrete Fourier Transform (DFT) in Eq. (4) which gives the response of the first $N/2$ circumferential modes according to the Nyquist-Shannon Sampling Theorem, [13]. For efficient computation of the DFT, the Fast Fourier Transform algorithm (FFT) is usually preferred.

$$W_m(x, t) = \frac{1}{\chi_m \pi} \int_0^{2\pi} w(x, \theta, t) \exp(-im\theta) d\theta \quad (3)$$

$$W_m(x, t) = \frac{2}{\chi_m N} \sum_{n=0}^{N-1} w(x, \theta_n, t) \exp(-im\theta_n) \quad (4)$$

where $\chi_{m=0} = 2, \chi_{m \neq 0} = 1$ and $\theta_n = \frac{2\pi n}{N}$.

This method is, however, only valid for the modal decomposition methods MD1, 3 and 4. For MD2 the decomposition proposed in [3] is used. In this decomposition the skew-symmetry/symmetry of the ideal response, see Eq. (1), is utilised to reduce the equation system to two separate systems; one for even modes and one for odd. This is done by alternately adding and subtracting the mobility functions when expanded as in Eq. (1) for which the system reduces to Eq. (5) (for accelerometer 1–6 in Fig. A.9) by virtue of the skew-/symmetric properties.

$$\begin{aligned} \begin{Bmatrix} w_0 + w_5 \\ w_1 + w_4 \\ w_2 + w_3 \end{Bmatrix} &= \begin{bmatrix} 2 & 2 & 2 \\ 2 & 2 \cos\left(\frac{2\pi}{5}\right) & 2 \cos\left(\frac{4\pi}{5}\right) \\ 2 & 2 \cos\left(\frac{4\pi}{5}\right) & 2 \cos\left(\frac{8\pi}{5}\right) \end{bmatrix} \begin{Bmatrix} W_0 \\ W_2 \\ W_4 \end{Bmatrix} \\ \begin{Bmatrix} w_0 - w_5 \\ w_1 - w_4 \\ w_2 - w_3 \end{Bmatrix} &= \begin{bmatrix} 2 & 2 & 2 \\ 2 \cos\left(\frac{\pi}{5}\right) & 2 \cos\left(\frac{3\pi}{5}\right) & -2 \\ 2 \cos\left(\frac{2\pi}{5}\right) & 2 \cos\left(\frac{6\pi}{5}\right) & 2 \end{bmatrix} \begin{Bmatrix} W_1 \\ W_3 \\ W_5 \end{Bmatrix} \end{aligned} \quad (5)$$

where w_n is the measured mobility function at θ_n such that $w_n = w(x, \theta_n, t)$ and $W_m = W_m(x, t)$ from Eq. (1). Subsequently, the amplitudes are retrieved simply by inverting the systems in Eq. (5). It should be noted that this method is more sensitive to leakage, since skew-/symmetry is strictly imposed for the measured mobility functions. Thus, MD2 is expected to display more leakage.

The methodology can also be adopted to the sine part to retrieve the imaginary part of the amplitudes and through Euler's Identity, see e.g. [14], get the phase, as given directly by the latter Fourier Transform. However, ideally, the imaginary (sine) part should be zero, since the radial response is ideally an even half-range expansion. Hence, the leakage from the cosine part into the sine part can be viewed as an indication of modal leakage and occurs e.g. due to lack of symmetry from inhomogeneities, imperfections or experimental errors, but may also arise from, unintentionally, measuring part of the circumferential response as this is ideally an odd half-range expansion. No matter the cause this will always occur, if not from the specimen then from experimental errors, and will be perceived, in our measurements, as the unfavourable modal leakage.

3. A sensitivity study on alternative leakage sources

First, we study the effects caused solely by lack of symmetry and added mass. For perfectly axi-symmetric specimens it is given that the vibration pattern in the vertical and horizontal plane is identical, meaning that each resonance will be a double resonance related specifically to each plane of motion. However, when not perfectly axi-symmetric specimens are considered the vibration pattern in the vertical plane differs from that of the horizontal plane and the double resonances start to depart for increasing breach of symmetry, see Fig. 4 (zoom of Fig. 1).

From this notion, it is obvious that departed double resonances is caused solely by lack of symmetry of the specimen itself e.g. from inhomogeneities or shape imperfections,

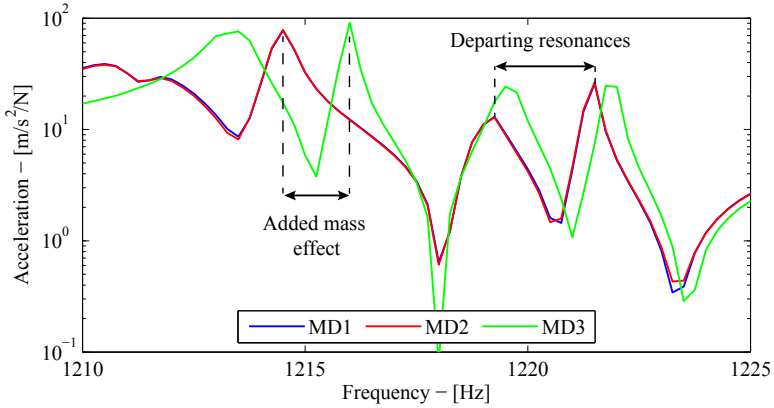


Fig. 4: Zoom of Fig. 1 around two authentic resonances of $m = 4$. Note the departing resonances due to lack of symmetry and the added mass effect from attached transducers.

and not as a consequence of experimental errors or imprecise transducers. Note also the shift in resonances between MD1-2 and MD3, caused strictly by the added mass effects i.e. the number of attached accelerometers.

Next, we focus on the effect of experimental sources of error on modal leakage through a sensitivity study. From the radial modal response, w_m , calculated in the mathematical model we can construct the general response, w , through Eq. (1). Obviously, this response can be decoupled completely by any of the latter decomposition methods provided that we have a number of equidistant sampling points around the circumference (chosen in accordance with the Nyquist-Shannon Sampling Theorem).

Now, to reflect the experiments, only the first five modes ($m = 0, 1, 2, 3, 4$) need be included in the general response and by virtue, at least, $N = 10$ measurement points are needed in the decomposition. From this general response we can easily study, as a function of frequency, the effect of imprecise transducers, not perfectly radial (off-axis) excitation and misplacement of accelerometers. This is done by, respectively:

1. Adding $\pm 5\%$ (accuracy of transducers – see Tab. A.2) of the calculated circumferential response to the radial response before decoupling
2. Calculating the general response when excited by a unit-vector different from the unit-vectors in the direction of the coordinate axis and decouple
3. Decomposing the general response with slightly perturbed equidistant 'measurement' points

Through these studies it is found that imprecise transducers and off-axis excitation have only small influence on the leakage – even for large perturbations, say $\pm 10\text{--}15\%$. The influence is mainly seen as moving anti-resonances and only for large perturbations, slightly decrease/increase in magnitude. The insignificance of these parameters is more or less obvious as these are somewhat 'controlled' parameters, meaning that the relative error stays within the same order of magnitude as the error (perturbation) introduced. For the misplacement, on the other hand, the decomposition is found to

be very sensitive to even the slightest perturbation in the measurement points. This is seen in Fig. 5 at $m = 4$ for randomly generated perturbations within $\pm 0.1\%$ of each equidistant measurement point. This corresponds to only $\pm 0.4\text{mm}$ on the circumference of the test specimen which is anticipated to be well below the actual accuracy at which the accelerometers can be attached.

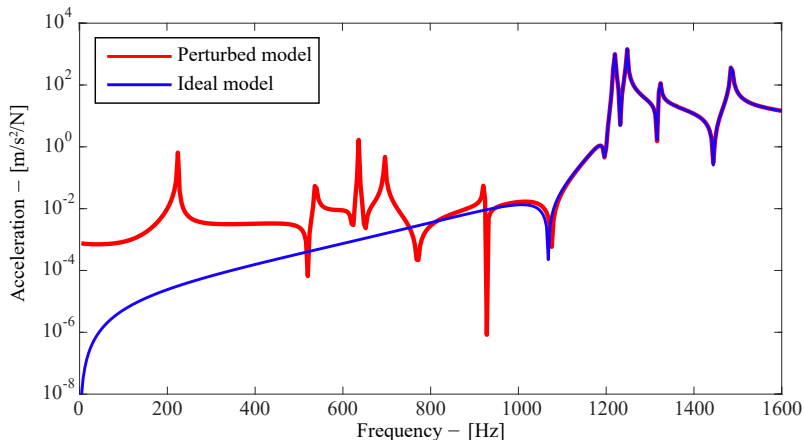


Fig. 5: Ideal modal response from the model (blue) compared with the decomposed response (red) at $m = 4$ when measurement points are perturbed randomly by $\pm 0.1\%$

From the figure it is clear that by even slightly perturbed measurement points the decomposed response diverge significantly from the authentic response. The significance of the misplacement is potentially large as it may be regarded as an ‘uncontrolled’ parameter, meaning that we may encounter relative errors of several orders of magnitudes higher than the error introduced – especially around resonances. Remark that introducing more measurement points do not improve the quality of the decomposition. Thus, it can immediately be concluded that the root cause of the modal leakage arises from misplacement of accelerometers and further that the decomposition is highly sensitive to such misplacements. This implies that the method of modal decomposition may be useless in practical applications, for instance, in model validation or mode characterisation of resonances due to the high sensitivities. Hence, simple methods to cope with these issues are needed to draw correct conclusions despite significant modal leakage.

4. Mode separation and model validation

In Fig. 1 the decomposed spectrum for $m = 4$ is presented. From this figure it is evident that the decomposition contains significant modal leakage and that resonances for this and other modes become inseparable. In this case, as the cut-on frequency is known, it is given that resonances below this frequency are spurious. However, to keep the methodologies completely general and applicable for other physics/applications no such information may be used to detect authentic/spurious resonances. Thus, our

knowledge is confined to a given set of data measured equidistantly around some circumference of a specimen that can be assumed uniform, axi-symmetric and obeys linearity.

Obviously, characterising the modal origin of the resonances becomes difficult even for perfectly axi-symmetric specimens due to the leakage introduced by the experimental errors. In fact, characterisation may be more or less impossible without, at least, comparing to some simple mathematical models. Typically, in industry, there is no 'easy' way of characterising the modes of the resonances. One approach may be to animate the deformation pattern based on the measured response and by visual means characterise each resonance. However, this becomes increasingly more difficult for increasing experimental errors and specimens moving away from perfect symmetry. Hence this requires some experience. Nevertheless, when comparing MD1 with MD2 it is given that there will be a difference in the decomposition – especially around spurious resonances as seen in Fig. 1 – due to the increased sensitivities in MD2 caused by imposing strict skew-/symmetry conditions. Yet, at the authentic resonances the modal response becomes so dominant that it abundantly exceeds the level of modal leakage and the two methods will eventually give the same result. This is immediately seen by comparing the decomposition methods MD1 and 2 at the authentic resonances from Fig. 4 with the spurious ones in Fig. 6.

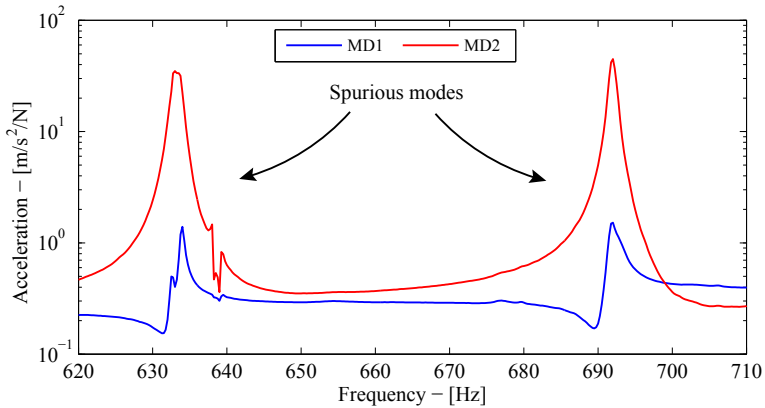


Fig. 6: Zoom of Fig. 1 around two spurious modes originating from $m = 3$. Note that the difference between the two methods is significant compared to Fig. 4. This is caused by the difference in leakage between MD1 and MD2.

In conclusion, it should be emphasised that this simple method/trick of separating modes and thereby characterising the resonances is very powerful as it is independent of the method used (MD1,3,4) and requires no additional measurements, only additional interpretation of the data.

On the other hand, in many engineering problems where mathematical models are used as tools for optimised/improved designs, experimental tests for validation is a prerequisite for using these. However, in modern engineering, experimental validation becomes increasingly more difficult due to the increasing complexity of structures. In

such cases, experimental sources of error may influence the results in a manner that restricts proper validation and/or insinuate ambiguous conclusions. A convincing example is the comparison between a model and decomposed experimental results containing significant modal leakage. A such comparison for the case treated in this paper was shown in Fig. 2 at $m = 1$, where only one authentic resonance is present – around 1315Hz. From Fig. 2 it is clear that the model predicts the region around the resonance reasonably well (for this mode) but in all other regions we fail to conclude whether the model is good or not. This was also concluded in [4]. For some industrial purposes this conclusion is sufficient, while for others a more elaborated or broader conclusion is needed. To get a better comparison – assuming that the model is profound – we need to reduce the experimental sources of error (the leakage) and try again.

Inasmuch as the main cause of leakage originate from misplacement this may be accounted for by introducing small random perturbations when decomposing the mathematical model, as it was done in Sec. 3. This is valid since the characteristics of the leakage is governed by the resonances and will therefore be similar no matter the size of the perturbations. This approach is simple and advantageous depending on the origin of the mathematical model. For instance, in case of transient or harmonic analysis using commercial software where the solution is the general response and therefore need be decoupled anyhow.

If, on the other hand, the governing equations are already decoupled and solved for each mode the 'detour' used in Sec. 3 need be applied to introduce leakage by misplacement i.e. assembly of the general response and subsequent decomposition back into the modes. In this case we can instead use the decoupled spectrum from experiments as a load scaling for proper comparison. Nevertheless, be aware that this short-cut calls for proper attention and sound physical understanding of the measured data in order not to over-interpret the results. The simple, but very useful, trick for introducing leakage (misplacement) into our model follow from Eq. (6).

$$w_m^{Exp.} \approx w_m^{Mod.} \quad \Leftrightarrow \quad \left(w_m^{Exp.}\right)^{1+\frac{1}{p}} \approx w_m^{Mod.} \left(w_m^{Exp.}\right)^{\frac{1}{p}} \quad p \in \mathbb{N} \quad (6)$$

where $^{Mod.}$ indicates response from the model and $^{Exp.}$ from the experiments, whereas p may be perceived as a 'visualisation-factor' belonging to the natural numbers, preferable > 1 .

At first instance, following the approach of Eq. (6) and multiplying each side by the same quantity may seem trivial. However, by this simple trick we conveniently introduce leakage from the experiments into the model and do thereby provide means for better comparison, as seen in Fig. 7. Thus, this simple trick ensures that model validation becomes somewhat transparent to leakage.

From this it is clear that there is a profound difference between the inconclusive comparison in Fig. 2 – illustrating the left-hand-side comparison of Eq. (6) – and the right-hand-side comparison shown in Fig. 7. The latter comparison reveals that there is an excellent agreement between model and experiments, whereas the former is inconclusive due to the substantial amount of leakage.

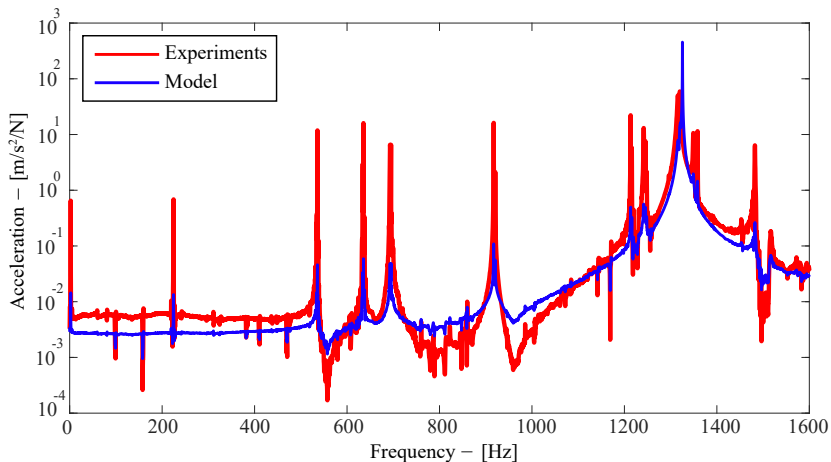


Fig. 7: The comparison in Fig. 2 scaled by the decomposed spectrum for $p = 2$. Experimental response (red) and model (blue) both scaled by the decomposed spectrum.

Nevertheless, to avoid a distorted picture and possible over-interpretation, p is restricted to the natural numbers as indicated in Eq. (6). This becomes obvious from Eq. (6) if we let p go to zero, as the model will then converge uniformly to the experimental results. On the other hand, by letting p go to infinity the right-hand-side will eventually converge uniformly to the initial comparison on the left-hand-side of Eq. (6). Thus, to avoid over-interpretation $p > 1$ is recommended. However, the choice of and sensitivity with respect to p should be considered for each individual case. Note also that the choice of p , can be perceived as an analogue to the size of the allowable perturbation in the former approach i.e. decreasing perturbation size is analogue to increasing p . Finally, it is important to notice that no matter the choice of p the absolute and relative errors between model and experiments are unaffected, why this simple method only provide visual aids to disregard modal leakage.

In addition to the mathematical arguments for using this simple method, the argument from a physical viewpoint is: As misplacement has shown to be the root cause of modal leakage, the leakage contaminated decomposed response can be perceived as a measure of leakage more than the authentic modal response, why this scaling may be appropriate for comparisons, depending on the choice of p .

5. Discussion

As discussed, the methods are developed to make the experimental results more transparent to the sources of error that introduce modal leakage, no matter whether they arise from inhomogeneities/shape imperfections or misplacement/imprecise transducers. However, one phenomenon of modal leakage that is not covered by these methods is the aspect of aliasing, see [13] for further details.

In general, aliasing is avoided on spectral level (spectral leakage) by using, for instance, low pass filters or controlled excitations to sort out higher order frequencies

before they are measured. Yet, leakage in the modal spectrum between circumferential modes in the sense of aliasing cannot be circumvented by the same techniques as it is a direct consequence of the chosen frequency spectrum and the mechanical and cross-sectional properties of the pipe. Thus, if the overall spectrum contains leakage in terms of aliasing, inevitably the leakage will also be present in the modal spectrum as a disguised spurious mode that cannot be detected by these (or any) methods. If, on the other hand, there is no leakage in the overall spectrum, the modal spectrums may still contain spurious aliasing modes. This occurs if N is chosen too small compared to the frequency range and mechanical and cross-sectional properties of the specimen. For instance, in the spectrum considered in this paper (0 – 1600Hz) the minimum number of sampling points around the circumference is chosen to $N = 10$ in accordance with the Nyquist-Shannon Sampling Theorem, [13], since the highest mode with cut-on frequency in this spectrum is the fifth mode ($m = 4$). In other words, N should be chosen such that; $N \leq 2(\tilde{m} + 1)$ where \tilde{m} is the highest mode that has cut-on frequency in the chosen spectrum. Thus, N is obviously highly dependent on the frequency range but likewise on the dimensions and mechanical properties of the pipe. In general, the cut-on frequency of the circumferential modes decreases for increasingly compliant structures e.g. increasing radius and/or decreasing thickness. In this case more sampling points are needed to analyse the same frequency range. Hence, to select a sufficient number of sampling points the cut-on frequencies of each mode need be known or estimated. In some areas of engineering and science approximations for the lower order cut-on frequencies exists, for instance, for empty pipes up to $m = 3$, see [6]. If such approximations do not exist, choosing the number of sampling points may not be a trivial task and needs to be studied for the individual cases. For certain problems, a frequency sweep may reveal the number of cut-on frequencies present in the response, however, a such method is, to the authors knowledge, yet to be developed.

6. Conclusion

In this paper we are concerned with studying the root cause of modal leakage in decomposition of experimental results as well as additional post-processing of experimental data to make conclusions transparent to such leakages. First, the root cause of leakage is found to arise from misplacement of accelerometers (or excitations points) as even slight misplacement will introduce significant leakage into the decomposed spectrums. To cope with these leakage issues two simple methods are developed – without demands for additional experimental work – just new approaches to post-processing. The first method is used for mode characterisation of resonances. The method compares different approaches to decomposition (one imposing strict skew-/symmetry) that will immediately distinguish authentic modes from spurious in the decomposed spectrum. The second method is used for model validation. In this method leakage is introduced into the mathematical model to provide the necessary means for comparison. This can, in general, be done in two ways depending on the mathematical model at hand: In one case by slightly perturbing the model before decomposing,

and in another case by utilising the decomposed spectrum as a scaling for both experiments and model. Finally, leakage caused by aliasing cannot be distinguished by these methods and we are therefore in need of methods for systematically determining the cut-on frequencies which we are yet to develop.

Appendix A. Experimental setup

As mentioned in Sec. 1 the experiments have been simplified to circumvent unnecessary sources of error. Effectively the experiments are confined to an empty thin-walled stainless steel pipe with the mechanical properties of Tab. A.1.

	Ref. name	Value	Unit
Geometry – Thin-walled pipe			
Radius – Median	R	68.3	mm
Pipe thickness	h	1.6	mm
Length	L	743.5	mm
Material properties – Stainless steel			
Young’s modulus	E	205.1	GPa
Poisson’s ratio	ν	0.3	-
Mass	m	4067.1	g
Density	ρ	7966.8	kg/m ³

Tab. A.1: Details of the test specimen. Young’s modulus is found by fitting model to experiments and the density calculated based on mass and volume.

The constraints used are free-free boundary conditions, mimicked by a soft suspension of compliant springs and fishline, as illustrated in Fig. A.8. For these boundary conditions to be feasible the overall resonance of the one degree-of-freedom mass-spring system should be low and not coincide with any structural resonances of the pipe itself. Using simple mass-spring considerations and the values from Tab. A.1 the system resonance can be approximated to 2.20Hz by Eq. (A.1), which is indeed anticipated to be well below the first resonance of the thin-walled pipe.

$$f_{sys} = \frac{1}{2\pi} \sqrt{\frac{k_{equiv}}{M}} = \sqrt{\frac{1}{2\pi^2} \frac{k}{M}} \quad (\text{A.1})$$

No.	Component	Type	Note
1	Fourier analyser (B&K)	PULSE LabShop	v18.0
2	Frontend (B&K)	3050-B-6/0	6 channels
3	Accelerometer (B&K)	4518-003	1.5g radial one-way ±5% circumferential
4	Modal hammer (B&K)	8202	w/ force transducer
5	Suspension line	Fishline	
6	Suspension spring	Tension	$k = 390\text{N/m}$

Tab. A.2: Equipment used in the experiments. Numbering associated with Fig. A.8. (B&K) abbrev. for Brüel & Kjør.

As illustrated in Fig. A.8 the specimen is excited by a modal hammer (tip chosen to comply with the given frequency range) and 10 accelerometers are placed equidistantly around the circumference according to Fig. A.9 at two arbitrarily chosen circumferences. Multiple measurements are needed to ensure that all modes are properly excited and that accelerometers and/or excitation points are not placed at stationary points (also known as nodal points).

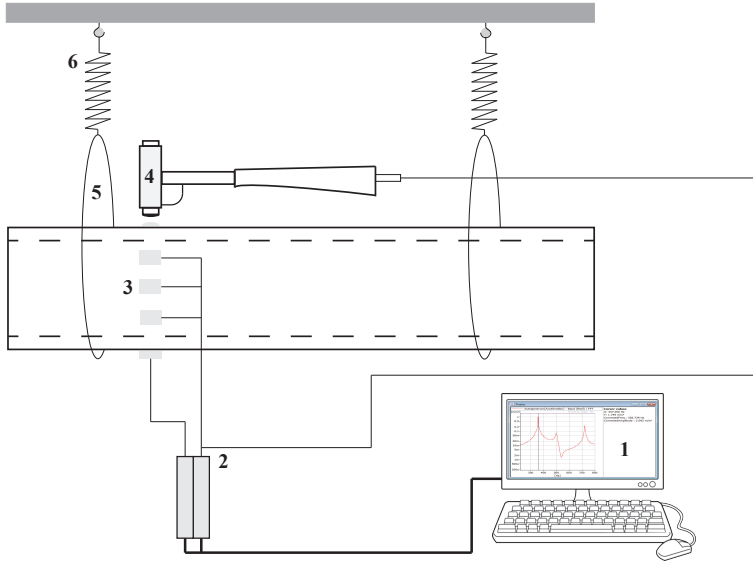
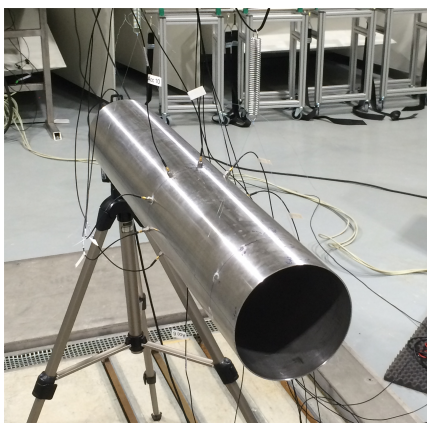
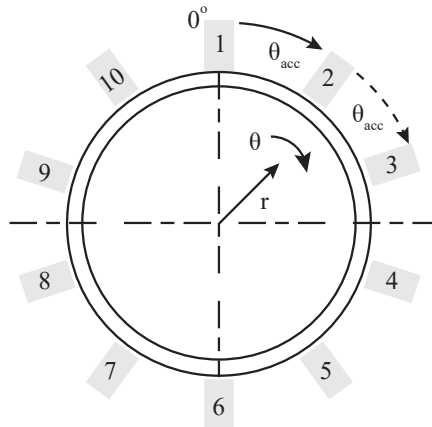


Fig. A.8: Sketch of experimental setup. Numbering elaborated in Tab. A.2.



(a)



(b)

Fig. A.9: Picture of the experimental setup (left) and graphical illustration of placement (and reference number) of the 10 accelerometers around the circumference (right).

References

- [1] J. Gieras, C. Wang, J. Lai, *Noise of Polyphase Electric Motors*, Taylor & Francis, 2005.
- [2] P. Timar, *Noise and Vibration of Electrical Machines*, vol. 34 Edition, Elsevier, 1989.
- [3] L. Feng, Experimental studies of the acoustic properties of a finite elastic pipe filled with water/air, *J. Sound Vib.* 189 (4) (1996) 511–524. doi : 10 . 1006 / j s v i . 1996 . 0032.
- [4] B. O. Olsen, Vibroacoustic power flow in infinite compliant pipes excited by mechanical forces and internal acoustic sources.
- [5] L. Cremer, M. Heckl, B. A. Petersson, *Structure-Borne Sound*, 3rd Edition, Springer, 2005. doi : 10 . 1017 / CB09781107415324 . 004.
- [6] F. J. Fahy, P. Gardonio, *Sound and Structural Vibration: Radiation, Transmission and Response*, 2nd Edition, Elsevier, 2007.
- [7] V. Novozhilov, *The theory of thin shells*, Groningen: P. Noordhoff Ltd., 1959.
- [8] S. V. Sorokin, The boundary integral equations method in vibro-acoustics., in: RASD - 10th Intl. Conf. Recent Adv. Struct. Dyn., 2010.
- [9] L. S. Ledet, S. V. Sorokin, Bi-orthogonality relations for fluid-filled elastic cylindrical shells: Theory, generalisations and application to construct tailored green's matrices, *J. Sound Vib.* 417 (2018) 315–340. doi : 10 . 1016 / j . j s v . 2017 . 12 . 010.
- [10] S. V. Sorokin, J. B. Nielsen, N. Olhoff, J. B. Larsen, N. Olhoff, Green's matrix and the boundary integral equation method for the analysis of vibration and energy flow in cylindrical shells with and without internal fluid loading, *J. Sound Vib.* 271 (3-5) (2004) 815–847. doi : 10 . 1016 / S0022 - 460X (03) 00755 - 7.
- [11] S. V. Sorokin, A. V. Terentiev, Flow-induced vibrations of an elastic cylindrical shell conveying a compressible fluid, *J. Sound Vib.* 296 (2006) 777–796. doi : 10 . 1016 / j . j s v . 2006 . 03 . 028.
- [12] A. S e-Knudsen, S. V. Sorokin, Modelling of linear wave propagation in spatial fluid filled pipe systems consisting of elastic curved and straight elements, *J. Sound Vib.* 329 (24) (2010) 5116–5146. doi : 10 . 1016 / j . j s v . 2010 . 06 . 015.
- [13] C. Phillips, J. Parr, *Feedback Control Systems*, 5th Edition, Pearson, 2011.
- [14] E. Kreyszig, *Advanced Engineering Mathematics*, 9th Edition, Wiley, 2006. doi : 10 . 15713 / ins . mmj . 3.

ISSN (online): 2446-1636
ISBN (online): 978-87-7210-453-9

AALBORG UNIVERSITY PRESS